

# **Towards Rhodium and Iridium Oxo Complexes**

Dissertation

zur Erlangung des akademischen Grades

Doktor der Naturwissenschaften

(Dr. rer. nat.)

von

Nevena Šušnjar

aus

Belgrad (Serbien)

Hamburg 2006

*"To dream anything that you want to dream. That is the beauty of the human mind.  
To do anything that you want to do. That is the strength of the human will.  
To trust yourself to test your limits. That is the courage to succeed."*

(Bernard Edmonds)

1. Gutachter: Prof. Dr. P. Burger
2. Gutachter: Prof. Dr. J. Heck

Dedicated to my parents

(Посвећено мојим драгим родитељима)

## Acknowledgements

I would like to express my deepest thanks and sincere gratitude to my supervisor, Professor Peter Burger for his invaluable advice, constant encouragement and discussion throughout my research.

Sincere thanks are due to Prof. Heinz Berke and all members of the research group at the University of Zürich who have created a wonderful atmosphere and made my first year of study most pleasant.

Many thanks must go to Dr. Stefan Nüchel who contributed to the improvement of my technical skills and introduction to this area of chemistry.

I would like to thank my colleagues at the University of Hamburg especially Julia Schöffel for her honest support and the students Jörg Storz, Nils Pagels, Jan-Philipp Mayer, Ulrich Tromsdorf, Viktoria Tonn and Angela Tomaszewski for help in the lab.

Sincere thanks to the technical staff of the department (X-ray and Elemental analysis service). Special thanks also to the NMR service and Dr. Erhard Haupt for constructive discussions.

I would like to thank to my husband, Andrew Hearley, for his patience, faith and support over the past 4 years.

Finally, I would like to gratefully acknowledge the financial support of the Swiss National Foundation and the University of Hamburg.

## List of abbreviations:

Al(pftb) <sub>4</sub>	Perfluorotertbutoxyaluminate
B3LYP	Becke-3 parameter functional with Lee-Yang-Parr correlation
BP-86	Becke-Perdew
Bn-tpen	N-benzyl-N,N',N'-tris(2-pyridyl-methyl)-1,2-diaminoethane
CCDC	Cambridge Crystallographic Data Center
C <sub>6</sub> H <sub>6</sub>	Benzene
CH <sub>2</sub> Cl <sub>2</sub>	Dichloromethane
CH <sub>3</sub> CN	Acetonitrile
DMAN	1,8-bis-(dimethylamino)naphthaline
DFT	Density functional theory
DME	1,2-Dimethoxyethane
Et <sub>2</sub> O	Diethyl ether
EPR	Electron Paramagnetic Resonance
HMBC	Heteronuclear Multiple Bond Correlation
HOMO	Highest Occupied Molecular Orbital
HPLC	High Performance Liquid Chromatography
HSQC	Heteronuclear Single Quantum Coherence
<sup>i</sup> Pr	Isopropyl
IRC	Intrinsic Reaction Coordinate
LACVP	Los Alamos Core Valence Potential
LUMO	Lowest Unoccupied Molecular Orbital
Me	Methyl
MeOH	Methanol
MLCT	Metal to Ligand Charge Transfer
NMR	Nuclear Magnetic Resonance
NOE	Nuclear Overhauser Effect
N4Py	N,N-bis(2-pyridylmethyl)-bis(2-pyridyl)methylamine
ORTEP	Oak Ridge Thermal Ellipsoid Plot Program
Ph	Phenyl
PPNCl	Bis-(triphenylphosphoranylidene)-ammonium chloride
TASF	Tris-(dimethylamino)sulfonium-difluorotrimethylsilicate
TBAF	Tetrabutyl-ammoniumfluoride

TDAE	Tetrakisdimethylaminoethylene
TD-DFT	Time Dependent Density Functional Theory
TEMPO	2,2,6,6-Tetramethyl-1-piperidinyloxo radical
THF	Tetrahydrofuran
TMC	1,4,8,11-Tetramethyl-1,4,8,11-tetraazacyclotetradecane
TZVP	Triple Zeta Split Valence

Abbreviations for the multiplicity of the NMR signals:

s (singlet), d (doublet), t (triplet), q (quartet) br (broad).

# Contents

<b>1 Introduction</b>	<b>1</b>
<b>1.1 Functionalization of alkanes to alcohols</b>	<b>1</b>
1.1.1 Examples in nature	2
1.1.2 Catalytic systems	4
<b>1.2 Our approach and goal</b>	<b>5</b>
<b>1.3 Late transition metal-oxo complexes</b>	<b>6</b>
<b>2 Towards Rh and Ir oxo complexes</b>	<b>11</b>
<b>2.1 Starting materials</b>	<b>11</b>
2.1.1 Synthesis of Ir(I) triflate complex	13
<b>2.2 Oxidation of Ir(I) hydroxo complex – unexpected results</b>	<b>15</b>
2.2.1 Oxidation with [thianthrene] <sup>+</sup> •	16
2.2.2 Oxidation with “ <i>magic blue</i> ”	19
2.2.3 Hydride abstraction with a trityl cation	22
<b>2.3 Ir(I) triflate as a precursor for an oxo complex</b>	<b>26</b>
2.3.1 Reactions with amine N-oxides	26
2.3.2 Reaction with TBA-Oxone	33
<b>2.4 Rh, Ir(III) peroxo complexes</b>	<b>34</b>
<b>2.5 The reactivity of the formal Rh<sup>III</sup>(0) complexes towards small molecules</b>	<b>38</b>
2.5.1 The formation of the Rh(I) azido complex	42
2.5.2 The reaction of V with adamantyl-1-azide	46
2.5.3 The activation of dinitrogen with complex V	47
<b>3 C-H activation by Rh, Ir(I) square planar complexes – mechanistic aspects</b>	<b>53</b>
<b>3.1 Improved synthesis of Ir(I) methyl complex</b>	<b>53</b>
<b>3.2 C-H activation of benzene</b>	<b>53</b>
3.2.1 Evidences for Ir(III) intermediate	57
3.2.2 Si-H activation process	61

<b>3.3 Ir, Rh(I) fluorides – precursors for the hydride complexes</b>	<b>64</b>
<b>3.4 C-O reductive elimination</b>	<b>73</b>
<b>4 Cationic complexes</b>	<b>79</b>
<b>4.1 Unexpected formation of the Ir(III) hydride</b>	<b>80</b>
<b>4.2 The formation of methanol from complex 4</b>	<b>83</b>
4.2.1 Proposed mechanism for the methanol formation	84
4.2.2 Alternative syntheses	86
<b>4.3 Synthesis of the novel formaldehyde complex 35</b>	<b>89</b>
4.3.1 Mechanistic aspects	93
4.3.2 Different reactivity of the Rh(I) methoxo complex 3	95
<b>5 Summary</b>	<b>98</b>
<b>6 Experimental section</b>	<b>102</b>
<b>6.1 General procedures</b>	<b>102</b>
<b>6.2 Synthesis and characterization of the novel Rh and Ir complexes</b>	<b>104</b>
6.2.1 Syntheses from Chapter 2	105
6.2.2 Syntheses from Chapter 3	110
6.2.3 Syntheses from Chapter 4	113
<b>7 References</b>	<b>119</b>
<b>8 Appendix</b>	<b>127</b>
<b>8.1 Summary of the isolated complexes</b>	<b>127</b>
8.1.1 Starting materials (1 – 7)	127
8.1.2 Summary of the isolated complexes (8 – 36)	128
8.1.3 Summary of the postulated complexes (I-VI)	130
<b>8.2 The X-ray crystallographic data and parameters</b>	<b>131</b>
<b>8.3 Lebenslauf</b>	<b>138</b>

# 1 Introduction

## 1.1 Functionalization of alkanes to alcohols

The selective oxidation and functionalization of alkenes under ambient conditions is an exciting scientific challenge and a highly valuable economic goal. Alkanes from natural gas and petroleum are the world's most abundant feedstocks (Fig. 1.1). The primary component of natural gas is methane ( $\text{CH}_4$ ). It may also contain heavier gaseous hydrocarbons such as ethane, propane and butane, as well as other gases, in varying amounts. During the geological formation of oil (and coal), large natural gas deposits are also formed. In former times, methane was released to the atmosphere when the oil (or coal) was extracted or it was simply burned at the oil field due to difficulties related to transportation. Most of the countries have abandoned this way of wasting methane, specifically because of environmental pressures. Nowadays, natural gas is transported through pipelines or by using tankers where the gas is liquefied. Although pipelines are economically feasible for inland gas transportation, they are not used across oceans. Alternatively, using tankers the cost of transport rises and safety problems emerge. In contrast, some platforms, where oil is extracted, pump the gas back into the ground in the hope that one day a new profitable method will be found to exploit this resource.

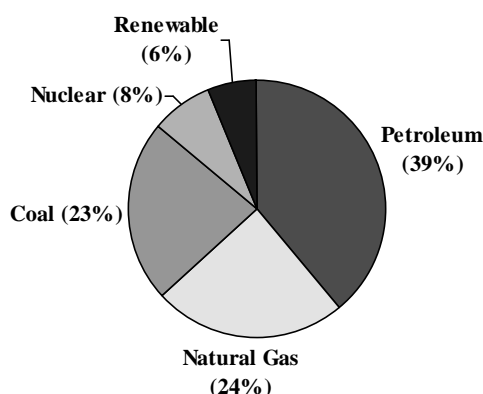


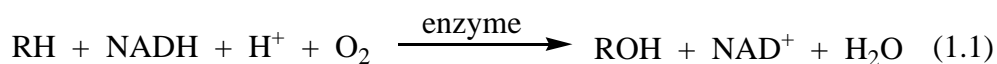
**Fig. 1.1** Abundance of natural gas and petroleum (left) and offshore platforms in California.

Currently, alkanes derived from both petroleum and natural gas are converted to energy, fuel and chemicals at high temperatures and multiple steps leading to inefficient environmentally and economically processes.

The development of a catalyst, which would selectively functionalize alkanes to alcohols under mild conditions, could lead to a new concept in production of energy in the 21<sup>st</sup> century.<sup>1, 2, 3</sup> The *selective* catalytic aerobic oxidation (O<sub>2</sub>) of one of the most inert substrates, methane, to methanol is still one of the "holy grails" of chemistry.<sup>4, 5</sup> In the past decades, there is an intense interest in C-H activation reactions, which are usually part of the catalytic cycle in functionalization of hydrocarbons to more useful products. However, there are very few examples of catalyst systems, that are capable of achieving this process and there are large gaps in our fundamental knowledge in how to design such a catalyst.<sup>3, 5</sup>

### 1.1.1 Examples in nature

The best examples of a selective alkane oxidation to a corresponding alcohol are found in nature. There are enzymes that can utilize dioxygen to oxidize saturated hydrocarbons to alcohols at ambient pressure and temperature (eq. 1.1).



The best known of these enzymes are cytochrome P450 and methane monooxygenase (MMO), which in the resting state contain an Fe(III) protoporphyrin IX and a  $\mu$ -oxo diiron or di-copper complex, respectively. The active species in the case of P450, is a terminal oxo-Fe(IV) porphyrin  $\pi$ -radical cation (Fig. 1.2- left), which can oxidize organic substrates by oxygen atom transfer. In methanotrophic organisms, there are two types of MMO: a soluble form (sMMO) containing oxygen bridged non-heme diiron (Fe(IV)) active sites, and particulate form (pMMO), which contains Cu(III) oxygen bridged metal centers (Fig. 1.2-right).<sup>6, 7, 8</sup>

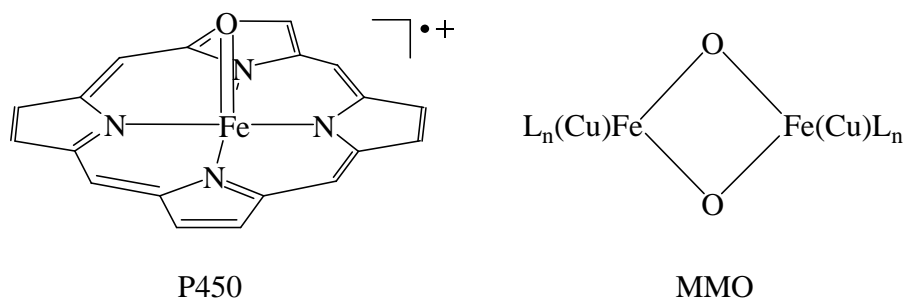


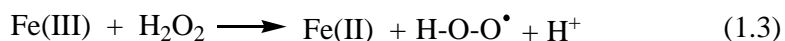
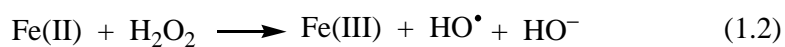
**Fig. 1.2** The active Fe(IV) site in P450 (left) and MMO enzyme.

A variety of Fe porphyrin complexes are able to mimic cytochrome P450 reactions *in vitro* using iodosylbenzene (PhIO) as the primary oxidant.<sup>9, 10</sup>

Recently, it was reported that Cu loaded zeolite (ZSM-5) after activating with oxygen, converts methane to methanol at 398 K.<sup>11</sup> In this case, the active core, containing a  $\mu$ -oxo bridged di-copper is responsible for methane oxidation, which was also proposed for pMMO.<sup>12</sup>

Only few examples are known in mimetics of non-heme iron enzymes. Wieghardt et al. postulated the formation of Fe(IV)-oxo compound  $[\text{Fe}(\text{O})(\text{cyclam-acetate})]^+$  in the reaction of corresponding Fe(II) complex and ozone.<sup>13</sup> This compound was characterized only by Mössbauer spectroscopy. The first crystal structure of the terminal  $[\text{Fe}^{\text{IV}}(\text{O})(\text{TMC})(\text{MeCN})](\text{OTf})_2$  complex was reported by Que Jr. et al..<sup>14</sup> It was obtained in high yield in the reaction of the related Fe(II) complex with iodosylbenzene. The corresponding Fe(IV)=O complex with pentadentate N5 ligands (N4Py or Bn-tpen) hydroxylates triphenylmethane or ethylbenzene to related alcohols.<sup>15</sup>

It is also worth mentioning that many of the postulated mechanisms involve radical pathways, which can be related to Fenton or Haber-Weiss chemistry. In 1898, Fenton reported the catalytic hydroxylation of alkanes with hydrogen peroxide and Fe(II) salts albeit with very low yield and conversion.<sup>16</sup> The mechanism of Fenton's reaction<sup>16</sup> was discovered later by Wilstätter, Haber and Weiss. They proposed that the actual oxidant in this reaction is the hydroxyl radical  $\cdot\text{OH}$  (eqs. 1.2 and 1.3).<sup>17, 18</sup>



They also worked on the mechanism of *catalase* (the enzyme which disproportionates hydrogen peroxide to water and oxygen) and proposed that a radical chain reaction takes place, which can be compared with their already proposed mechanism.<sup>19, 20, 21</sup> This reaction activated further research in the field of biomimetics.

## 1.1.2 Catalytic systems

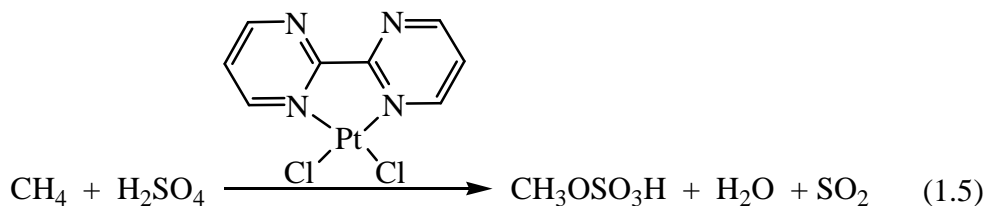
The classical Shilov system is one of the first examples where methane is selectively oxygenated to methanol (eq. 1.4).<sup>22, 23, 24</sup> The C-H bond in methane showed an 100 times higher reactivity than C-H in methanol.



Unfortunately, this catalyst showed to be unpractical. Pt(II) disproportionates to Pt(0) and Pt(IV) leading to a metal precipitation with concomitant deactivation. Further investigations of this system showed its high selectivity towards a terminal alkyl chain in the presence of the hydroxyl group.<sup>25</sup>

Another example of methane oxidation to methanol is known as “*Catalytica*” process. This process involves either a Hg(II) or Pt(II) catalyst and sulfuric acid as the oxidant.<sup>26</sup> Periana et al. improved the original Shilov system using a Pt(II) chloro complex with a bidentate 2,2'-dipyrimidine ligand (eq. 1.5).<sup>27</sup> The conversion to methylsulfate yields up to 70 %, selectivity of 90 % and turnover number ~ 300.

Apart from low turn over number, the disadvantage of this system is the high cost for the recovery of methanol from sulfuric acid.



So far, the Shilov and Periana catalysts are the closest to producing a practical system for selective methane oxidation.

## 1.2 Our approach and goal

The main goal in this work is to develop a novel selective catalyst for the aerobic functionalization of methane to methanol. Combining an organometallic and coordination approach in alkane functionalization, monomeric Rh, Ir(III) oxo complexes with a terminal oxo unit  $L_nM=O$  were the key compounds of the catalytic cycle presented in Figure 1.3.<sup>28</sup>

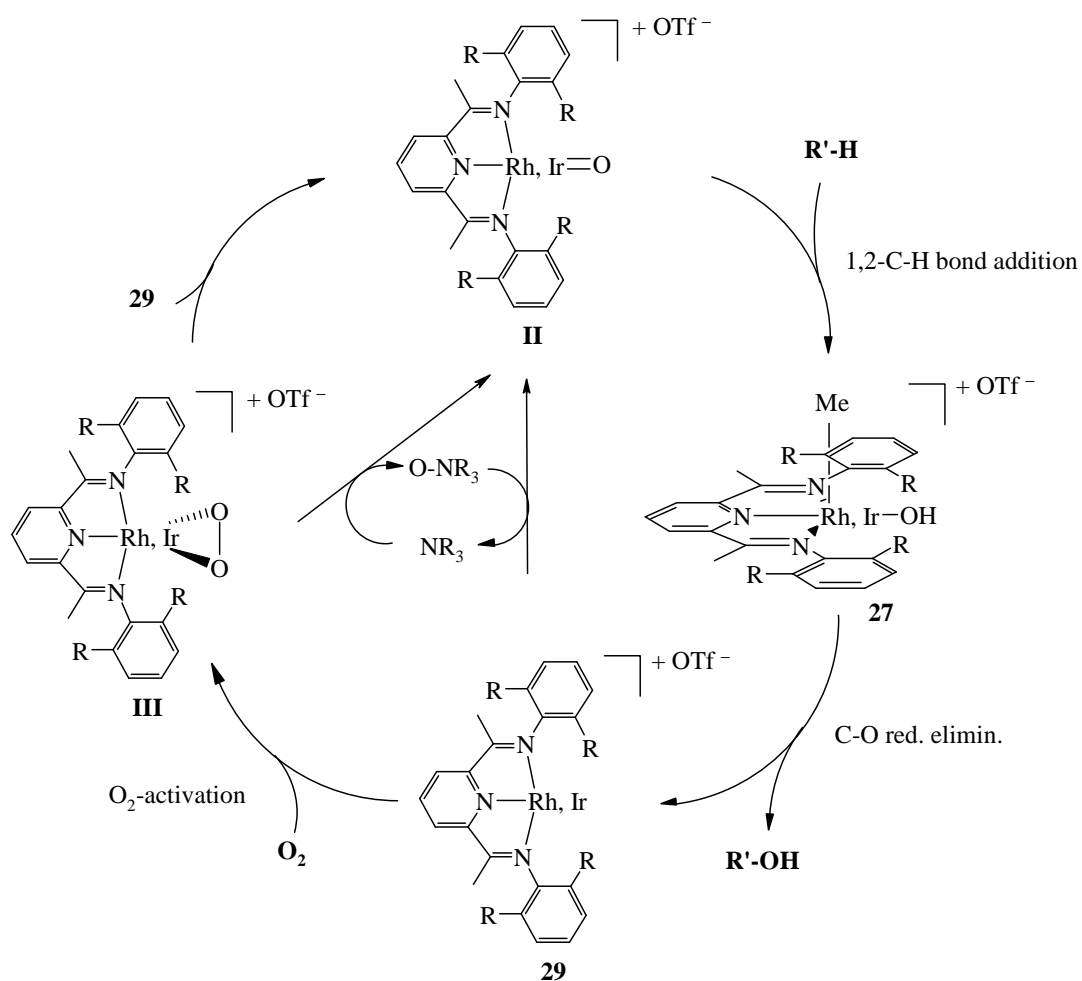


**Fig. 1.3** Proposed catalytic cycle for alkane hydroxylation with Ir, Rh(III) oxo complex.

Starting from the oxo complex **II**, 1,2-C-H bond addition would lead to alkyl hydroxo complex **27**. The next step involves C-O reductive elimination of an alcohol and the formation of a cationic complex **29**. The latter gives a peroxo species **III** after  $O_2$  activation. The metal oxo complex **II** is then restored from **III** and one equivalent of **29**.

According to DFT calculations, the step from the peroxo **III** to oxo complex **II** is thermodynamically favored. If the energy barrier is greater than expected, suitable amines such as dimethylphenyl amine can be used as a cocatalyst to convert **III** to **II**. The amine would also play a role in oxygen transfer. When amine-N-oxide is formed, it reacts further with **29** giving the desired oxo complex **II**.

### 1.3 Late transition metal-oxo complexes

Terminal metal-oxo complexes for high valent early and middle transition metals are well known.<sup>29, 30</sup> Moving from left to right in the periodic table, the number of stable terminal oxo complexes decreases. For the systems with a  $d^n$  electron configuration with  $n > 4$ , the oxo ligand is destabilized by repulsion (*vide infra*).

The aforementioned Fe(IV)=O complexes reported by Que Jr. et al.<sup>14</sup> together with the four coordinate trimesityl Ir(V) oxo complex have  $d^4$  configuration (Fig. 1.4).<sup>31</sup>

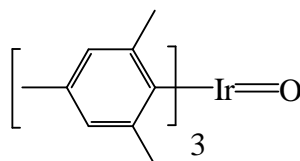


**Fig. 1.4** Ir(V) trimesityl oxo complex.

The latter was obtained under aerobic conditions from the corresponding Ir(III) trimesityl complex and  $O_2$  and is the only example of a terminal Ir-oxo complex reported in the literature. In the case of  $d^6$  configuration, there are only two complexes isolated for which a crystal structure was determined. One is  $NaRe(O)(PhCCPh)_2$  reported by Mayer et al.<sup>32</sup> (Fig. 1.5-left) and the second is Pt(IV)=O complex ( $K_7Na_9[Pt(O)(H_2O)L_2]$ ,  $L = [PW_9O_{34}]^{9-}$ ) (Fig. 1.5-right) recently isolated by Hill et al.<sup>33</sup> The platinum metal center is situated between two polyoxotungstate ligands, which are found to be highly effective  $\pi$  acceptors.

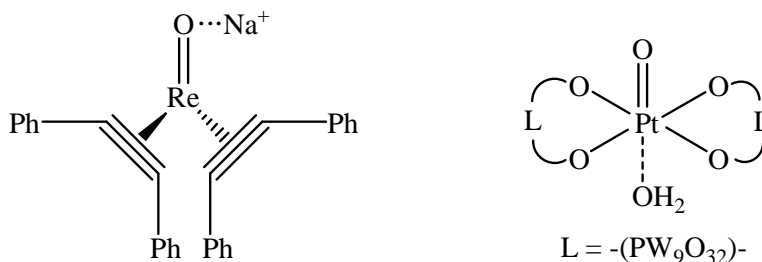


**Fig. 1.5** Re(I) and Pt(IV) terminal oxo complexes.

However, square planar transition metal-oxo complexes with  $d^8$  configuration are unknown. They are destabilized and a metal-oxygen multiple bond ( $L_3M=O$ ) is less feasible. This was rationalized by qualitative molecular orbital theory for Ni, Pd and Pt complexes by Mayer et al.<sup>34</sup> The lack of an available  $\pi$  acceptor orbital on the metal center ( $d\pi$ ), leads to 4 electron 2 orbital repulsion and destabilization of the system (Fig. 1.6).

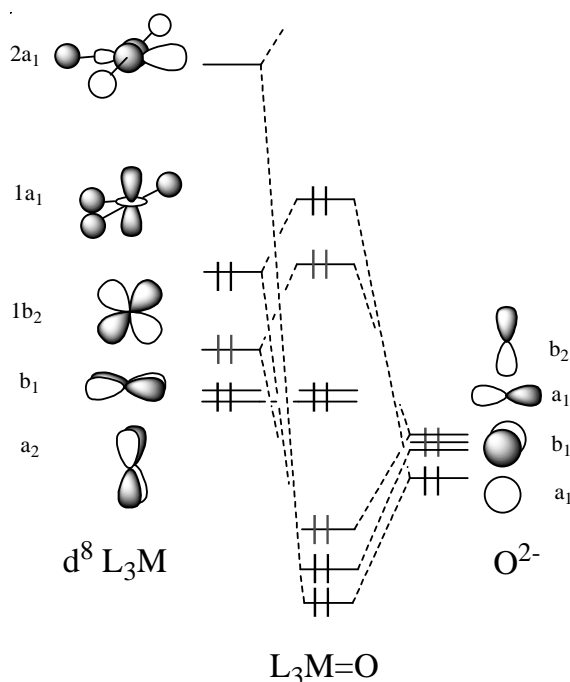


**Fig. 1.6** Destabilization of  $d^8$  square planar  $L_3M=O$  complexes.

Recently the group of Cinellu postulated the formation of a reactive terminal Au(III) oxo intermediate in the reaction of the related gold bis- $\mu$ -oxo bipyridine  $[Au_2(bipy^{Me})_2(\mu-O)_2]^{2+}$  and norbornene.<sup>35</sup> The square-planar intermediate would have  $d^8$  configuration.

In complexes of the type  $L_3M=O$  with  $d^6$  electron configuration destabilization by 4 electron 2 orbital repulsion may be still present (Fig. 1.7-left). However, there is a possibility to overcome this problem. The electrons from  $d_{xz}$  orbital ( $b_2$ , HOMO) of the  $L_3M$  fragment have to be promoted to a  $d_z^2$  orbital ( $a_1$ , LUMO). This way  $\pi$  bonding of the  $O^{2-}$  ligand with  $b_2$  symmetry is possible with the now empty  $d_{xz}$  orbital of the same symmetry and the system is stabilized (Fig. 1.7-right).

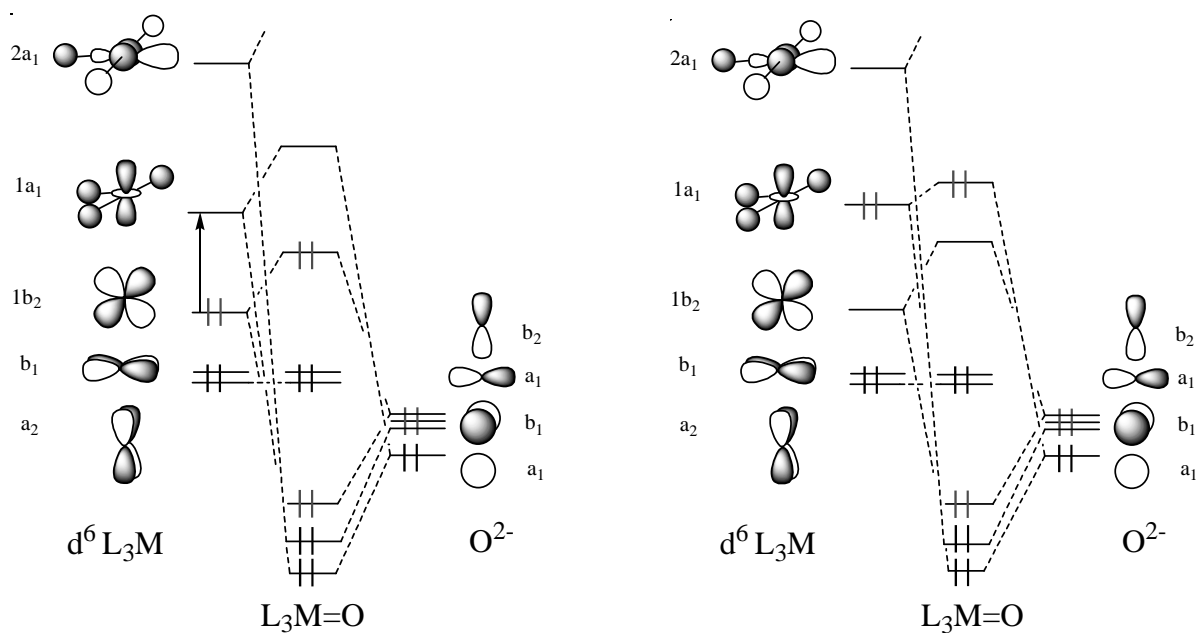


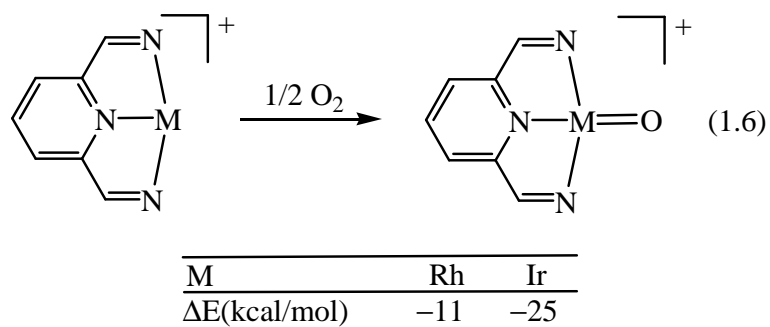
**Fig. 1.7** M-O bonding in  $d^6$  square-planar  $L_3M=O$  complexes (left-destabilized; right-stabilized).

The energy for promoting these electrons depends on the gap between the HOMO and LUMO. For the weaker donors, such as amines or imines, with smaller splitting of these levels, the estimated promotion energy is small.

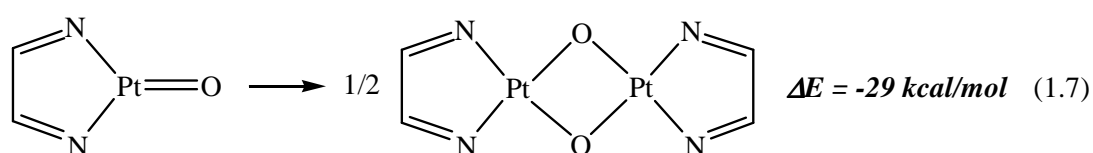
Conversely, the terdentate pyridine, diimine ligands, show excellent  $\pi$ -acceptor abilities and have been chosen in this work.<sup>36, 37</sup> It is believed that the M=O interaction will be stabilized through a push-pull-interaction.<sup>28, 38</sup>

It is noteworthy that HOMO-LUMO gaps in  $d^6$  configured  $L_3M=O$  complexes are anticipated to be small and that an open shell  $S=1$  states might be encountered.<sup>38</sup>

According to previous investigations in our group,<sup>28</sup> it was calculated that the formation of an oxo complex with a pyridine diimine ligand is thermodynamically favored for Rh and Ir (eq. 1.6).



However, the dimerization process of the terminal oxo complexes to mono or bis- $\mu$ -oxo bridged compounds is also strongly thermodynamically favored (eq. 1.7).<sup>28</sup>



To prevent dimerization, sterically demanding pyridine diimine ligands with alkyl (Me, <sup>i</sup>Pr, t-Bu) substituted phenyl groups were suggested. Intermolecular steric repulsion between the substituents on the ligands will prevent two possible dimerization pathways, denoted as “head to head” and “top on top” (Fig. 1.8).

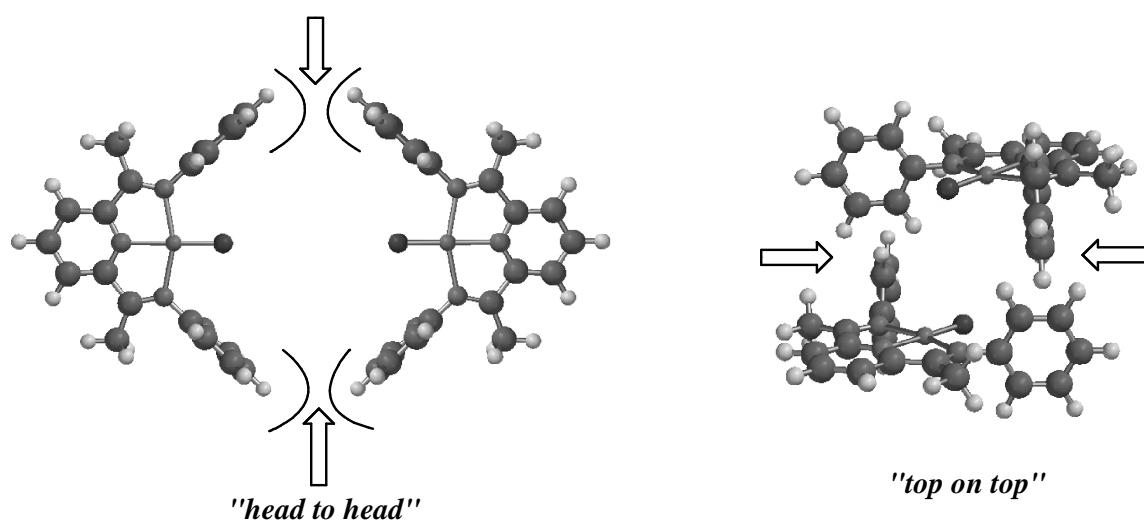


**Fig. 1.8** Prevention of dimerization using steric repulsion of the ligand substituents.

Although, sterically demanding ligands will be used, facile access of substrates is still possible from above or below the metal ligand plane.

The bond dissociation enthalpy of the metal-oxo moiety for the model complexes (depicted in eq. 1.6) was calculated to be in the range from 70-105 kcal/mol.<sup>28</sup> These values are significantly lower than for early to middle transition metals. For the tungsten oxo complex  $(C_5MeH_4)_2W=O$ ,<sup>39</sup> the BDE equals 132 kcal/mol (experimentally determined). It may be concluded that low BDE's of M=O in late transition metal oxo complexes will imply a great reactivity of the latter, which is important for alkane oxidation.

Part of this research was related to provide evidence for every step of the proposed cycle for the selective alkane activation (*vide supra*). The thesis is divided into three chapters. In Chapter 2, different approaches to the synthetic access to the desired oxo and peroxy species will be described. In Chapter 3 a focus on the C-H activation and C-O reductive elimination reactions of the catalytic cycle will be made. The last part explains different synthetic routes to cationic complexes.

## 2 Towards Ir and Rh oxo complexes

As mentioned in the introduction, the selective, aerobic oxidation of methane to methanol is believed to involve a monomeric late transition metal oxo complex ( $L_nM=O$ ) with a terminal oxo unit of the proposed catalytic cycle (see Fig. 1.3). The focus of this chapter will be on the synthetic progress in the preparation and characterization of rhodium and iridium oxo complexes as shown in Figure 2.1.

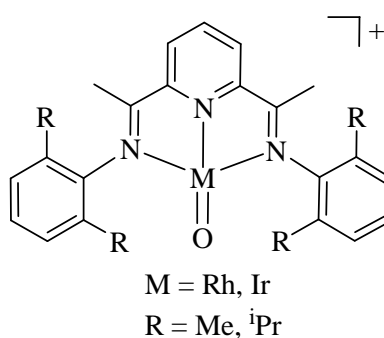
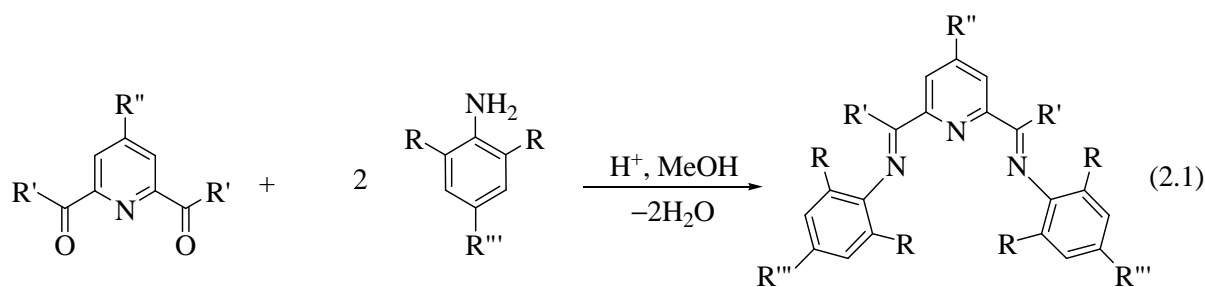


**Fig. 2.1** An example of a Rh or Ir(III) oxo complex.

This chapter is divided into four sections. The first section describes the synthesis of the starting materials. The other sections are related to different approaches to obtain oxo complexes: 1) by oxidizing an Ir(I) hydroxo complex, 2) reaction with amine N-oxides and a cationic triflate complex, and from peroxo complexes. Although not directly related to the chemistry of the oxo complexes, the last part describes the reactions of “Rh(0)” complexes. These are suspected as potential precursors for the formation of a Rh(II) oxo or peroxo complexes.

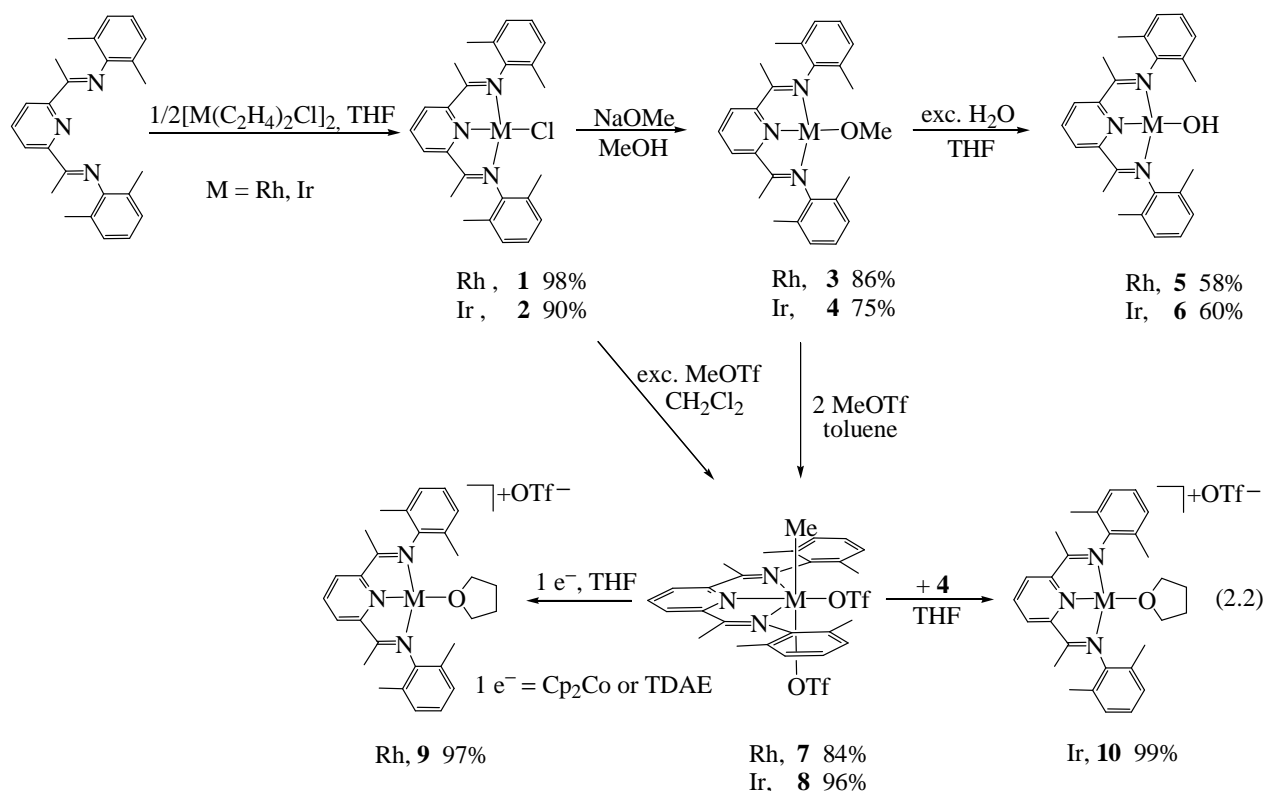
### 2.1 Starting materials

As indicated, in order to prevent dimerization of the terminal  $L_nM=O$  systems, terdentate pyridine diimine ligand systems, with sterically demanding alkyl substituted groups, have been selected for this study. The terdentate pyridine diimine ligands ( $N_3Me_4$ ) are prepared by the condensation of two equivalents of the desired aniline with 2,6-diacetylpyridine in 80 % yield (eq. 2.1).<sup>40, 41, 42, 43, 44</sup>



R = H, Me, <sup>i</sup>Pr; R' = Me, CF<sub>3</sub>; R'', R''' = H, t-Bu

The chloro complexes **1** and **2** were prepared from the bis( $\mu$ -chloro) dimers [M(C<sub>2</sub>H<sub>4</sub>)<sub>2</sub>Cl]<sub>2</sub> (M = Rh, Ir) in good yields.<sup>43, 45, 46</sup> The other starting materials, **3** – **6** were prepared by methoxide or hydroxide metathesis of the chloro ligand in a straight forward procedure as previously described.<sup>44</sup> Compounds **7** and **8** were obtained by oxidative addition of methyl triflate to **3** and **4** dissolved in toluene (or **1** and **2** in dichloromethane). Complex **9** was prepared in excellent yield by a 1e<sup>-</sup> reduction of the Rh(III) methyl bistriflate **7** with either TDAE or cobaltocene (Cp<sub>2</sub>Co) in THF (eq. 2.2).<sup>47, 48</sup>

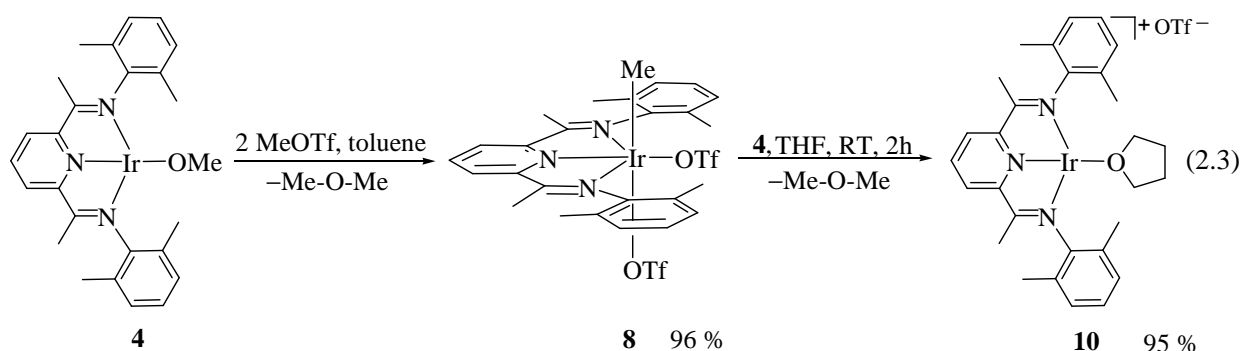


As previously established by Nüchel,<sup>44, 47</sup> according to the <sup>1</sup>H, <sup>13</sup>C-NMR spectroscopic data and X-ray crystal structure analyses, complexes **1** – **6** have a square planar geometry with a C<sub>2v</sub> symmetrical ligand environment. All complexes are soluble in THF and dichloromethane.

However, after two days at room temperature in dichloromethane, compounds **3**, **4** reconverted to the starting material **1**, **2** and methanol. The presence of methanol was observed by  $^1\text{H-NMR}$  spectroscopy in the reaction mixture as well in the transferred volatiles (singlet peak at  $\delta = 3.43$  ppm in  $\text{CD}_2\text{Cl}_2$ ). According to the  $^1\text{H}$  and  $^{13}\text{C-NMR}$  of the residual product in  $\text{CD}_2\text{Cl}_2$ , the formation of **1** and **2** was unambiguously confirmed. Incorporation of alkyl substituents on the pyridine and phenyl rings increases the overall complex solubility in less polar solvents such as benzene or toluene.

### 2.1.1 Synthesis of Ir(I) triflate complex

The novel complex **10** was synthesized in quantitative yield by a different route than Rh analogue,<sup>44</sup> starting from the methoxide complex **4** (eq. 2.3). The reaction between complex **4** and two equivalents of methyl triflate resulted in the formation of the light green Ir(III) methyl bis triflate complex **8**, which was fully characterized by  $^1\text{H}$ ,  $^{19}\text{F}$  and  $^{13}\text{C-NMR}$  spectroscopy. The desired triflate compound **10** was obtained in the second step, when an equimolar THF solution of **4** and **8** were stirred together, until the color changed from green to brown. Both steps lead to C-O bond formation yielding dimethyl ether. The latter was identified in the  $^1\text{H-NMR}$  of the transferred volatiles revealing a singlet peak at  $\delta = 3.21$  ppm in  $\text{THF-d}_8$  (the observed resonance was compared to a reference sample). A possible reaction mechanism of this transformation will be discussed in Chapter 3.



Complex **10** is soluble in THF and DME and completely insoluble in benzene, toluene, diethyl ether and pentane.  $^{19}\text{F-NMR}$  spectroscopy of **10** revealed a singlet peak at  $\delta = -78.9$  ppm in  $\text{THF-d}_8$ . Proton resonances from the coordinated THF (in  $\text{THF-d}_8$ ) are observed as multiplets at  $\delta = 1.61$  and  $1.81$  ppm in the  $^1\text{H-NMR}$  spectrum. Based on the  $^1\text{H}$ ,  $^{13}\text{C}$  and  $^{19}\text{F-NMR}$  spectroscopic data, it was concluded that compound **10** is ionic with a THF ligand coordinated to

the metal center. This was later unambiguously confirmed by X-ray crystal structure analysis (Fig. 2.2).

Brown crystals suitable for an X-ray crystal structure analysis were obtained from a THF/pentane solution. Selected structural parameters of complex **10** are summarized in Table 2.1.

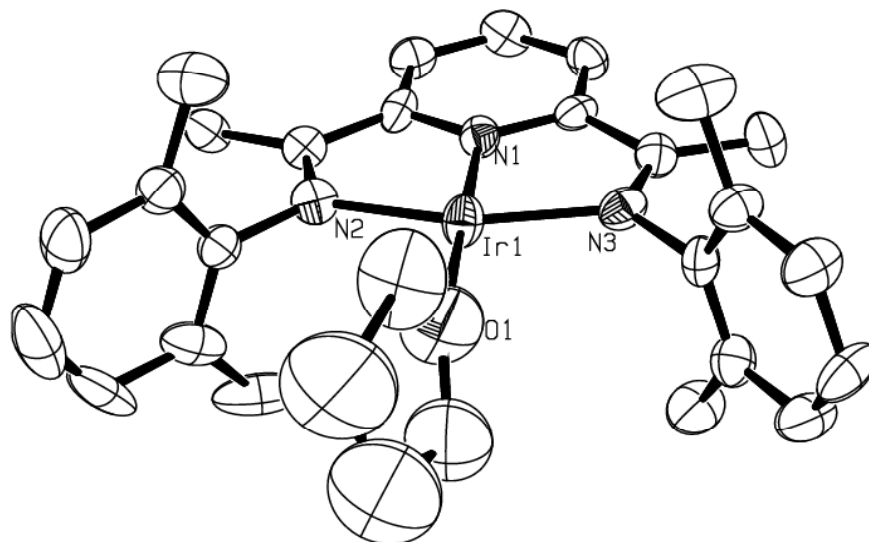


**Fig. 2.2** ORTEP plot of complex **10** with 50% thermal ellipsoids (triflate group and hydrogen atoms were omitted for clarity).

Table 2.1 Selected bond lengths [Å] and angles [°] for complex **10**.

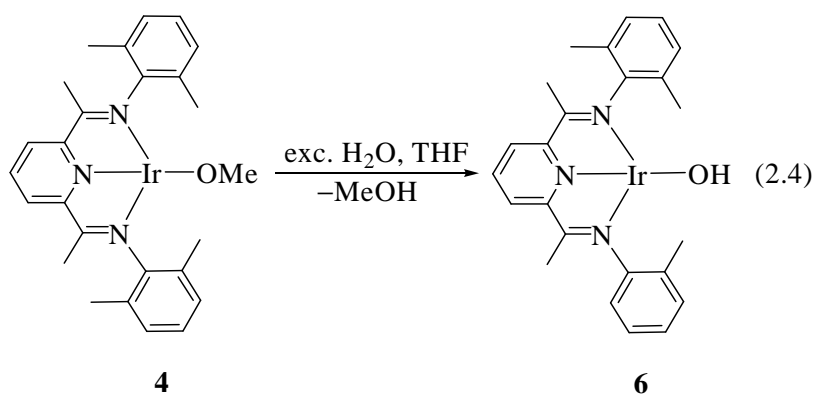
Ir1-N1	1.905(7)	Ir1-N2	1.999(7)	Ir1-N3	2.017(7)
Ir1-O1	2.102(8)				
N1-Ir1-N2	80.0(3)	N3-Ir1-N1	78.8(3)	N3-Ir1-N2	158.8(3)
N1-Ir1-O1	179.6(3)	N2-Ir1-O1	100.4(3)	N3-Ir1-O1	100.8(3)

The geometry around the Ir(I) center is essentially square planar with the sum of the bond angles equaling 359°. The fourth coordination site is occupied by a THF molecule displaying an Ir1-O1 distance of 2.102(8) Å, which indicates a strong interaction between the oxygen atom and the

positively charged metal center. Literature values for Ir-O distances are in the range of 2.025 – 2.339 Å.<sup>44, 49, 50</sup> The only crystal structure found in CCDC database, where a THF molecule is bound to iridium metal center, is [IrH<sub>2</sub>(THF)(H<sub>2</sub>O)(PPh<sub>3</sub>)<sub>2</sub>]SbF<sub>6</sub>·THF with the Ir-O distance 2.308(8) Å. In the latter the Ir-O bond is greatly elongated due to the trans influence of the hydride ligand.<sup>51</sup> The reactions of complex **10** will be discussed later in this chapter.

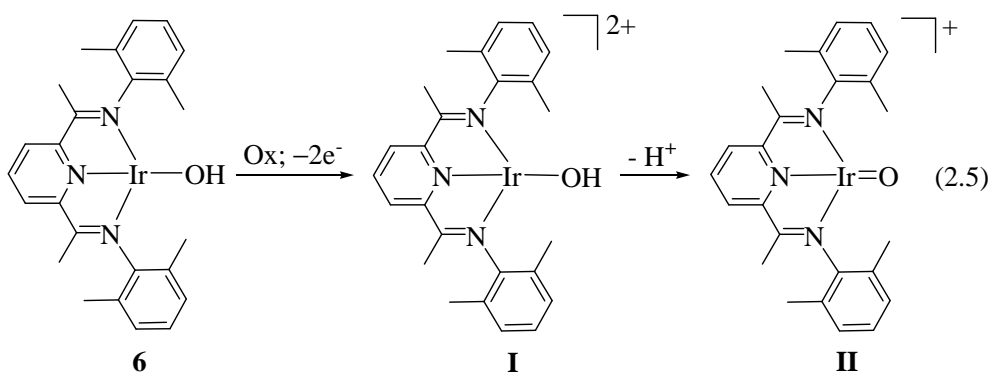
## 2.2 Oxidation of the Ir(I) hydroxo complex – unexpected results

The hydroxo complex **6** has been used as a starting material in a number of attempts to synthesize an oxo complex. It is obtained in 60 % yield from the methoxo complex **4** by the addition of excess degassed water (eq. 2.4).<sup>47</sup>



Complex **6** was fully characterized by <sup>1</sup>H, <sup>13</sup>C - NMR, IR spectroscopy and elemental analysis.

Synthetic access to oxo complexes was sought via oxidation of the readily available basic Ir(I) hydroxide complex **6** to the presumed corresponding acidic Ir(III) compound **I**, followed by deprotonation of **I** to give the desired oxo complex **II**\* (eq. 2.5).



\* Isolated and postulated complexes are labelled using arabic and roman numbers, respectively.

In order to have a better insight into the oxidation of complex **6**, cyclic voltammetry experiments were performed (Fig. 2.3).

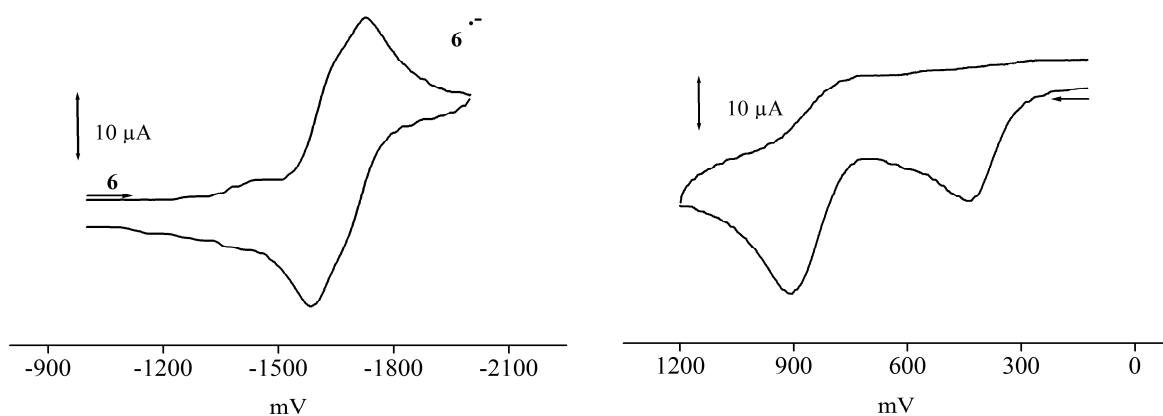


**Fig. 2.3** Cyclic voltammograms of complex **6** recorded in THF (working electrode, gold; reference electrode, Ag/Ag<sup>+</sup>; c[Bu<sub>4</sub>NPF<sub>6</sub>] = 0.4 M; scan rates = 400 mV (left) and 250 mV (right)).

The redox response for complex **6** is *quasireversible* with  $\Delta E_p = 152$  mV. The approximate redox potential of complex **6** is ca.  $-1.7$  V vs Cp<sub>2</sub>Fe<sup>+</sup>/Cp<sub>2</sub>Fe.

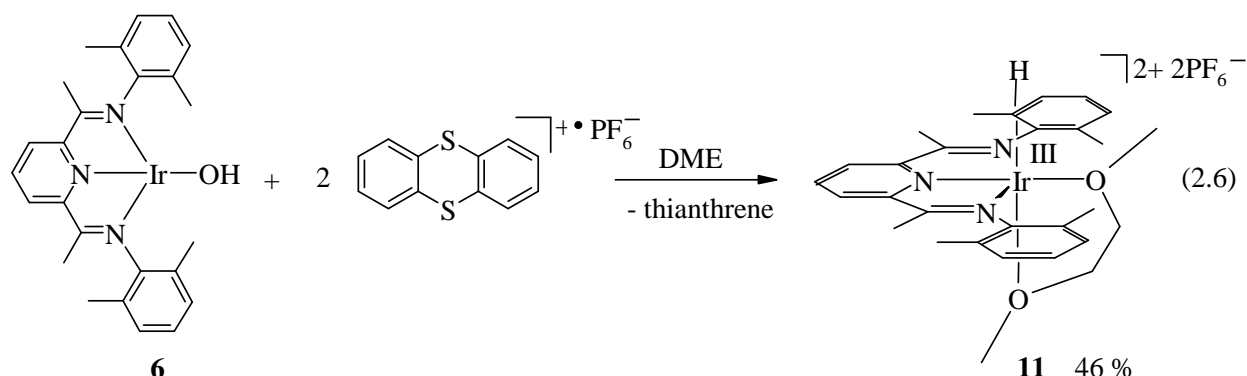
The oxidation process is *irreversible*. Two oxidation waves are observed with potentials of 0.44 and 0.91 V vs Cp<sub>2</sub>Fe<sup>+</sup>/Cp<sub>2</sub>Fe. It is presumed that the first oxidation wave at 0.44 V corresponds to the [Ir<sup>I</sup>(N<sub>3</sub>Me<sub>4</sub>)OH] / [Ir<sup>II</sup>(N<sub>3</sub>Me<sub>4</sub>)OH]<sup>+</sup> pair and the second wave at 0.91 V to the [Ir<sup>II</sup>(N<sub>3</sub>Me<sub>4</sub>)OH]<sup>+</sup> / [Ir<sup>III</sup>(N<sub>3</sub>Me<sub>4</sub>)OH]<sup>2+</sup> couple. However, it is not clear whether a simple E process (one electron transfer) or more complex mechanisms such as EC and ECE are involved in the oxidation of **6**.

In order to oxidize complex **6**, different oxidizing reagents such as [thianthrene]<sup>•+</sup>, [NO]<sup>+</sup>, [N-(C<sub>6</sub>H<sub>4</sub>Br-4)<sub>3</sub>]<sup>•+</sup>, [TEMPO]<sup>+</sup> with high formal potentials ( $E^\circ$ ) in the range from 0.7 – 1.0 V have been used. Each are classified as very strong oxidants.<sup>52</sup>

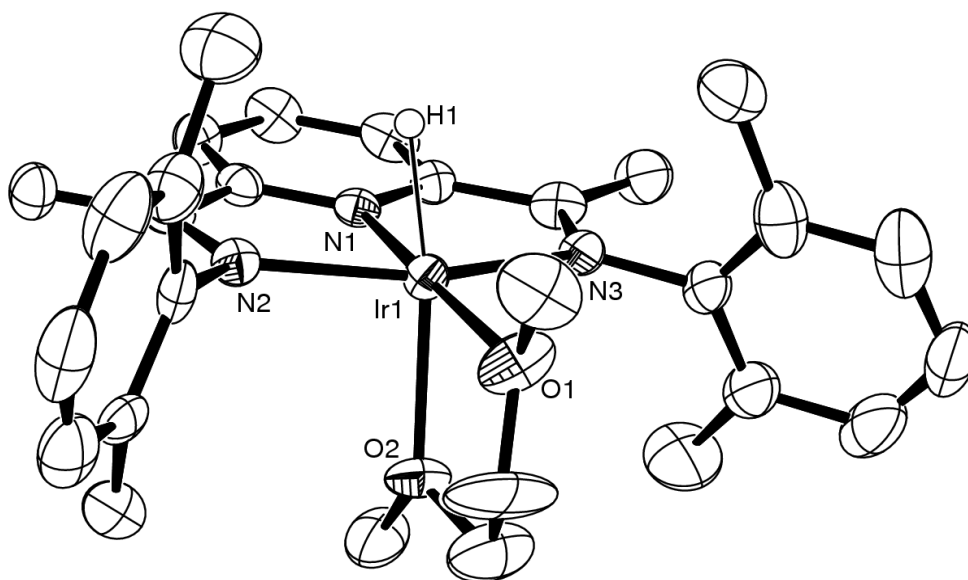
### 2.2.1 Oxidation with [thianthrene]<sup>•+</sup>

When the green solution of complex **6** in DME was added to a violet solution of the radical cation thianthrene<sup>•+</sup> in DME, the color changed to red. However, instead of the desired oxo

complex, a diamagnetic Ir(III) hydride complex **11**, with a molecule of DME coordinated to the metal center was obtained in 46 % of yield (eq. 2.6).



The product **11** was fully characterized by  $^1\text{H}$ ,  $^{13}\text{C}$  and  $^{19}\text{F}$ -NMR spectroscopy. The presence of the Ir-H moiety was confirmed by  $^1\text{H}$ -NMR spectroscopy (in  $\text{CD}_2\text{Cl}_2$ ) through a singlet peak at  $\delta = -32.5$  ppm. The DME ligand reveals four different sets of peaks (two singlets and two multiplets) in the aliphatic region. This is in agreement with the adopted essential  $C_s$  symmetrical environment found around the Ir metal center observed in X-ray crystal structure of **11**. Red crystals of **11** were obtained by layering a DME solution with pentane (Fig. 2.4). Selected bond lengths and angles of complex **11** were presented in Table 2.2.



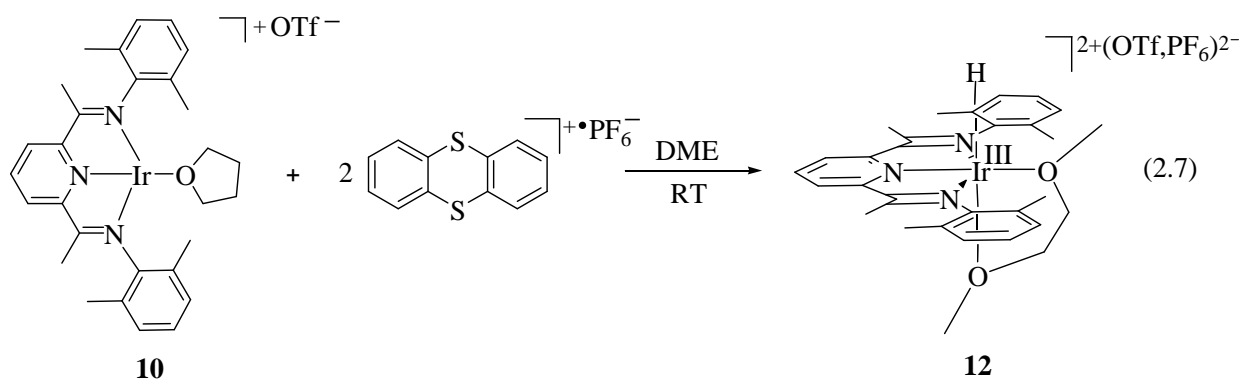
**Fig. 2.4** ORTEP plot of complex **11** with 50% probability thermal ellipsoids (the  $\text{PF}_6^-$  groups and H atoms except for the hydride ligand were omitted for clarity).

Table 2.2 Selected bond lengths [ $\text{\AA}$ ] and angles [ $^\circ$ ] for complex **11**.

Ir1-N1	2.058(4)	Ir1-N2	1.921(5)	Ir1-N3	2.061(5)
Ir1-O1	2.120(5)	Ir1-O2	2.263(5)	Ir1-H1	1.681(2)
N2-Ir1-N3	159.4(2)	N2-Ir1-N1	79.8(2)	N3-Ir1-N1	79.9(2)
O1-Ir1-O2	75.6(2)	N1-Ir1-O1	177.7(2)	N1-Ir1-O2	93.6(2)
N2-Ir1-O1	98.2(2)	N2-Ir1-O2	103.3(2)	N3-Ir-O1	102.2(9)
N3-Ir1-O2	93.8(2)				

The sum of angles of the equatorial ligands is  $359.8^\circ$  and of  $\text{N1-Ir1-O2} = 93.6(2)^\circ$  and  $\text{N2-Ir1-O2} = 103.3(2)^\circ$ . This shows that the geometry around the Ir(III) center is slightly distorted octahedral. The position of the hydride was located in the difference Fourier map and was isotropically refined. The Ir1-H1 distance of  $1.68 \text{ \AA}$  is in the expected range for Ir(III) hydrides ( $1.47 - 1.81 \text{ \AA}$ ).<sup>53, 54, 55</sup> As displayed in Figure 2.4, DME is coordinated to the metal center. The *trans* influence of the hydride is reflected in the elongation of the *trans* Ir1-O2 bond distance of  $2.263(5) \text{ \AA}$ , compared to the shorter equatorial Ir1-O1 bond distance of  $2.120(5) \text{ \AA}$ .

The origin of the hydride is still unclear, as well as the fate of the hydroxide ligand. Less likely, the hydride originates from the OH group, since the independent experiment presented in eq. 2.7 leads to the product **12**, which differs from **11** only in the counter ion.

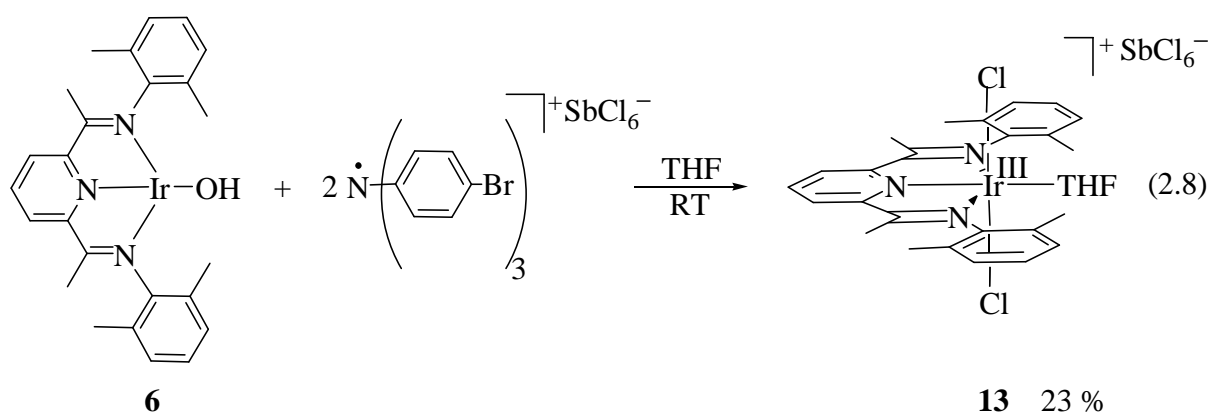


Comparing with the  $^1\text{H-NMR}$  spectrum of **11**, all proton signals except for the hydride peak display the same chemical shift. The hydride peak is slightly shifted ( $\delta = -32.6 \text{ ppm}$ ,

$\Delta\delta = 0.1$  ppm) presumably caused by the change of the counter ion. Until now, it is assumed that the hydride originates either from the glassware or the solvent.

### 2.2.2 Oxidation with “magic blue”

In another attempt to produce an iridium oxo complex, two equivalents of a different oxidizing agent, N-(p-bromophenyl)<sub>3</sub>SbCl<sub>6</sub>, which is also known as “magic blue” was added to complex **6**. After stirring for 2 h in THF, the color changed from green to brown. The reaction resulted in the formation of the unexpected dichloro iridium(III) complex **13** in 23% yield (eq. 2.8).



According to the <sup>1</sup>H-NMR spectrum, the diamagnetic complex **13** was formed, which was confirmed by an X-ray crystal structure analysis. Complex **13** displays C<sub>2v</sub> symmetry in the solution, as confirmed by the observation of two singlet peaks assigned to the methyl groups of the phenyl rings and the ketimine methyl group with the integration ratio 2:1. The peaks from coordinated THF in THF-d<sub>8</sub> are found at  $\delta = 1.58$  and 3.36 ppm, indicating slow exchange on the NMR time scale at 200 MHz as expected for a d<sup>6</sup> configured octahedral complexes.

The ORTEP plot of complex **13** is displayed in Fig. 2.5 and the corresponding data with selected distances are listed in Table 2.3.

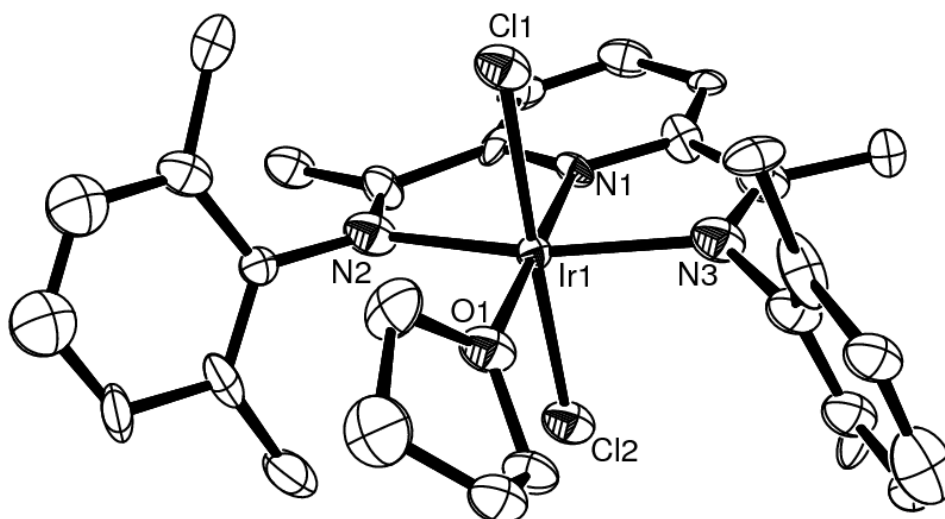


**Fig. 2.5** ORTEP plot of complex **13** with 50% probability thermal ellipsoids (the  $\text{SbCl}_6^-$  group and hydrogen atoms were omitted for clarity).

Table 2.3 Selected bond lengths [Å] and angles [°] for complex **13**.

Ir1-N1	1.934(9)	Ir1-N2	2.098(9)	Ir1-N3	2.092(9)
Ir1-Cl1	2.347(3)	Ir1-Cl2	2.339(3)	Ir1-O1	2.121(9)
N1-Ir1-N2	80.1(4)	N1-Ir1-N3	79.8(4)	N2-Ir1-N3	159.8(3)
Cl1-Ir1-Cl2	177.7(1)	O1-Ir1-Cl1	90.9(4)	O1-Ir1-Cl2	91.1(4)
N1-Ir1-O1	179.0(2)	N2-Ir1-O1	100.7(4)	N3-Ir1-O1	99.5(4)
N1-Ir1-Cl1	88.5(4)	N2-Ir1-Cl1	88.9(3)	N3-Ir1-Cl1	91.8(3)
N1-Ir1-Cl2	89.4(4)	N2-Ir1-Cl2	91.7(3)	N3-Ir1-Cl2	86.9(3)

The geometry at the Ir(III) center is slightly distorted octahedral. This is confirmed by the sum of angles for the equatorially coordinated ligands which is  $360^\circ$  and the angles:  $\text{N1-Ir1-Cl1} = 88.5(4)^\circ$ , and  $\text{N2-Ir1-Cl1} = 88.9(3)^\circ$ . The two chloro ligands are positioned *trans* to each other with an angle,  $\text{Cl1-Ir1-Cl2}$ , of  $177.7(1)^\circ$ . The iridium chloro distances  $\text{Ir1-Cl1} = 2.347(3) \text{ \AA}$  and  $\text{Ir1-Cl2} = 2.339(3) \text{ \AA}$  are in good agreement with typical Ir-Cl distances ( $2.35 \text{ \AA}$ ) reported in the literature for octahedral Ir(III) complexes.<sup>56, 57</sup> The fourth

equatorial site is occupied by THF molecule displaying Ir-O1 distance 2.121(9) Å, slightly longer than Ir-O distance in complex **10** (2.102(8) Å). The THF ring is coordinated to the Ir center in a chair conformation as opposed to [Rh(NCN)(THF)Cl<sub>2</sub>] where the THF ring has a tilted coordination.<sup>58</sup>

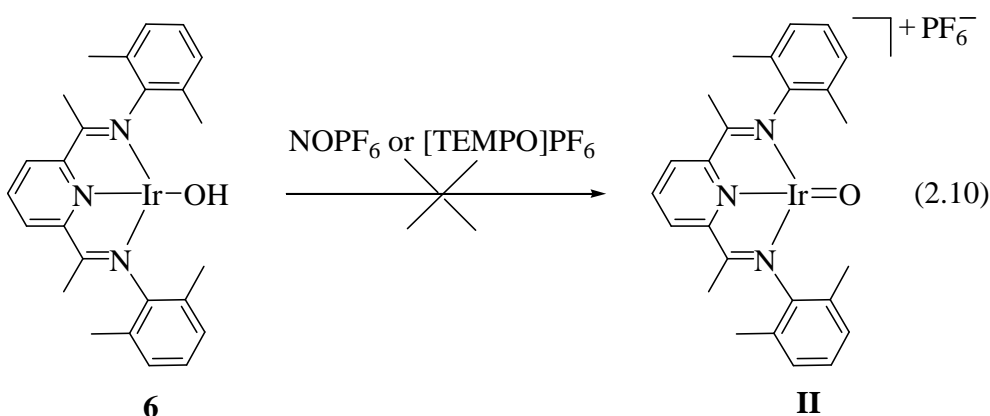
### *The source of the chloro ligand*

It appears that [SbCl<sub>6</sub>]<sup>-</sup> is not always innocent. It can as well be an oxidant and undergo dissociation (reduction) to [SbCl<sub>4</sub>]<sup>-</sup> and 2 Cl<sup>-</sup> (eq. 2.9).<sup>52</sup>



Two chloro ligands in complex **13** presumably originate from the reaction according to equation 2.9. Similar chloride transfer was previously reported in the literature. Using N-(p-bromophenyl)<sub>3</sub>SbCl<sub>6</sub> in the oxidation of [Fe<sub>2</sub>(μ-CO)<sub>2</sub>(CO)<sub>2</sub>Cp<sub>2</sub>] the undesired chloro complex [FeCl(CO)<sub>2</sub>Cp] was formed<sup>59</sup> and the oxidation of [Mn(CO)(dppe)Cp\*] gave [MnCl(CO)(dppe)Cp\*]<sup>+</sup>.<sup>60</sup>

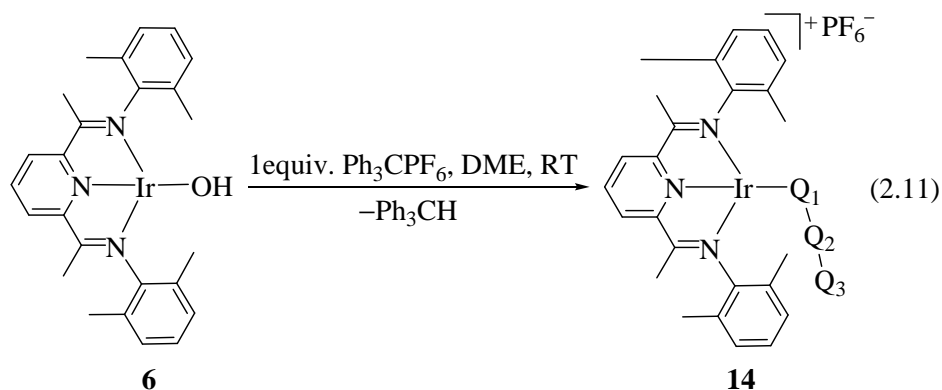
The oxidation reaction of complex **6** with [TEMPO]PF<sub>6</sub> and [NO]<sup>+</sup>PF<sub>6</sub><sup>-</sup> was also attempted. However, it did not succeed owing to their low solubility in the non-polar solvents (eq. 2.10). Due to problems with polymerization of the solvent, THF could not be used.



According to Conelly and Geiger,<sup>52</sup> nitrosonium salts are soluble in CH<sub>3</sub>CN, but react with solvents such as diethyl ether, acetone, and alcohols. Hence, based on our experience acetonitrile would interfere with the reaction and possibly coordinate to the metal center.

### 2.2.3 Hydride abstraction with a trityl cation

The hydride abstraction with trityl ( $\text{Ph}_3\text{CPF}_6$ )<sup>61</sup> from complex **6** was another anticipated method to access the desired Ir(III) oxo complex. Upon addition of a solution of complex **6** in DME to solid trityl-hexafluorophosphate, a color change from green to red was observed (eq. 2.11).

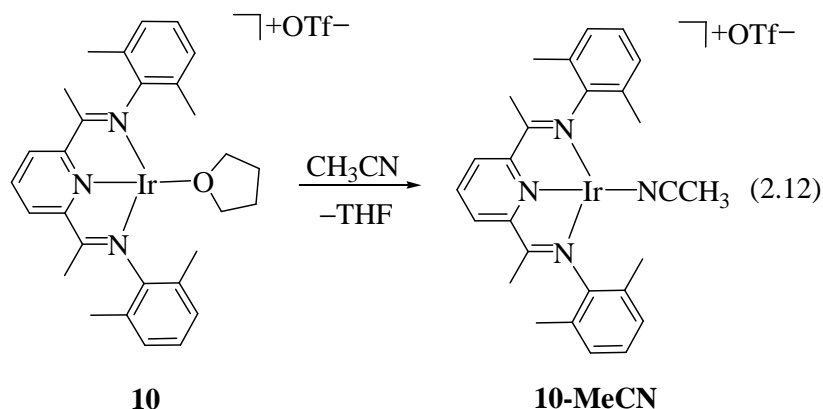


The  $^1\text{H-NMR}$  spectrum of the pentane extraction of the reaction mixture revealed a singlet resonance at  $\delta = 5.40$  ppm in  $\text{C}_6\text{D}_6$ , which corresponds to triphenylmethane. The  $^1\text{H-NMR}$  of the residual product in  $\text{THF-d}_8$  appears to be diamagnetic with sharp peaks in the aliphatic (singlets at  $\delta = 0.92$ , 1.83 and 1.89 ppm with 1:1:1 integration ratio) and aromatic region (multiplet at  $\delta = 6.84$ , doublet at  $\delta = 7.37$  and triplet at  $\delta = 7.7$  ppm).

The IR spectrum of **14** shows a sharp, medium intensity peak at  $1967\text{ cm}^{-1}$ .

An electrospray mass spectrum of complex **14** (ESI-MS +ve ion mode) was recorded and revealed a single peak at  $603.2\text{ m/z}$ . This mass matches the complex with a coordinated acetonitrile ligand. The latter could originate from the atmosphere of the glovebox.

In order to provide more evidence for acetonitrile coordination, an independent experiment was performed. Upon addition of  $\text{CH}_3\text{CN}$  to complex **10**, the reddish brown acetonitrile complex **10-MeCN** was formed in a quantitative yield (eq. 2.12).



The  $^1\text{H-NMR}$  spectrum of **10-MeCN** in  $\text{THF-d}_8$  revealed a new resonance at  $\delta = 1.77$  ppm, which was assigned to the coordinated acetonitrile. The integration ratio of the observed peaks for the methyl groups (on the phenyl ring, diimine and acetonitrile) is 4:2:1. The stretching  $\nu_{\text{CN}}$  frequency of the coordinated acetonitrile ligand in complex **10-MeCN** was found at  $\nu_{\text{CN}} = 2294 \text{ cm}^{-1}$  (non-coordinated  $\text{CH}_3\text{CN}$ ;  $\nu_{\text{CN}} = 2250 \text{ cm}^{-1}$ ).

Upon dissolving the obtained crystals of complex **14** in  $\text{THF-d}_8$  and transferring the volatiles, a singlet peak at  $\delta = 2.47$  ppm in  $^1\text{H-NMR}$  spectrum was observed\*. It was later discovered that the water resonance in  $\text{THF-d}_8$  appears at essentially the same chemical shift ( $\delta = 2.48$  ppm). The same peak was observed when  $\text{PPNCl}$  was added to complex **14** and volatiles were transferred. The  $^1\text{H-NMR}$  of the residual compound confirmed the formation of **2**.

Compound **14** can be reproduced and several X-ray crystal analyses have been undertaken. Red crystals were obtained from DME/pentane solution at  $-35$  °C. The X-ray crystal structure analysis suggested a linear, possibly three-atom ligand, Q1-Q2-Q3. The residual electron density (Q1-Q2-Q3) as shown in Figure 2.6 is so far unresolved. The full pyridine-diimine ligand could be anisotropically refined and the R-values ( $I > 2\sigma(I)$ ) for the complete molecule are  $R1 = 0.0383$ ,  $wR2 = 0.0843$ . The distances between Ir-N1 are  $1.967(7) \text{ \AA}$  and Ir-N2 are  $2.036(4) \text{ \AA}$ .

\* The acetonitrile resonance in  $\text{THF-d}_8$  displays a singlet peak at  $\delta = 1.95$  ppm in  $^1\text{H-NMR}$  spectrum.

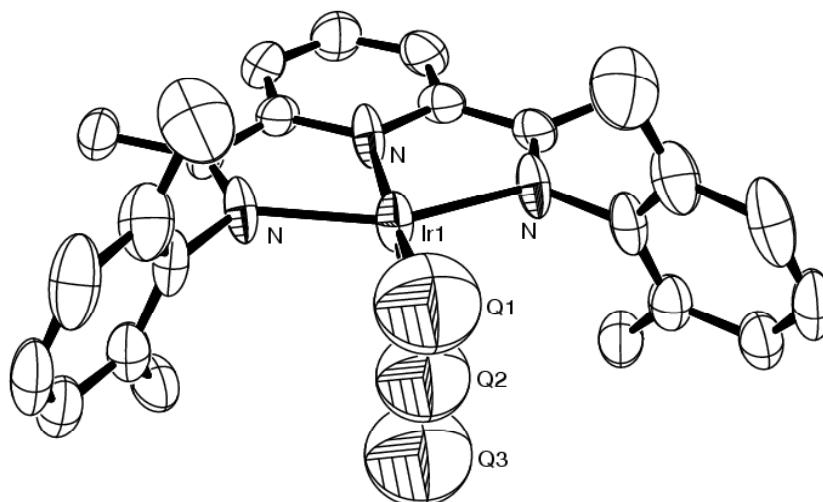


**Fig. 2.6** ORTEP plot of complex **14** (Q1, Q2 and Q3 represent unresolved residual electron densities found in the difference Fourier map).

According to the literature, acetonitrile is mostly coordinated in the linear rather than bent fashion, due to increased overlap between the N donor and the metal center. However, there are also examples for the group 6 transition metals, where acetonitrile is coordinated to the metal center in  $\eta^2$ -fashion.<sup>62</sup>

In order to address this point, DFT calculations (B3LYP hybrid, LACVP\*\* basis set) for the model complex **14a** and **14b** have been performed (Fig. 2.7).

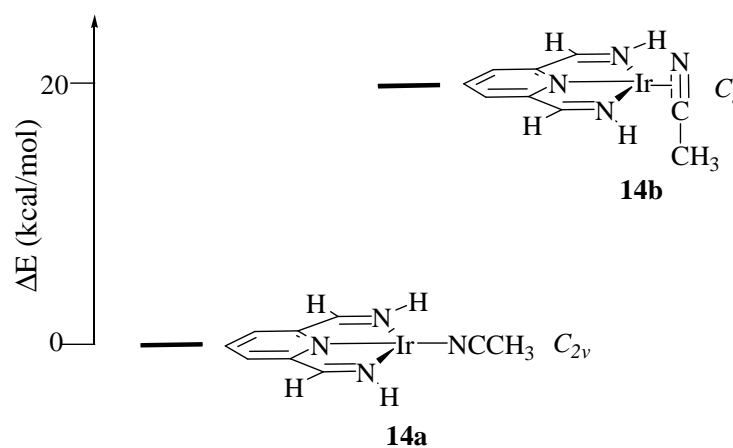


**Fig. 2.7** Energy diagram for the optimized structures **14a**, **b**.

As displayed in Fig. 2.7, complex **14a** is 20 kcal/mol lower in energy than the  $\eta^2$  analogue **14b**. During the optimization of structure **14b**, the angle N-Ir-C was constrained. When constraints are released, **14b** relaxes to **14a**.

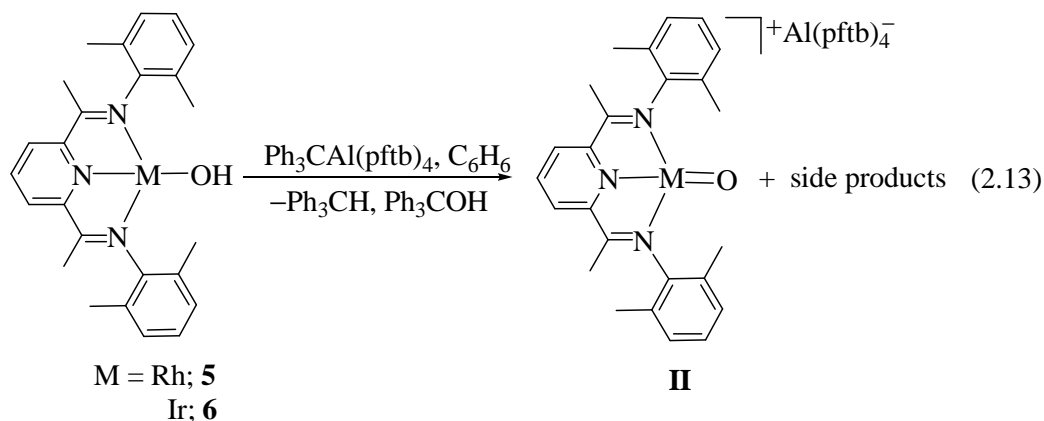
Comparing and summarizing all the results related to reaction according to eq. 2.11 allows us to exclude the coordination of acetonitrile.

Unfortunately, until now it has not been possible to establish the nature of the ligand that resides in the fourth coordination site in complex **14**.

Due to the disorder observed in the  $\text{PF}_6^-$  anion (not shown in Fig. 2.6) in the crystal structure of complex **14** and aforementioned refinement, it was decided to exchange the  $\text{PF}_6^-$  counter ion of the trityl cation with a more bulky perfluorinated alkoxyaluminate anion.<sup>63, 64</sup>

Unfortunately, the experiment could not be performed applying the same conditions as in eq. 2.11 using DME as solvent. The trityl-Al(pftb)<sub>4</sub> reacts with DME very fast giving a violet-blue solution of unknown products. Therefore, benzene was used as solvent.

When complexes **5** or **6** were dissolved in benzene and added to  $\text{Ph}_3\text{CAI}(\text{pftb})_4$  the color changed from green to reddish brown. Pentane extraction of the reaction mixture contained a 1:1 mixture of  $\text{Ph}_3\text{CH}$  ( $\delta = 5.40$  ppm) and  $\text{Ph}_3\text{COH}$  ( $\delta = 2.67$  ppm) according to the <sup>1</sup>H-NMR in  $\text{C}_6\text{D}_6$  (eq. 2.13).



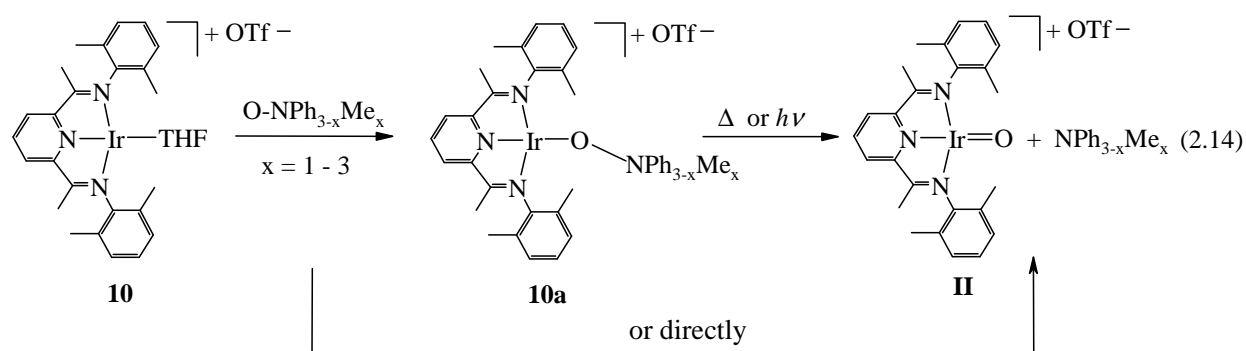
The <sup>1</sup>H-NMR spectrum of **II** in THF-d<sub>8</sub> revealed that a mixture of at least three different products was formed (three sets of triplet and doublet peaks at different chemical shifts were

observed in the aromatic region). The mixture could not be separated by either extraction or by precipitation due to comparative solubilities.

## 2.3 Ir(I) triflate as a precursor for an oxo complex

### 2.3.1 Reactions with amine N-oxides

Based on the previous investigations by our group,<sup>28, 47</sup> a straight forward route to Ir-oxo complex **II** from Ir(I) triflate **10** and amine N-oxides has been suggested (eq. 2.14). The proposed mechanism, supported by kinetics will be discussed later in more details.



Upon the addition of a solution of  $\text{Ph}_2\text{MeNO}$  or  $\text{PhMe}_2\text{NO}$  in THF to complex **10**, the corresponding amine  $\text{Ph}_2\text{MeN}$  or  $\text{PhMe}_2\text{N}$  were formed, as confirmed by  $^1\text{H-NMR}$  spectroscopy in  $\text{THF-d}_8$  ( $\text{Ph}_2\text{MeN}$ :  $\delta = 3.28$  (s, 3 H, Me), 6.88 (tt, 2 H,  $\text{CH}_{\text{arom}}$ ), 6.98 (dd, 4 H,  $\text{CH}_{\text{arom}}$ ), 7.20 (tt, 4 H,  $\text{CH}_{\text{arom}}$ );  $\text{PhMe}_2\text{N}$ :  $\delta = 2.86$  (s, 6 H, Me), 6.56 (tt, 1 H,  $\text{CH}_{\text{arom}}$ ), 6.66 (dd, 2 H,  $\text{CH}_{\text{arom}}$ ), 7.10 (tt, 2 H,  $\text{CH}_{\text{arom}}$ ). Unfortunately, the expected “Ir-oxo” complex **II** precipitated from solution as a dark brown solid.

The IR spectrum of the precipitate in Nujol revealed a sharp, medium intensity band at  $723 \text{ cm}^{-1}$ , which can be tentatively assigned to Ir=O stretching frequency (*note*: this band was observed after subtracting the spectrum of precipitate in Nujol and Nujol\*). The only Ir-oxo complex in the literature by Wilkinson et al. reported that Ir=O band was found at  $802 \text{ cm}^{-1}$  (in Nujol) for the related  $\text{Ir(V)}(\text{mes})_3(\text{O})$  complex.<sup>31</sup>

\* Nujol absorption bands were found at  $\nu = 2924$  (vs), 1462 (s), 1384 (s), 726 (vw)  $\text{cm}^{-1}$ .

The reaction according to eq. 2.14 was also monitored by UV-Vis spectroscopy at room temperature during a period of 3 hours. The spectrum displayed in Figure 2.8 was observed.

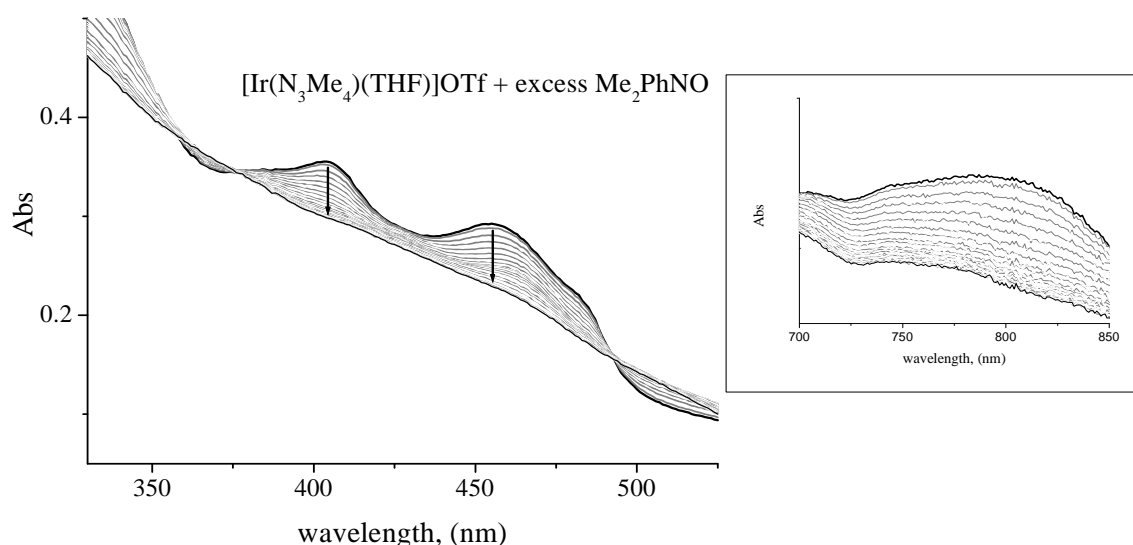
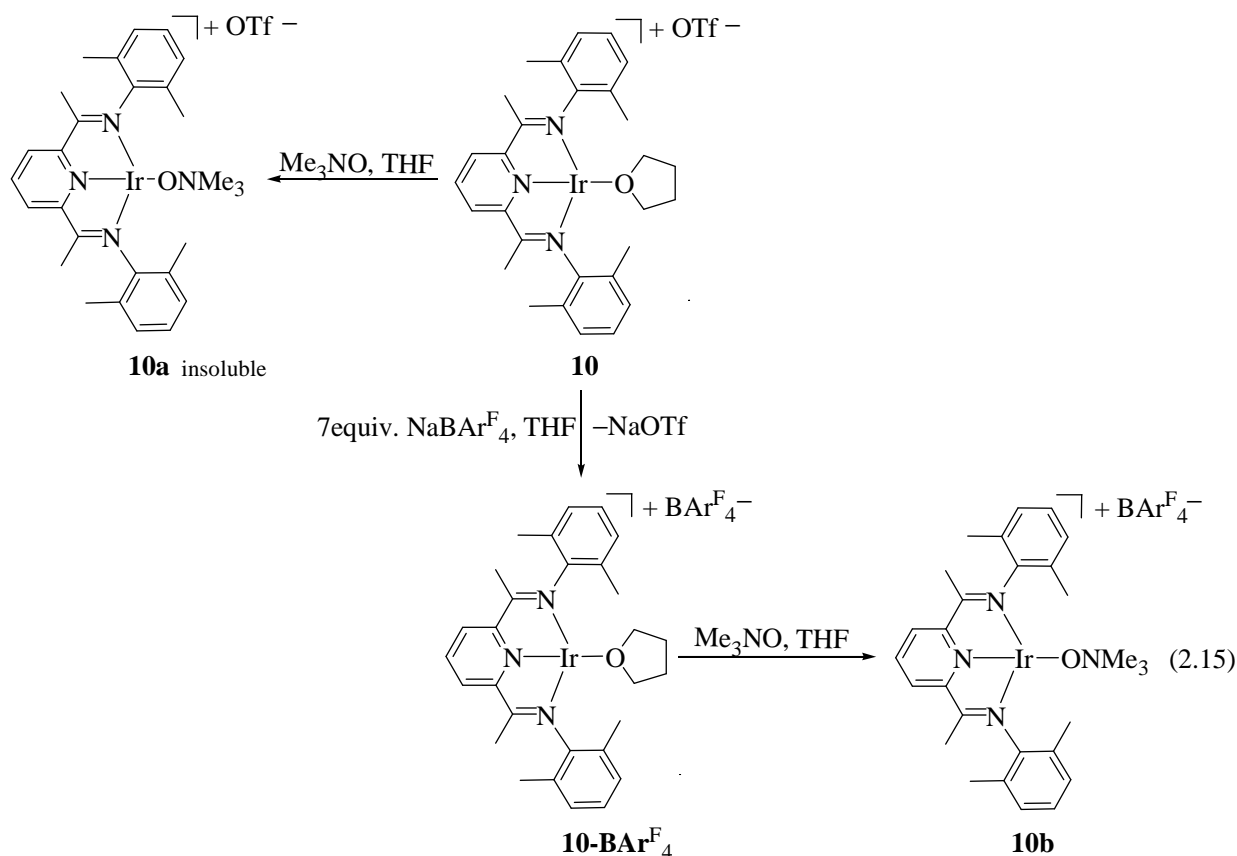


**Fig. 2.8** Isobestic points for the reaction of complex **10** and excess of Me<sub>2</sub>PhNO (left); decay of the absorbance at 800 nm (right).

The decay of the absorption bands at 404 and 455 nm corresponds to the decrease in the concentration of complex **10**. As displayed in Fig. 2.8, there are three isobestic points at 357, 376 and 490 nm. The absorption, which has been tentatively assigned to a d-d transition at 800 nm decreases also with time.

The reaction is suggested to proceed via substitution of the THF ligand by the amine N-oxide group and formation of Ir-ONPh<sub>3-x</sub>Me<sub>x</sub> intermediate **10a**. The latter dissociates to an Ir=O complex and a free amine (see eq. 2.14). This proposed mechanism is supported by the previous isolation of [Rh(N<sub>3</sub>Me<sub>4</sub>)ONMe<sub>3</sub>]OTf which was fully characterized and the crystal structure was determined.<sup>47</sup>

In order to obtain an Ir analogue, the similar reaction between complex **10** and Me<sub>3</sub>NO has been performed (eq. 2.15). However, due to the low solubility of the obtained complex **10a**, the same reaction with Me<sub>3</sub>NO after anion exchange of OTf with BAR<sup>F</sup><sub>4</sub> was attempted. Upon addition of Me<sub>3</sub>NO to a THF solution of complex **10-BAR<sup>F</sup><sub>4</sub>**, the color changed from brown to green and complex **10b** was formed.



The coordination of  $\text{Me}_3\text{NO}$  to the Ir center is confirmed by  $^1\text{H-NMR}$  spectroscopy, revealing a singlet peak at  $\delta = 2.45$  ppm (in  $\text{THF-d}_8$ ). This peak is considerably shifted in comparison to free  $\text{Me}_3\text{NO}$ , which reveals a singlet peak at  $\delta = 3.06$  ppm. The integration ratio of the methyl groups on the N-oxide, phenyl rings and diimine ligand is 3:4:2. Unfortunately, the crystals obtained were not of suitable quality for an X-ray structure analysis.

Photolytic studies (using a mercury medium-pressure lamp 125HPKW, shielded by a Quartz jacket water cooling mantle and  $\text{K}_2\text{CrO}_4$  or  $\text{H}_2\text{O}$  UV-Vis cutoff filters) were performed on complex **10b** in order to cleave the N-O bond and therefore obtain an oxo complex. The photolysis reaction was done in a Young's NMR tube in  $\text{THF-d}_8$ . Unfortunately, an insoluble black precipitate was formed. However, the  $^1\text{H-NMR}$  spectrum of the supernatant revealed a singlet peak at  $\delta = 2.1$  ppm assigned to free trimethylamine. The fate of the oxygen from  $\text{Me}_3\text{NO}$  is unclear.

There are a few structurally characterized transition-metal complexes with  $\text{Me}_3\text{NO}$  as a ligand in the literature. Examples involve the octahedral rhenium dinuclear complex  $[(\mu\text{-H})\text{Re}_2(\text{CO})_7(\mu\text{-NC}_5\text{H}_4)(\text{Me}_3\text{NO})]^{65}$ , tetrahedral  $[\text{Co}(\text{ONMe}_3)]\text{I}_2^{66}$  and pseudo tetrahedral

[Cu(Me<sub>2</sub>CNOCO)(ONMe<sub>3</sub>)<sub>2</sub>].<sup>67</sup> Further, Herrmann et al.<sup>68</sup> reported the formation of an air stable trinuclear Rh μ<sup>3</sup>-oxo complex [(Cp\*Rh)<sub>3</sub>(μ-CO)(μ-O)] in the reaction of Me<sub>3</sub>NO and Cp\*Rh(CO)<sub>2</sub>. If we address the reaction according to eq. 2.14 as a deoxygenation of an amine N-oxides to amines, there are examples where Cp<sub>2</sub>TiCl<sub>2</sub>/In or FeCl<sub>3</sub>·6H<sub>2</sub>O/In convert the N-oxide into the corresponding amines under ultrasonication.<sup>69, 70</sup> This process is also well known in the catalytic cycle of enzymes such as trimethylamine-N-oxide reductase where the active site is Mo(IV) metal center.<sup>71</sup>

As already established by DFT calculations,<sup>28</sup> for the model compound, the formation of the Ir-oxo complex **II** is expected to be thermodynamically more favorable for amine N-oxide of the type O-NPh<sub>3-x</sub>Me<sub>x</sub> with a larger number of phenyl groups (Fig. 2.9).

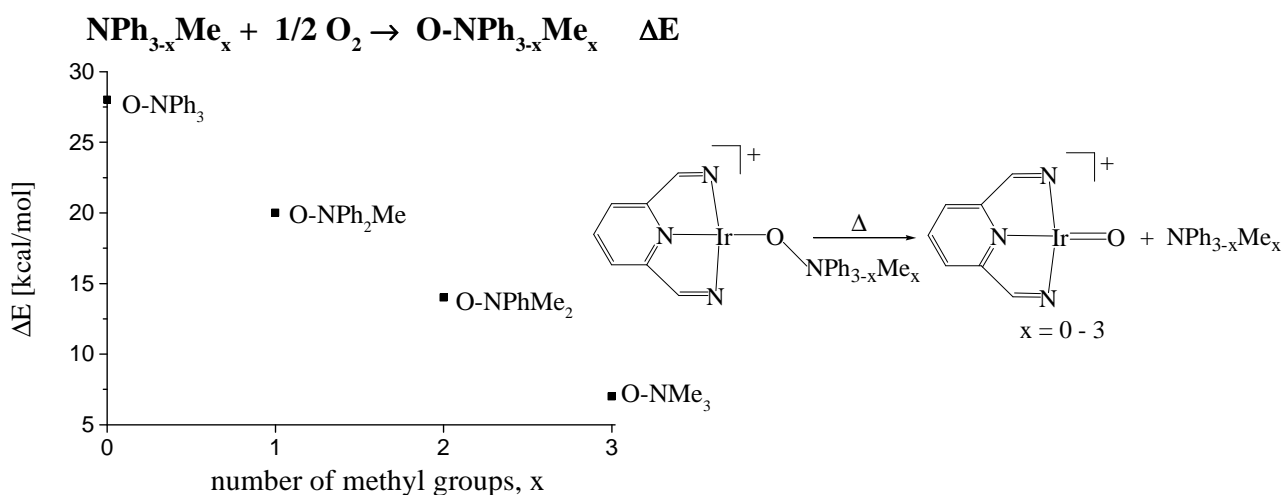
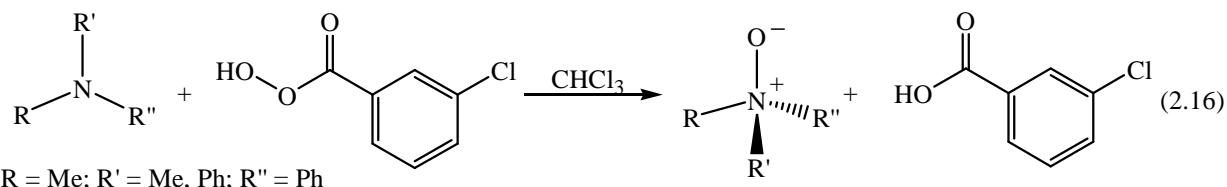


**Fig. 2.9** Energy diagram for the N-O bond strength in O-NPh<sub>3-x</sub>Me<sub>x</sub> based on DFT (BP86/TZVP) calculations.

As shown in Figure 2.9, there is a nearly linear trend observed for the N-O bond strength in O-NPh<sub>3-x</sub>Me<sub>x</sub> vs. number of methyl groups. When all methyl groups are substituted with phenyl groups, N-O bond is weakened by 22 kcal/mol.

To establish whether the N-O bond length changes by increasing the number of phenyl groups (as might be expected according to the calculations), Me<sub>2</sub>PhNO and MePh<sub>2</sub>NO were synthesized. The N-oxides (Me<sub>2</sub>PhNO or MePh<sub>2</sub>NO) were prepared according to the literature by using a tertiary N-amine and *m*-chloroperbenzoic acid<sup>72</sup> in 70 % yield and high purity (eq. 2.16).



Colorless crystals of Me<sub>2</sub>PhNO and MePh<sub>2</sub>NO suitable for X-ray structure analyses were obtained from concentrated acetone/pentane solutions. The crystal structures and the selected bond distances are presented in Figure 2.10a, b and Table 2.4.

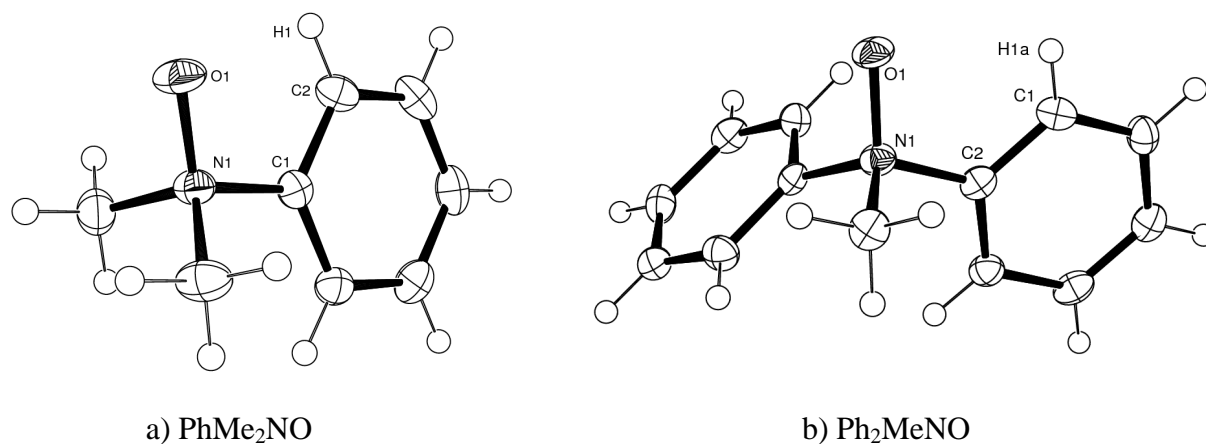


**Fig. 2.10** ORTEP plot of tertiary amine N-oxide at the 50% probability level.

Table 2.4 Selected bond lengths [Å] and angles [°] for **PhMe<sub>2</sub>NO** and **Ph<sub>2</sub>MeNO**.

O1-N1	1.388(1)	C1-N1	1.500(1)	O1...H1	2.345
O1-N1-C1	111.2(1)	N1-C1-C2	118.5(1)		
O1-N1-C1-C2	17.4				
O1-N1	1.401(4)	N1-C1	1.501(1)	O1...H1a	2.314
O1-N1-C2	109.6(3)	N1-C1-C2	117.5(4)		
O1-N1-C2-C1	13.7				

Both N-oxides crystallize in the orthorhombic crystal system. PhMe<sub>2</sub>NO crystallizes in the Pbc<sub>a</sub> (Z = 8) space group, whilst Ph<sub>2</sub>MeNO crystallizes in the Pna2<sub>1</sub> space group (Z = 8) with two

independent molecules in the asymmetric unit. They display a pseudo tetrahedral geometry around the N atom with average O-N-C bond angle of  $109.6^\circ$  for PhMe<sub>2</sub>NO and  $109.0^\circ$  for Ph<sub>2</sub>MeNO. The N-O distances, 1.388 Å for Me<sub>3</sub>NO,<sup>73</sup> 1.388(1) Å for PhMe<sub>2</sub>NO and 1.401(4) Å for Ph<sub>2</sub>MeNO do not differ significantly, when one methyl group is replaced with phenyl group.

The dihedral angle O1-N1-C1-C2, which is  $17.4^\circ$  for PhMe<sub>2</sub>NO and  $13.7^\circ$  for Ph<sub>2</sub>MeNO is of particular interest since it suggested C-H-O hydrogen bonding. In order to address this point, DFT calculations were performed. In this case, the recently published X3LYP hybrid functional and 6G-311G\*\*<sup>++</sup> basis set was used to describe hydrogen bonding and Van-der-Waals interactions.<sup>74</sup> According to the calculations, the minimum energy corresponds to the structure with the dihedral angle O-N-C-C =  $0^\circ$  (Fig. 2.11). Increasing the dihedral angle from 0– $90^\circ$ , the energy rises and the maximum is reached when the angle is  $90^\circ$ .

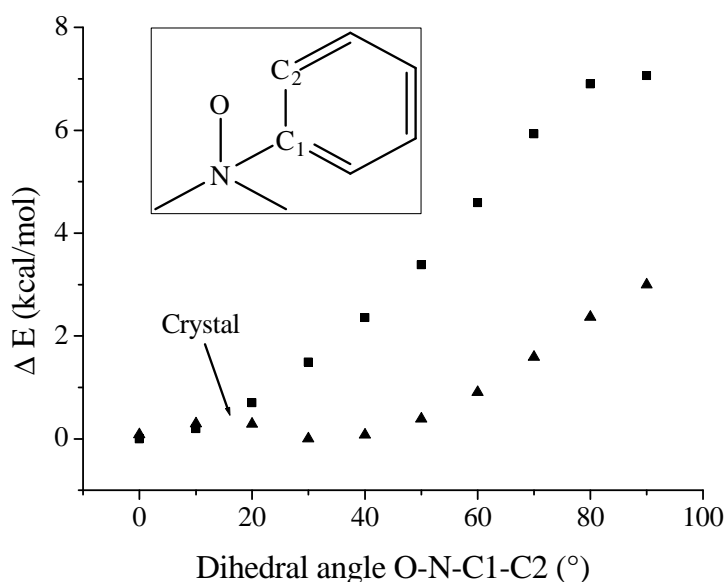


**Fig. 2.11** Energy diagram of PhMe<sub>2</sub>NO (■) and Ph<sub>2</sub>MeNO (▲) based on the change of the dihedral angle O-N-C1-C2 from 0– $90^\circ$ .

The calculated energy difference between the optimized and the crystal structure is approximately 0.5 kcal/mol for both N-oxides. A likely explanation for this observed difference is the additional *intramolecular* and *intermolecular* (calculated above) hydrogen bonding observed in the crystal packing (Fig. 2.12).

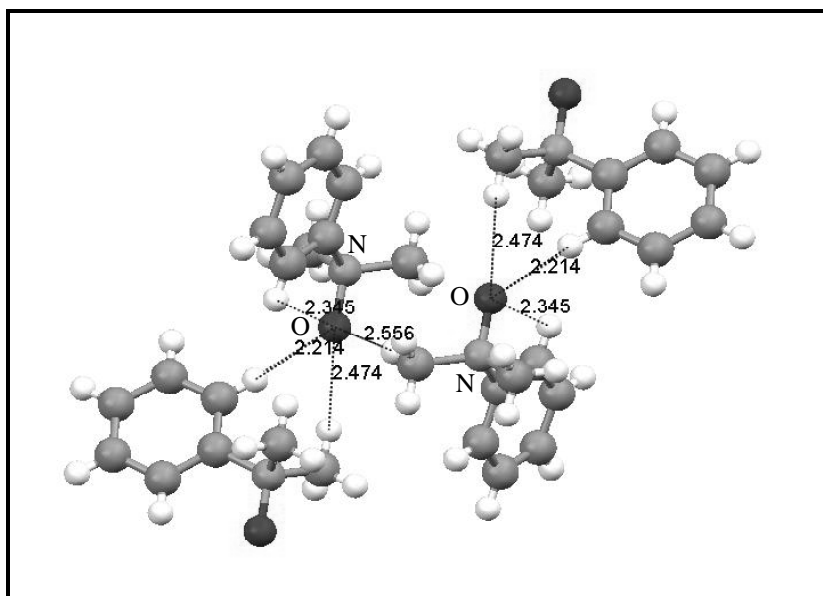


**Fig. 2.12** *Intramolecular and intermolecular CHO hydrogen bonding in Me<sub>2</sub>PhNO.*

The positions of all hydrogen atoms were located in the difference Fourier map and refined isotropically. *Note:* All C-H distances were averaged to 0.96 Å.

Non-linear *intramolecular* hydrogen bonding is apparent between O1...H1-C1 with the bond distance O1-H1 = 2.345 Å for PhMe<sub>2</sub>NO (O1-H1a = 2.314 Å for Ph<sub>2</sub>MeNO). The C1-H1...O1 angle is 102°, which is the lower limit for what can be accepted as bent hydrogen bonding according to the classification of Desiraju.<sup>75</sup> An example of hydrogen bonding with a small angle (116°) is reported for the case of methoxy substituted cyclopenta[a]phenantrenes.<sup>76</sup> *Intermolecular* CH...O hydrogen bonding, depicted in Figure 2.12, with the distances from 2.2 – 2.6 Å and an average angle from 170°, is classified as a strong CH...O hydrogen bond.<sup>75</sup>

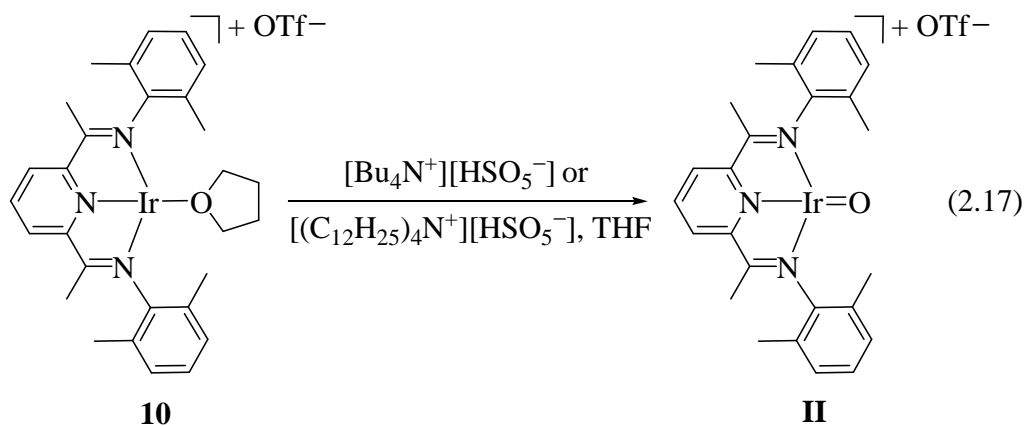
With respect to equation 2.14, the deoxygenation reaction of PhMe<sub>2</sub>NO and Ph<sub>2</sub>MeNO to the corresponding free amines under mild conditions with complex **10** is observed. However, the fate of the oxygen atom is still unclear due to the low solubility of the obtained compound.

### 2.3.2 Reaction with TBA-Oxone

“Oxone”, i.e. monopersulfate tetrabutylammonium salt has been used as an oxidant (for example it oxidizes sulfides to sulfones)<sup>77</sup> and as an efficient single oxygen transfer reagent. It contains an unsymmetrical O-O bond that can be heterolytically cleaved with various transition metal

complexes.<sup>78, 79</sup> It is also used in the asymmetric epoxidation of alkenes with Mn(III)-salen complexes as a cocatalyst.<sup>80</sup>

The direct conversion of complex **10** to the oxo complex **II** with tetrabutylammonium monopersulfate ( $\text{Bu}_4\text{NHSO}_5$ ) or for increased solubility with dodecylammonium monopersulfate ( $(\text{C}_{12}\text{H}_{25})_4\text{NHSO}_5$ ), was attempted (eq. 2.17).

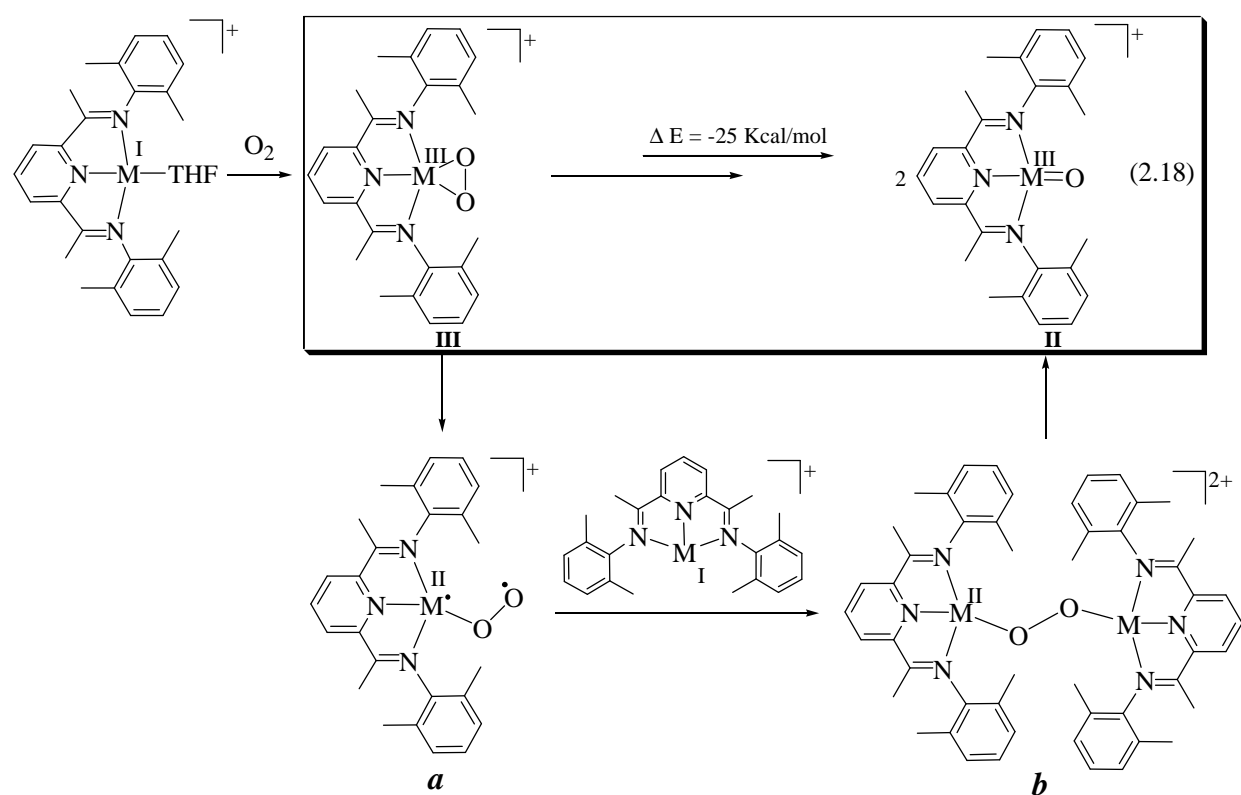


Unfortunately, complete characterization of the obtained compound was not possible due to its low solubility. The solubility can be improved by changing the anion with more sterically demanding group. Alternatively, the methyl groups located on the phenyl rings could be exchanged by *tert*-butyl groups. Both suggestions are left for future work.

## 2.4 Rh, Ir(III) peroxo complexes

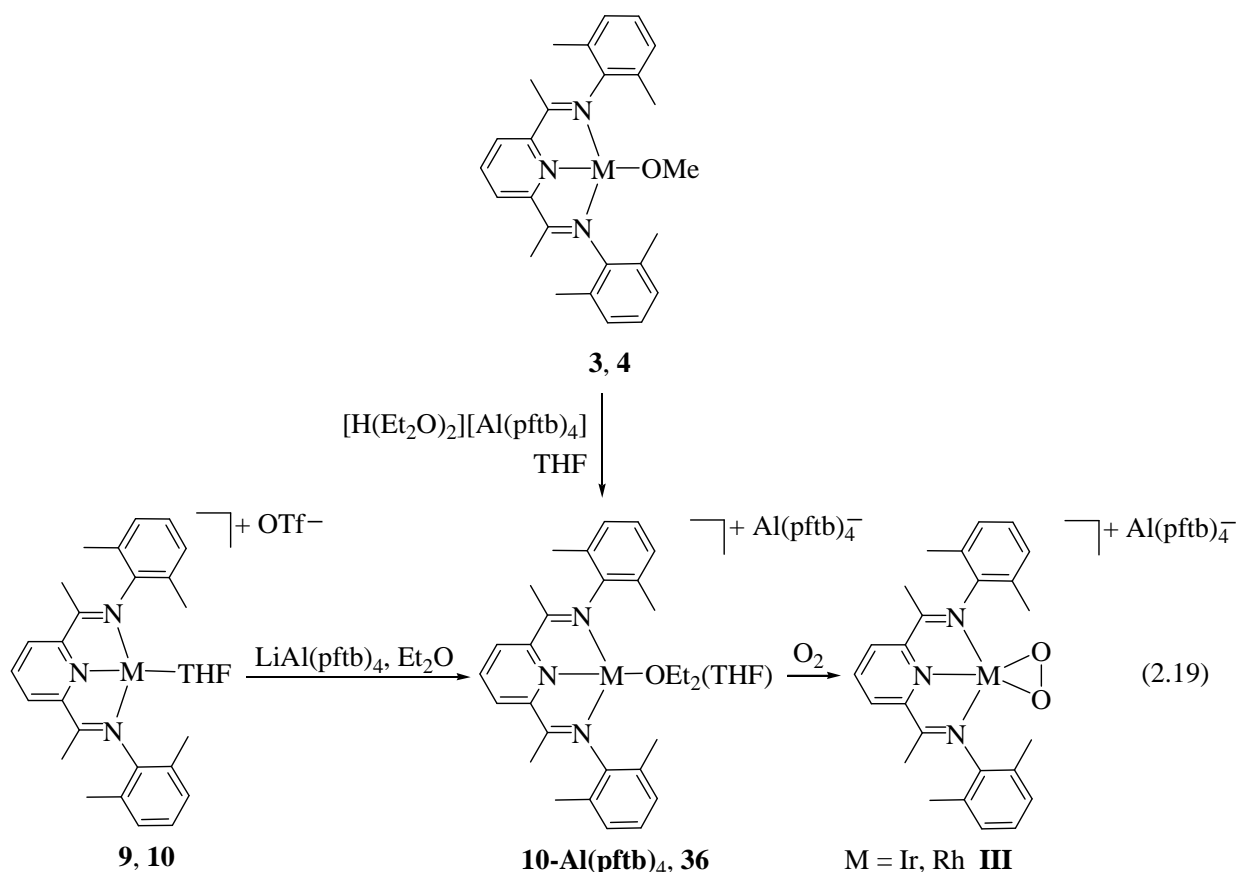
The activation of dioxygen at transition metal centers is a fundamentally important process in the aerobic oxidation of organic molecules<sup>81, 82</sup> and many other biological systems.<sup>83, 84, 85, 86</sup> According to the literature, most of the available evidence shows that bound dioxygen is not very reactive, compared to a metal-oxo species.<sup>87, 49</sup>

Based on the previous investigations,<sup>28</sup> a different approach to an oxo moiety was planned through the synthesis of a peroxo complex **III** (eq. 2.18).



The overall proposed pathway involves cleavage of an M-O bond and formation of the superoxo transient **a**. Addition of one equivalent of the cation complex would lead to the  $\mu$ -peroxo bridged species **b**, which transforms into oxo complex **II**. In general, the formation of an oxo complex is expected to be smooth because it does not involve energetically too high lying species.

Exposure of a diethyl ether solution of complex **10-Al(pftb)<sub>4</sub>** (synthesis – see Chapter 4) to an excess of dioxygen resulted in the formation of reddish-brown precipitate. After the solvent was evaporated, a microcrystalline product **III** was obtained (eq. 2.19).



The IR spectrum of complex **III** (in methylene chloride or diethyl ether) exhibited a new band (when compared to starting materials) at  $976 \text{ cm}^{-1}$ , which was tentatively assigned to an O-O stretching frequency  $\nu_{\text{O-O}}$ . This band is blue shifted by approximately  $100 \text{ cm}^{-1}$  when compared Rh, Ir(III)-peroxo chloride complexes.<sup>8</sup> The O-O stretching frequency is used in the classification of peroxo complexes ( $930\text{-}740 \text{ cm}^{-1}$ ) and superoxo complexes ( $1200\text{-}1700 \text{ cm}^{-1}$ ).<sup>88</sup> This criterion failed in our case and it was also reported by Theopold et al. for  $\text{TpCo}(\text{O}_2)$  (Tp = hydrotrispyrazolyl-borate).<sup>87</sup> The O-O stretching frequency in the latter was found at  $961 \text{ cm}^{-1}$ .

The  $^1\text{H-NMR}$  spectrum of **III** (M = Ir) in  $\text{THF-d}_8$  revealed three broad resonances (at  $\delta = 2.1, 7.2$  and  $8.3 \text{ ppm}$ ), which suggested that the complex **III** is paramagnetic. In the  $^{19}\text{F-NMR}$ , a singlet peak assigned to the counter ion is slightly shifted to  $\delta = -73.7 \text{ ppm}$  when compared to the starting material  $\text{10-Al(pftb)}_4$  ( $\delta = -75.6 \text{ ppm}$ ). These observations are supported by DFT calculations, which revealed a preference of  $\sim 4 \text{ kcal/mol}$  for  $S = 1$  over  $S = 0$  state when the peroxo ligand is perpendicular to the IrNNN plane (Fig. 2.13 left).







The difficulties in preparation and handling of complex **V**, deserves a special mention. The lifetime of **V** depends strongly on the quality (purity) of the solvent (HPLC solvents required) as well as on the quality of argon. However, even when the synthesis of **V** was performed under very rigorous Schlenk conditions, the lifetime of the methyl substituted complex **V** was in order of 1 hour at  $-35\text{ }^{\circ}\text{C}$ . Therefore, it was anticipated that by changing the methyl groups (on the phenyl rings) with isopropyl groups would lead to a more stable radical complex. This was indeed accomplished, and the isopropyl substituted compound can be stored for days at low temperatures. Unfortunately, after many attempts, the crystals of **V** suitable for an X-ray analysis were not obtained. The lifetime of **V** can be related to a color change from violet to green or brown.

The UV-Vis spectrum of complex **V** in THF shows a relatively intense band at 459 nm and a weaker at 508 nm. Since the molecular weight of **V** was unknown, in order to support the band assignment, TD-DFT calculations were performed. Calculated extinction coefficients for the model compounds **Vb** and **Vc** (*vide infra*) were in the order of  $10^4\text{ l/mol cm}$ , which is in agreement with literature values for MLCT bands.<sup>99</sup> The shape of the spectrum is identical to the one obtained experimentally. The other bands in the visible region found at 581 nm and 650 nm with weaker intensities are assigned to a d-d transition (calculated  $\epsilon = 10^3\text{ l/mol cm}$ ). The corresponding UV-Vis spectrum of the complex **V** is displayed in Figure 2.14 together with the related chloro complex and the ligand for comparison.

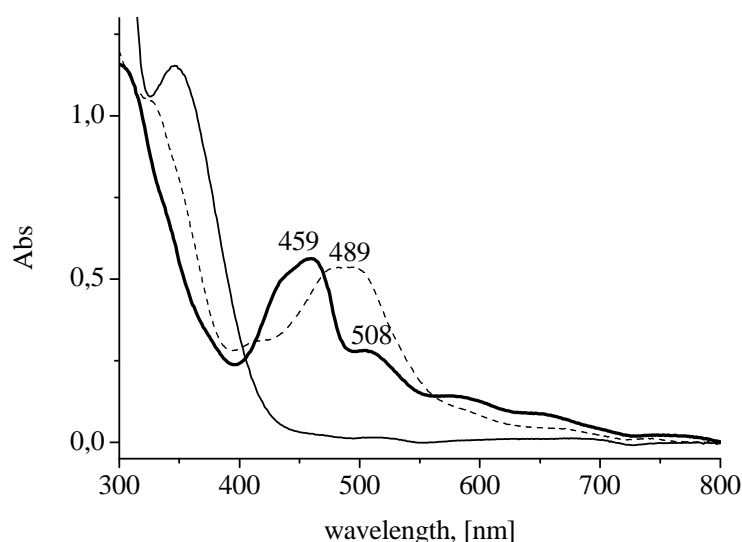
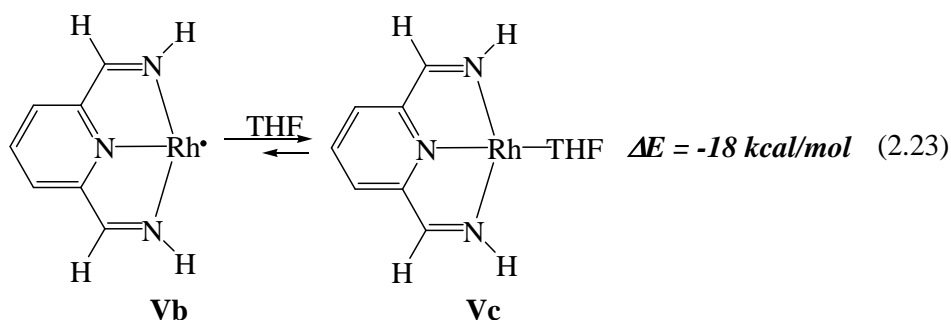


**Fig. 2.14** UV-Vis spectra of the chloro complex **1** (---), the radical complex **V** (—) and the ligand (—).

The dimerization of the 15 electron complex **V** and the formation of metal-metal bond is prevented by sterically demanding ligand. However, coordination of the THF at the rhodium "(0)" metal center was not excluded. According to DFT calculations (B3LYP, LACVP\*\* basis set), the preference for THF coordination in **Vc** is approximately 18 kcal/mol (eq. 2.23).



The electronic structure was also of particular interest. Based on DFT calculations (B3LYP, LACVP\*\* basis set) on the model compounds **Vb** and **Vc**, the spin density of the electron is essentially located within the pyridine diimine ligand (Fig. 2.15).

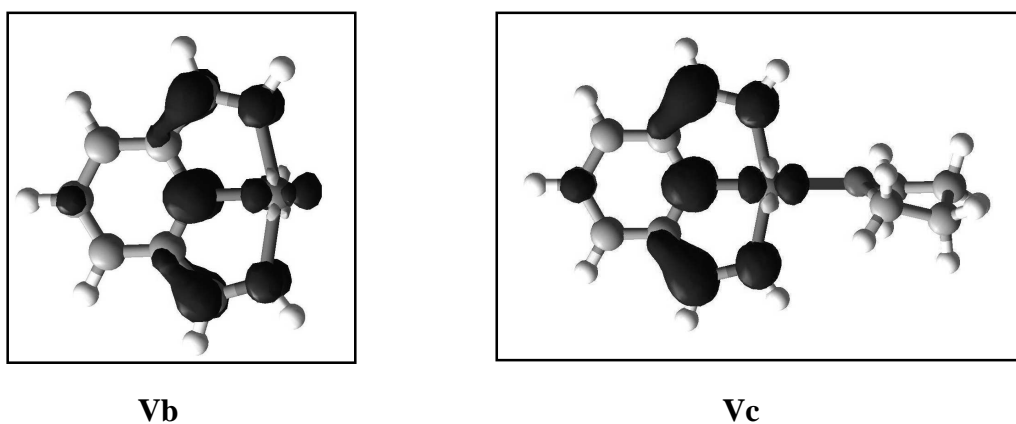
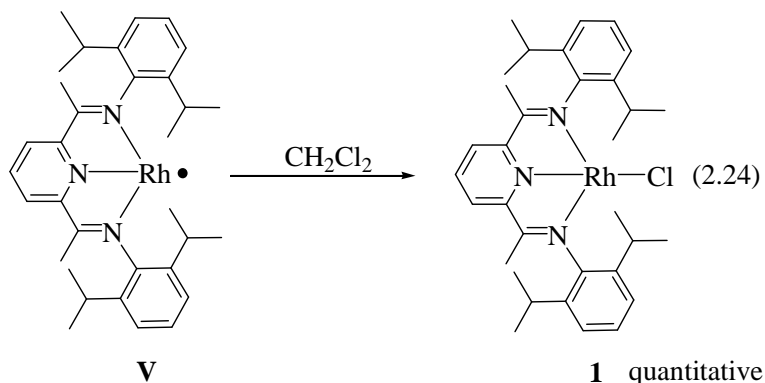


**Fig. 2.15** Calculated spin density for the model compounds **Vb** and **Vc**.

The non-innocent behavior of the pyridine diimine ligands has already been established. They are readily engaged in to a metal-to-ligand charge transfer and sometimes undergo alkyl migrations.<sup>100, 101, 102, 103</sup> DFT calculations of **V** showed that the pyridine diimine ligand demonstrates a great capacity to accept an additional electron. This was also observed for the Rh"(0)" dinitrogen complex (see part 2.5.3).

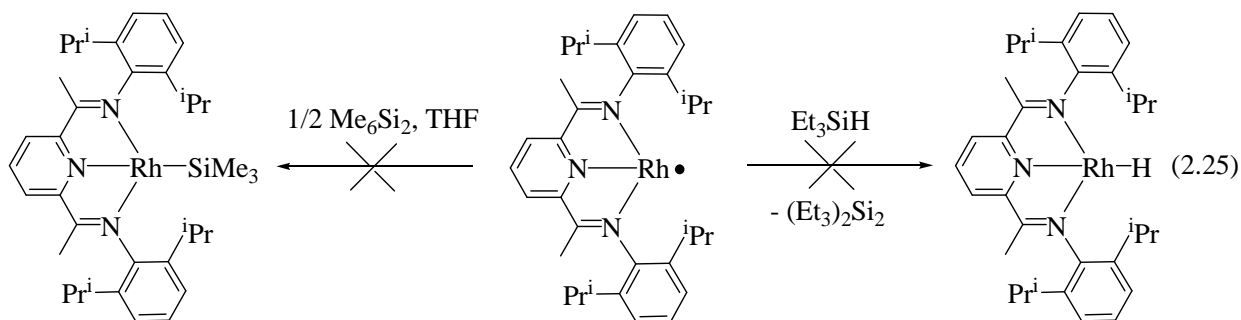
Since compound **V** has a “delicate” structure, different anticipated trapping reactions were attempted.

In dichloromethane, complex **V** immediately changed color from violet to green yielding the chloro complex **1** (eq. 2.24).



According to the  $^1\text{H-NMR}$  spectrum (in  $\text{CD}_2\text{Cl}_2$ ), the observed resonances ( $\delta = 1.03$  (d, 12 H,  $\text{CH}(\text{CH}_3)_2$ ); 1.12 (d, 12 H,  $\text{CH}(\text{CH}_3)_2$ ); 1.64 (s, 6 H,  $\text{CH}_3$ ); 3.02 (sept, 4 H,  $\text{CH}(\text{CH}_3)_2$ ); 7.19-7.27 (m, 6 H,  $\text{CH}_{\text{arom}}$ ); 7.69 (d, 2 H,  $\text{CH}_{\text{pyr}}$ ); 8.52 (t, 1 H,  $\text{CH}_{\text{pyr}}$ )) and their integration ratio unambiguously confirmed the formation of **1**.

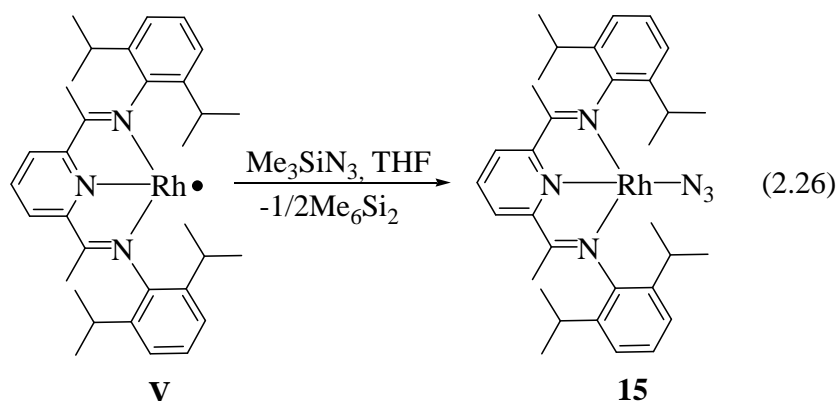
Complex **V** was completely un-reactive towards hexamethydisilane ( $\text{Me}_6\text{Si}_2$ ) at room temperature. In the reaction of **V** with triethylsilane ( $\text{Et}_3\text{SiH}$ ), only a mixture of different unknown compounds was observed with no hydride resonance in the expected region in the  $^1\text{H-NMR}$  spectrum (eq. 2.25).



### 2.5.1 The formation of the Rh(I) azido complex

Rh-imido complexes are of general interest, since they are isoelectronic to the related oxo ligand. The focus of this section will be to describe attempts to isolate a Rh(II) imido complex. As a preparative route to the desired Rh(II) imido complex, trimethylsilyl azide and adamantyl-1-azide have been used. According to the literature, the facile Si-N cleavage and elimination of N<sub>2</sub> has been used as a successful method in synthesis of organic imides and imines.<sup>104</sup>

However, in this case, addition of one equivalent of Me<sub>3</sub>SiN<sub>3</sub> to a THF solution of complex **V** resulted in the formation of the green Rh(I) azido complex **15** in quantitative yield based on starting material **1** (eq. 2.26).



The loss of hexamethyldisilane was confirmed by <sup>1</sup>H-NMR spectroscopy of the transferred volatiles from the reaction mixture in THF-d<sub>8</sub>. A singlet peak at δ = 0.04 was observed and compared to a standard reference.

The IR spectrum of complex **15** in toluene showed a strong characteristic absorption band at ν = 2031 cm<sup>-1</sup> (Fig. 2.16 left). This band is assigned to the ν<sub>as</sub> stretching frequency of the coordinated azido ligand. The expected ν<sub>s</sub> band for the azido ligand was not detected. This was also reported by Werner et al. for [Rh(<sup>i</sup>Pr<sub>3</sub>P)<sub>2</sub>(C<sub>2</sub>CPh<sub>2</sub>)N<sub>3</sub>] (ν<sub>as</sub> = 2050 cm<sup>-1</sup>).<sup>105</sup>

The UV-Vis spectrum of **15** in THF revealed three bands, at 474 nm (strong intensity) and at 615 and 676 nm (weak intensity) (Fig. 2.16 right).

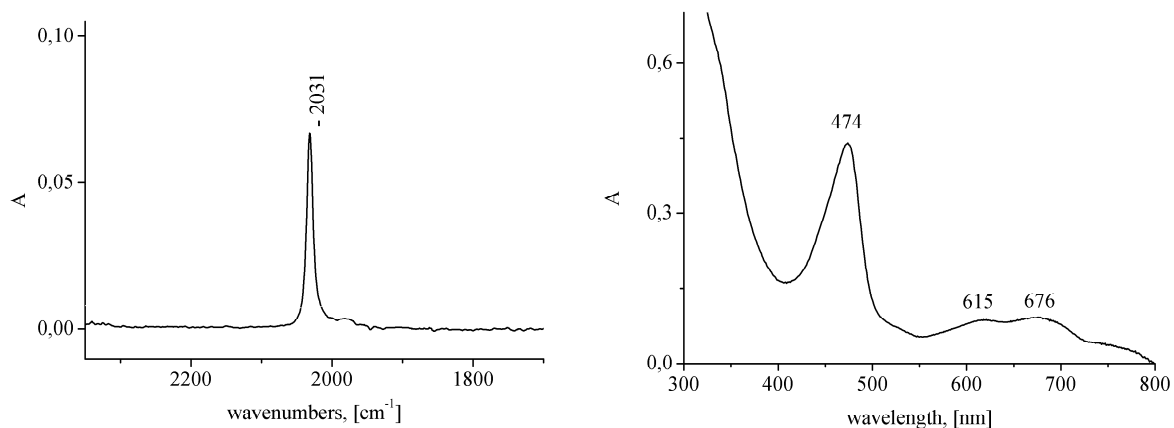


**Fig. 2.16** IR and UV/Vis spectra of complex **15** recorded at RT.

Crystals of **15** suitable for X-ray crystal structure analysis were obtained from a THF/pentane solution.

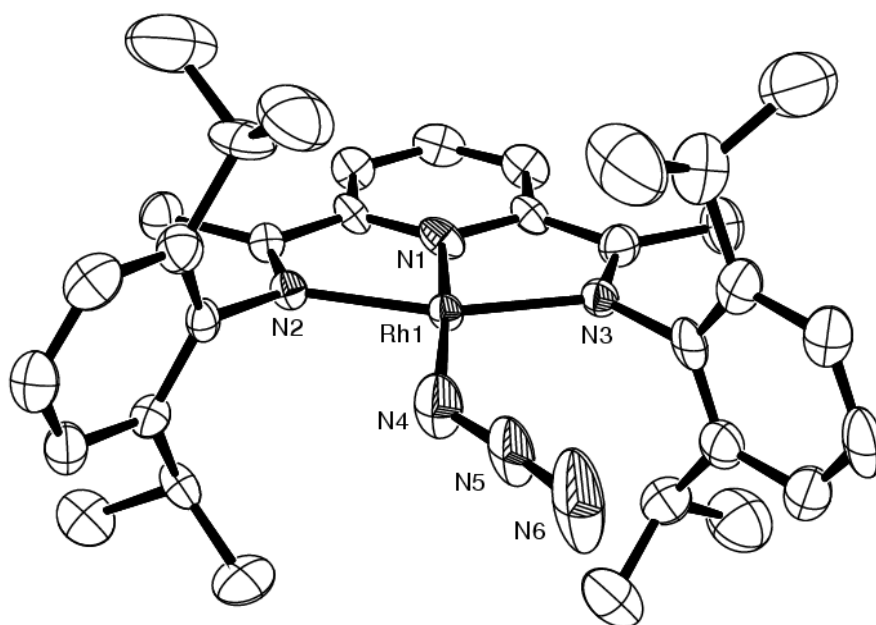


**Fig. 2.17** ORTEP plot of complex **15** with 50% probability ellipsoids (hydrogen atoms were omitted for clarity).

---

Table 2.5 Selected bond lengths [ $\text{\AA}$ ] and angles [ $^\circ$ ] for complex **15**.

---

Rh1-N1	1.887(7)	Rh1-N3	2.029(7)	N4-N5	1.204(1)
Rh1-N2	2.010(7)	Rh1-N4	2.030(8)	N5-N6	1.159(1)
N1-Rh1-N2	80.2(3)	N1-Rh1-N3	78.2(3)	N5-N4-Rh1	132.2(7)
N2-Rh1-N3	158.3(3)	N1-Rh1-N4	174.9(4)	N6-N5-N4	175.0(1)
N2-Rh1-N4	104.2(3)	N3-Rh1-N4	97.5(3)		

---

Complex **15** adopts a square planar coordination with the sum of angles around Rh center equaling  $360^\circ$ . The azido ligand N4-N5-N6 displays an angle of  $175.0(1)^\circ$ . The angle Rh1-N4-N5 of  $132.2(7)^\circ$  suggests  $sp^2$  hybridisation of nitrogen atom N4, while the bond distances N4-N5 ( $1.204(1) \text{\AA}$ ) and N5-N6 ( $1.159(1) \text{\AA}$ ) describe nitrogen atom N5 as  $sp$  hybridised.

As displayed in Figure 2.17, the molecule has an approximate  $C_s$  symmetry in the solid state. However, the integration ratio between the methyl groups on the ketimine and phenyl rings, in the (time averaged)  $^1\text{H-NMR}$  spectrum (in THF- $d_8$ ) at RT, is 1:2. This indicates  $C_{2v}$  symmetry of **15** in the solution.

To address this point, DFT calculations on a model complex **15a** were performed. The geometry of the ground state ( $S=0$ ) has  $C_s$  symmetry and a bent conformation of the azido ligand. The azido ligand can rotate fast around the Rh-N bond or it can move as a “windshield wiper” going through a linear structure, which could explain the observed  $C_{2v}$  symmetry (Fig. 2.18). Both suggested processes are much faster than the NMR time scale.

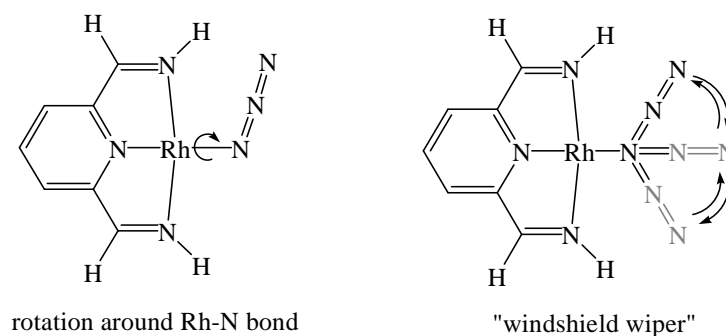


**Fig. 2.18** Possible ways to accomplish time averaged  $C_{2v}$  symmetry.

The linear structure was found to be a transition state, with the energy barrier of approximately 5 kcal/mol. The Walsh diagram (displayed in Fig. 2.19) shows an increase in energy by  $\sim 1$  kcal/mol when angle  $\alpha$  was increased by  $10^\circ$ . Since the energy barrier is so small, the calculation related to the rotation around the Rh-N bond were not performed.

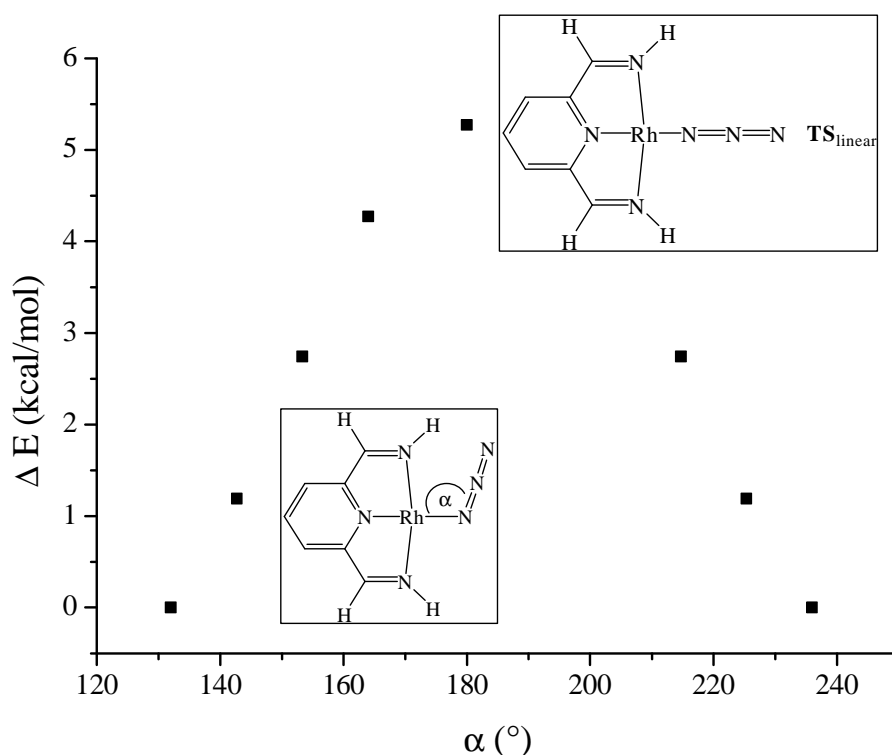
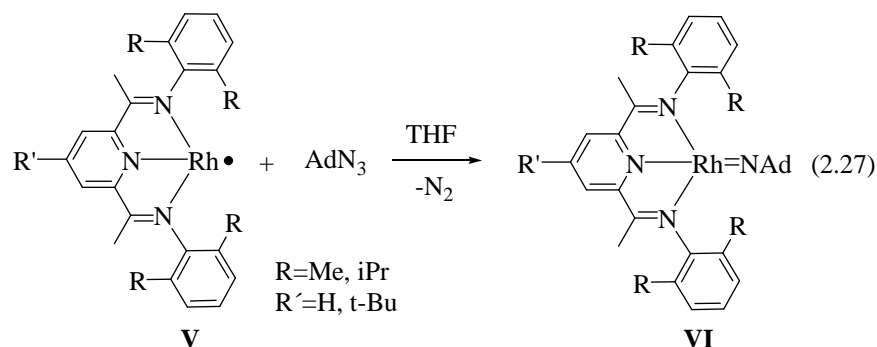


**Fig. 2.19** Walsh diagram for in plane bending of the azide related by symmetry.

Further, calculated bond distances for the model complex (B3LYP, LACVP\*\* basis set) are in good agreement with those found in the X-ray structure analysis. This is the best illustrated with  $N4-N5 = 1.217 \text{ \AA}$  ( $1.204(1) \text{ \AA}$ ) and  $N5-N6 = 1.156 \text{ \AA}$  ( $1.159(1) \text{ \AA}$ ) bond distances.

## 2.5.2 The reaction of **V** with adamantyl-1-azide

Addition of one equivalent of adamantyl-1-azide ( $\text{AdN}_3$ ) to a THF solution of the radical complex **V** at room temperature resulted in the evolution of gas bubbles (presumably  $\text{N}_2$ ) accompanied by a color change from violet to burgundy to yield complex **VI** as a plausible product (eq. 2.27).



The UV-Vis spectrum of **VI** in THF showed two bands at 465 nm and 520 nm. In the  $^1\text{H-NMR}$  spectrum ( $\text{THF-d}_8$ ), broad peaks at  $\delta = 4.3$  and  $7.2$  ppm were observed, indicating the presence of a paramagnetic compound, most likely a Rh(II) species. A group of resonances at  $\delta = 1.1$  ppm were assigned to the adamantyl protons. Fast relaxation of the unpaired electron does not affect significantly adamantyl moiety since it is further away (Fermi and through space coupling decreases with the increase in distance ( $\sim 1/r^2$  and  $1/r^3$ )). Therefore, the observed peaks were not broad. The EPR spectroscopy reveals a sharp signal with  $g = 1.997$  (3500 G) at RT (Fig. 2.20). Measurements at low temperature showed only minor splitting.

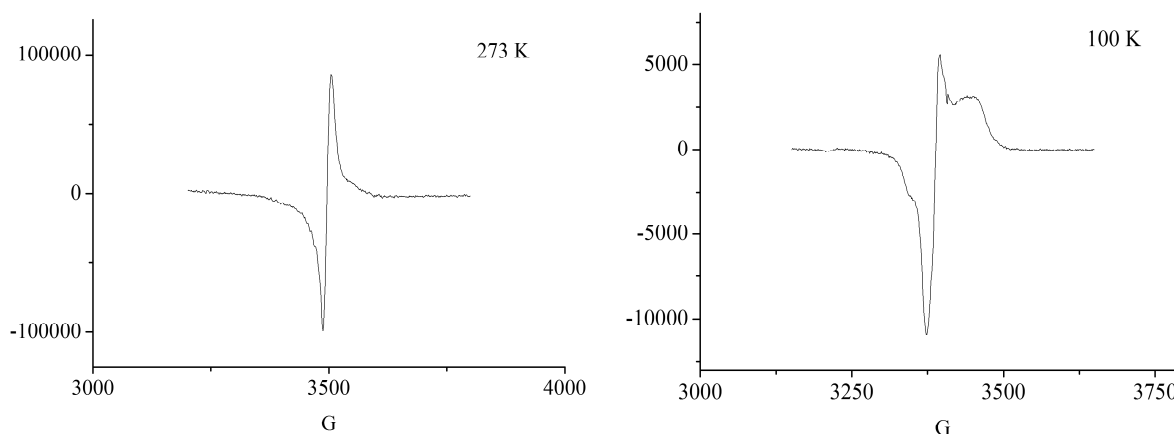


**Fig. 2.20** EPR spectra of complex **VI**.

In the literature p-tolyl azide or adamantyl azide have been used to generate imido complexes. Meyer et al. described the formation of the  $d^6$  low spin ( $S=0$ ) Co(III) imido complex, supported by a tris-carbene ligand, using p-tolyl azide.<sup>106</sup> An open shell Co(III) imido complex ( $S=1$ ) was obtained with a Tp ligand system using adamantyl azide, as described by Theopold et al.<sup>107</sup> High reactivity of the  $\beta$ -diketiminato Co(I) arene complex towards organic azides and the formation of diverse imido complexes have been described by Warren et al.<sup>108</sup>

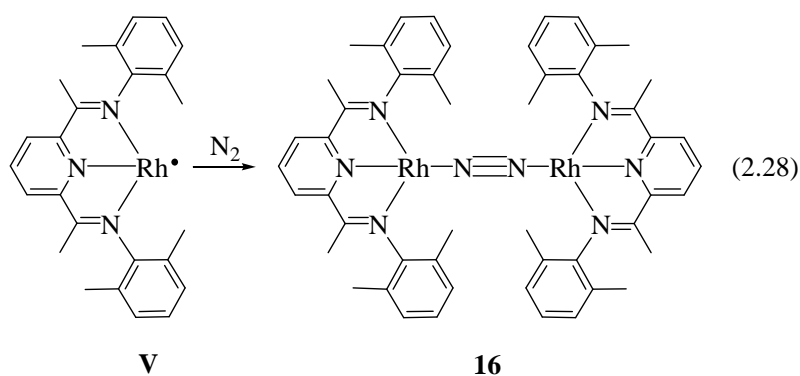
### 2.5.3 The activation of dinitrogen with complex **V**

Dinitrogen is inert to reactions due to its low polarity and strong triple bond. In comparison to the isoelectronic CO ligand, chemistry of dinitrogen is less well developed owing to its weak  $\sigma$  donor and poor  $\pi$  acceptor characteristics. Depending on the metal, oxidation state and the neighboring ligands, dinitrogen can be bonded to the metal center in different ways. For example, it can bind to the metal in *end-on* or *side-on* mode, forming mono or dinuclear complexes.<sup>109</sup>

Dinitrogen complexes can be obtained by displacement of weakly coordinated ligands. They can also be prepared by reduction of metal complexes and formation of low-valent metal center that can activate and bind  $N_2$ . It is also possible, that during the reaction a vacant site is formed on the metal center where  $N_2$  may coordinate.<sup>109</sup> As it will be described in this part, the activation of dinitrogen with complex **V** has been accomplished.

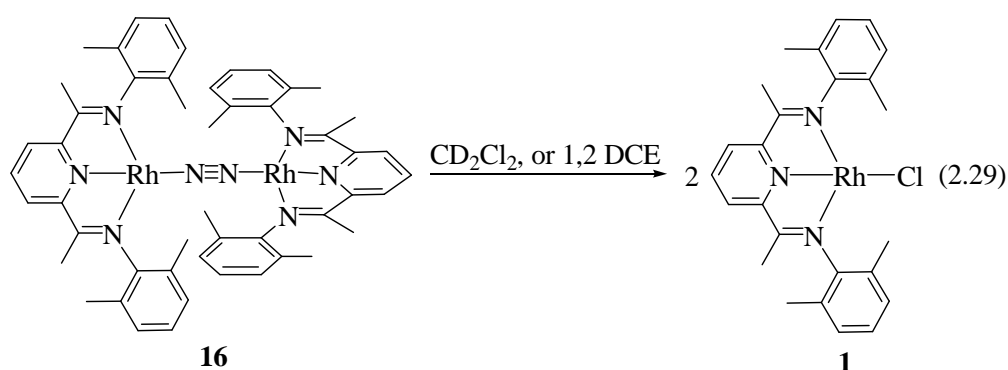
#### *Dinuclear dinitrogen complex 16*

When the tentative radical violet complex **V**, with the methyl groups on the aryl substituents was exposed to a nitrogen atmosphere, the color immediately changed from violet to dark brown and complex **16** is formed in quantitative yield (eq. 2.28). Complex **16** can be independently synthesized by the reduction of Rh(I) chloro or methoxo complex with Na/Hg under  $N_2$  atmosphere. The synthesis and characterization of complex **16** as well as magnetic properties have already been described by Nüchel.<sup>47</sup>

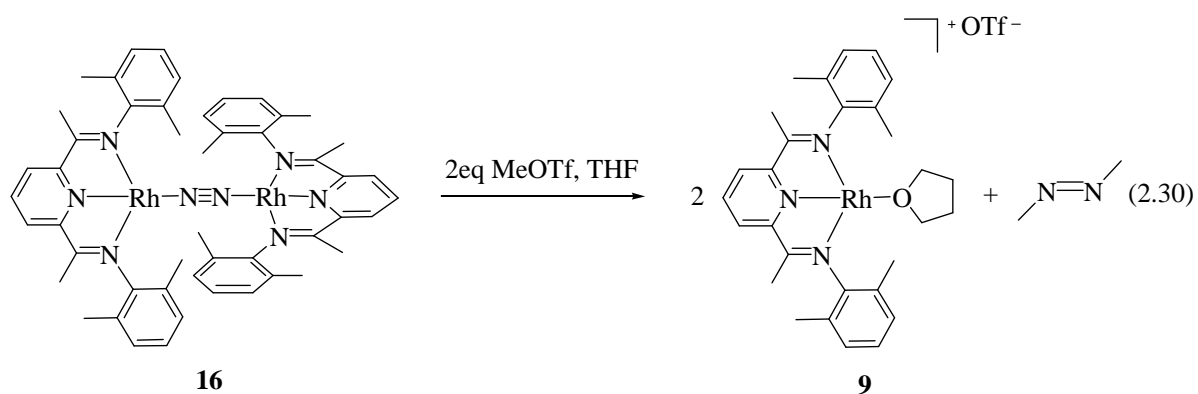


Both metal centers in complex **16** have a formal Rh(0) oxidation state. According to the crystal structure analysis, the N-N bond in complex **16** is 1.129(7) Å, slightly elongated in comparison to free N<sub>2</sub> (1.0975 Å). The elongation of the N-N bond is often related with the reactivity of dinitrogen complexes (*vide infra*).

Complex **16** reacts with chlorinated solvents such as dichloromethane and 1,2-dichloroethane forming the complex **1** in quantitative yield (eq. 2.29). The formation of **1** was unambiguously confirmed by <sup>1</sup>H-NMR spectroscopy in CD<sub>2</sub>Cl<sub>2</sub> and compared with reference.



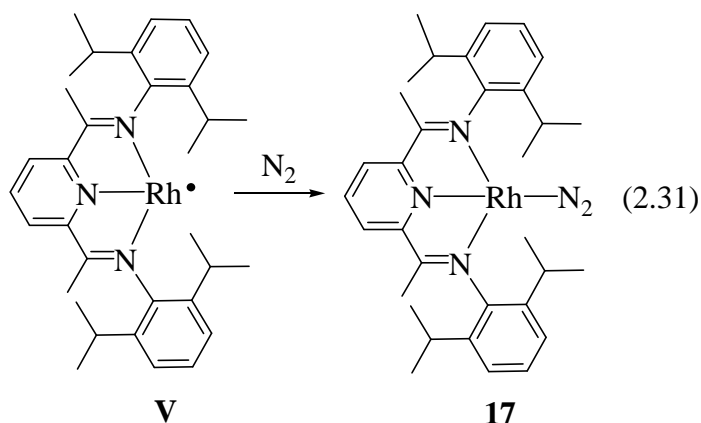
The reaction between complex **16** and two equivalents of methyl-triflate leads to the formation of the Rh (I) triflate complex **9** (eq. 2.30).



The  $^1\text{H-NMR}$  analysis of the transferred volatiles (in  $\text{THF-d}_8$ ) revealed a singlet peak at  $\delta = 2.94$  ppm. Based on the  $^1\text{H-NMR}$  spectrum, the formation of  $\text{Me}_2\text{N}_2$  as a side product is proposed.<sup>110, 111</sup> The chemical shift for  $\text{Me}_2\text{N}_2$  reported in the literature was found at  $\delta = 3.76$  ppm in  $\text{CDCl}_3$  and  $\delta = 2.84$  ppm in  $\text{D}_2\text{O}$ .<sup>112</sup> (No reference was found for  $\text{THF-d}_8$ ). Further supporting evidence was obtained by GC-MS of the volatiles displaying a peak at 58 m/z as expected for  $\text{N}_2\text{Me}_2^{+\bullet}$ .

### ***Mononuclear dinitrogen complex 17***

When the violet complex **V** with ortho isopropyl aryl substituents was exposed to  $\text{N}_2$  atmosphere the color changed to brown and the mononuclear dinitrogen complex **17** was formed in quantitative yield (eq. 2.31). Alternatively, complex **17** can be obtained by reduction of the chloro complex with  $\text{Na/Hg}$  under  $\text{N}_2$  atmosphere. To the best of our knowledge, this is the first example of a mononuclear  $\text{Rh}(0)$  dinitrogen complex. The cationic cobalt(I) complex was reported by Gibson et al.<sup>113</sup>



Based on NMR and EPR spectroscopy, complex **17** is paramagnetic with the formal oxidation state of (0) for Rh center. In the  $^1\text{H-NMR}$  spectrum in  $\text{C}_6\text{D}_6$ , broad peaks typical for paramagnetic compounds were detected at  $\delta = 2.28, 3.55$  and  $5.60$  ppm. The IR spectrum in toluene revealed a N-N stretching frequency at  $\nu = 2139$   $\text{cm}^{-1}$  (Fig. 2.21). A small shoulder at  $\nu = 2101$   $\text{cm}^{-1}$  presumably originates from the solvent.

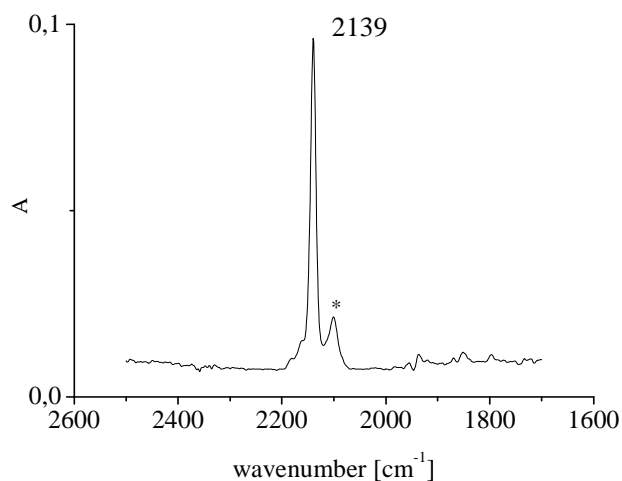


**Fig. 2.21** IR spectrum of complex **17** in toluene (\*– toluene).

According to the IR spectrum, it can be concluded that there is no enhanced back bonding to the  $N_2$  ligand. The observed frequency at  $\nu_{NN} = 2139 \text{ cm}^{-1}$  reveals that the  $N_2$  molecule is polarized but still retains its triple bond character (free  $N_2$  is IR inactive, whilst in the Raman spectrum displays a frequency at  $\nu_{NN} = 2331 \text{ cm}^{-1}$ ).<sup>114</sup>

Crystals suitable for an X-ray structure analysis were obtained from a concentrated toluene solution of **17** at  $-35 \text{ }^\circ\text{C}$ . The molecular representation of **17** and selected bond distances and angles are displayed in Figure 2.22 and Table 2.6.

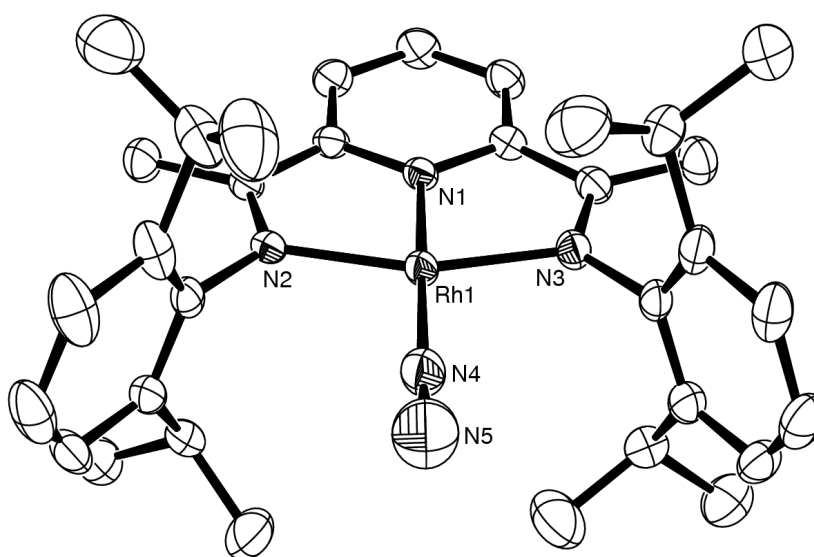


**Fig. 2.22** ORTEP plot of complex **17** with 50% probability ellipsoids (hydrogen atoms were omitted for clarity).

Table 2.6 Selected bond lengths [ $\text{\AA}$ ] and angles [ $^\circ$ ] for complex **17**.

Rh1-N1	1.914(1)	Rh1-N2	2.011(1)	Rh1-N3	2.012(1)
Rh1-N4	1.950(2)	N4-N5	1.087(3)		
N1-Rh1-N4	179.3(1)	Rh1-N4-N5	178.8(3)	N4-Rh1-N2	100.6(8)
N1-Rh1-N2	79.55(7)	N1-Rh1-N3	79.05(7)	N4-Rh1-N3	100.8(8)
N2-Rh1-N3	158.6(7)				

The geometry of complex **17** at the Rh center is square planar with the sum of bond angles equaling  $360^\circ$ . The  $\text{N}_2$  ligand completes the fourth coordination site of the N1-N2-Rh1-N3 plane. The molecule adopts approximate  $\text{C}_{2v}$  symmetry. The N1-Rh1-N4 angle is  $179.3(1)^\circ$ . The distance between N4-N5 bond is  $1.087(3) \text{\AA}$  and it is comparable with the N-N distance in free  $\text{N}_2$  ( $1.0975 \text{\AA}$ ). The dinitrogen distance in the cationic cobalt system is  $1.112(6) \text{\AA}$ .<sup>113</sup>

### *EPR spectroscopy and DFT calculations*

The EPR spectrum revealed a sharp signal at room temperature measurement with  $g = 1.999$  (3500 G). However, the unpaired electron did not show hyperfine splitting either with the  $^{103}\text{Rh}$  metal center ( $I=1/2$ ) or  $^{14}\text{N}$  atoms ( $I = 1$ ). At low temperature measurements (100 K), a small shoulder is observed. No hyperfine coupling for either complex **16** and **17** was detected (Fig. 2.23).

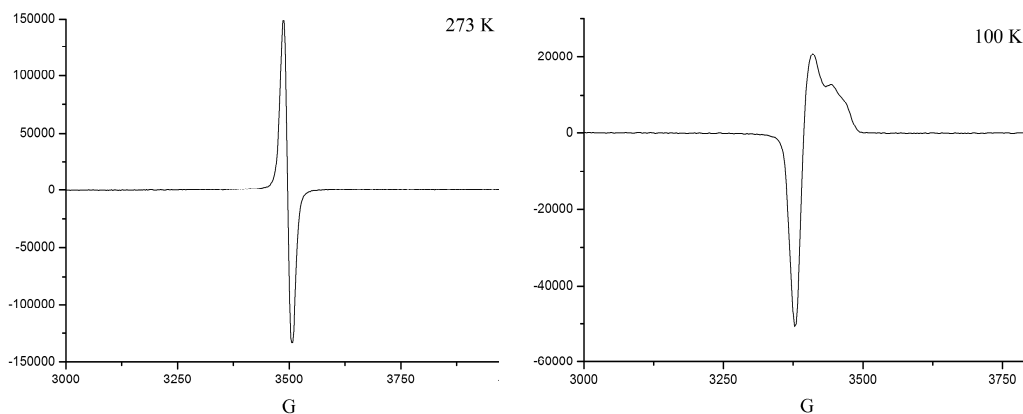


**Fig. 2.23** EPR spectra of complex **17** at RT and 100 K.

According to DFT calculations, the spin density of the electron is delocalized within the pyridine ligand (Fig. 2.24-left). This could be a possible explanation why hyperfine splitting was not observed in the EPR experiment.

Calculated distances for the model compound **17a** (B3LYP, LACVP\*\* basis set) are in good agreement with those found in the X-ray crystal analysis (Fig. 2.24-right).

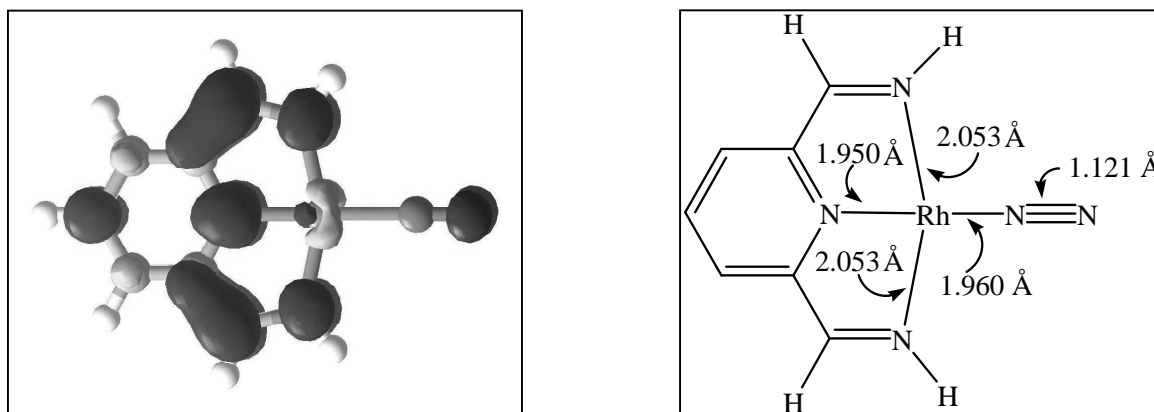


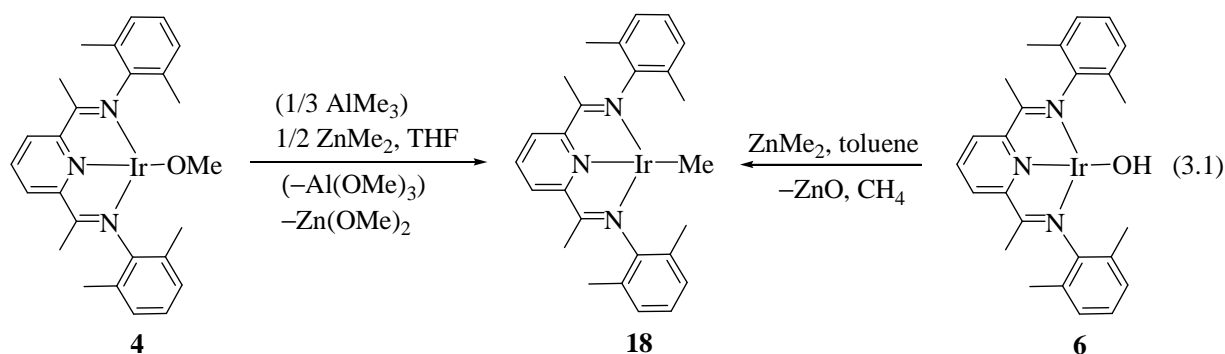
**Fig. 2.24** Calculated bond distances and spin density for the model complex **17a**.

In this part, it was shown that the activation of  $\text{N}_2$  is feasible with very reactive radical complex **V**. The reactivity of the isolated complexes **16** and **17** with different reagents (such as  $\text{H}_2$ ,  $\text{O}_2$ , etc.) will be of great interest in the future.

### 3 C-H activation by Rh, Ir(I) square planar complexes – mechanistic aspects

#### 3.1 Improved synthesis of Ir(I) methyl complex

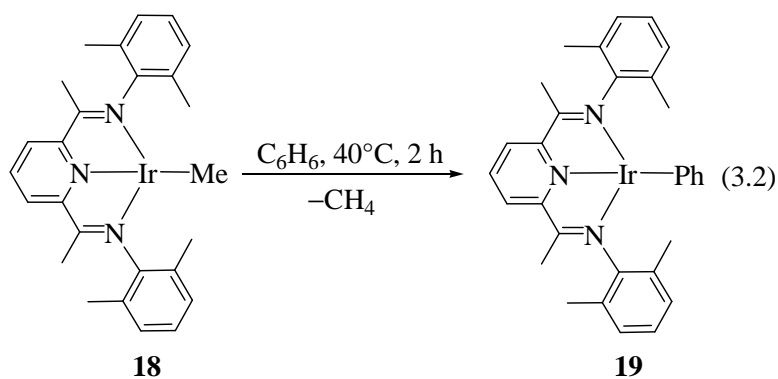
It has been previously shown that the methyl complex **18** can be synthesized from complex **4** by the addition of  $\text{AlMe}_3$ .<sup>44</sup> However, the trimethoxy aluminium  $\text{Al}(\text{OMe})_3$  side product formed is difficult to remove from the reaction mixture. If traces of  $\text{Al}(\text{OMe})_3$  remain in the solution together with complex **18**, for a prolonged period of time, a mixture of unknown products is obtained. Therefore, an improved synthesis of **18**, employing the alternative methylating agent,  $\text{ZnMe}_2$ , was performed. Complex **18** can be prepared by the addition of  $\text{ZnMe}_2$  to a THF solution of complex **4** or complex **6** in approximately 70 % yield for both reactions (eq. 3.1).



The insoluble byproducts ( $\text{Zn}(\text{OMe})_2$  and  $\text{ZnO}$ ) can be easily removed by filtration. However, the stability of **18** in diethyl ether or THF solution even at the lower temperatures ( $-35\text{ }^\circ\text{C}$ ) is still a great problem. Interestingly, by using this route (especially from complex **6**), decomposition of complex **18** is much slower than in the previously reported synthesis, suggesting that less side products remained in the solution.

#### 3.2 C-H activation of benzene

The facile *intermolecular* C-H activation of complex **18** in benzene under ambient temperature leads quantitatively to the phenyl complex **19** and methane (eq. 3.2). This reaction, as well as the DFT analysis of the proposed mechanism were previously reported in some detail by our group.<sup>36</sup>



The proposed mechanism for this reaction is anticipated to proceed via a two-step mechanism, via oxidative addition followed by C-H reductive elimination rather than  $\sigma$ -bond metathesis (Fig. 3.1). The oxidative addition pathway leads to an octahedral Ir(III) intermediate, with a “square-pyramidal” transition state.

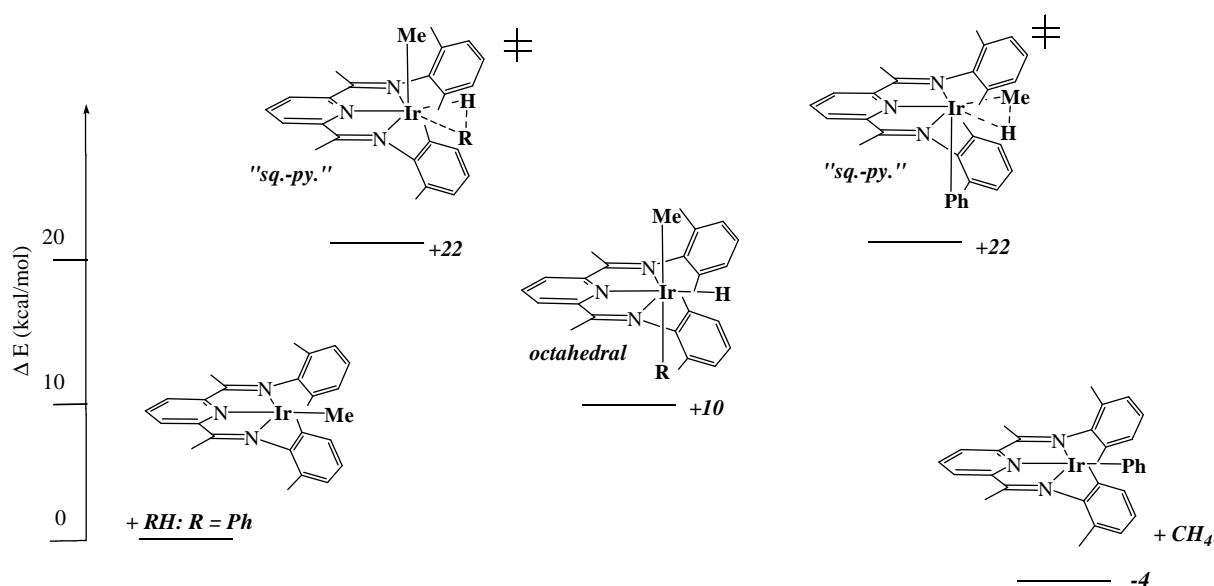


**Fig. 3.1** The proposed two-step mechanism for C-H activation process.<sup>36</sup>

The crucial step in the C-H activation mechanism is the bending of the Ir-Me bond out of the metal-NNN<sub>ligand</sub> plane. This bending process in **18** requires energy of approximately 12 kcal/mol for  $\alpha = 70^\circ$ .<sup>36</sup> However, if the ketimine methyl groups are replaced with CF<sub>3</sub> groups, enhancing the  $\pi$ -acceptor properties of the ligand, the bent over the square-planar structure is preferred (Fig. 3.2).

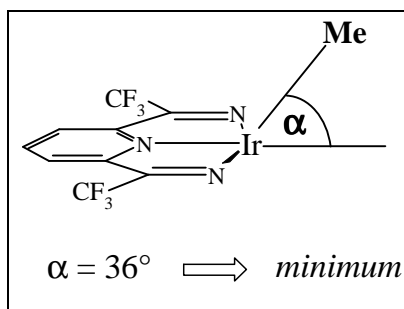
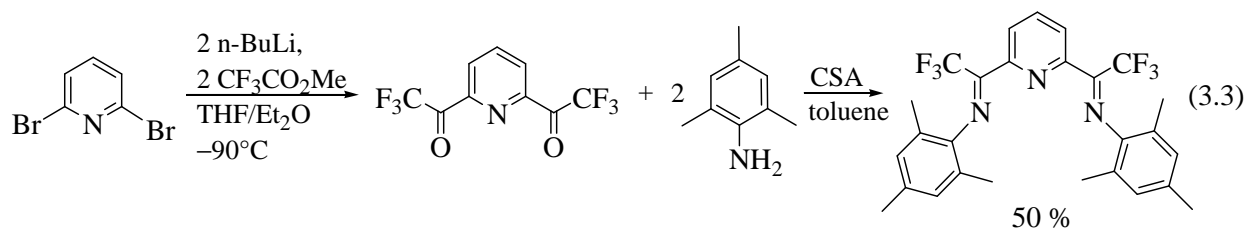
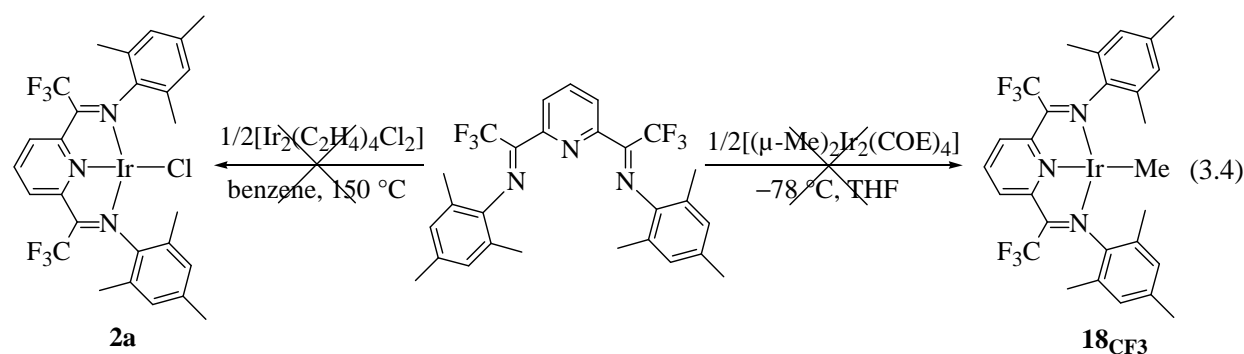


**Fig. 3.2** Calculated minimum for model complex **18<sub>CF3</sub>**.

To probe experimentally, the synthesis of methyl complex **18<sub>CF3</sub>** was attempted. The ligand was synthesized according to the procedure of Brookhart et al.<sup>115</sup> The first step of ligand synthesis involves the sequential treatment of 2,6-dibromopyridine with n-BuLi and methyltrifluoroacetate at  $-90^\circ\text{C}$  and the formation of 2,6-bis(trifluoroacetyl)pyridine. The following step is a simple condensation reaction between the diketopyridine derivative and 2,4,6-trimethylaniline (eq. 3.3).



The syntheses of the chloro and methyl complexes (**2a** and **18<sub>CF3</sub>**) according to eq. 3.4 were attempted.



According to the  $^1\text{H-NMR}$  in  $\text{C}_6\text{D}_6$ , no reaction proceeds when the  $\text{CF}_3$ -ligand and  $[\text{Ir}_2(\text{C}_2\text{H}_4)_4(\mu\text{-Cl})_2]$  was mixed together and heated up to  $150^\circ\text{C}$  over a period of 6 days.

In one step reaction, by using freshly prepared  $[(\mu\text{-Me})_2\text{Ir}_2(\text{COE})_4]^{116}$  and  $\text{CF}_3$ -ligand (in THF) at  $-78\text{ }^\circ\text{C}$  and warming up the reaction mixture gradually to room temperature (eq. 3.4), the isolation of methyl complex  $\mathbf{18}_{\text{CF}_3}$  failed.

The unsuccessful complexation could be traced to strongly reduced  $\sigma$ -donor properties of the diimine ligand, which originate from a very strong electron withdrawing nature of the  $\text{CF}_3$  groups.

### *Low temperature NMR studies*

In order to learn more about the bending process of the Ir methyl moiety, low temperature NMR studies were performed (Fig. 3.3).

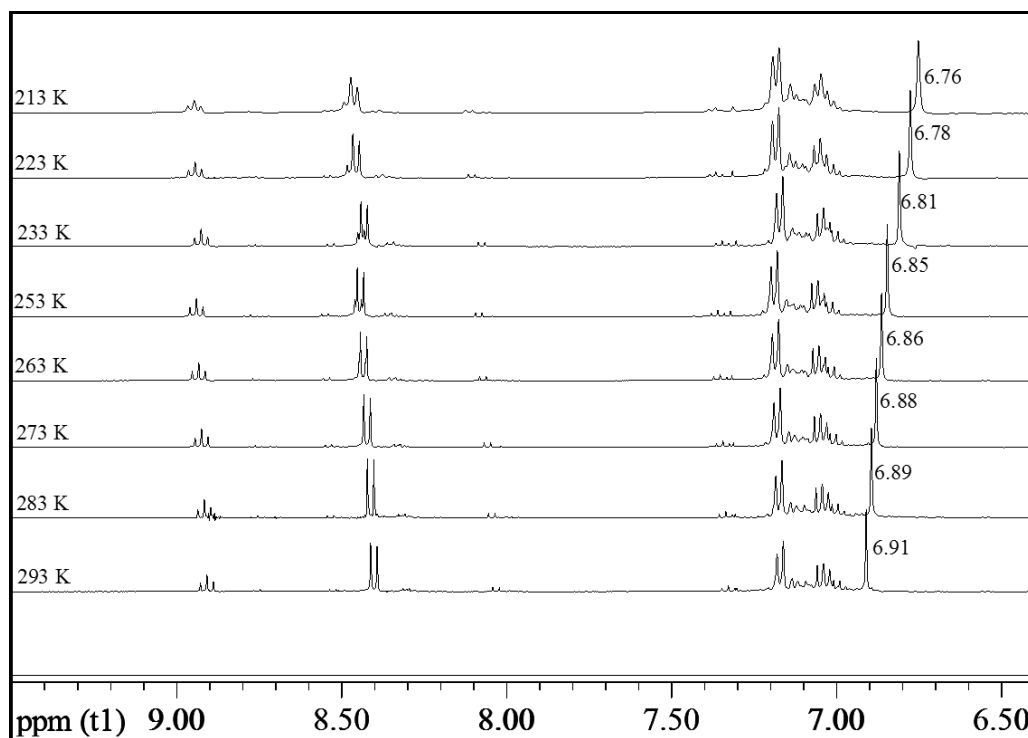


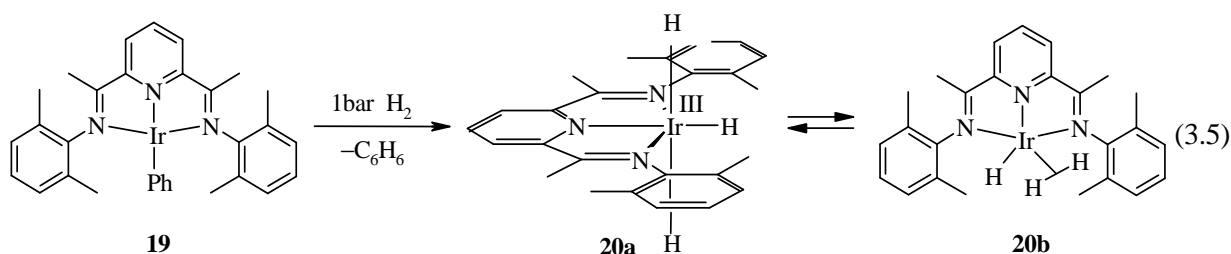
**Fig. 3.3** Temperature dependent NMR of complex **18**.

The  $^1\text{H}$ -NMR of the Ir methyl group in complex **18** shows an unusual down field shift at 6.91 ppm. As displayed in Figure 3.3, by decreasing the temperature, the Ir methyl signal is shifted towards higher field (6.91 – 6.76 ppm). The signals (doublet and triplet) from the pyridine ring are slightly shifted towards lower field. As previously described,<sup>36</sup> complex **18** has

a very shallow potential for the “bending process” of the methyl group. This low energy barrier may provide a possible explanation for the observed strong dependence in the low temperature NMR study. The ability of phenyl rings to induce a ring-current effect and shift the protons towards higher field is similar to the previous observations made by Crabtree et al..<sup>117</sup>

### 3.2.1 Evidences for Ir(III) intermediate

In the context of the aforementioned C-H activation process, support for the proposed mechanism with an Ir(III) intermediate was obtained by the reaction of the iridium phenyl complex **19** with excess hydrogen. The reaction leads to the formation of the trihydride complex **20a** (eq. 3.5).



The trihydride peak was observed as a broad “triplet” at  $-8.76$  ppm in toluene-*d*<sub>8</sub>. The integration ratio between the proton in the *para* position on the pyridine ring and the trihydride peak is approximately 1:3 as required. The broadness of the triplet is attributed to the fast exchange process between the hydride ligands. It is proposed that complex **20a** is in equilibrium with the dihydrogen hydride complex **20b**, which will be discussed below.

#### *Low temperature NMR studies*

In an attempt to gain a better insight into the dynamic processes of the hydride ligands, the low temperature NMR behavior of complex **20a** was studied. NMR investigations between 313 and 183 K in toluene demonstrated a classical (incoherent) exchange process (Fig. 3.4).

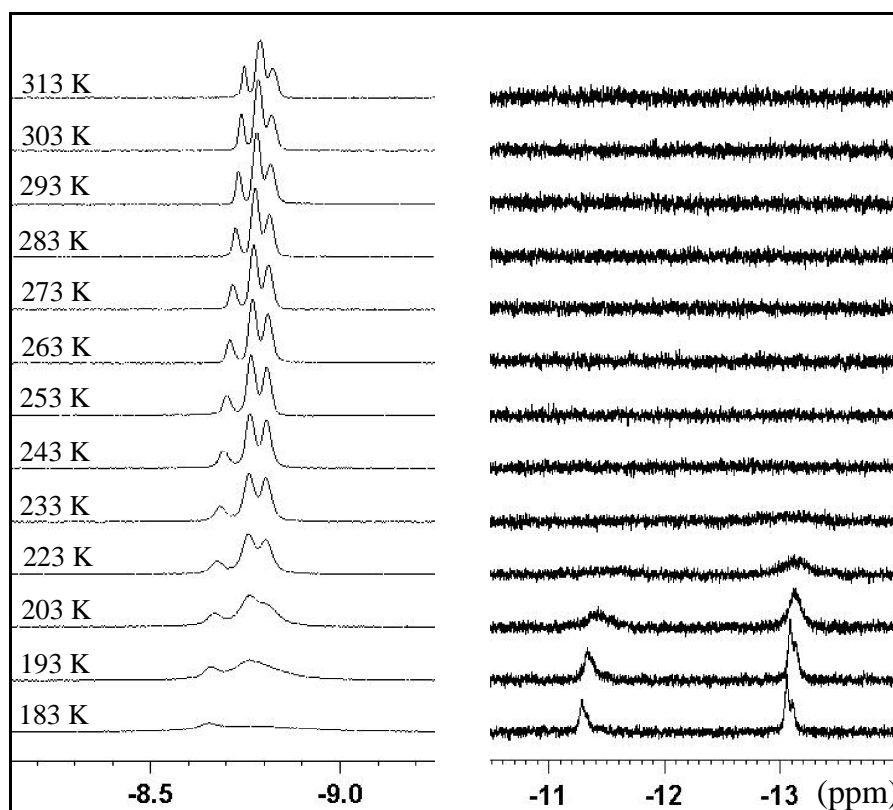


**Fig. 3.4**  $^1\text{H}$ -NMR spectra of the hydride resonances at different temperatures.

As the temperature was decreased, a broadening of the signal at  $-8.76$  ppm was observed. Also, the integral, starting from 233 K, became smaller (in comparison to the *para* proton from the pyridine ring). The value is reduced by half at 193 K. Starting from 223 K, (Fig. 3.3 right) peaks at  $-11.3$  and  $-13.1$  ppm were observed with increasing signal intensity at lower temperatures. Unfortunately the shapes of the peaks do not appear as a doublet and a triplet, which might be expected for the trihydride complex **20a**. However, the integration ratio of these newly observed signals at 183 K is approximately 2:1.

The unsymmetrical shape of the triplet and its further broadening, when the temperature is decreased, did not allow for the coupling constants in complex **20a** to be measured.

According to the overall data from the low temperature NMR study, it is proposed that at room temperature, equilibrium between **20a** and **20b** is present. Fast exchange between the hydride ligands resulted in the broadness of the “triplet” peak at  $-8.76$  ppm. Upon decreasing the temperature, the exchange process (between the hydride ligands) slows down and at 183 K the predominantly structure observed is **20a**.

According to the literature, if the barrier is too low (between dihydrogen and hydride complexes), fluxional behavior (incoherent process) will be observed rather than the coherent exchange process (*vide infra*).<sup>118, 119</sup> A barrier between 8.7 and 16.7 kcal/mol must be present in order that two species can be observed by NMR.<sup>120</sup>

### *T<sub>1</sub> measurements*

The determination of relaxation time for the hydride resonances of complex **20a** was carried out using the standard inversion recovery method. The obtained  $T_1$  value was 276 ms at room temperature (400 MHz), confirming the presence of a classical trihydride complex. Unfortunately, due to technical problems of the NMR spectrometer,  $T_{1\min}$  measurements were not performed, thus it was not possible to show the existence of a dihydrogen hydride species **20b**.

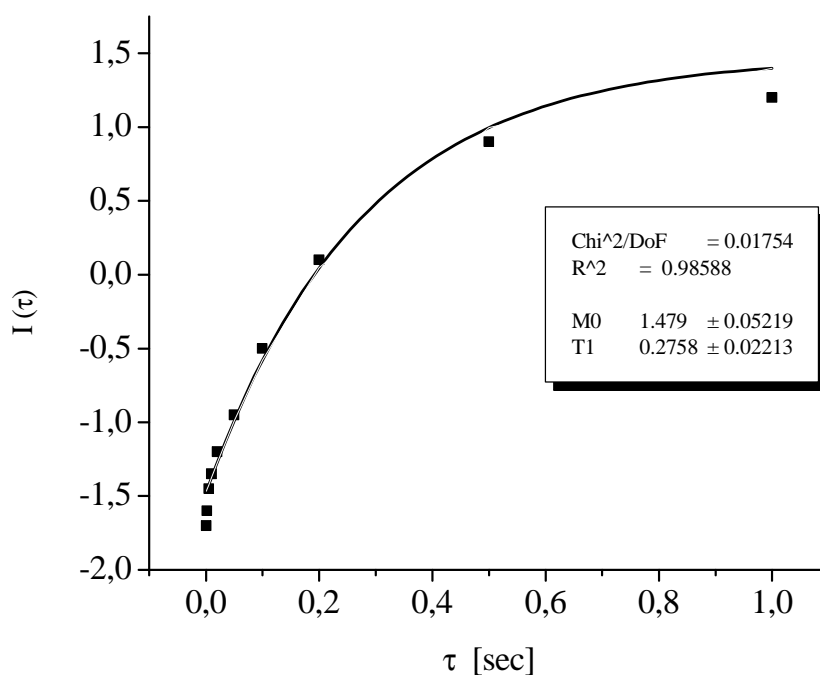


**Fig. 3.5**  $T_1$  for complex **20**.

Short  $T_{1\min}$  values (< 80 ms) are usually diagnostic to the presence of dihydrogen bound to the metal center, such as in the case of  $\text{Ir}(\text{PCy}_3)_2\text{H}_6^+$ .<sup>121</sup> In contrast, larger  $T_{1\min}$  values (> 150 ms) imply that the relaxation time is much slower, the distance between the hydrogen nuclei is larger and that classical hydrides are present.<sup>122, 123, 124, 125</sup>

### DFT calculations

DFT calculations have been used extensively in order to provide a fundamental understanding of both structure and bonding, as well as the dynamic processes in dihydrogen complexes.<sup>122, 126</sup> DFT calculations with the BP-86 functional were therefore performed on complex **20** (Fig. 3.6).<sup>127</sup> The distance between the hydrogen atoms was varied from 1 Å ( $\eta^2$ -dihydrogen hydride complex) up to 1.7 Å (trihydride complex).

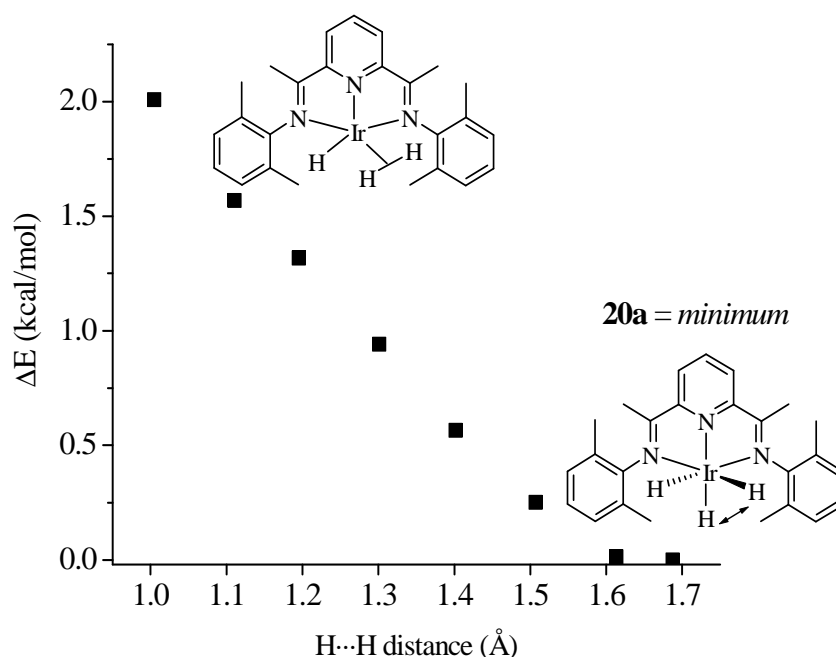


**Fig. 3.6** Energy diagram for the conversion of the complex **20a** to **20b** by varying the H-H distance (DFT model, BP-86; basis set: TZVP (for Ir) and SV(P) (for the rest of atoms)).

The minimum for complex **20** was found to be the trihydride complex **20a**, lying 2 kcal/mol below the  $\eta^2$ -dihydrogen hydride complex **20b**. This energy difference between the two structures is very small, which is the reason why **20a** and **20b** could not be distinguished by NMR spectroscopy.

Also, molecular dynamics calculations were undertaken for complex **20a**. The intramolecular H-H site exchange between hydrogen atoms is displayed in Figure 3.7.

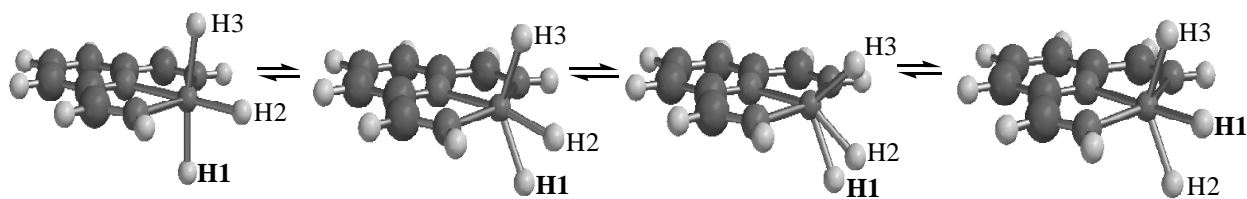
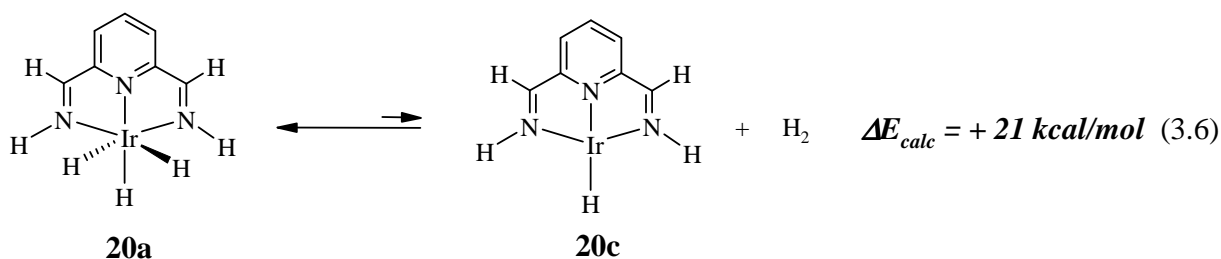


**Fig. 3.7** H-H site exchange in complex **20a**.

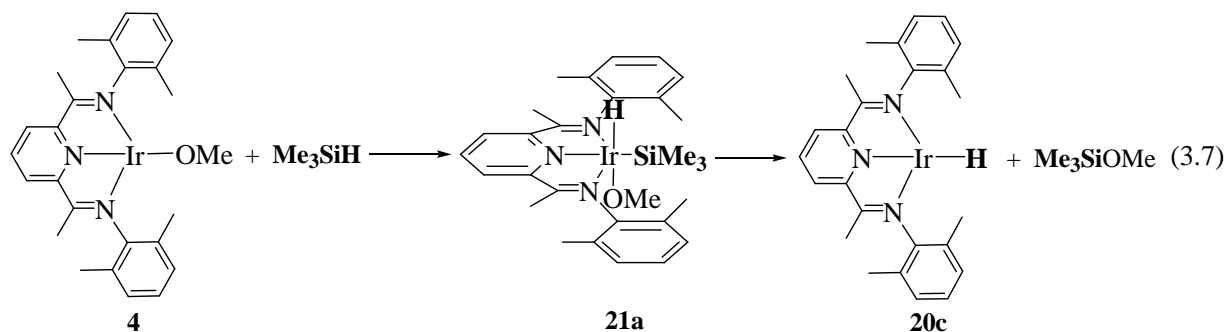
The extrusion of dihydrogen from the trihydride (model) complex **20c** was calculated (eq. 3.6).



It was found to be a thermodynamically unfavorable process (+ 21 kcal/mol). If an entropical contribution (~ 10 kcal/mol at RT for the formation of dihydrogen and monohydride complex **20c**) is also considered, then  $\Delta G$  for the overall process is in the order of 10 kcal/mol. This encountered problem may be the reason why the crystals of complex **20a** were not obtained.

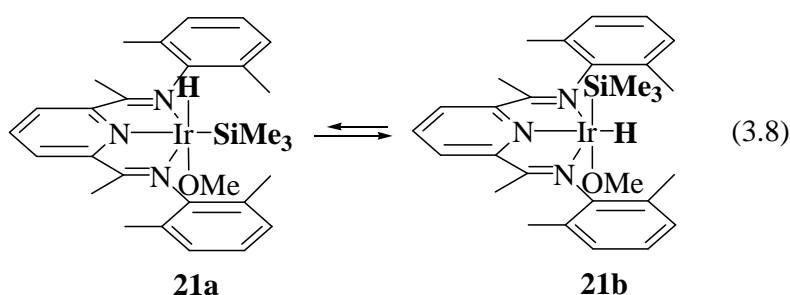
### 3.2.2 Si-H activation process

Further evidence for a two-step C-H activation mechanism was provided by low temperature NMR studies of complex **4** for the Si-H activation process in trimethylsilane. It is assumed that upon the addition of  $\text{Me}_3\text{SiH}$  to complex **4**, Ir(III) intermediate **21a** is formed (eq. 3.7).



The reaction was carried out on the NMR scale in THF- $d_8$ . Excess of  $\text{Me}_3\text{SiH}$  was condensed to a frozen solution of complex **4**, the tube sealed and then allowed to warm up to  $-80\text{ }^\circ\text{C}$ .

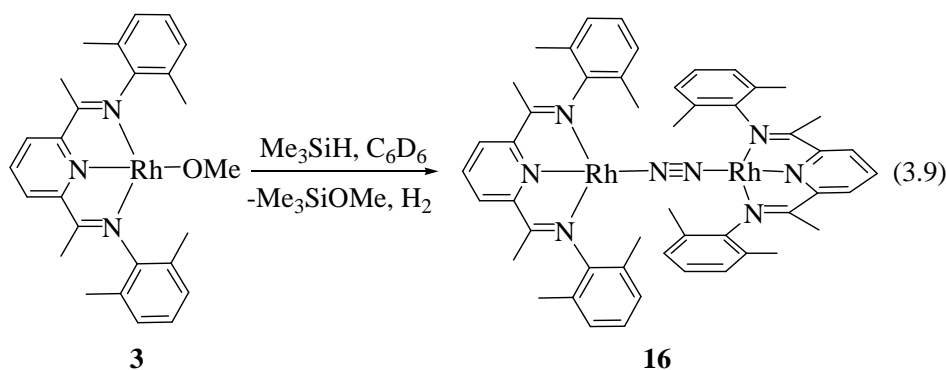
The  $^1\text{H}$ -NMR spectrum of the reaction mixture was monitored starting from  $-80\text{ }^\circ\text{C}$ . Upon warming up to  $-59\text{ }^\circ\text{C}$ , two hydride resonances at  $-28.30$  and  $-11.50$  ppm started to grow in. Both of the signals appeared as singlets and no  $^{29}\text{Si}$  satellites were detected. The  $^{29}\text{Si}$  satellites have been observed in cases of  $\eta^2$ -silane complexes.<sup>128, 129</sup> Therefore, it is anticipated that octahedral intermediate isomers (cis/trans) **21a** and **21b** are present (eq. 3.8).



Upon warming to  $-50\text{ }^\circ\text{C}$ , the peak at  $\delta = -28.30$  ppm disappeared and the intensity of the hydride resonance at  $\delta = -11.50$  ppm increased. At  $-35\text{ }^\circ\text{C}$ , another singlet peak in the hydride region ( $\delta = -6.20$  ppm) begins to appear while the other peak (at  $\delta = -11.50$  ppm) starts to decrease in intensity. This newly observed hydride peak has been tentatively assigned to the Ir-H complex **20c**. An additional resonance at  $\delta = 3.36$  ppm, later assigned to free  $\text{Me}_3\text{SiOMe}^*$ , appeared. The Ir-OMe peak at  $\delta = 4.67$  ppm decreased in intensity upon warming up the reaction mixture with a small shift ( $\sim 0.1$  ppm) towards lower field. Finally, upon reaching room temperature only the hydride resonance assigned to the monohydride (at  $\delta = -6.10$  ppm) remained. Unfortunately, after 1-2 hours at room temperature, the postulated monohydride complex decomposed to a mixture of unknown products (a broad peak at  $\delta = 18$  ppm was detected, similar to the one observed for the dinitrogen complex **16**;  $\text{N}_2$  residue originates from THF).

The same reaction with trimethylsilane was investigated for the Rh analogue **3** (eq. 3.9).

\*  $^1\text{H}$ -NMR of the  $\text{Me}_3\text{SiOMe}$ : in THF- $d_8$   $\delta = 0.06$  ppm ( $\text{Me}_3\text{SiOMe}$ ), 3.36 ppm ( $\text{Me}_3\text{SiOMe}$ );  
in  $\text{C}_6\text{D}_6$   $\delta = 0.06$  ppm ( $\text{Me}_3\text{SiOMe}$ ), 3.24 ppm ( $\text{Me}_3\text{SiOMe}$ ).



The mixture of **3** and  $\text{Me}_3\text{SiH}$  was gradually allowed to warm up (from the frozen solution to room temperature) and the  $^1\text{H-NMR}$  spectra were recorded over period of 30 minutes. The reaction proceeded rapidly and broad signals at  $\delta = 5$  ppm and 21 ppm were detected after only 5 min. No hydride peak was detected during the reaction. By comparing the observed, characteristic broad resonances (at  $\delta = 5.01, 5.26, 17.2$  and  $20.2$  ppm), the formation of the dinuclear Rh dinitrogen complex **16** was confirmed. The peak at  $\delta = 0.58$  and  $3.24$  ppm was assigned to free  $\text{Me}_3\text{SiOMe}$ .

Based on the  $^1\text{H-NMR}$  experiments, the mechanism presented in Figure 3.8 for the Si-H activation is proposed. DFT calculations on the model complex (B3LYP, LACVP\*\* basis set), excluding the aryl substituents and the ketimine methyl groups were performed.

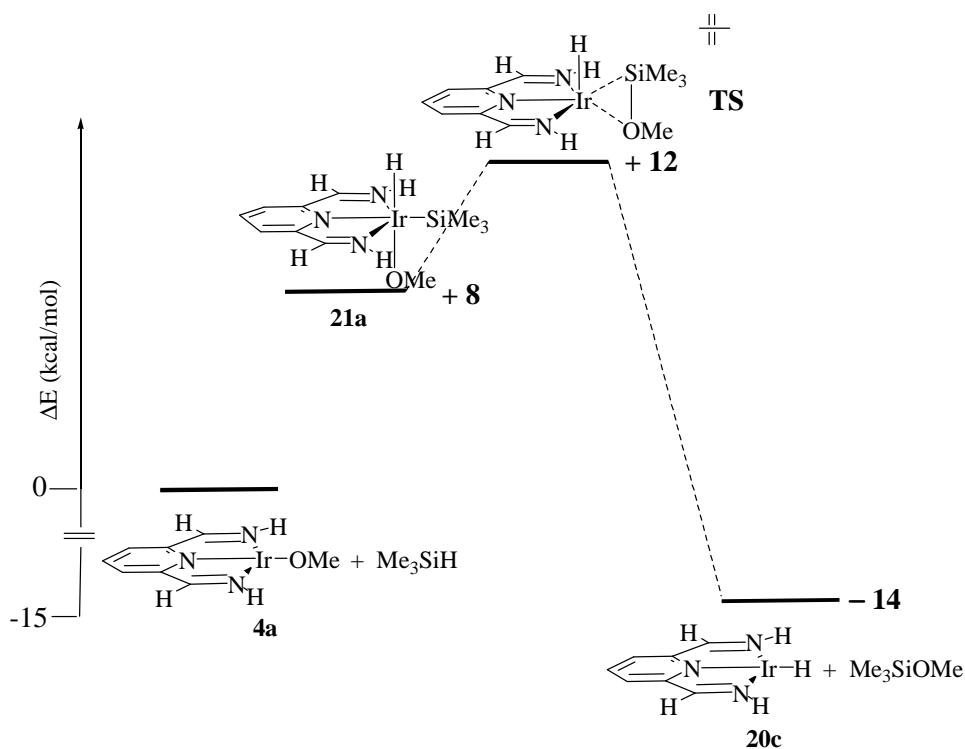


**Fig. 3.8** The proposed mechanism for Si-H activation.

The oxidative addition of Me<sub>3</sub>SiH to **4a** leads initially to the octahedral intermediate **21a**, which is 8 kcal/mol higher in energy. The second step of the reaction involves reductive elimination of Me<sub>3</sub>SiOMe, which is thermodynamically favourable by 14 kcal/mol relative to the reactants (**4a** + Me<sub>3</sub>SiH). The transition state (TS) for the reductive elimination of Me<sub>3</sub>SiOMe is 12 kcal/mol uphill starting from **4a** and silane.

IRC calculations were also carried out (B3LYP, LACVP\*\* basis set) starting at the saddle point to check the connections between the transition state, intermediate and the final product. As expected, the forward step leads to the product (**20c** + Me<sub>3</sub>SiOMe) and reverse to the intermediate (**21a**).

DFT calculations for the reductive elimination of methanol from the intermediate **21b**, were also performed. The reaction is uphill by 13 kcal/mol in comparison to the reactants, presumably because of the formation of weaker Ir-Si bond (compared with **20c** Ir-H).

### 3.3 Ir, Rh(I) fluorides – precursors for the hydride complexes

It has been shown that fluoride complexes provide a convenient synthetic route to hydride complexes.<sup>130</sup> With respect to the mechanistic studies related to C-H activation, suitable synthetic routes to the rhodium and iridium hydrides via the appropriate fluoride complexes were investigated. It is also believed that a rhodium hydride compounds would provide a good starting materials for the synthesis of a rhodium hydroperoxo complex, which is anticipated to be one of the intermediates in catalytic epoxidation of ethylene observed in previous studies.<sup>47</sup> The F<sup>-</sup> ligand is classified as a strong  $\pi$ -donor. It was expected that a pyridine diimine ligand could stabilize the Ir(Rh)-F bond due to its good  $\pi$ -acceptor abilities, as in the case for methoxo ligand in complex **4**.<sup>44</sup>

In the last decade, adequately characterized fluoro complexes started to appear in the literature.<sup>131, 132, 133, 134</sup> The difficulties involved in isolating pure metal-fluoro compounds arises from the great affinity of the fluoride anion towards protic reagents. Often, the target compounds are contaminated with hydroxide or bifluoride moiety. Another obstacle to isolate metal fluoride complexes is the possible reactions with glassware. Often plastic containers are used to overcome this problem. Elemental fluorine and hydrogen fluoride are not convenient reagents in



rhodium fluoride complex a doublet in the  $^{19}\text{F}$ -NMR due to the direct  $^1J_{\text{RhF}}$  coupling would be expected. In the literature there is also an example of  $\text{RhF}(\text{COD})(\text{PPh}_3)$  where coupling between Rh-F was not observed in the  $^{19}\text{F}$ -NMR even at  $-90^\circ\text{C}$  presumably due to the fast Rh-F dissociation.<sup>136</sup> This could also apply for complex **22**.

Crystals suitable for an X-ray structure analysis were obtained from a THF/pentane solution (Fig. 3.9).

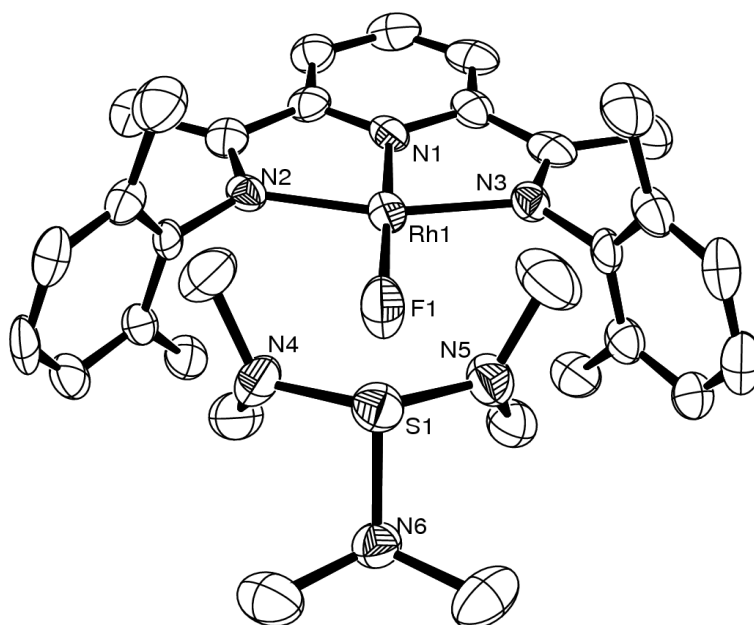


**Fig. 3.9** ORTEP plot of **22** shown at 50% thermal ellipsoid probability (hydrogen atoms and triflate anion were omitted for clarity).

Table 3.1 Selected bond lengths [ $\text{\AA}$ ] and angles [ $^\circ$ ] for complex **22**.

Rh1-F1	2.000(5)	Rh1-N1	1.854(6)	Rh1-N2	1.999(6)
Rh1-N3	2.015(6)	S1-N4	1.626(6)	S1-N5	1.601(6)
S1-N6	1.697(6)				
F1-Rh1-N2	99.9(2)	F1-Rh1-N3	100.3(2)	N1-Rh1-F1	178.3(2)
N1-Rh1-N3	80.4(2)	N2-Rh1-N1	79.3(2)	N2-Rh1-N3	159.7(2)

Complex **22** is isostructural with complex **23**. It crystallizes in an orthorhombic Pbc<sub>a</sub> space group. The bond distance Rh1-N1 is 1.854(6) Å, a significantly shorter than for chloro analogue (Rh-N1 = 1.889(2) Å).<sup>44</sup> The N-S bond distances are in agreement to the literature values for a sulfonium moiety.<sup>137</sup> A possible explanation why complexes **22** and **23** co-crystallize with a molecule of sulfonium triflate will be discussed later (*vide infra*).

### *Ir(I) fluoride complex – 23*

The <sup>1</sup>H-NMR spectrum of **23** displays singlet peaks assigned to the methyl groups on the ketimine ( $\delta = 1.01$  ppm), phenyl rings ( $\delta = 1.98$  ppm) and sulfonium cation ( $\delta = 2.73$  ppm) with an integration ratio 1:2:3.

In the <sup>19</sup>F-NMR spectrum of **23** (in THF-*d*<sub>8</sub>), besides the triflate peak at  $\delta = -80$  ppm an additional peak at  $\delta = -128$  ppm was found and was assigned to Ir-F ligand.

Crystals suitable for an X-ray diffraction of complex **23** were obtained from a THF/pentane (2:1) solution (Fig. 3.10). Selected bond distances and angles are given in the Table 3.2.

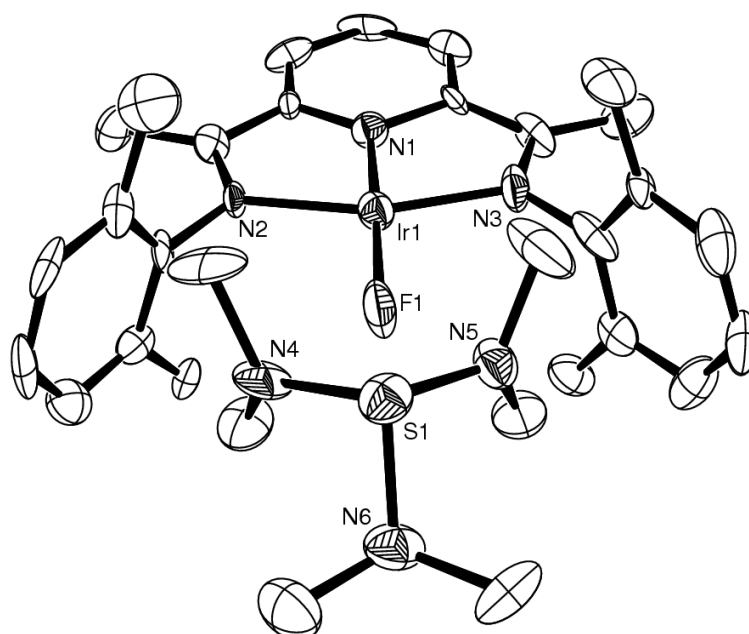


**Fig. 3.10** ORTEP plot of complex **23** (hydrogen atoms and triflate anion are omitted for clarity).

Table 3.2 Selected bond lengths [ $\text{\AA}$ ] and angles [ $^\circ$ ] for complex **23**.

Ir1-F1	1.983(5)	Ir1-N1	1.825(6)	S1-N5	1.611(9)
Ir1-N2	1.992(8)	Ir1-N3	1.998(9)	S1-N4	1.627(2)
S1-N6	1.699(9)				
N1-Ir1-F1	177.5(4)	N2-Ir1-F1	100.4(3)	N3-Ir1-F1	100.5(4)
N2-Ir1-N1	78.9(4)	N1-Ir1-N3	80.3(4)	N2-Ir1-N3	159.1(4)

Complex **23** has a square planar geometry with the sum of the angles equaling  $360^\circ$ . The Ir-F distance is  $1.983(5) \text{ \AA}$ , while the distance between Ir1-N1 =  $1.825(6) \text{ \AA}$  is significantly shorter than in other iridium(I) complexes of this type (Table 3.3).<sup>47,44</sup>

Table 3.3	[Ir]-Cl <b>2</b>	[Ir]-OMe <b>4</b>	[Ir]-Me <b>18</b>	[Ir]-F <b>23</b>
Ir-N1 [ $\text{\AA}$ ]	1.889(4)	1.891(5)	1.942(3)	<b>1.825(6)</b>

A possible reason for the decrease in the distance in the Ir-N1 bond could be explained by molecular orbital analysis. As displayed in Fig. 3.11, a three-orbital–four-electron interaction between occupied  $p_z(\text{F})$ ,  $d_{xz}(\text{Ir})$  orbitals and an empty ligand pyridine based  $\pi^*$  acceptor orbital is observed in HOMO. The interaction between  $p_z(\text{F})$  and  $d_{xz}(\text{Ir})$  orbitals is antibonding. Nevertheless, by in-phase mixing of the pyridine  $\pi^*$  orbital, the system becomes strongly stabilized. This back donation to the  $\pi^*$  pyridine orbital could explain shortening of the Ir-N1 bond. The same kind of interaction was observed for the methoxo complex **4**.<sup>44</sup>

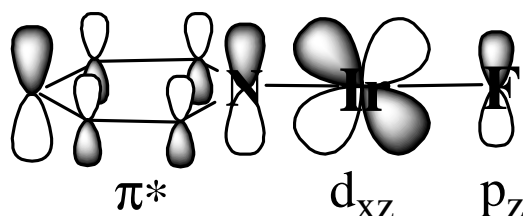
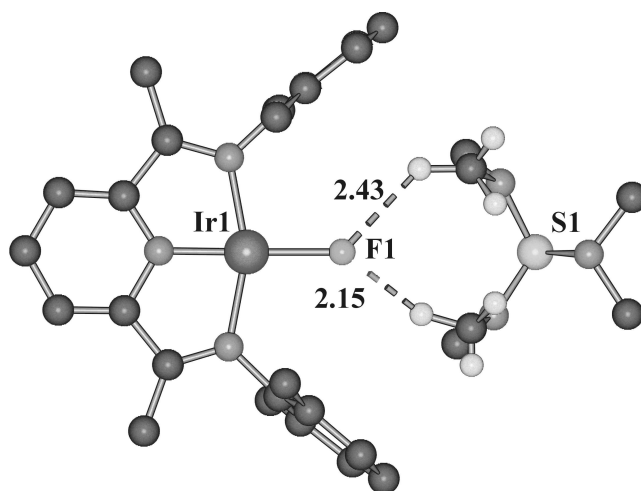


Fig. 3.11 HOMO of complex **23** (DFT, B3LYP hybrid, LACVP\*\* basis set).

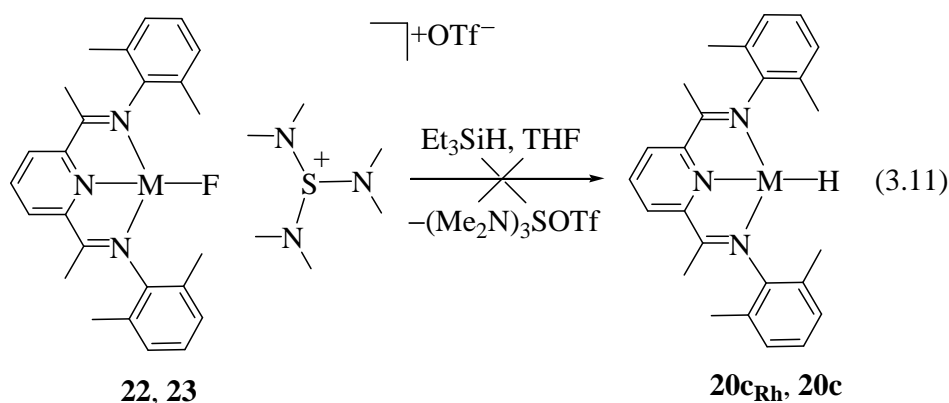
The aforementioned co-crystallization of the sulfonium triflate was of particular interest. A possible explanation for this behavior might be attributed to hydrogen bonding between the C-H...F atoms. The position of the protons on the tris-(dimethylamino)sulfonium cation were located in the difference Fourier map and were isotropically refined. As depicted in Figure 3.12, H...F1 distances are 2.43 Å and 2.15 Å, respectively. Both protons are only 0.62 Å (0.52 Å) above the IrNNF plane, whilst the sulphur atom is out of the plane by 2.32 Å. The H...F distances are in agreement with the values reported by Mews et al. between one of the axial fluoride from Me<sub>3</sub>SiF<sub>2</sub> anion and protons from (Me<sub>2</sub>N)<sub>2</sub>CF<sub>3</sub>S cation.<sup>138</sup> Other groups, such as Desiraju<sup>139</sup> and Scheiner<sup>140</sup> investigated hydrogen C-H...F bonding in fluorobenzenes and fluoromethanes and reported similar to CH...F distances.



**Fig. 3.12** CH...F bonding in complex **23**.

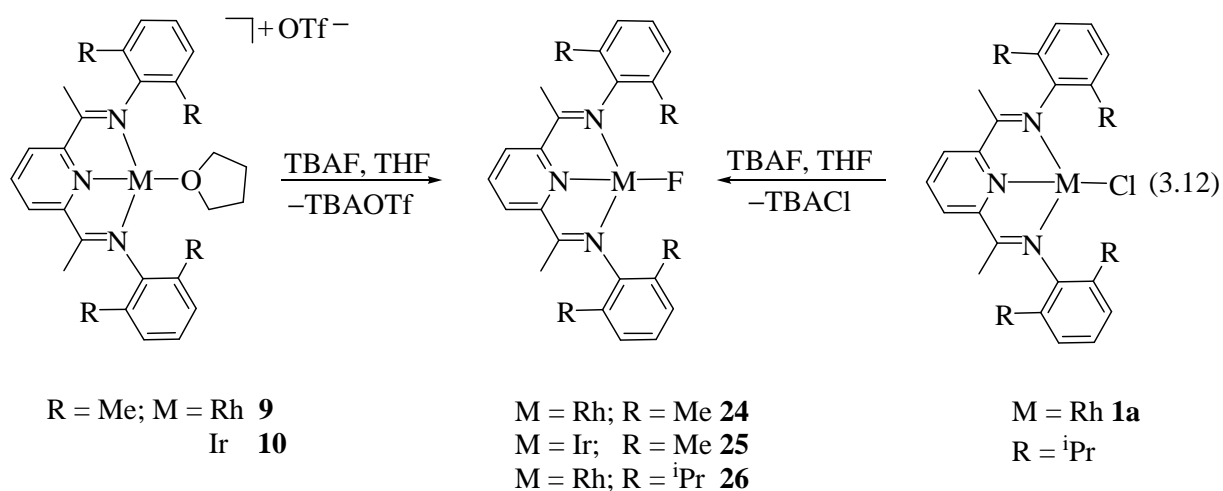
According to the literature, hydride complexes can be obtained from fluoride complexes through reaction of the latter with organosilanes. The driving force is the formation of a very strong Si-F bond (approximately 159 kcal/mol).<sup>141</sup>

The reactivity of complex **22** and **23** towards triethylsilane was tested. However, neither the formation of a metal hydride nor Si-F bond was detected in the <sup>1</sup>H and <sup>19</sup>F-NMR experiment. The reaction did not take place probably because the fluoride is shielded by the sulfonium cation (eq. 3.11).



In another attempt to obtain rhodium and iridium fluoride complexes, tetrabutylammonium fluoride (TBAF) was used. It has been recently reported that TBAF exceeds the reactivity of other nucleophilic fluorinated reagents. Anhydrous TBAF has been synthesized from tetrabutylammonium cyanide and hexafluorobenzene at low temperature through nucleophilic aromatic substitution reaction.<sup>142</sup>

When a cold THF solution of triflate complex **9** or **10** was added to a cold solution of freshly prepared TBAF in THF ( $-35\text{ }^\circ\text{C}$ ) and stirred for 1 hour at room temperature, complexes **24** or **25** were formed in 70 % yield (eq. 3.12).



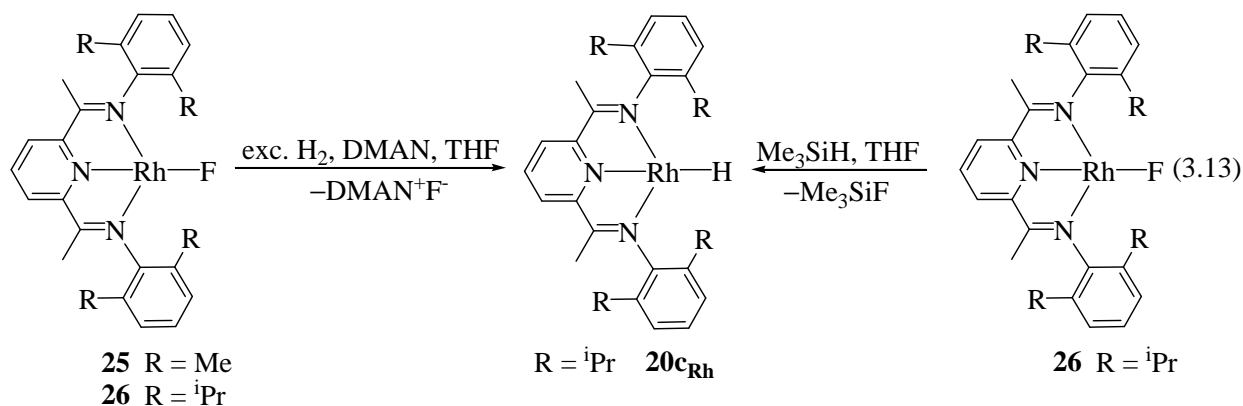
Complexes **24** and **25** have been characterized by  $^1\text{H}$  and  $^{19}\text{F}$ -NMR spectroscopy. The  $^1\text{H}$ -NMR spectrum (in THF- $d_8$ ) of **24**, **25** and **26** revealed the traces of tetrabutylammonium chloride, which could not be removed. Proton resonances of **24** and **25** are slightly shifted in the aliphatic region (0.1 ppm) when compared to the  $^1\text{H}$ -NMR of **22** and **23**. The resonances of the aromatic region are on the same shift. The presence of doublet in  $^{19}\text{F}$ -NMR spectrum at  $\delta = -151.5$  ppm

with the coupling constant  $^1J_{\text{RhF}} = 121$  Hz, confirms the formation of Rh-F bond in complexes **24** and **26**. The peak at  $\delta = -262.3$  ppm ( $^{19}\text{F}$ -NMR) was assigned to the fluoride for complex **25**, which is significantly shifted in comparison to complex **23**. This observation could be attributed to the less shielded fluoro ligand in **25** leading to a shift towards higher fields in the  $^{19}\text{F}$ -NMR spectrum.

It is worth mentioning that metathesis of the chloro ligand (by fluoro ligand) in **1a** could be also accomplished. In the cases with different substituents on the phenyl ligand, chloride could not be substituted with the fluoride via this route.

In order to obtain a mono-hydride complex, complex **24** and **26** were treated with excess hydrogen (eq. 3.13). The released HF was trapped with a base 1,8-bis-(dimethylamino)naphthalin, known as proton sponge. Since the reaction was not stoichiometrically controlled and hydrogen was used in excess, a mixture of mono and tri-hydride species were formed in the solution according to the  $^1\text{H}$ -NMR where several singlet peaks in the range from  $-9$  to  $-35$  ppm were observed.

In order to use the formation of the strong Si-F bond (*vide supra*) as a driving force for the formation of Rh-H, trimethylsilane ( $\text{Me}_3\text{SiH}$ ) was added to complex **26** (eq. 3.13). Trimethylsilane was prepared from  $\text{Me}_3\text{SiCl}$  by the reduction with  $\text{LiAlH}_4$ .<sup>143, 144</sup> As  $\text{Me}_3\text{SiH}$  has a boiling point of  $-10$  °C, it was treated as a gas and transferred to the  $\text{THF-d}_8$  solution of complex **26** using a known volume bulb manometer. The color of the reaction mixture changed from green to violet and then brown.



A doublet at  $\delta = -29.9$  ppm in the  $^1\text{H}$ -NMR spectrum was observed and assigned to the hydride complex **20c<sub>Rh</sub>**. In the  $^{19}\text{F}$ -NMR spectrum, the doublet from Rh-F coupling (at  $\delta = -151.5$  ppm)

disappears and the singlet peak at  $\delta = -158.4$  ppm assigned to Si-F appears. The Si-F resonance for Me<sub>3</sub>Si-F can be compared with the literature value found at  $\delta = -159$  ppm (Fig. 3.13).<sup>145</sup>

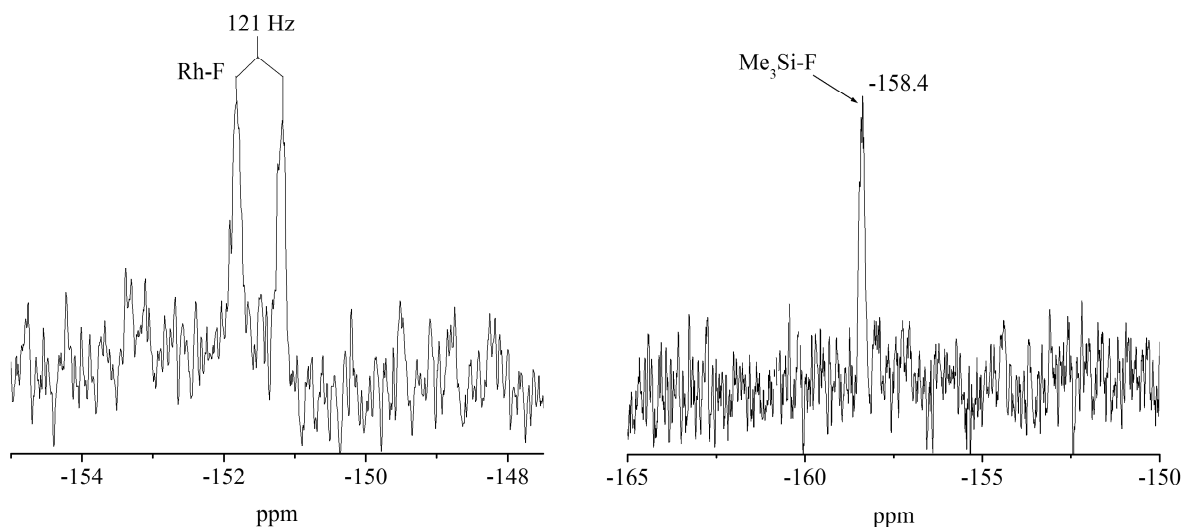


**Fig. 3.13** <sup>19</sup>F-NMR before and after reaction of **26** with Me<sub>3</sub>SiH.

Although, the obtained crystals of complex **20c<sub>Rh</sub>** were not of good enough quality for the X-ray structure analysis, the NMR spectroscopy indicated that the formation of the Rh(I) hydride from the fluoride analogue is feasible.

The formation of the Rh(I) hydride species from Rh(I) fluoride was calculated for the model compounds **20c<sub>Rh</sub>** and **26a** at B3LYP/LACVP\*\* level (Fig. 3.14).

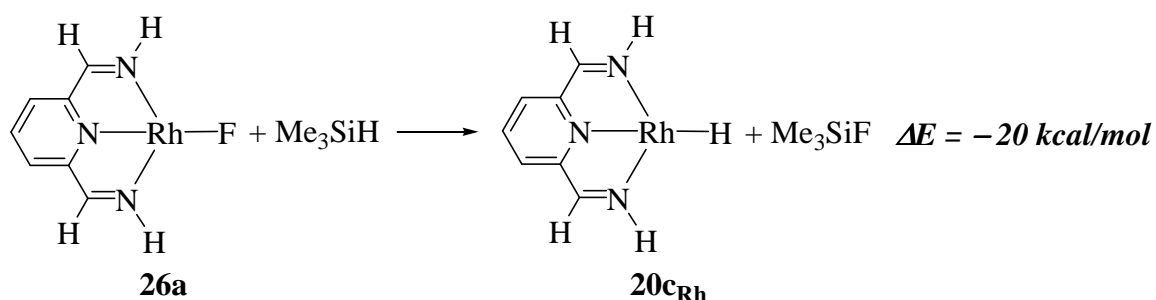


**Fig. 3.14** DFT calculations for the formation of **20c<sub>Rh</sub>**.

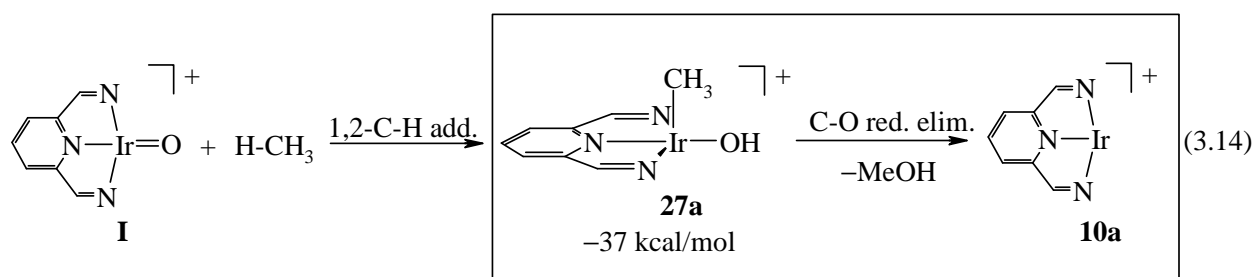
As depicted above, the formation of the hydride complex **20c<sub>Rh</sub>** is thermodynamically favorable by 20 kcal/mol.

### 3.4 C-O reductive elimination

The formation of a C-O bond by reductive elimination is an important part in an alkane functionalization process. The final products are usually alcohols, amines, ethers and esters. Despite the great importance of this reaction in homogeneous catalysis<sup>24, 27</sup> a limited number of the directly observed metal centered C-O bond formation reactions are known.<sup>146, 147, 148, 149, 150</sup>

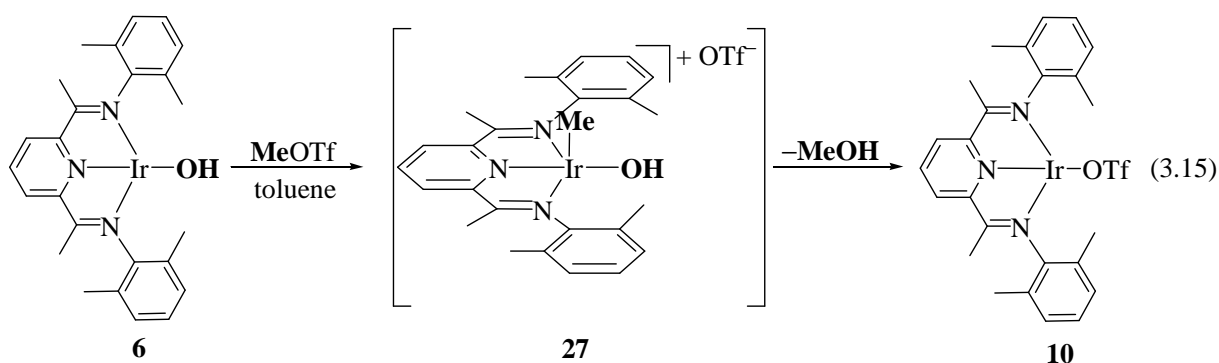
The reductive elimination from  $d^6$  octahedral complexes mostly proceeds via ligand dissociation and formation of five-coordinate intermediate prior to the actual reductive elimination step.<sup>151, 152, 153</sup> The energy barriers for the C-O or C-C reductive elimination in square-pyramidal penta-coordinated systems are much smaller than the energy barriers for same process which occurs without the ligand loss, from the six-coordinated complexes. This process has been studied by Goldberg et al. for the Pt(IV) complexes.<sup>154, 155</sup>

The C-O bond formation is one important part in the proposed catalytic cycle for methane functionalization (Chapter 1). Based on the DFT calculations for the Ir model complex (eq. 3.14), C-H bond addition, which is strongly thermodynamically favorable, leads to the hydroxy alkyl intermediate **27a**. The second step involves reductive elimination of methanol, which leads to the formation of the cationic species **10a**.



In order to provide support for C-O reductive elimination of methanol via intermediate **27a** (eq. 3.14), a low temperature NMR experiment of the reaction 3.15 was performed (*vide infra*).

Addition of MeOTf to a toluene solution of **6** at room temperature leads to the fast and clean formation of complex **10** and methanol. To provide the evidence for intermediate **27**, low temperature NMR experiment was performed.



The reaction shown in eq. 3.15 was monitored from  $-80\text{ }^{\circ}\text{C}$  to  $25\text{ }^{\circ}\text{C}$  for 2 hours in toluene- $d_8$ . During, the first 45 minutes, the temperature was held at  $-80\text{ }^{\circ}\text{C}$ . Even after 2 minutes at  $-80\text{ }^{\circ}\text{C}$ , three new singlet peaks appeared at  $\delta = 2.60$ ,  $2.98$  and  $5.30$  ppm. The resonances at  $\delta = 2.60$  (Ir-CH<sub>3</sub>) and  $5.30$  ppm (OH-broad) were tentatively assigned to the intermediate species **27**. When the reaction mixture was further warmed up, the intensity of peaks at  $2.60$  and  $5.30$  ppm decreased, while the peak at  $2.98$  ppm gained intensity. At  $-30\text{ }^{\circ}\text{C}$ , of these three peaks the singlet resonance at  $\delta = 2.98$  ppm remained. This resonance was assigned to free methanol ( $^1\text{H-NMR}$  of MeOH in toluene- $d_8$ :  $\delta = 3$  ppm).

In the  $^{19}\text{F-NMR}$  spectra (at  $-80\text{ }^{\circ}\text{C}$ ) three peaks are observed at:  $\delta = -76.0$  ppm assigned to the free MeOTf ( $^1\text{H-NMR}$  of MeOTf in toluene- $d_8$ :  $\delta = 3.03$  ppm;  $^{19}\text{F-NMR}$ :  $\delta = -76.1$  ppm),  $\delta = -79.2$  ppm assigned to the intermediate **27** and  $\delta = -80.0$  ppm assigned to the triflate complex **8**. After the reaction was completed, the solvent was evaporated. The  $^1\text{H}$  and  $^{19}\text{F-NMR}$  spectra of the final product (in THF- $d_8$ ) unambiguously confirmed the formation of complex **10**.

### *Mechanistic aspects*

The highly nucleophilic character of  $d^8$ -configured metal centers in the square planar coordination geometry is based on the  $^1\text{H-NMR}$  experiment.<sup>28</sup> A nucleophilic attack on the carbon as the first step followed by reductive elimination of methanol is proposed. It was also observed in the  $^1\text{H-NMR}$  study that the nucleophilic substitution step in MeOTf is significantly faster than the C-O reductive elimination of methanol. The presence of an intermediate provided further support for the proposed mechanism.

DFT calculations presented in Fig. 3.15 are concerned with the C-O reductive elimination part starting from the proposed intermediate **27a**. The calculations were carried out at the B3LYP/LACVP\*\* level in toluene.

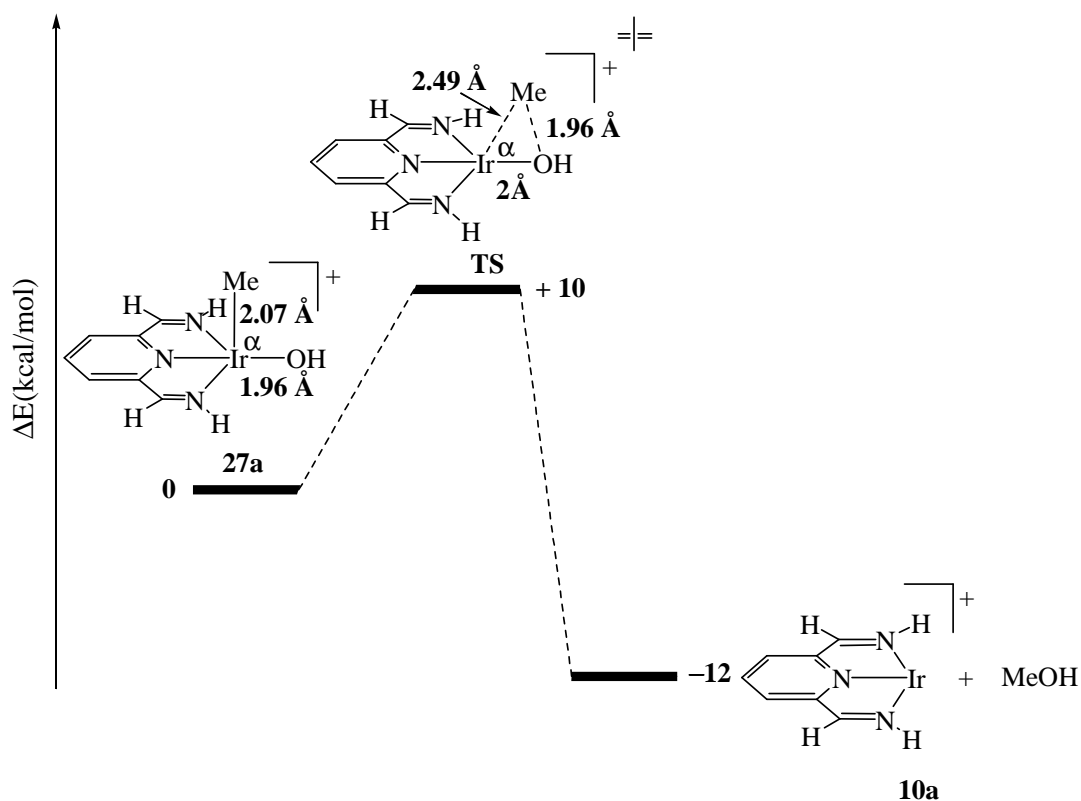
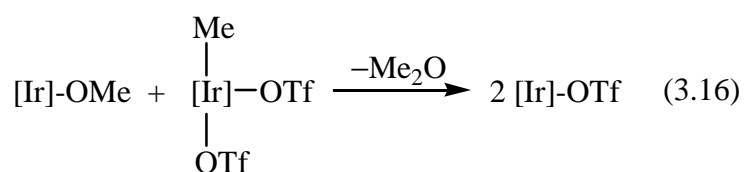


**Fig. 3.15** Reaction profile for the C-O reductive elimination of methanol from **27a**.

The reductive elimination (**27a**  $\rightarrow$  **10a**) is exothermic with an energy difference of  $\sim 12$  kcal/mol and a calculated energy barrier for this process of 10 kcal/mol. In the transition state **TS**, the C-Ir-O angle becomes more acute (starting from  $100^\circ$  in **27a** to  $50^\circ$  in **TS**) with concomitant elongation of the Ir-Me bond. By decreasing the angle between the methyl group and the hydroxide, the C-O bond distance shortens and methanol is formed.

C-O bond formation is independently observed in the synthesis of the triflate complex **10** (Chapter 2.1.1). When **4** and **8** were stirred together dimethyl ether was formed (eq. 3.16).

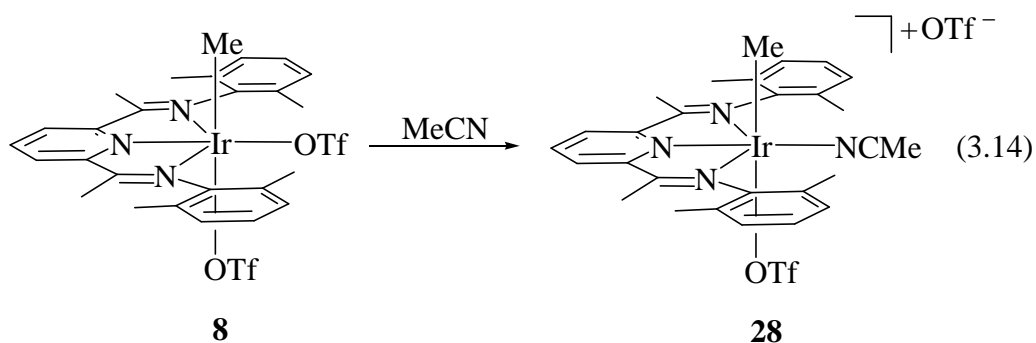


The mechanism proposed for the reaction according to eq. 3.16 was adopted from the C-C coupling reaction of **7** and Rh(I) methyl complex.<sup>28</sup>

In both cases (C-C<sup>44</sup> or C-O bond formation), the methyl group on the Rh, Ir(III) centers has attributed an *electrophilic* character. To address this point, <sup>13</sup>C labeled bistriflate complexes (**7** and **8**) were prepared and <sup>1</sup>H-NMR spectra in CD<sub>2</sub>Cl<sub>2</sub> were measured. The coupling constant (<sup>1</sup>J<sub>CH</sub>) of the methyl group, in complex **7** is <sup>1</sup>J<sub>CH</sub> = 140 Hz and 135 Hz in **8**. According to the literature, polar substituents in alkanes (for example CH<sub>4</sub>) influence on the coupling constant and hybridization of the carbon. Depending on the nature of the substituent, the carbon centers are more *electrophilic* or *nucleophilic*, which is determined by field-gradient factor *F*. As a result, by comparison to the literature values,<sup>156</sup> it was proposed that carbon bonded to metal centers have an *electrophilic* character in complexes **7** and **8**.

In addition, it is worth mentioning that the methyl group exhibits a strong *trans* influence. Therefore, the bond distances between the metal and the oxygen from the triflate group, in the apical position is elongated (Rh-O<sub>ap</sub> = 2.305(4) Å) in comparison to the Rh-O<sub>eq</sub> equatorial bond (2.093(3) Å).<sup>44</sup> After spectroscopic (IR, <sup>19</sup>F-NMR) and conductivity measurements, the triflate *trans* to the methyl group was described with partially ionic character. The same observations were reported by Brookhart et al. for the Rh(III)-methyl-bistriflate complex with the isopropyl groups on the phenyl rings. In this complex Rh-O<sub>ap</sub> distance is 2.358 Å and the author describes the Rh metal center as pentacoordinate. For this reason, it could be expected that the triflate in the apical position would be substituted in further reactions.

Addition of acetonitrile to the light green complex **8**, resulted in the color change to red and the formation of **28** in quantitative yield (eq. 3.14).



Complex **28** is fully characterized by  $^1\text{H}$ ,  $^{13}\text{C}$  and  $^{19}\text{F}$ -NMR spectroscopy. The  $^1\text{H}$ -NMR spectrum in  $\text{CD}_2\text{Cl}_2$  revealed a new singlet peak at  $\delta = 2.21$  ppm assigned to the acetonitrile ligand. The integration ratio between different methyl groups is 1:1:2:4. Two singlets at  $\delta = -79.50$  and  $-79.62$  ppm were observed in the  $^{19}\text{F}$ -NMR spectrum.

Crystals suitable for an X-ray structure analysis were obtained from a THF/pentane solution. The molecular structure and the selected bond distances and angles were presented in Figure 3.16 and Table 3.4.

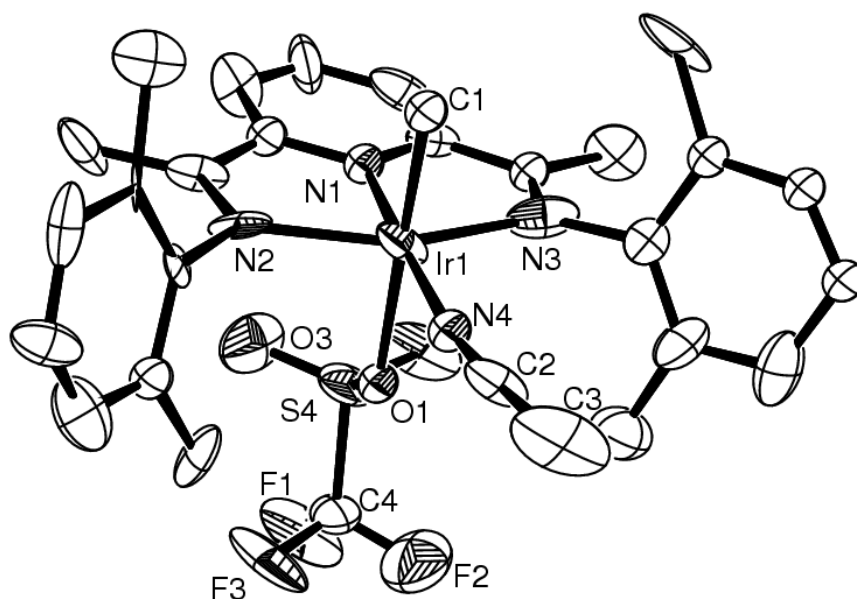


**Fig. 3.16** ORTEP plot of complex **28** with 50% thermal ellipsoids (non-coordinated triflate and hydrogen atoms were excluded for clarity).

Table 3.4 Selected bond lengths [Å] and angles [°] for complex **28**.

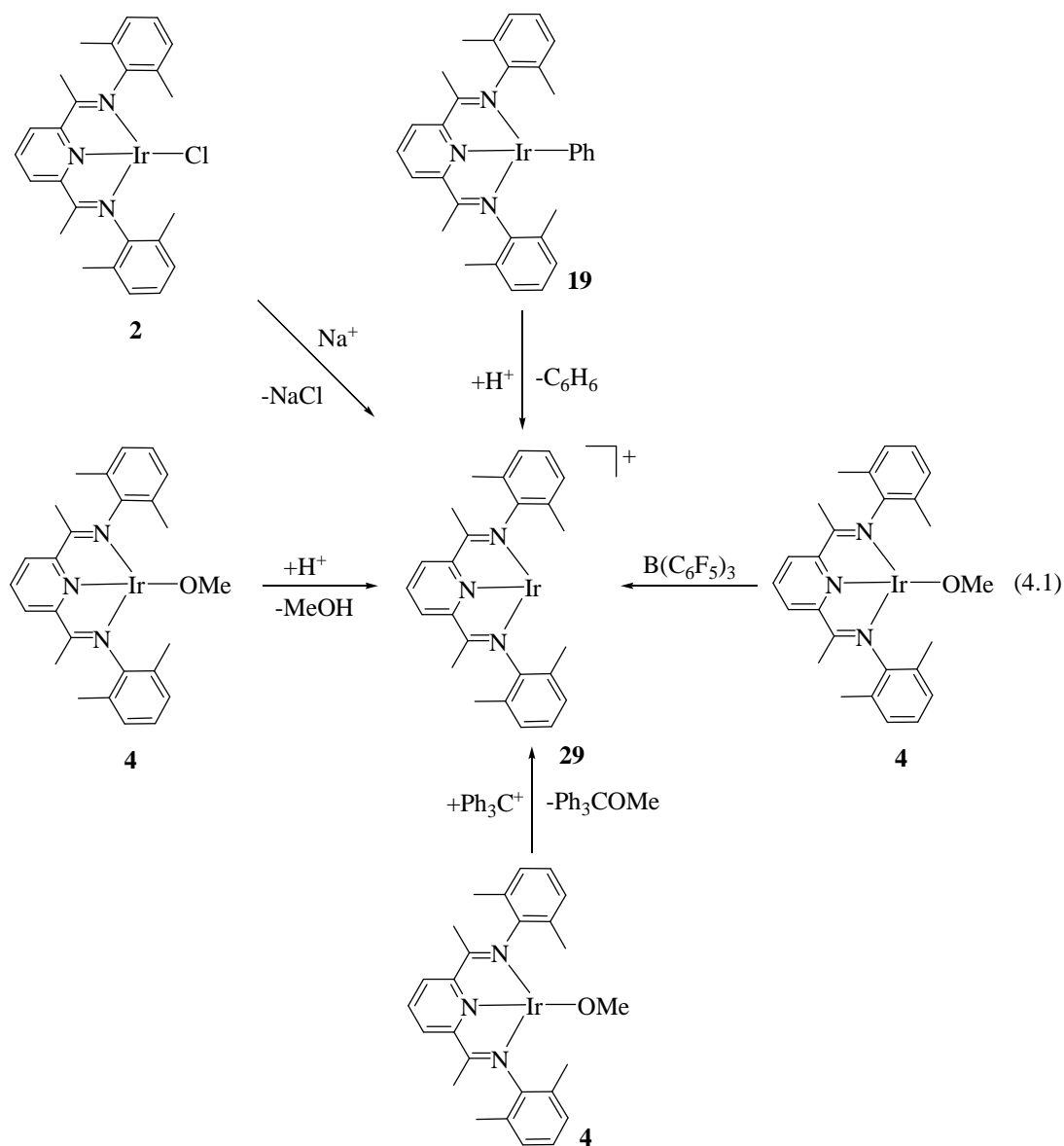
Ir1-N1	1.88(4)	Ir1-N2	2.10(3)	Ir1-N3	2.05(4)
Ir1-N4	1.95(4)	Ir1-C1	2.05(4)	Ir1-O1	2.26(2)
N1-Ir1-N4	178.1(1)	N2-Ir1-N1	80.1(1)	N3-Ir1-N1	79.1(1)
C1-Ir1-O1	177.6(1)	N1-Ir1-O1	88.2(1)	N1-Ir1-C1	94.1(1)
N2-Ir1-O1	93.0(9)	N2-Ir1-C1	86.9(1)	N2-Ir1-N4	101.8(1)
N3-Ir1-O1	91.2(1)	N3-Ir1-C1	89.8(1)	N3-Ir1-N4	99.0(1)
N3-Ir1-N2	158.6(1)	N4-Ir1-C1	85.9(1)	N4-Ir1-O1	91.8(1)

The ligand environment around the Ir(III) center is octahedral with the sum of the equatorial angles equaling 360° and N2-Ir1-O1 = 93.0(9)° N2-Ir1-C1 = 86.9(1)°. The methyl group is *trans* to the triflate group with the C1-Ir1-O1 angle equaling 177.6°. The bond distance Ir1-O1 (2.26(2) Å) is in the range of the reported values.<sup>44, 49, 50, 48</sup> Compared to Rh1-O1 bond distance in **7**, Ir1-O1 is shortened by 0.1 Å. Nevertheless, the *trans* influence of the methyl group is still evident. The equatorial coordination site is occupied by the acetonitrile ligand with Ir1-N4 = 1.95(4) Å. The ligand shows an almost linear arrangement with the angle Ir1-N4-C2 = 170.0° and N4-C2-C3 = 176.4° similar to the one found in cationic [Rh(PPh<sub>3</sub>)<sub>3</sub>(CH<sub>3</sub>CN)]BF<sub>4</sub> or neutral [Rh(PNP)(CH<sub>3</sub>CN)] complexes.<sup>157, 158</sup>

The results reported in this section are focused on the first two steps proposed in the catalytic cycle (Chapter1); C-H activation and C-O reductive elimination. Further evidence that C-H activation occurs via a two-step process (oxidative addition and reductive elimination) was provided. This was supported by the formation of Ir(III) trihydride intermediate as well as the Si-H activation in trimethylsilane. The second part was related to C-O bond formation, which was investigated by NMR spectroscopy and compared to the findings from our previous research.<sup>47, 28</sup>

## 4 Cationic complexes

This chapter focuses on different approaches for the synthesis and isolation of three-coordinated cationic complexes. The syntheses and characterization of cationic compounds **9**<sup>47</sup> and **10** with a THF molecule coordinated to the metal center have been described in Chapter 2.1.1. However, the main goal of this work is the isolation of cationic complex or related compounds with more weakly coordinated ligands such as, for example, diethyl ether. As will be described later, the purity of the solvents plays an important role in the crystallization process of these types of compounds. Cationic complexes are part of the proposed alkane functionalization cycle (Chapter 1) and several reactions were anticipated as good routes to the desired species **29** (eq. 4.1).

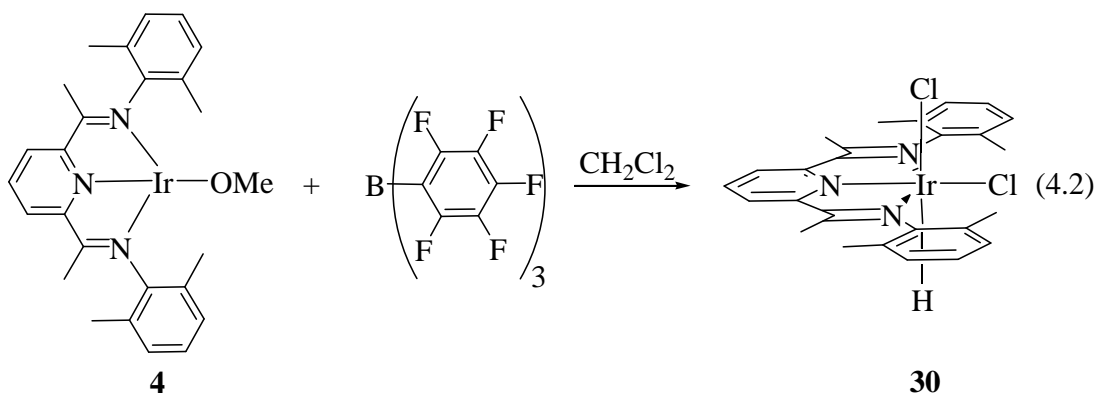


Based on results of Brookhart et al.,<sup>159</sup> one promising route was to use sodium salts of weakly coordinated anions (such as  $\text{NaBAr}^{\text{F}}_4$ ) together with complex **2** in non-coordinated solvent to form complex **29** in salt–metathesis reaction. In order to avoid further reaction between complex **29** and chlorinated solvents such as  $\text{CH}_2\text{Cl}_2$  or  $\text{C}_2\text{H}_4\text{Cl}_2$  (*vide infra*), diethyl ether was used. However, the reaction did not take place even after 3 days of stirring at room temperature (no visible changes in the  $^1\text{H-NMR}$  spectrum were observed).

This contrasts results reported by Brookhart et al. for the formation of Rh analogue.<sup>159</sup> For the synthesis of the latter, dichloromethane was used. The different reactivity observed for the Ir complex **29** and the Rh analogue could be attributed to the change in solvent.

#### 4.1 Unexpected formation of the Ir(III) hydride

Upon addition of a dichloromethane solution of tris-(pentafluorophenyl)borane into complex **4**, the color changed from green to reddish-brown and complex **30** was formed in 60 % yield (eq. 4.2).



The presence of an Ir-H moiety was confirmed by  $^1\text{H-NMR}$  spectroscopy, revealing a singlet peak at  $\delta = -18$  ppm in  $\text{CD}_2\text{Cl}_2$ . The methyl groups on the phenyl rings are chemically non-equivalent (opposite as in the square planar complexes), leading to two sets of singlet peaks at  $\delta = 2.02$  and  $2.40$  ppm with an integration ratio of 1:1. Finally, the formation of **30** was confirmed by an X-ray crystal structure analysis. The crystals were obtained from  $\text{CH}_2\text{Cl}_2$ /pentane solution at  $-35$  °C. A molecular representation of **30** and selected bond distances and angles are presented in Figure 4.1 and Table 4.1.

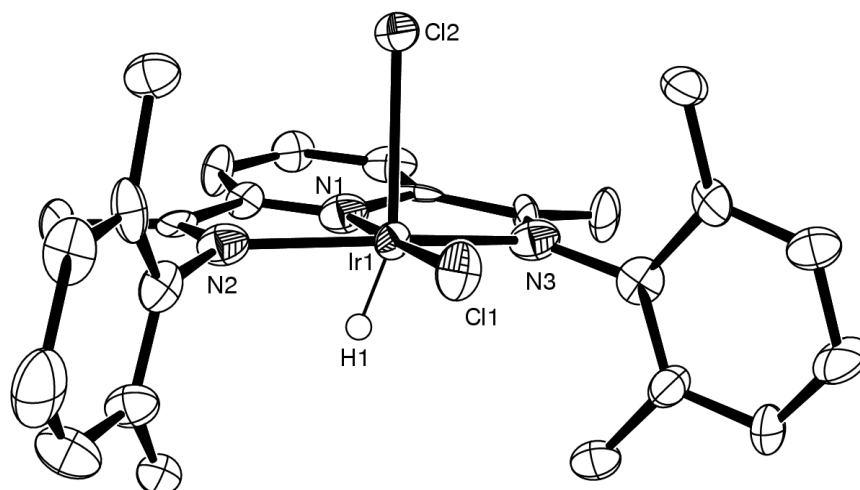


**Fig. 4.1** ORTEP plot of complex **30** with 50% probability level (hydrogen atoms except H1 were excluded for clarity).

Table 4.1 Selected bond lengths [Å] and angles [°] for complex **30**.

Ir1-N1	1.945(2)	Ir1-N2	2.050(2)	Ir1-N3	2.049(2)
Ir1-Cl1	2.354(5)	Ir1-Cl2	2.502(5)		
N2-Ir1-N3	158.2(6)	N2-Ir1-N1	78.1(7)	N3-Ir1-N1	81.0(6)
Cl1-Ir1-Cl2	93.7(2)	N1-Ir1-Cl1	177.5(5)	N1-Ir1-Cl2	83.9(4)
N2-Ir1-Cl1	101.3(5)	N2-Ir1-Cl2	92.4(4)	N3-Ir1-Cl1	99.8(4)
N3-Ir1-Cl2	91.4(4)				

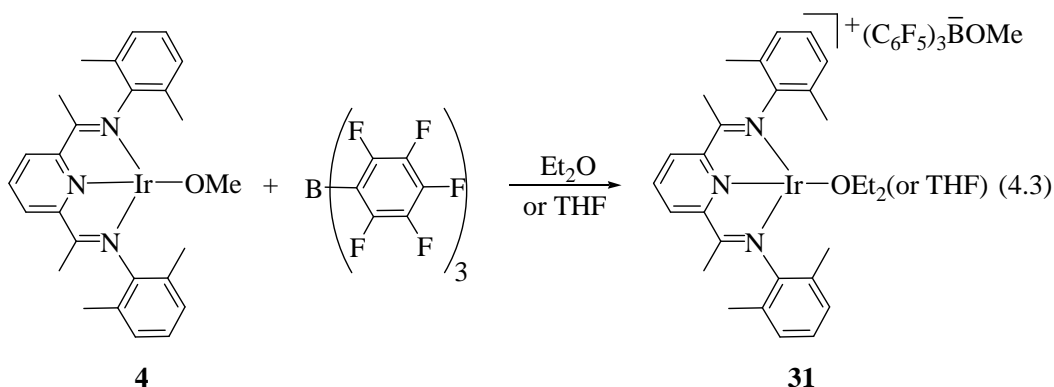
The coordination geometry around the iridium center is pseudo octahedral with the equatorial angles equaling  $359.3^\circ$  and  $\text{N2-Ir1-Cl2} = 92.4(4)^\circ$ . Two chloro ligands are arranged *cis* to each other with a  $\text{Cl1-Ir1-Cl2}$  angle  $93.7(2)^\circ$ . The position of the hydride was located in the difference Fourier map and was isotropically refined. The Ir1-Cl2 bond distance is elongated ( $2.502(5)$  Å) when compared to the Ir1-Cl1 bond distance ( $2.354(5)$  Å), due to the *trans* influence of the hydride ligand. It is in the range of Ir-Cl distances found for other complexes containing chloro ligands *trans* to the hydride ligand, as reported for  $[\text{Ir}(\eta^3\text{-cyclooctenyl})(\text{Sb}^i\text{Pr}_3)_2\text{Cl}(\text{H})]^{160}$ ,

$[\text{Ir}(\text{PN})(\text{PPh}_3)\text{ClH}_2]$  (PN = (4S)-2-(2-(diphenylphosphino)phenyl)-4-isopropyl-1,3-oxazoline)<sup>161</sup> or  $[\text{Ir}(\text{NH}=\text{O})(\text{PPh}_3)_2\text{Cl}_2\text{H}]$ .<sup>162</sup>

In complex **30**, it may be assumed that the chloro ligands originate from the solvent. Complex **4** is not stable in chlorinated solvents (dichloromethane or 1,2-dichloroethane), forming **2** after 3 days (Chapter 2.1). The origin of the hydride is still unclear.

Similar reactions with  $\text{B}(\text{C}_6\text{F}_5)_3$  in dichloromethane and the formation of chloro complexes were already reported in the literature. For example, the exchange reaction between a methyl and a chloro ligand in dichloromethane have been described for  $[\text{CpTi}(\text{NP-}t\text{Bu}_3)(\text{NC}_5\text{H}_4\text{NMe}_2)\text{Cl}][\text{B}(\text{C}_6\text{F}_5)_4]$  and  $[\text{CpTi}(\mu\text{-Cl})(\text{NPPh}_2(\text{NP-}t\text{Bu}_3))_2][\text{B}(\text{C}_6\text{F}_5)_4]_2$ .<sup>163, 164</sup>

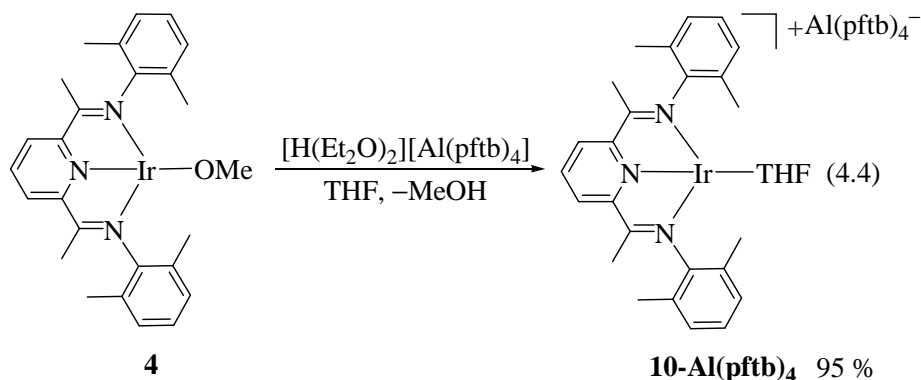
In order to avoid the formation of chloro complex **30**, the reaction (equation 4.2) was repeated using diethyl ether as a solvent. A color change from green to reddish-brown was observed and according to the spectroscopic data, complex **31** was obtained in 62 % yield.



Compound **31** is soluble in THF, diethyl ether and DME, partially soluble in non-polar solvents such as benzene or toluene and insoluble in pentane. According to the <sup>1</sup>H-NMR spectrum in THF-d<sub>8</sub>, the obtained complex is diamagnetic displaying sharp resonances in the aliphatic and aromatic region comparable to resonances observed for complex **10** (see Experimental part). The resonance assigned to the methoxo ligand in **4** was shifted from 4.67 ppm to 2.97 ppm (broad) in the newly formed complex **31**. The integration ratio of the different methyl groups is 4:2:1 as in **4**. The <sup>19</sup>F-NMR spectrum in THF-d<sub>8</sub> revealed three resonances at  $\delta = -133.9$ ,  $-165.4$  and  $-168.4$  ppm assigned to the *ortho*, *para* and *meta* fluorine in  $[\text{MeOB}(\text{C}_6\text{F}_5)_3]^-$  anion. Minor shifts are observed when compared with the resonances of free  $\text{B}(\text{C}_6\text{F}_5)_3$  ( $\delta = -135$ ,  $-159.6$  and  $-166.3$  ppm).

## 4.2 The formation of methanol from complex **4**

The addition of the strong cationic Brønsted acid  $[\text{H}(\text{Et}_2\text{O})_2][\text{Al}(\text{pftb})_4]^{165}$  to a THF solution of complex **4** at room temperature, resulted in the formation of the Ir(I) cationic complex **10-Al(pftb)<sub>4</sub>**. The color immediately changed to reddish-brown and complex **10-Al(pftb)<sub>4</sub>** was formed with concomitant elimination of methanol (eq. 4.4).



Compound **10-Al(pftb)<sub>4</sub>** was fully characterized with  $^1\text{H}$ ,  $^{13}\text{C}$  and  $^{19}\text{F}$ -NMR spectroscopy. The solubility of **10-Al(pftb)<sub>4</sub>** is comparable with **31**. However, in benzene or toluene, **10-Al(pftb)<sub>4</sub>** precipitates and turns to an oily material.

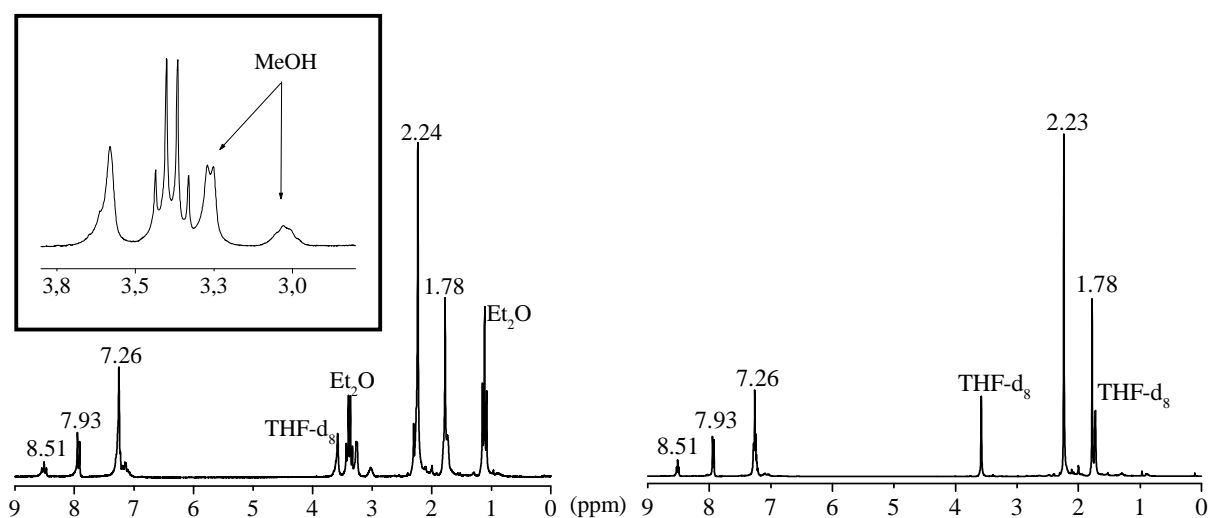


**Fig. 4.2** The  $^1\text{H}$ -NMR spectrum of the reaction mixture in eq. 4.4 and **10-Al(pftb)<sub>4</sub>** in  $\text{THF-d}_8$ .

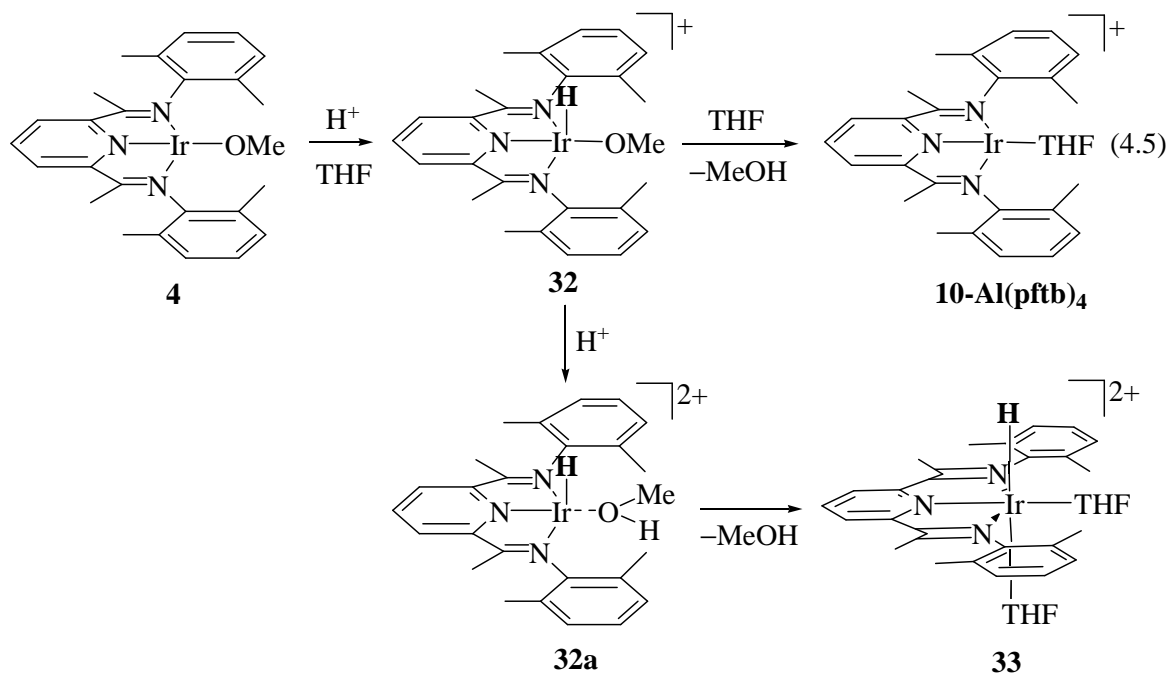
According to the  $^1\text{H}$ -NMR spectrum of the (1:1) reaction mixture (**4** :  $[\text{H}(\text{Et}_2\text{O})_2]^+$ ) in  $\text{THF-d}_8$ , the methoxide resonance ( $\delta = 4.67$  ppm) disappeared. New peaks, doublet at  $\delta = 3.26$  ppm and quartet at  $\delta = 3$  ppm appeared, which were assigned to methanol (Fig. 4.2 - left).

Methanol resonances are also found in the transferred volatiles at the aforementioned chemical shift. The coupling between the methyl group and hydroxide proton through the oxygen atom was observed, revealing a doublet and a quartet peak with the coupling constant  $^3J_{\text{HH}} = 5$  Hz. Diethyl ether from the acid was also observed in the transferred volatiles. In the  $^{13}\text{C}$ -NMR spectrum in  $\text{THF-d}_8$ , the methanol resonance appeared at  $\delta = 50$  ppm.

The proton resonances of  $\mathbf{10-Al(pftb)}_4$  (Fig. 4.2 - right) are found at the same chemical shift as in the complexes  $\mathbf{10}$  and  $\mathbf{31}$  leading to the conclusion that no influence of the different anion is present.

#### 4.2.1 Proposed mechanism for the methanol formation

The following mechanism for the formation of complex  $\mathbf{10-Al(pftb)}_4$  is proposed. Initially, protonation at the metal center occurs and compound  $\mathbf{32}$  is formed. Consecutively, reductive elimination of methanol and formation of  $\mathbf{10-Al(pftb)}_4$  takes place. This part of the proposed mechanism is equal to the mechanism anticipated for eq. 3.15 (Chapter 3.4). As it will be discussed later, another process involves further protonation of  $\mathbf{32}$  on the methoxide ligand and formation of Ir(III) hydrido methanol complex  $\mathbf{32a}$  is observed.



In order to provide a support for the proposed mechanism, the reaction according to eq. 4.5 was monitored from  $-90\text{ }^{\circ}\text{C}$  to  $50\text{ }^{\circ}\text{C}$  over a period of 6 hours by  $^1\text{H}$ -NMR spectroscopy. Both components (**4** and  $[\text{H}(\text{Et}_2\text{O})_2]^+$ ) were placed in the NMR tube and the solvent ( $\text{THF-d}_8$ ) was condensed over (at liq.  $\text{N}_2$  temperature). The mixture was then warmed up to  $-90\text{ }^{\circ}\text{C}$  and placed into the pre-cooled probe-head of the NMR spectrometer. In the first spectrum obtained at  $-90\text{ }^{\circ}\text{C}$ , two peaks in the high field region were observed at  $\delta = -32.90$  and  $-33.30$  ppm. The peak at  $-33.30$  ppm was assigned to the hydride ligand in **32** (Fig. 4.3).

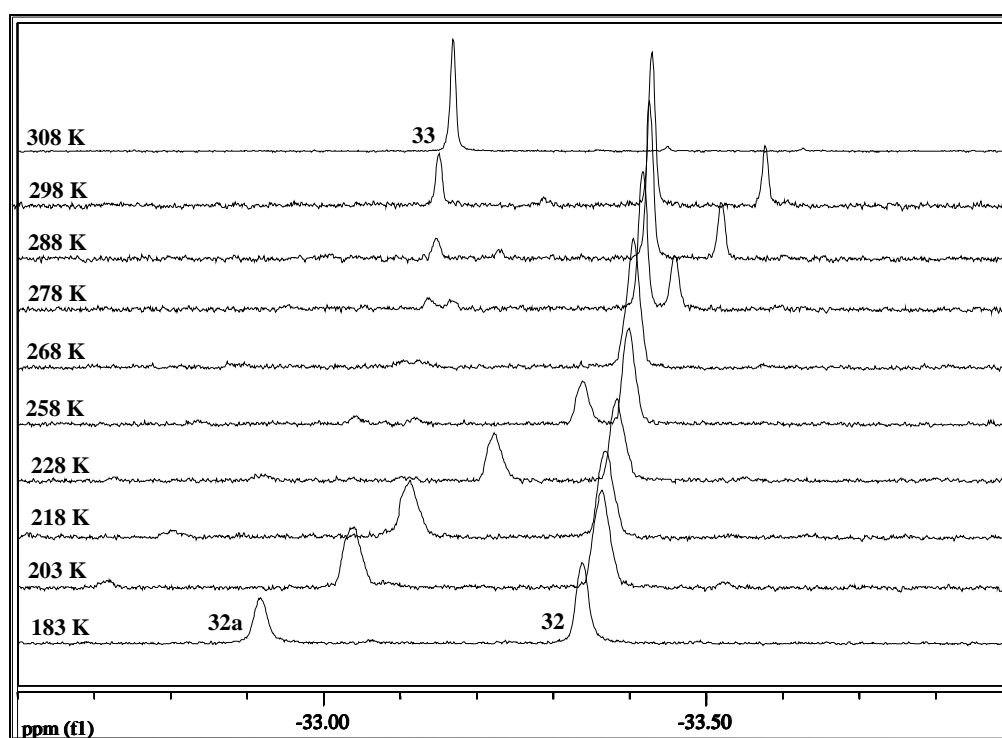
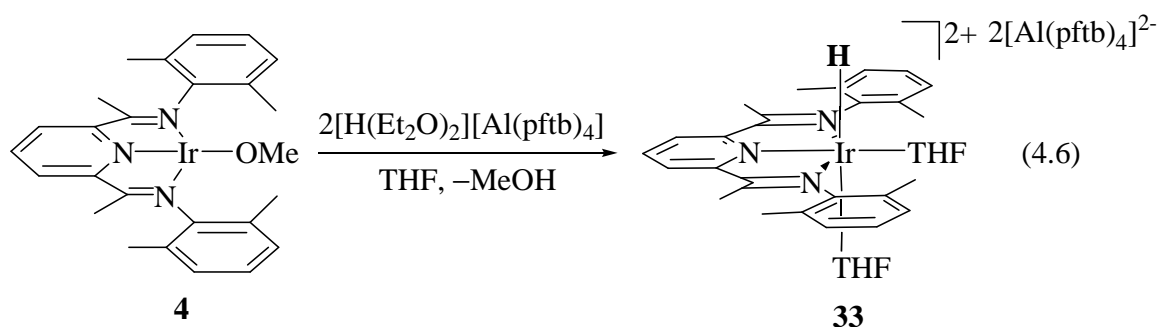


**Fig. 4.3** Temperature dependent NMR of the reaction according to eq. 4.5 (hydride region).

The methoxo ligand (in **32**) was found at  $\delta = 2.33$  ppm, significantly shifted towards higher field when compared to chemical shift in **4** ( $\delta = 4.67$  ppm). The assignment derived from the  $^1\text{D}$ -NOE NMR experiment. When the hydride peak at  $\delta = -33.30$  ppm is irradiated, the peak at  $\delta = 2.33$  ppm showed NOE enhancement. The resonance of protonated methanol in **32a** appeared at  $\delta = 2.90$  ppm. During a period of 1 hour, the temperature was increased gradually by  $10\text{ }^{\circ}\text{C}$  and the spectra recorded every 3 min. Nevertheless, apart from the slight shift of the hydride peak at  $\delta = -32.90$  towards higher field no significant changes were observed. At  $-5\text{ }^{\circ}\text{C}$  methanol was eliminated. The two hydride peaks crossed-over giving only one resonance at

$\delta = -33.40$  ppm (see spectrum at 268 K in Fig. 4.3). At +5 °C, the second hydride peak (at  $\delta = -33.45$  ppm) reappeared again reducing the intensity with further temperature rise and it completely disappeared at 25 °C. Also, at 10 °C a new hydride resonance was observed at  $\delta = -33.10$  ppm which was assigned to complex **33**. This resonance was the only one that remained when the temperature was elevated to 50 °C. In the aromatic region two sets of doublet and triplet peaks were detected. The triplet at  $\delta = 8.5$  ppm and the doublet at  $\delta = 7.91$  ppm were assigned to **10-Al(pftb)<sub>4</sub>** whilst the doublet at  $\delta = 8.36$  and triplet at  $\delta = 8.21$  ppm were assigned to complex **33**. At the end, the mixture of **10-Al(pftb)<sub>4</sub>**, **33** and methanol remained.

Complex **33** was synthesized independently when two equivalent of the aforementioned acid were added to a THF solution of **4** and the color changed from green to red (eq. 4.6).

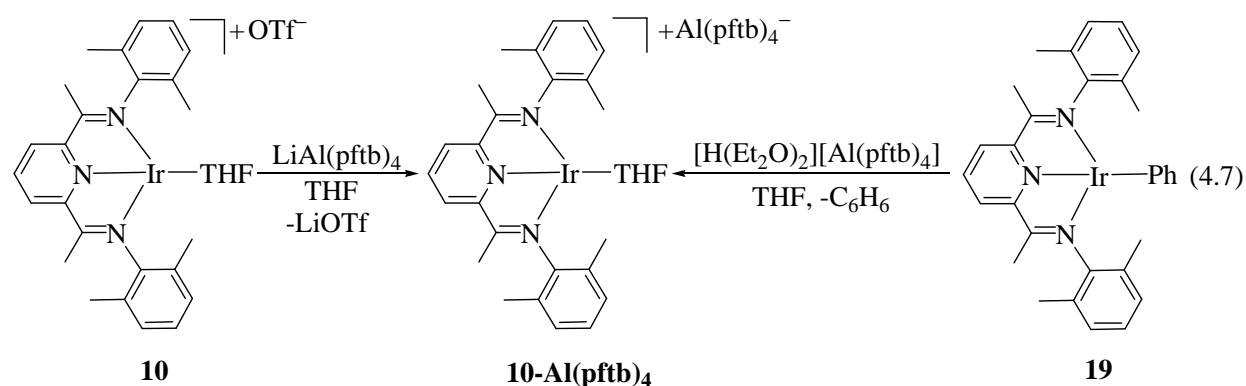


This compound was characterized with <sup>1</sup>H, <sup>13</sup>C, and <sup>19</sup>F-NMR spectroscopy. Methanol was found in the transferred volatiles. According to the <sup>1</sup>H-NMR spectrum (in THF-d<sub>8</sub>) the symmetry of the obtained compound is lowered, suggesting solvent coordination to the metal center. Methyl groups attached to the phenyl displayed a 1:1 integration ratio. The resonance of the methyl group on the diimine part of the ligand is shifted downfield revealing a peak at  $\delta = 2.84$  ppm. The assignments of the proton resonances were confirmed with 2D-HSQC and HMBC (<sup>1</sup>H/<sup>13</sup>C) NMR spectra.

#### 4.2.2 Alternative syntheses

Complex **10-Al(pftb)<sub>4</sub>** can be obtained via different routes. One way is by adding LiAl(pftb)<sub>4</sub> to a THF solution of **10**. This procedure is straightforward employing only one equivalent of lithium salt in comparison to the reaction of **10** with NaBAR<sub>4</sub><sup>F</sup> where 7 equivalents of latter were used in order to complete the exchange of the triflate anion. The other method to synthesize

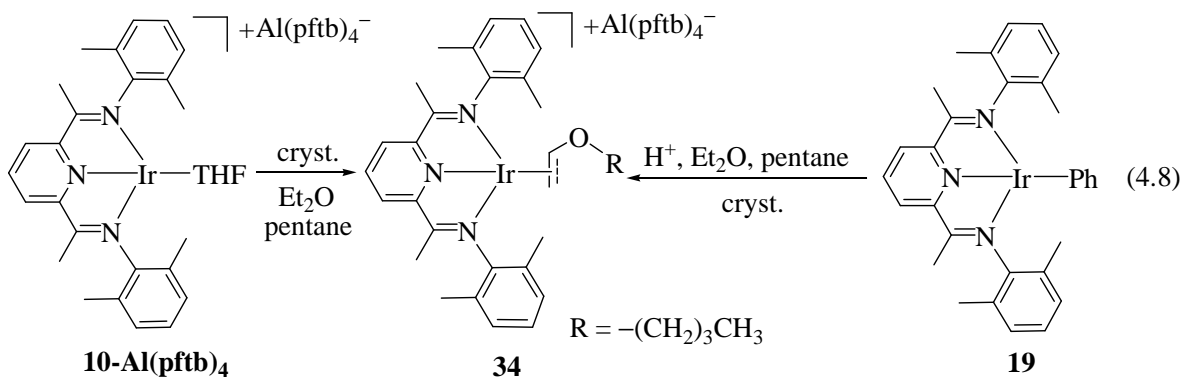
**10-Al(pftb)<sub>4</sub>** was by adding a THF solution of [H(Et<sub>2</sub>O)<sub>2</sub>][Al(pftb)<sub>4</sub>] to a THF solution of **19** (eq. 4.7). The yield in both reactions is approximately 90 %.



According to the <sup>19</sup>F-NMR spectrum in THF-d<sub>8</sub> for the reaction of LiAl(pftb)<sub>4</sub> and **10** the resonance for the triflate anion at δ = -79.0 ppm disappeared and the new peak at δ = -75.6 ppm was assigned to Al(pftb)<sub>4</sub> anion. This observation showed that the anion exchange was complete. The proton resonances are on the same chemical shift (see Experimental part).

In the <sup>1</sup>H-NMR spectrum in THF-d<sub>8</sub> for the reaction of **19** and [H(Et<sub>2</sub>O)<sub>2</sub>][Al(pftb)<sub>4</sub>], peaks from the phenyl group attached to the metal center (d, 5.57; t, 5.81; t, 6.58) disappeared and the resonances of the methyl groups at δ = 0.67 and 1.97 ppm (in **19**) shifted to δ = 1.78 and 2.24 ppm in newly formed complex **10-Al(pftb)<sub>4</sub>**. The other aromatic peaks from the pyridine ligand were also shifted by 0.35 ppm towards higher field (comparing **19** and **10-Al(pftb)<sub>4</sub>**). The formation of benzene was confirmed in the transferred volatiles (in THF-d<sub>8</sub>), revealing a singlet peak at δ = 7.25 ppm in <sup>1</sup>H-NMR and at δ = 130 ppm in the <sup>13</sup>C-NMR spectrum.

In order to crystallize complex **10-Al(pftb)<sub>4</sub>**, different ether solutions (THF, Et<sub>2</sub>O or DME) were layered with non-polar solvents (pentane, toluene or benzene) or vapor diffusion was used. In this case, the crystals were obtained by slow vapor diffusion of pentane into a diluted Et<sub>2</sub>O solution of **10-Al(pftb)<sub>4</sub>** at -35 °C. After a long period of time, during crystallization, complex **34** was obtained (eq. 4.8). Dehydrogenation of diethyl ether and coordination of the ethoxyethene could be the possible explanation for the formation of complex **34**.



The  $^1\text{H-NMR}$  spectrum of the crystals was measured in  $\text{Et}_2\text{O-d}_{10}$  revealing two resonances at lower field (at  $\delta = 4.08$  ppm and  $5.44$  ppm), with an integration ratio 2:1. These peaks were assigned to the  $\eta^2$ -coordinated vinyl ether ligand and compared with the literature values.<sup>166, 167, 168</sup> The other resonances from the ethyl group were found at higher field (at  $\delta = 1.01$  and  $1.42$  ppm). In the  $^{19}\text{F-NMR}$  spectrum, a singlet peak at  $\delta = -79$  ppm was observed for the  $\text{Al(pftb)}_4^-$  anion. Unfortunately, the concentration of **34** in  $\text{Et}_2\text{O-d}_{10}$  was too low to perform  $^{13}\text{C}$  or 2D-NMR analyses.

Molecular representation of **34** and selected bond distances and angles are displayed in Figure 4.4 and Table 4.2.

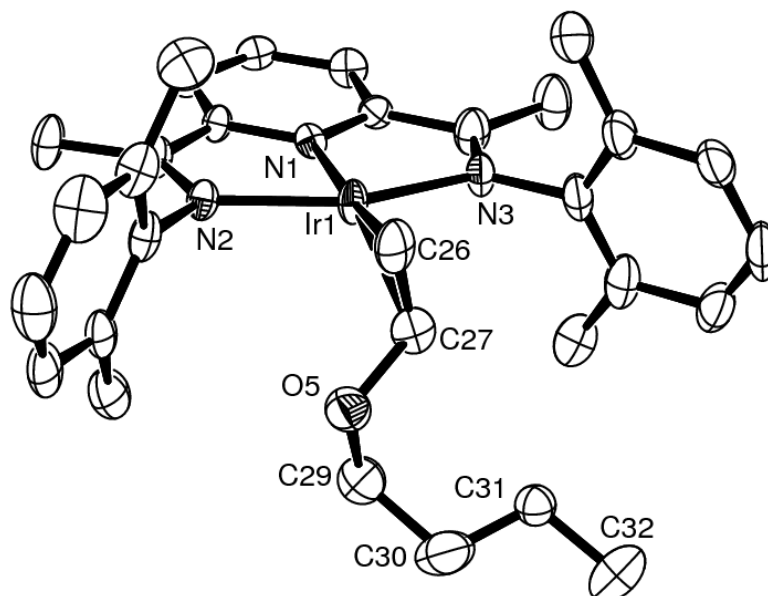


**Fig. 4.4** ORTEP plot of **34** with 50% probability level (hydrogen atoms and  $\text{Al(pftb)}_4^-$  anion were omitted for clarity).

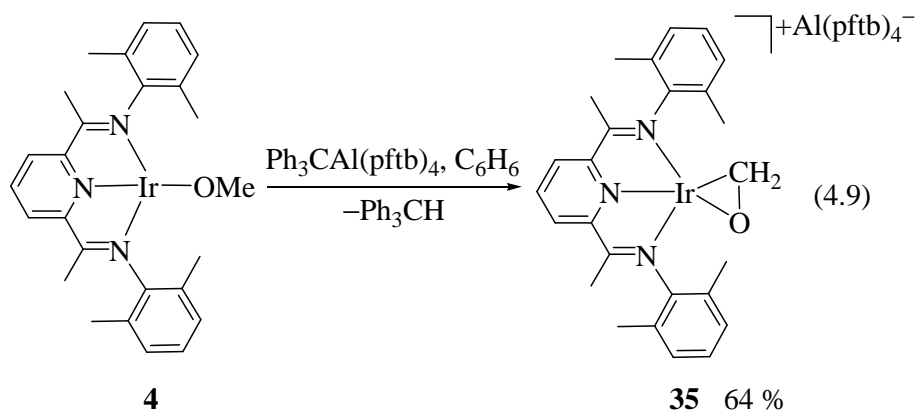
Table 4.2 Selected bond lengths [Å] and angles [°] for complex **34**.

Ir1-N1	1.948(5)	Ir1-N2	2.033(5)	Ir1-N3	2.019(5)
Ir1-C26	2.139(7)	Ir1-C27	2.223(6)	C26-C27	1.381(1)
C27-O5	1.340(9)	O5-C29	1.432(1)	C29-C30	1.489(1)
C30-C31	1.379(1)	C31-C32	1.415(1)		
N2-Ir1-N3	157.4(2)	N2-Ir1-N1	79.2(2)	N3-Ir1-N1	78.3(2)
N1-Ir1-C26	168.7(3)	N2-Ir1-C26	97.1(3)	N3-Ir1-C26	104.7(3)
N1-Ir1-C27	154.5(3)	N2-Ir1-C27	106.6(2)	N3-Ir1-C27	94.6(3)
C26-Ir1-C27	36.8(3)	Ir1-C27-O5	112.1(5)	C27-O5-C29	115.9(6)
O5-C29-C30	113.6(8)	C29-C30-C31	110.1(7)	C30-C31-C32	112.2(8)

The square planar coordination around the Ir center is slightly distorted with the sum of the angles equalling 359.2°. The ligand occupying the fourth coordination site is perpendicular to the IrNNN plane. The bond distance Ir1-C26 = 2.139(7) Å is by 0.086 Å shorter than Ir1-C27. Both are in the range of reported Ir-C<sub>sp2</sub> distances.<sup>169, 170</sup> The C26-C27 distance is 1.381(1) Å, comparable with the C=C bonds reported for the metallo vinyl ether complexes.<sup>168, 171</sup> According to the literature, the C=C distance in the free vinyl ether is 1.340(5) Å.<sup>172</sup> The atoms from C29-C32 are disordered.

### 4.3 Synthesis of the novel formaldehyde complex **35**

The methoxide abstraction with trityl (Ph<sub>3</sub>CAI(pftb)<sub>4</sub>) from complex **4** was another anticipated method to access the desired Ir(I) cation complex in non polar, less coordinative solvents (see eq. 4.1). Upon addition of a green solution of complex **4** in benzene to a yellow solution of Ph<sub>3</sub>CAI(pftb)<sub>4</sub> and stirring for 2 hours a color change to reddish-brown was observed. However, instead of the desired cationic compound, the novel *dihapto*-Ir(III) formaldehyde complex **35** was obtained in 64 % yield (eq. 4.9).



The  $^1\text{H}$ -NMR spectrum of the colorless pentane extraction of the reaction mixture revealed a singlet resonance at  $\delta = 5.4$  ppm in  $\text{C}_6\text{D}_6$ , which corresponds to triphenylmethane. Complex **35** was fully characterized with  $^1\text{H}$ ,  $^{13}\text{C}$  and  $^{19}\text{F}$ -NMR spectroscopy and elemental analysis. The  $^1\text{H}$ -NMR spectrum of **35** in THF- $d_8$  is consistent with  $\text{C}_{2v}$  symmetry, indicating a fast rotation of the formyl group in solution. The formaldehyde ligand revealed a proton resonance at  $\delta = 4.0$  ppm and  $^{13}\text{C}$  resonance at  $\delta = 69.1$  ppm, which are highfield in comparison with the free aldehyde. These chemical shifts are in the good agreement with the ones reported for complexes with a  $\eta^2$ -coordinated formaldehyde, for example  $[(\text{tmeda})\text{Ni}(\eta^2\text{-CH}_2\text{O})(\text{C}_2\text{H}_4)]$  (in THF- $d_8$ : ( $^1\text{H}$ )  $\delta = 3.64$ , ( $^{13}\text{C}$ )  $\delta = 70.9$  ppm)<sup>173</sup> and  $[\text{Cp}'_2\text{Nb}(\eta^2\text{-CH}_2\text{O})]$  (in  $\text{C}_6\text{D}_6$ : ( $^1\text{H}$ )  $\delta = 3.37$  ppm, ( $^{13}\text{C}$ )  $\delta = 67.8$  ppm).<sup>174</sup> The integration ratio of the formaldehyde ligand and the methyl groups is 1:6:3. The  $^{13}\text{C}$ -NMR resonance at  $\delta = 69.2$  ppm, which was assigned to  $\text{CH}_2$  group is based on a DEPT-135 experiment. In the coupled  $^{13}\text{C}\{^1\text{H}\}$ -NMR experiment, the  $\text{CH}_2$  group revealed a triplet with a coupling constant  $^1J_{\text{CH}} = 166$  Hz, typical for  $\text{sp}^2$ -hybridized carbon. According to the literature,  $^1J_{\text{CH}}$  coupling constants depend also on the nature of the neighboring atom. Electronegative substituents lead to an increase of the  $^1J_{\text{CH}}$  value.<sup>175</sup> In case for **35**, it is anticipated that the carbon atom (in  $\text{CH}_2\text{O}$  group) is  $\text{sp}^3$ -hybridized, which is in agreement with results obtained by X-ray crystal structure analysis. For the  $^1\text{H}$  and  $^{13}\text{C}$  resonances of the formaldehyde ligand a cross peak in the HSQC experiment was observed (Fig. 4.5).

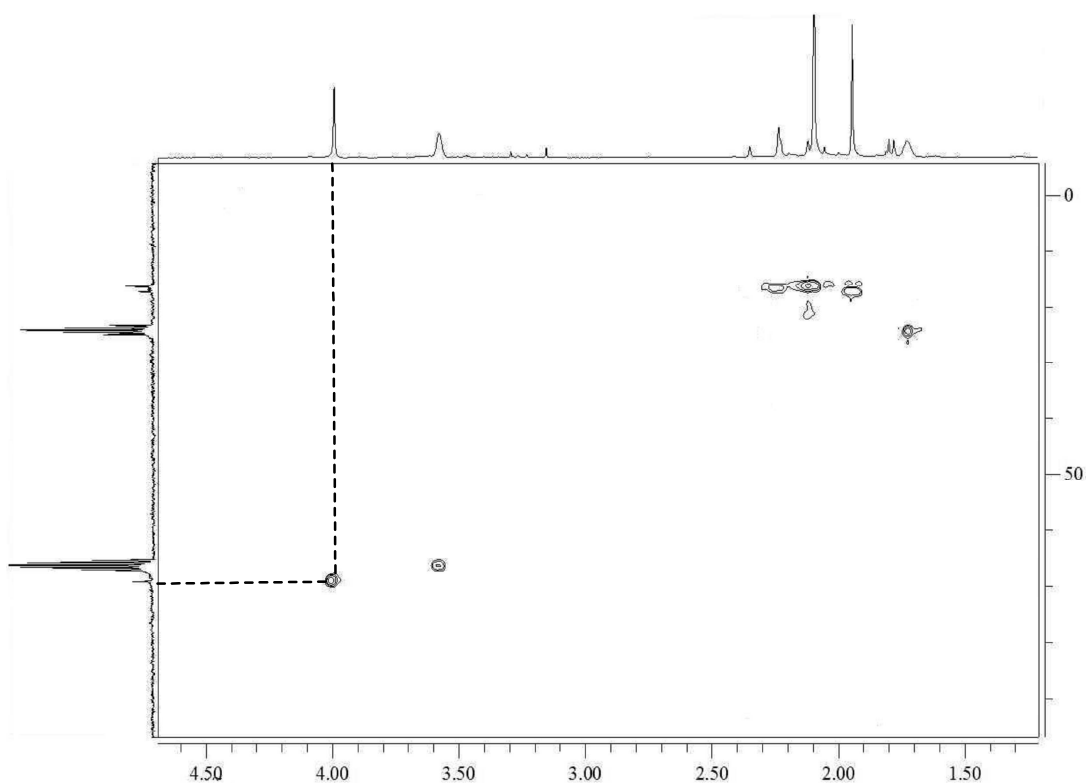
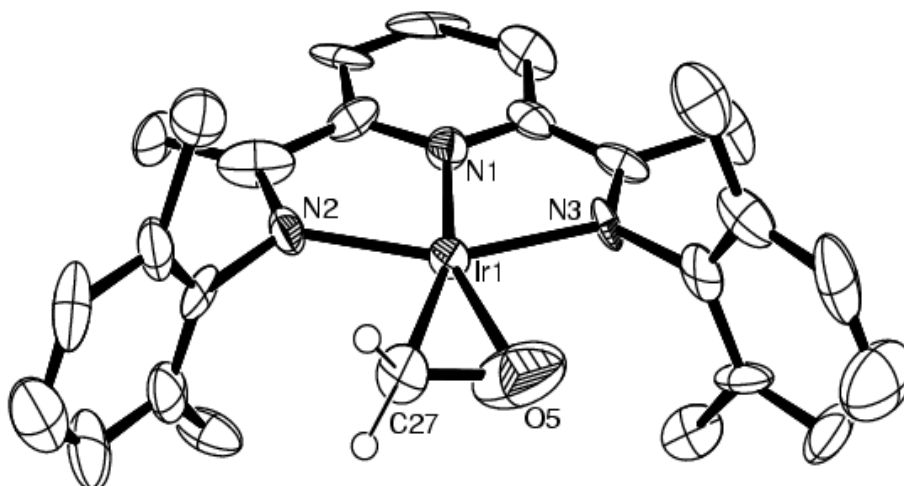


Fig. 4.5 HSQC for complex **35** in THF- $d_8$ .

The  $\nu(\text{CO})$  stretching frequency at  $1031\text{ cm}^{-1}$  in toluene strongly suggested an  $\eta^2$  coordination of the formaldehyde ligand for which typical stretching frequencies vary from  $1000\text{--}1200\text{ cm}^{-1}$ .<sup>176</sup> Opposite to  $\eta^2$ ,  $\eta^1$  formaldehyde ligands show much higher energy C-O stretching frequencies ( $\sim 1600\text{ cm}^{-1}$ ).<sup>177, 178</sup> It is noteworthy that the assigned frequency is indicative for back donation and lengthening of the C-O bond which is confirmed by X-ray crystal structure analysis.

Reddish-brown crystals were obtained from  $\text{Et}_2\text{O}$ /pentane solution by vapor diffusion (Fig. 4.6). Selected bond lengths and angles of **35** are presented in Table 4.3.



**Fig. 4.6** ORTEP plot of complex **35** with 50% probability thermal ellipsoids (the  $\text{Al}(\text{pftb})_4$  anion and hydrogen atoms (except the formyl ones) were excluded for clarity).

Table 4.3 Selected bond lengths [ $\text{\AA}$ ] and angles [ $^\circ$ ] for complex **35**.

Ir1-N1	1.962(1)	Ir1-N2	2.098(1)	Ir1-N3	2.113(1)
Ir1-O5	2.146(1)	Ir1-C27	2.172(2)	C27-O5	1.390(2)
N2-Ir1-N3	152.9(6)	N2-Ir1-N1	75.5(6)	N3-Ir1-N1	77.5(6)
N1-Ir1-C27	164.3(7)	N2-Ir1-C27	89.5(7)	N3-Ir1-C27	117.1(7)
N1-Ir1-O5	156.9(8)	N2-Ir1-O5	127.1(7)	N3-Ir1-O5	79.6(7)
C27-Ir1-O5	37.6(6)				

The molecule adopts a square planar geometry around the metal center with the sum of the angles equaling  $358.8^\circ$ . The formyl ligand lies in the IrNNN plane. The angle between the plane defined by Ir1-C27-O1 is  $37.6^\circ$ . The C27-O5 bond distance ( $1.390(2) \text{ \AA}$ ) is in the range of the other formaldehyde complexes reported.<sup>179, 174, 173</sup> The observed lengthening of the C-O bond, compared to free formaldehyde ( $1.225 \text{ \AA}$ )<sup>180</sup> strongly suggested  $\pi$  back-bonding. In the literature, the osmium complex  $[\text{Os}(\text{PPh}_3)_2(\text{CO})_2(\eta^2\text{-CH}_2\text{O})]$  with the unusually long C-O bond ( $1.59(1) \text{ \AA}$ ) was reported and the interaction between osmium and formaldehyde was described as the oxirane like structure.<sup>181</sup> It is worth noticing that the C-O bond distance in the starting material **4**

(1.392(8) Å) is only 0.002 Å longer than in **35** (*vide infra*), which suggests that the ligand (C-O) retained the same hybridization after the reaction. The Ir1-O5 bond distance (2.146(1) Å) is shorter than the Ir-C27 distance (2.172(2) Å). This behaviour is mostly observed when the metal centers have an oxophilic character<sup>181, 182, 179</sup> as it could be suggested in case for complex **35**.

### 4.3.1 Mechanistic aspects

There are several different routes for the synthesis of aldehyde complexes. Mostly, they are prepared by using paraformaldehyde as the source of the desired ligand<sup>183, 184</sup> or reduction of the carbon monoxide by appropriate metal hydrides.<sup>185, 186</sup> The third possibility for the synthesis of aldehyde complexes is  $\beta$ -hydride elimination of alkoxide complexes to give hydridoformaldehyde intermediates.<sup>187, 188, 189</sup> Formation of such an intermediate is anticipated for the reaction according to eq. 4.9.

The proposed mechanism (Fig. 4.7), involves the formation of the formyl hydrido complex. The hydride ligand is then abstracted by the trityl cation giving **35** and triphenylmethane. DFT calculations (B3LYP, LACVP\*\* basis set) on the model complex **4a** were performed for the formation of the formyl hydride.

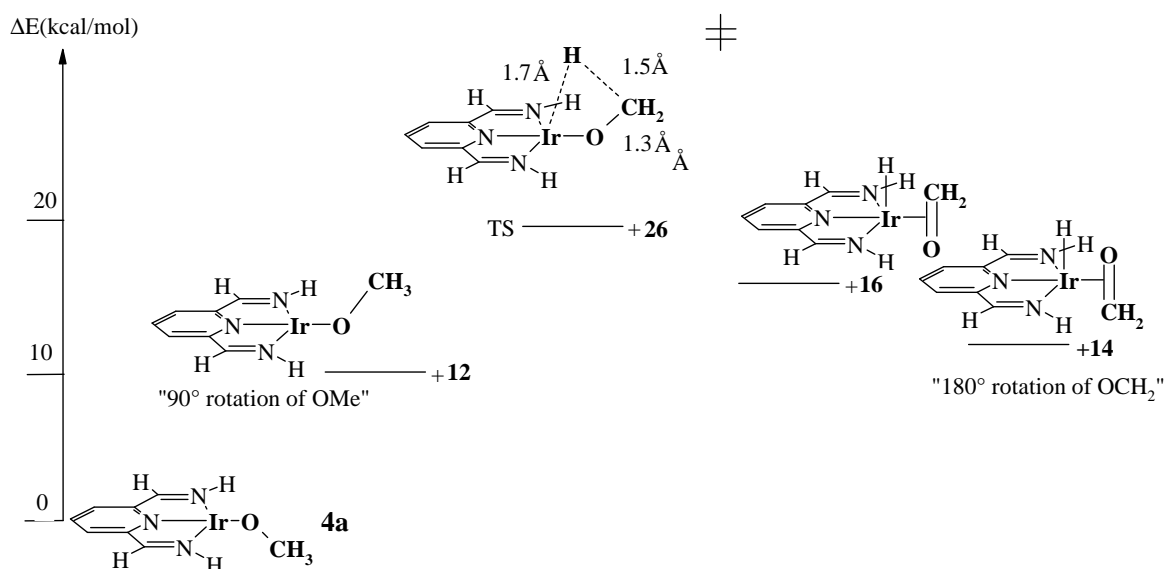


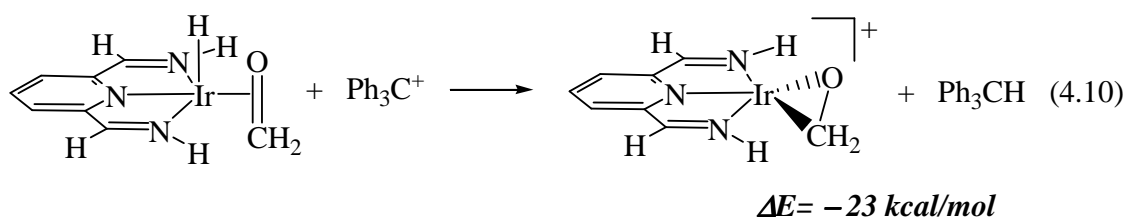
**Fig. 4.7** Energy barrier for the formation of formyl hydrido complex.

Previously, the preference for the in-plane coordination of the methoxide group in **4a** was established by our group, with an energy difference of 12 kcal/mol.<sup>44</sup> The energy barrier from **4a**

to the formyl hydride is 26 kcal/mol. The transition state (TS) resembles the product and can be described as late transition state according to the Hammond postulate.<sup>190</sup> The imaginary frequency for the transition state corresponds to shortening of Ir-H bond distance. The formyl hydrido complex is 14 kcal/mol higher in energy than **4a** with the hydride and oxygen in the *cis* position.

In order to confirm the reaction pathway, IRC calculations were carried out (B3LYP, LACVP\*\* basis set). Starting from the saddle point (TS), the forward direction led to the formyl hydride and the reverse reaction mode to the starting material **4a**.

The second part of the proposed mechanism involves hydride abstraction. According to DFT calculations, the reaction is thermodynamically favored (in the gas phase) for the formation of the formaldehyde complex and triphenylmethane by 23 kcal/mol (eq. 4.10).

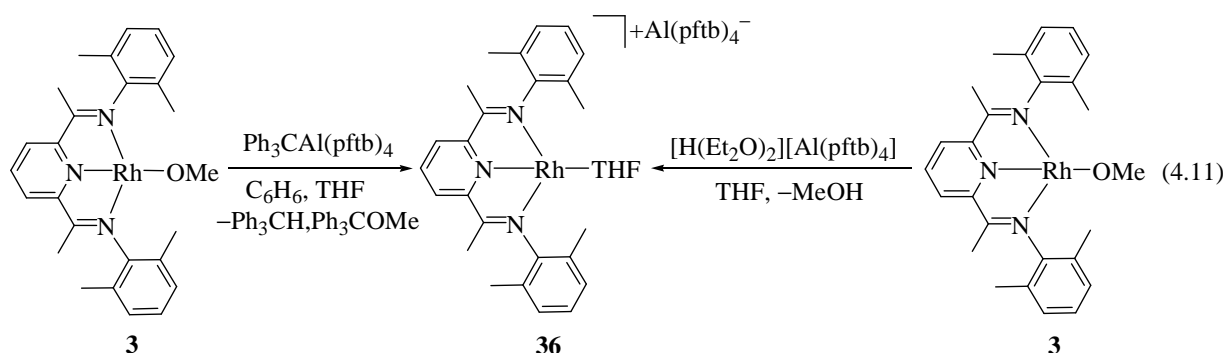


The  $\beta$ -hydride elimination from methoxo complexes was already reported by Bryndza et al. in the case for Pt(II)(DPPE)(OMe)<sub>2</sub>. The thermolysis of the latter, which generates methanol and formaldehyde oligomers at 30 °C, was explained by a mechanism involving a pre-equilibrium with a  $\beta$ -hydride elimination.<sup>187</sup> Milstein et al. established the same mechanism for an octahedral Ir(III)Cl(H)(OMe)(PR<sub>3</sub>)<sub>3</sub> complex.<sup>188</sup>

To the best of our knowledge this is the first fully characterized and isolated iridium  $\eta^2$ -formaldehyde complex. The reactivity of latter, especially towards H<sub>2</sub> and CO, is still unexplored and will be left for further studies.

### 4.3.2 Different reactivity of the Rh(I) methoxo complex **3**

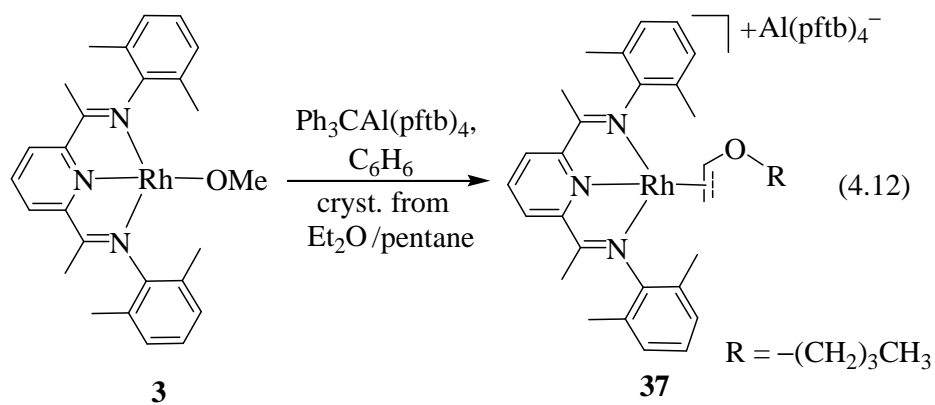
The reaction according to equation 4.9 was repeated for the Rh analogue. Upon addition of a green solution of **3** in benzene to a yellow solution of  $\text{Ph}_3\text{CAI}(\text{pftb})_4$ , a color change to brown was observed. However, instead of formaldehyde compound, the cationic complex **36** was obtained (eq. 4.11).



The  $^1\text{H-NMR}$  spectrum of the colorless pentane extraction of the reaction mixture revealed singlet resonances at  $\delta = 5.40$  ppm (for the CH group) and 2.96 ppm (for the methyl group) in  $\text{C}_6\text{D}_6$  with a 1:1 integration ratio, which correspond to triphenylmethane and trityl-methyl ether (*Note*: the residual compound is not soluble in pentane). The  $^1\text{H-NMR}$  spectrum of **36** in  $\text{THF-d}_8$  revealed two singlet peaks of the methyl groups (at  $\delta = 1.98$  and 2.30 ppm) with an 1:2 integration ratio as expected for  $\text{C}_{2v}$  symmetry in complex **36**. In the  $^{19}\text{F-NMR}$  spectrum, one resonance at  $\delta = -76.30$  ppm assigned to the  $\text{Al}(\text{pftb})_4$  anion was observed.

The alternative route to synthesize complex **36** was by mixing THF solutions of **3** and  $[\text{H}(\text{Et}_2\text{O})_2][\text{Al}(\text{pftb})_4]$ . As in the reaction according to eq. 4.4, methanol was eliminated (see section 4.2). Proton and carbon resonances of **36** can be compared with the resonances from triflate complex **9**<sup>47</sup>, confirming that there is no anion effect involved.

The crystals were grown by a slow vapor diffusion of pentane to a diluted diethyl ether solution of **36**. During crystallization, compound **37** was obtained, which was confirmed by X-ray crystal structure analysis (eq. 4.12).



Molecular presentation and selected bond distances and angles were displayed in Figure 4.8 and Table 4.4.

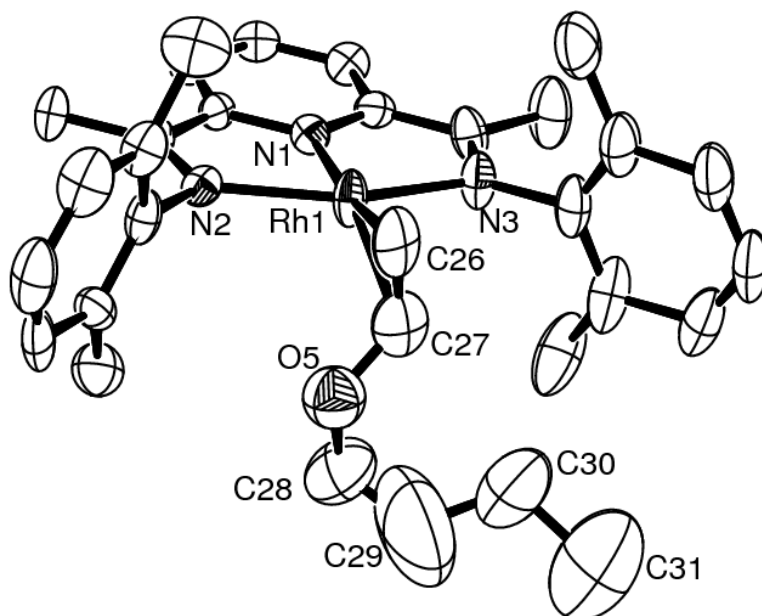


**Fig. 4.8** ORTEP plot of complex **37** at 50% probability level (hydrogen atoms and the  $\text{Al(pftb)}_4$  anion were omitted for clarity).

Table 4.4 Selected bond lengths [Å] and angles [°] for complex **37**.

Rh1-N1	1.946(6)	Rh1-N2	2.053(6)	Rh1-N3	2.046(6)
Rh1-C26	2.160(8)	Rh1-C27	2.195(1)	C26-C27	1.310(1)
C27-O5	1.308(1)	C29-O5	1.451(1)		
N2-Rh1-N3	157.4(2)	N2-Rh1-N1	79.0(2)	N3-Rh1-N1	78.5(2)
N1-Rh1-C26	167.7(3)	N2-Rh1-C26	98.2(3)	N3-Rh1-C26	103.4(3)
N1-Rh1-C27	157.3(4)	N2-Rh1-C27	105.3(4)	N3-Rh1-C27	96.1(3)
C26-Rh1-C27	34.9(3)	Rh1-C27-O5	113.9(6)	C27-O5-C29	114.6(9)
O5-C29-C30	74.0(2)				

Complex **37** is isostructural with complex **34**, crystallizing in the space group  $P2_1/n$ . The geometry around the Rh center is distorted square planar with the sum of the angles equaling  $359^\circ$ . The alkene, as the fourth ligand is oriented perpendicularly to the plane defined by Rh1, N1, N2 and N3 atoms. The rhodium center is bound to C26 and C27 with the distance Rh-C26 = 2.160(8) Å and Rh-C27 = 2.195(1) Å, respectively. The C26-C27 bond distance (1.310(1) Å) is slightly longer than in Ir analogue. The R values are less than 10 % for both complexes ( $R_1(\mathbf{34}) = 0.0661$ ,  $R_1(\mathbf{37}) = 0.0772$ ).

In this chapter, syntheses of novel cationic complexes were presented. In comparison to the synthesis of complex **10**, a new, straightforward synthesis was described for preparation of the **10-Al(pftb)<sub>4</sub>** followed by the elimination of methanol. This reaction was studied by low temperature NMR and the mechanism was proposed.

Synthesis and characterization of the novel  $[\text{Ir}(\text{N}_3\text{Me}_4)(\eta^2\text{-CH}_2\text{O})]^+$  complex as well as DFT calculations concerning the mechanism for the formation of the latter was also described.

## 5 Summary

The research described herein is an extension and continuation of previous research work developed within the group, in the area of C-H activation of alkanes to alcohols *via* square planar late transition metal monomeric Rh, Ir(III) oxo complexes with a terminal oxo unit  $L_nM=O$ . The central theme of the current work was to try and provide further evidence for each sequential step of the proposed catalytic cycle for this process. Syntheses and characterization of the desired complexes and direct observation or isolation of reactive intermediates and products was the focus of the experimental work.

A range of square planar starting materials (**1-10**) using sterically demanding terdentate pyridine diimine ligands was prepared. The first approach to an Ir oxo complex was the direct oxidation of the Ir(I)-hydroxo complex **6** with different strong oxidizing reagents. However, unexpected compounds were obtained. Using 2 equivalents of the thianthrene radical cation and **6** in a dimethoxyethane (DME) solution, the Ir(III)-hydride complex **11** with DME coordinated to the metal center was isolated. The source of the hydride was not conclusive. An independent experiment (formation of **12**) showed that the hydride did not originate from the hydroxide group in **6**. The use of a different oxidizing reagent, “magic blue” led to the formation of the Ir(III)-dichloro complex **13** with THF coordinated to the metal center.

Another route to the oxo complex **II** by hydride abstraction from the hydroxide group in **6** was pursued with trityl-PF<sub>6</sub>. However, due to crystallographic problems, the ligand occupying the fourth site on the metal center in **14** was not resolved. It is noteworthy, that several X-ray crystal structure analyses were undertaken and apart from the fourth ligand, all the other atoms from the terdentate ligand were anisotropically refined with small R-values.

According to DFT calculations, amine N-oxides were proposed as possible co-catalysts in the catalytic cycle that can react with the cationic complex **29** to yield **II**. It was also calculated that by increasing the number of phenyl groups coordinated to the nitrogen of the amine N-oxide, starting from trimethylamine N-oxide, the formation of **II** would be thermodynamically more favorable. Therefore, **Me<sub>2</sub>PhNO** and **MePh<sub>2</sub>NO** were synthesized and their X-ray crystal structures determined. The distances between two amine N-oxides (including Me<sub>3</sub>NO) were comparable. This finding was opposite from what was expected, since electron withdrawing

phenyl groups were introduced. Through a crystal packing analysis, it was found that strong *intermolecular* and *intramolecular* CH...O hydrogen bonding is present and presumably responsible for the aforementioned result. In the reaction of the triflate complex **10** and **Me<sub>2</sub>PhNO**, the formation of free amine was confirmed. Unfortunately, the fate of the oxygen atom is still unclear.

The activation of molecular oxygen and the formation of a peroxo species was also at the center of this work. In order to improve the solubility of the desired complexes, the exchange of the triflate anion in **10** was accomplished either with NaBAr<sup>F</sup><sub>4</sub> or LiAl(pftb)<sub>4</sub> giving complexes **10-BAr<sup>F</sup><sub>4</sub>** and **10-Al(pftb)<sub>4</sub>**, respectively. When the latter was reacted with oxygen, the tentative, paramagnetic peroxo complex **III** was obtained. DFT calculations indeed confirmed that a triplet state (S=1) is preferable. In the reaction with Ph<sub>3</sub>P and **III**, the cationic phosphine complex **IV** and free Ph<sub>3</sub>PO were formed.

The reaction chemistry of the formal Rh<sup>0</sup> complexes was a significant part of this project. Compound **V** was synthesized by the reduction of the Rh(I) chloro or methoxo complexes (**1a** or **3a**) with Na/Hg in THF solution under argon atmosphere. Paramagnetic character of **V** was confirmed with EPR experiment. DFT calculations revealed that the spin density of the electron is essentially located within the pyridine diimine ligand. Unfortunately, attempts to obtain crystals for an X-ray crystal structure analysis were unsuccessful.

The reactivity of **V** was tested with different reagents. In dichloromethane, it reconverts to the chloro complex **1a**. Upon addition of Me<sub>3</sub>SiN<sub>3</sub> in **V**, the Rh(I) azido complex **15** was obtained. In the reaction with adamantyl-1-azide, the paramagnetic, species **VI** was formed. Although further characterization was unsuccessful, the structure of **VI** was tentatively assigned to a Rh(II) imido species.

Alternatively, when the reduction of **1a** was performed under an N<sub>2</sub> atmosphere, depending on the alkyl substituents on the phenyl rings, dinuclear or mononuclear dinitrogen complexes **16** and **17** were isolated. To the best of our knowledge, **17** is the first example of a mononuclear Rh(0) dinitrogen complex. As in the case of **V**, DFT calculations showed that the spin density is delocalized within the pyridine diimine ligand.

Further focus of this research was the improvement of the synthesis of methyl complex **18** and establish evidence for the Ir(III) intermediate proposed for the mechanism in the case of *intermolecular* C-H activation of **18** in benzene. In the reaction of the phenyl complex **19** and H<sub>2</sub>, the Ir(III) trihydride **20a** was obtained. This compound showed fluxionality of the hydrido ligands in the <sup>1</sup>H-NMR spectra. Low temperature NMR and T<sub>1</sub> measurements confirmed the presence of a trihydride species. DFT calculations revealed that the energy difference between the trihydride **20a** and the dihydrogen hydride **20b** complexes is very small.

Further evidence for a two-step C-H activation mechanism (oxidative addition and reductive elimination) was the extended low temperature NMR study of the Si-H activation process in trimethylsilane of the methoxo complex **4**. The Ir(I) mono-hydride **20** was obtained, followed by the formation of trimethylsilylmethoxide.

A suitable route to both iridium and rhodium mono-hydride complexes from the related fluoride complexes was investigated. Using TASF as a fluorinating reagent in the reaction with the triflate complexes **9** and **10**, the Rh,Ir(I)-fluoro complexes **22** and **23** were obtained. Both complexes crystallize with (Me<sub>2</sub>N)<sub>3</sub>SOTf. Using a new fluoride source, TBAF, by metathesis of the chloride ligand from **1**, **1a** or **2**, the fluoro complexes **24**, **25** and **26** were obtained.

One of the most important reactions in the alkane functionalization is the C-O reductive elimination process. During this study, C-O elimination of methanol (from the hydroxo complex **6** and methyltriflate) was followed by low temperature <sup>1</sup>H-NMR spectroscopy. The formation of the hydroxo, methyl intermediate **27** was detected. DFT calculations on the mechanism of C-O reductive elimination were also investigated. Another example of C-O bond formation was observed in the reaction of the methoxo complexes **3** or **4** and two equivalents of methyltriflate. In both examples dimethyl ether was eliminated.

Finally, different approaches to obtain cationic complexes were pursued. In the reaction of **4** and tris-(pentafluorophenyl)borane, depending on the solvent, complexes **30** and **31** were obtained. If the reaction was performed in dichloromethane, the Ir(III)-dichloro hydride **30** was isolated. In the case when diethyl ether was used, the cationic complex **31** was formed.

When one equivalent of the Brønsted acid [H(Et<sub>2</sub>O)<sub>2</sub>][Al(pftb)<sub>4</sub>] was added to the methoxo complex **4**, complex **10-Al(pftb)<sub>4</sub>** was formed and methanol was eliminated. Low temperature

<sup>1</sup>H-NMR measurements were undertaken in order to provide evidence for the proposed mechanism. The formation of the Ir(III)-hydrido methoxide complex **32**, followed by reductive elimination of methanol strongly support the mechanistic scenario. However, a competing reaction also takes place and depending on the concentration of the acid, the Ir(III)-hydrido complex **33** can be obtained.

Complex **10-Al(pftb)<sub>4</sub>** can be synthesized via different routes, either by the simple metathesis of the triflate anion from **10** with LiAl(pftb)<sub>4</sub> already described above or upon addition of the aforementioned acid to the phenyl complex **19**.

In the reaction of **4** and trityl-Al(pftb)<sub>4</sub>, the novel η<sup>2</sup>-Ir(III) formaldehyde complex **35** was prepared. A possible mechanism for this reaction was investigated with DFT calculations. The proposed mechanism involves the formation of the formaldehyde hydride species obtained by β-hydride elimination from the methoxide ligand, followed by a hydride abstraction with trityl. The outcome for the reaction of the analogous Rh(I) methoxo complex **3** and trityl-Al(pftb)<sub>4</sub>, was different. Instead of the formaldehyde complex, a cationic species **36** was obtained. The same compound was independently synthesized when **3** was reacted with the acid, [H(Et<sub>2</sub>O)<sub>2</sub>][Al(pftb)<sub>4</sub>].

## 6 Experimental Section

### 6.1 General Procedures

Unless otherwise noted, all manipulations were performed at room temperature under an atmosphere of purified nitrogen or argon either in a glove box (M. Braun) or using standard Schlenk/vacuum line techniques. Solvents used for syntheses were dried thoroughly using appropriate drying agent and distilled under nitrogen atmosphere. Deuterated NMR solvents were purified, dried and degassed with “freeze-pump-thaw” method. Pentane used for the preparation of the cation complexes was purified by following procedure from the literature.<sup>191</sup>

Instruments used for characterization:

<sup>1</sup>H-NMR spectra were recorded on Varian Gemini 2000 and Bruker Avance 400 spectrometers operating at 200 and 400 MHz respectively.

<sup>13</sup>C{<sup>1</sup>H}-NMR spectra were recorded on a Varian Gemini 2000 and Bruker Avance 400 spectrometer operating at 50 and 100 MHz respectively.

<sup>19</sup>F{<sup>1</sup>H}-NMR spectra were recorded on a Varian Gemini 2000 spectrometer operating at 188.1 MHz.

<sup>31</sup>P{<sup>1</sup>H}-NMR spectra were recorded on Bruker Avance 400 spectrometer operating at 162 MHz.

Chemical shifts are given in ppm and were referenced to the residual <sup>1</sup>H solvent shift or <sup>13</sup>C-NMR solvent shift. If not specially noted, all spectra were recorded at RT.

The assignment of <sup>1</sup>H NMR and <sup>13</sup>C NMR resonances is based on C-H correlation in 2D-NMR spectra (DEPT, HSQC and HMBC experiments).

IR spectra were measured on a FT-IR Perkin Elmer Spectrometer 1720.

ESI mass spectra were measured on a Bruker *ESQUIRE-LC* quadrupole ion trap instrument equipped with a combined Hewlett-Packard Atmospheric Pressure Ion (API) source at the University of Zürich.

Mass spectra were measured on Finnigan MAT 8430 specrometer at the University of Zürich.

ESR spectra were recorded in the X-Band (9.45-9.75 GHz) on a Bruker ESP-300E instrument.

UV/Vis spectra were measured on a Cary 50 Scan UV-VIS spectrophotometer.

X-ray crystal structure analyses were performed on a STOE-IPDS image plate system with monochromated Mo- $K\alpha$  (0.70713 Å) beam at the University of Zürich and on a Bruker SMART CCD diffractometer with Mo- $K\alpha$  (0.70713 Å) beam at the University of Hamburg. For the structure determination and refinement SHELXS-86 and SHELX-97 programs were used.<sup>192, 193</sup>

Elemental analyses were measured on a Heraeus CHN Rapid analyzer.

Cyclic voltammetry was carried out in THF/0.4 M Bu<sub>4</sub>NPF<sub>6</sub> using a three-electrode configuration in the glove box at room temperature. The potential was controlled with a BAS-100W potentiostat (Bionalytical Systems Inc.).

DFT calculations were performed with Jaguar (version 6.0) using B3LYP (X3LYP) hybrid and LACVP\*\* (6G-311G\*\*<sup>++</sup>) basis set.

## 6.2 Synthesis and characterization of the novel Rh and Ir complexes

The below mentioned compounds were synthesized following the procedure from the literature:

- Di- $\mu$ -chloro-tetrakis(ethene)dirhodium(I)  $[\text{Rh}(\text{C}_2\text{H}_4)_2\text{Cl}]_2$ <sup>194</sup>
- Di- $\mu$ -chloro-tetrakis(cyclooctene)diiridium(I)  $[\text{Ir}(\text{COE})_2\text{Cl}]_2$ <sup>194</sup>
- Di- $\mu$ -chloro-tetrakis(ethene)diiridium(I)  $[\text{Ir}(\text{C}_2\text{H}_4)_2\text{Cl}]_2$ <sup>46</sup>
- Tetrabutylammonium-fluoride TBAF<sup>142</sup>
- Dimethylphenyl amine N-oxide  $\text{Me}_2\text{PhNO}$ <sup>72</sup>
- Diphenylmethyl amine N-oxide  $\text{MePh}_2\text{NO}$ <sup>195, 72</sup>
- Trimethylsilane  $\text{Me}_3\text{SiH}$ <sup>144</sup>
- $\text{LiAl}(\text{pftb})_4$ ,  $\text{AgAl}(\text{pftb})_4$ <sup>196</sup>
- $\text{Ph}_3\text{CAI}(\text{pftb})_4$ <sup>63</sup>
- $[\text{H}(\text{Et}_2\text{O})_2][\text{Al}(\text{pftb})_4]$ <sup>165</sup>
- 2,6-Bis-[1-(2,6-Dimethylphenylimino)ethyl]pyridine  $\text{N}_3\text{Me}_4$  and 2,6-Bis-[1-(2,6-Diisopropylphenylimino)ethyl]pyridine  ${}^i\text{Pr}_4\text{N}_3$ <sup>41, 197</sup>
- 4-tert-butyl-2,6-diacetylpyridine and related ligand<sup>44</sup>
- Complexes **1-7**, **9** and **17**, **19**, **20**<sup>44, 47</sup>

The general numbering scheme used for the assignment of proton and carbon resonances in the  ${}^1\text{H}$  and  ${}^{13}\text{C}\{{}^1\text{H}\}$ -NMR spectra for all complexes **1 - 36** is shown in Fig. 6.1.

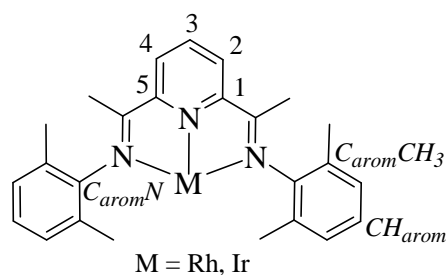


Fig. 6.1 Numbering scheme for NMR resonances used in complexes **1 - 36**.

## 6.2.1 Syntheses from Chapter 2

### [Ir(N<sub>3</sub>Me<sub>4</sub>)Me(OTf)<sub>2</sub>] - **8**

[Ir(N<sub>3</sub>Me<sub>4</sub>)OMe] **4** (840 mg, 1.51 mmol) was dissolved in 10 ml of toluene. MeOTf (0.33 ml, 3 mmol) was added via syringe at room temperature. The mixture was stirred over night. The solvent was removed in vacuum and a light green product was obtained. The crude product was washed with pentane (2 × 10 ml).

Yield: 96 % (1.26 g, 1.44 mmol).

<sup>1</sup>H-NMR (CD<sub>2</sub>Cl<sub>2</sub>): δ = 1.08 (s, 3 H, Ir-CH<sub>3</sub>); 2.12 (s, 6 H, CH<sub>3</sub>); 2.40 (s, 6 H, CH<sub>3</sub>); 2.79 (s, 6 H, CN-CH<sub>3</sub>); 7.18 (m, 6 H, CH<sub>arom</sub>); 7.95 (s, 3 H, CH(2,3,4)).

<sup>13</sup>C{<sup>1</sup>H}-NMR (CD<sub>2</sub>Cl<sub>2</sub>): δ = 18.3 (CN-CH<sub>3</sub>); 19.5 (CH<sub>3</sub>); 19.8 (CH<sub>3</sub>); 21.4 (Ir-CH<sub>3</sub>); 127.6 (CH(2,4)); 128.7, 129.3, 129.5 (C<sub>arom</sub>H); 134.1 (C<sub>arom</sub>-CH<sub>3</sub>); 138.5 (CH(3)); 144.6 (C<sub>arom</sub>-N); 184.0 (C=N).

<sup>19</sup>F{<sup>1</sup>H}-NMR (CD<sub>2</sub>Cl<sub>2</sub>): δ = -80.1 (s, 3 F, OTf); -80.7 (s, 3 F, OTf).

### [Ir(N<sub>3</sub>Me<sub>4</sub>)(THF)]OTf - **10**

[Ir(N<sub>3</sub>Me<sub>4</sub>)Me(OTf)<sub>2</sub>] **8** (506 mg, 579 μmol) was dissolved in 10 ml of THF. A solution of [Ir(N<sub>3</sub>Me<sub>4</sub>)OMe] **4** (344 mg, 579 μmol) in THF (10 ml) was added at room temperature to the reaction vial. The mixture was stirred for 2 hours. The color changed from green to dark brown. The solvent was evaporated. The crude product was recrystallized from THF/pentane (-35 °C).

Yield: 94 % (778 mg, 994 μmol).

<sup>1</sup>H-NMR (THF-d<sub>8</sub>): δ = 1.80 (s, 6 H, CN-CH<sub>3</sub>); 1.61 (m, 4 H, THF); 1.81 (m, 4 H, THF) 2.24 (s, 12 H, CH<sub>3</sub>); 7.23 (m, 6 H, CH<sub>arom</sub>); 8.10 (d, 2 H, J = 8 Hz, CH(2,4)); 8.55 (t, 1 H, J = 8 Hz, CH(3)).

<sup>13</sup>C{<sup>1</sup>H}-NMR (THF-d<sub>8</sub>): δ = 17.6 (CN-CH<sub>3</sub>); 18.5 (CH<sub>3</sub>); 123.9 (C<sub>arom</sub>-CH<sub>3</sub>); 125.1 (CH(2,4)); 128.2 128.5, 129.7 (C<sub>arom</sub>H); 131.9 (CH(3)); 150.0 (C<sub>arom</sub>-N); 166.4 (C(1,5)); 179.8 (C=N).

$^{19}\text{F}\{^1\text{H}\}$ -NMR (THF- $d_8$ ):  $\delta = -78.92$  (s, 3 F, OTf).

Elemental analysis:

Calculated for  $\text{C}_{30}\text{H}_{35}\text{N}_3\text{O}_4\text{F}_3\text{SIr}$ : C 46.00, H 4.47, N 5.37;

Found: C 45.73, H 4.13, N 5.65.

### **$[\text{Ir}(\text{N}_3\text{Me}_4)(\text{THF})]\text{Bar}^{\text{F}}_4$ - **10- $\text{Bar}^{\text{F}}_4$****

$[\text{Ir}(\text{N}_3\text{Me}_4)\text{THF}]\text{OTf}$  **10** (100 mg, 0.13 mmol) was dissolved in 10 ml of THF and added to  $\text{NaBar}_4^{\text{F}}$  (0.8 g, 0.91 mmol). The mixture was stirred for 1 h, filtered and the solvent was evaporated. The crude product was extracted with diethyl ether and left at  $-35\text{ }^\circ\text{C}$  to crystallize off the excess of  $\text{NaBar}_4^{\text{F}}$ . The latter was filtered and the solvent was evaporated.

Yield: 33 % (61 mg, 43  $\mu\text{mol}$ ).

$^1\text{H}$ -NMR (THF- $d_8$ ):  $\delta = 1.77$  (s, 6 H, CN- $\text{CH}_3$ ); 2.22 (s, 12 H,  $\text{CH}_3$ ); 7.24 (m, 6 H,  $\text{CH}_{\text{arom}}$ ); 7.57 (s, 4 H,  $\text{Bar}_4^{\text{F}}$ ); 7.79 (s, 8 H,  $\text{Bar}_4^{\text{F}}$ ); 7.92 (d, 2 H,  $J = 8$  Hz, CH(2,4)); 8.45 (t, 1 H,  $J = 8$  Hz, CH(3)).

$^{19}\text{F}\{^1\text{H}\}$ -NMR (THF- $d_8$ ):  $\delta = -64.0$  (s, 24 F,  $\text{Bar}_4^{\text{F}}$ ).

### **$[\text{Ir}(\text{N}_3\text{Me}_4)\text{ONMe}_3]\text{Bar}^{\text{F}}_4$ - **10b****

$\text{Me}_3\text{NO}$  (3.3 mg, 44  $\mu\text{mol}$ ) was added to a solution of  $[\text{Ir}(\text{N}_3\text{Me}_4)\text{THF}]\text{OTf}$  **10** (50 mg, 33  $\mu\text{mol}$ ) in THF (10 ml). The mixture was stirred for 15 min. The solvent was evaporated and the crude product was washed with pentane (2 x 5 ml). The crude product was dissolved in THF and left to crystallize at  $-35\text{ }^\circ\text{C}$ .

$^1\text{H}$ -NMR (THF- $d_8$ ):  $\delta = 1.11$  (s, 6 H, CN- $\text{CH}_3$ ); 2.10 (s, 12 H,  $\text{CH}_3$ ); 2.45 (s, 9 H,  $\text{Me}_3\text{NO}$ ); 7.15 (m, 6 H,  $\text{CH}_{\text{arom}}$ ); 7.57 (s, 4 H,  $\text{Bar}_4^{\text{F}}$ ); 7.80 (s, 8 H,  $\text{Bar}_4^{\text{F}}$ ); 8.05 (d, 2 H,  $J = 8$  Hz, CH(2,4)); 8.75 (t, 1 H,  $J = 8$  Hz, CH(3)).

### **[Ir(N<sub>3</sub>Me<sub>4</sub>)(H)DME](PF<sub>6</sub>)<sub>2</sub> - 11**

[Ir(N<sub>3</sub>Me<sub>4</sub>)OH] **6** (50 mg, 92 μmol) was dissolved in 5 ml of DME and added to a violet solution of thianthrene<sup>+</sup>PF<sub>6</sub> (66 mg, 184 μmol) in DME. The color changed from violet to dark red. The solvent was evaporated in vacuo and the crude product was crystallized from DME/pentane (−35 °C).

Yield: 46 % (48 mg, 43 μmol).

<sup>1</sup>H-NMR (CD<sub>2</sub>Cl<sub>2</sub>): δ = −32.50 (s, Ir-H); 2.25 (s, 6 H, CH<sub>3</sub>); 2.28 (s, 6 H, CH<sub>3</sub>); 2.82 (s, 6 H, CN-CH<sub>3</sub>); 3.10 (m, 2 H, DME); 3.32 (s, 3 H, DME); 3.48 (m, 2 H, DME); 3.67 (s, 3 H, DME); 7.02-7.32 (m, 6 H, CH<sub>arom</sub>); 8.26 (s, 1 H, CH(3)).

<sup>19</sup>F{<sup>1</sup>H}-NMR (CD<sub>2</sub>Cl<sub>2</sub>): −71.2 (6 F, PF<sub>6</sub>), −75.69 (6 F, PF<sub>6</sub>).

<sup>1</sup>H-NMR (THF-d<sub>8</sub>): δ = −31 (Ir-H); 2.20 (s, 6 H, CH<sub>3</sub>); 2.38 (s, 6 H, CH<sub>3</sub>); 2.80 (s, 6 H, CN-CH<sub>3</sub>); 3.28 (s, 3 H, DME); 3.42 (m, 2 H, DME); 4.11 (t, 4 H, DME); 6.42 (d, 2 H, CH(2,4)); 7.1-7.30 (m, 6 H, CH<sub>arom</sub>); 8.30 (t, 1H, CH(3)).

<sup>19</sup>F{<sup>1</sup>H}-NMR (THF-d<sub>8</sub>): δ = −72.5 (6 F, PF<sub>6</sub>); −76.3 (6 F, PF<sub>6</sub>).

<sup>31</sup>P{<sup>1</sup>H}-NMR (THF-d<sub>8</sub>): δ = −143.4 (sept, PF<sub>6</sub>).

### **[Ir(N<sub>3</sub>Me<sub>4</sub>)(DME)(H)]PF<sub>6</sub>OTf - 12**

[Ir(N<sub>3</sub>Me<sub>4</sub>)THF]OTf **10** (50 mg, 64 μmol) was dissolved in 5 ml of DME and added to a solution of thianthrene<sup>+</sup>PF<sub>6</sub> (64 μmol) in DME. The color changed from dark brown to red. The mixture was stirred for 15 min and solvent was evaporated. The crude product was extracted with DME and filtered. The solvent was evaporated. The complex was crystallized from DME/pentane (−35°C).

<sup>1</sup>H-NMR (THF-d<sub>8</sub>): δ = −32.7 (Ir-H); 1.94 (s, 6 H, CH<sub>3</sub>); 2.18 (s, 6 H, CH<sub>3</sub>); 2.49 (s, 6 H, CN-CH<sub>3</sub>); 2.79 (m, 2 H, DME); 3.27 (s, 3 H, DME); 3.43 (m, 2 H, DME); 6.62 (d, 2 H, CH(2,4)); 7.04-7.30 (m, 6 H, CH<sub>arom</sub>); 8.38 (t, 1H, CH(3)).

$^{13}\text{C}\{^1\text{H}\}$ -NMR (THF- $d_8$ ):  $\delta = 15.3$  ( $\text{CH}_3$ , DME);  $15.5$  ( $\text{CH}_2$ , DME);  $16.6$  ( $\text{CH}_3$ -CN);  $23.3$  ( $\text{CH}_3$  (overlaps with THF signal));  $127.1$ ,  $128$ ,  $128.4$  ( $\text{C}_{\text{arom}}\text{H}$ );  $129.3$  ( $\text{C}_{\text{arom}}\text{-CH}_3$ );  $130.1$  ( $\text{C}_{\text{arom}}\text{-CH}_3$ );  $134.5$  ( $\text{CH}(3)$ );  $140.2$  ( $\text{CH}(2,4)$ );  $143.8$  ( $\text{C}_{\text{arom}}\text{-N}$ );  $160.7$  ( $\text{C}(1,5)$ );  $184.6$  ( $\text{C}=\text{N}$ ).

$^{19}\text{F}\{^1\text{H}\}$ -NMR (THF- $d_8$ ):  $\delta = -72.5$  (3 F,  $\text{PF}_6$ );  $-76.2$  (3 F,  $\text{PF}_6$ );  $-80.4$  (3 F, OTf).

### **[Ir(N<sub>3</sub>Me<sub>4</sub>)(THF)Cl<sub>2</sub>]SbCl<sub>6</sub> - 13**

[Ir(N<sub>3</sub>Me<sub>4</sub>)OH] **6** (53 mg, 97,6  $\mu\text{mol}$ ) was dissolved in 5 ml THF and added to a solution of N-(p-bromophenyl)<sub>3</sub>SbCl<sub>6</sub> (159 mg, 195  $\mu\text{mol}$ ) in THF. The reaction mixture was stirred for 2 hours. The color changed from green to brown. The solvent was evaporated. The crude product was dissolved in THF and filtered through a glass filter. The solvent was reduced to half of its volume and pentane was added ( $-35$  °C).

Yield: 23 % (23 mg, 22  $\mu\text{mol}$ ).

$^1\text{H}$ -NMR (THF- $d_8$ ):  $\delta = 1.58$  (m, 4 H,  $\text{CH}_{2\text{thf}}$ );  $2.44$  (s, 12 H,  $\text{CH}_3$ );  $3.10$  (s, 6 H,  $\text{CN-CH}_3$ );  $3.36$  (m, 4 H,  $\text{CH}_2\text{-O}_{\text{thf}}$ );  $7.20$  (m, 6 H,  $\text{CH}_{\text{arom}}$ );  $8.43$  (t, 1 H,  $\text{CH}(3)$ );  $8.55$  (d, 2 H,  $\text{CH}(2,4)$ ).

$^{13}\text{C}\{^1\text{H}\}$ -NMR (THF- $d_8$ ):  $\delta = 19.1$  ( $\text{CN-CH}_3$ );  $21.7$  ( $\text{CH}_3$ );  $26.4$  ( $\text{CH}_{2\text{thf}}$ );  $74.9$  ( $\text{CH}_2\text{-O}_{\text{thf}}$ );  $129.4$ ,  $131.4$ ,  $133.0$  ( $\text{C}_{\text{arom}}\text{H}$ );  $130.8$  ( $\text{C}_{\text{arom}}\text{-CH}_3$ );  $142.2$  ( $\text{CH}(2,4)$  or  $\text{CH}(3)$ );  $145.7$  ( $\text{C}_{\text{arom}}\text{-N}$ );  $160.3$  ( $\text{C}(1,5)$ );  $186.7$  ( $\text{C}=\text{N}$ ).

Elemental analysis:

Calculated for  $\text{C}_{36}\text{H}_{49}\text{Cl}_8\text{IrN}_3\text{O}_3\text{Sb}$ : C 36.98, H 4.22, N 3.59;

Found: C 36.46, H 4.44, N 3.64.

### **[Rh(N<sub>3</sub><sup>i</sup>Pr<sub>4</sub>)OMe] - 3a**

[Rh(N<sub>3</sub><sup>i</sup>Pr<sub>4</sub>)Cl] **1a** (300 mg, 485  $\mu\text{mol}$ ) and NaOMe (42 mg, 775  $\mu\text{mol}$ ) were placed in a Schlenk tube and 20 ml of methanol was added. The mixture was stirred for 1h and the solvent was evaporated. The crude product was washed with pentane (2 $\times$ 5 ml) and dried in vacuum. The

product was extracted into toluene and filtered through a glass filter. The solvent was removed in vacuo. Green crystals were obtained from a toluene/pentane by vapor diffusion ( $-35\text{ }^{\circ}\text{C}$ ).

Yield: 71 % (212 mg, 344  $\mu\text{mol}$ ).

$^1\text{H-NMR}$  ( $\text{C}_6\text{D}_6$ ):  $\delta = 1.09$  (d, 12 H,  $^3J = 7$  Hz,  $\text{CH}(\text{CH}_3)_2$ ); 1.24 (d, 12 H,  $^3J = 7$  Hz,  $\text{CH}(\text{CH}_3)_2$ ); 2.10 (s, 6 H, CN- $\text{CH}_3$ ); 3.16 (sept, 4 H  $^3J = 7$  Hz,  $\text{CH}(\text{CH}_3)_2$ ); 4.28 (s, 3 H, O $\text{CH}_3$ ); 6.98-7.19 (m, 6 H,  $\text{CH}_{\text{arom}}$ ); 6.80 (d, 2H, CH (2,4)); 7.82 (t, 1H,  $^3J = 8$  Hz, CH (3)).

$^{13}\text{C}\{^1\text{H}\}$ -NMR ( $\text{C}_6\text{D}_6$ ):  $\delta = 17.5$  (CN- $\text{CH}_3$ ); 24.0 ( $\text{CH}(\text{CH}_3)_2$ ); 24.2 ( $\text{CH}(\text{CH}_3)_2$ ); 28.8 ( $\text{CH}(\text{CH}_3)_2$ ); 121.8 (CH(3)); 123.6 ( $\text{C}_{\text{aromH}}$ ); 124.5 (CH(2,4)); 127.1 ( $\text{C}_{\text{aromH}}$ ); 140.5 ( $\text{C}_{\text{arom}}\text{-}^i\text{Pr}$ ); 146.2 ( $\text{C}_{\text{arom}}\text{-N}$ ); 156.3 (C(1,5)); 166.9 (C=N).

Elemental analysis:

Calculated for  $\text{C}_{34}\text{H}_{46}\text{N}_3\text{ORh}$ : C 66.33, H 7.53, N 6.83;

Found: C 64.16, H 7.22, N 6.82.

### **[Rh( $\text{N}_3^i\text{Pr}_4$ ) $\text{N}_3$ ] - 15**

The rhodium radical **V** (20 mg) was dissolved in 5 ml of THF and  $\text{Me}_3\text{SiN}_3$  (4.6  $\mu\text{l}$ , 34.2  $\mu\text{mol}$ ) was added. The mixture was stirred for 2 hours. The color changed from violet to green. The solvent was evaporated and the crude product was washed with pentane (2 x 2 ml). Crystals were obtained from a solution of THF/pentane at  $-35\text{ }^{\circ}\text{C}$ .

Yield: 71 % (15.6 mg, 24  $\mu\text{mol}$  – based on complex **1a**).

$^1\text{H-NMR}$  (THF- $d_8$ ):  $\delta = 1.05$  (d, 12 H,  $^3J = 7$  Hz,  $\text{CH}(\text{CH}_3)_2$ ); 1.14 (d, 12 H,  $^3J = 7$  Hz,  $\text{CH}(\text{CH}_3)_2$ ); 1.65 (s, 6 H, CN- $\text{CH}_3$ ); 3.06 (sept, 4 H  $^3J = 7$  Hz,  $\text{CH}(\text{CH}_3)_2$ ); 7.08-7.20 (m, 6 H,  $\text{CH}_{\text{arom}}$ ); 7.87 (d, 2 H,  $^3J = 8$  Hz, CH (2,4)); 8.47 (t, 1 H,  $^3J = 8$  Hz, CH (3)).

$^{13}\text{C}\{^1\text{H}\}$ -NMR (THF- $d_8$ ):  $\delta = 16.4$  (CN- $\text{CH}_3$ ); 22.7 ( $\text{CH}(\text{CH}_3)_2$ ); 27.9 ( $\text{CH}(\text{CH}_3)_2$ ); 122.2 (CH(3)); 122.5 ( $\text{C}_{\text{aromH}}$ ); 124.5 (CH(2,4)); 126.1 ( $\text{C}_{\text{aromH}}$ ); 139.5 ( $\text{C}_{\text{arom}}\text{-}^i\text{Pr}$ ); 145.3 ( $\text{C}_{\text{arom}}\text{-N}$ ); 155.2 (C(1,5)); 166.6 (C=N).

IR (toluene):  $\nu_{\text{NN}} = 2031\text{cm}^{-1}$ .

Elemental analysis results were not adequate after repeating the measurements several times.

### **[Rh(N<sub>3</sub><sup>i</sup>Pr<sub>4</sub>)N<sub>2</sub>] - 17**

[Rh(N<sub>3</sub><sup>i</sup>Pr<sub>4</sub>)Cl] **1a** (100 mg, 161 μmol) was dissolved in 5 ml of THF and added to Na/Hg (550 mg, 183 μmol) in THF. The mixture was stirred for 1.5 h. The color of the mixture changed from green to brown. The solvent was evaporated and the crude product was washed with pentane (2×5 ml). After removing pentane in vacuum, the brown product was extracted into toluene and filtered. The solvent was evaporated. The crystals were obtained from toluene/pentane solution at -35 °C.

Yield: 76 % (75 mg, 122 μmol).

<sup>1</sup>H-NMR (C<sub>6</sub>D<sub>6</sub>): δ = 2.28 (br); 3.55(br); 5.60 (br).

IR (toluene): ν<sub>NN</sub> = 2139 cm<sup>-1</sup>

ESR (in toluene): g = 1.99 (3500 G) at RT.

Elemental analysis:

Calculated for C<sub>33</sub>H<sub>43</sub>N<sub>5</sub>Rh: C 64.70, H 7.07, N 11.43;

Found: C 65.04, H 7.39, N 9.59.

## **6.2.2 Syntheses from Chapter 3**

### **[Ir(N<sub>3</sub>Me<sub>4</sub>)Me] - 18**

#### ***Alternative syntheses***

a) [Ir(N<sub>3</sub>Me<sub>4</sub>)OMe] **4** (21 mg, 36 μmol) was dissolved in 5 ml of toluene and cooled down to -35°C. A 2M solution of ZnMe<sub>2</sub> in toluene (9 μl, 18 μmol) was added. The reaction mixture was allowed to warm up to room temperature and was stirred for 2 days. The solvent was evaporated

and the crude product was extracted into diethyl ether. After filtration, the solvent was evaporated and  $^1\text{H-NMR}$  recorded.

Yield: 70 % (14 mg, 24  $\mu\text{mol}$ ).

b)  $[\text{Ir}(\text{N}_3\text{Me}_4)\text{OH}]$  **6** (20 mg, 34  $\mu\text{mol}$ ) was dissolved in 5 ml of THF and cooled down to  $-35^\circ\text{C}$ . A 2M solution of  $\text{ZnMe}_2$  in toluene (17  $\mu\text{l}$ , 34  $\mu\text{mol}$ ) was added. The mixture was stirred until room temperature was reached. The mixture was filtered and the solvent was evaporated.

Yield: 72 % (15 mg, 26  $\mu\text{mol}$ ).

$^1\text{H-NMR}$  (THF- $d_8$ ): 0.21 (s, 6 H, CN- $\text{CH}_3$ ); 1.97 (s, 12 H,  $\text{CH}_3$ ); 6.91 (s, 3 H, Ir- $\text{CH}_3$ ); 7.0 – 7.19 (m, 6 H,  $\text{CH}_{\text{arom}}$ ); 8.40 (d,  $J = 8$  Hz, 2 H, CH(2,4)); 8.91 (t,  $J = 8$  Hz, 1 H, CH(3)).

#### **$[\text{Rh}(\text{N}_3\text{Me}_4)\text{F}](\text{Me}_2\text{N})_3\text{SOTf} - \mathbf{22}$**

$[\text{Rh}(\text{N}_3\text{Me}_4)\text{THF}]\text{OTf}$  **9** (100 mg, 144  $\mu\text{mol}$ ) was dissolved in 10 ml of THF and added to a solution of TASF (40 mg, 144  $\mu\text{mol}$ ) in THF. The color changed from brown to dark green. The mixture was stirred for 15 min and then filtered through a glass filter. The solvent was evaporated. The crude product was dissolved in 5 ml of THF and 1 ml of pentane was added to precipitate colorless crystals (of  $\text{Me}_3\text{SiF}$ ). The product was re-filtered to yield green crystals.

Yield: 61 % (71 mg, 88  $\mu\text{mol}$ ).

$^1\text{H-NMR}$  (THF- $d_8$ ):  $\delta = 1.64$  (s, 6 H, CN- $\text{CH}_3$ ); 2.14 (s, 12 H,  $\text{CH}_3$ ); 2.76 (18 H,  $(\text{Me}_2\text{N})_3\text{S}$ ); 7.03-7.08 (m, 6 H,  $\text{CH}_{\text{arom}}$ ); 7.85 (d, 2 H,  $J = 8$  Hz); 8.49 (t, 1 H,  $J = 8$  Hz).

$^{13}\text{C}\{^1\text{H}\}$ -NMR (THF- $d_8$ ):  $\delta = 16.5$  (CN- $\text{CH}_3$ ); 18.5 (4  $\text{CH}_3$ ); 38.2 ( $(\text{Me}_2\text{N})_3\text{S}$ ); 122.9 (CH(3)); 126.1 (CH(2,4)); 128.7, 131.2 ( $\text{C}_{\text{arom}}\text{H}$ ); 149.1 ( $\text{C}_{\text{arom}}\text{-N}$ ); 158.1 (C(1,5)); 168.1 (C=N).

$^{19}\text{F}\{^1\text{H}\}$ -NMR (THF- $d_8$ ):  $\delta = -80.0$  (3 F, OTf), -158.1 (1 F, Rh-F).

Elemental analysis:

Calculated for  $C_{32}H_{45}F_4N_6O_3RhS_2$ : C 47.76, H 5.64, N 10.44, S 7.97;

Found: C 47.46, H 5.65, N 10.49, S 7.69.

### **[Ir(N<sub>3</sub>Me<sub>4</sub>)F](Me<sub>2</sub>N)<sub>3</sub>SOTf - 23**

[Ir(N<sub>3</sub>Me<sub>4</sub>)THF]OTf **10** (73.3 mg, 94 μmol) was dissolved in 10 ml of THF and added to a solution of TASF (26 mg, 94 μmol) in THF. The color changed from brown to dark green. The mixture was stirred for 15 min and filtered through a glass filter. The solvent was evaporated. The crude product was dissolved in 5 ml of THF and 1 ml of pentane was added to precipitate colorless crystals (of Me<sub>3</sub>SiF). After a second filtration product was placed at -35 °C and green crystals were obtained.

Yield: 60 % (50 mg, 56 μmol).

<sup>1</sup>H-NMR (THF-d<sub>8</sub>): δ = 1.01 (s, 6 H, CN-CH<sub>3</sub>); 1.98 (s, 12 H, CH<sub>3</sub>); 2.73 (18 H, (Me<sub>2</sub>N)<sub>3</sub>S); 7.03-7.05 (m, 6 H, CH<sub>arom</sub>); 8.01 (d, 2 H, *J* = 8 Hz); 8.45 (t, 1 H, *J* = 8 Hz).

<sup>13</sup>C{<sup>1</sup>H}-NMR (THF-d<sub>8</sub>): δ = 18.6 (CN-CH<sub>3</sub>); 18.4 (4 CH<sub>3</sub>); 38.3 ((Me<sub>2</sub>N)<sub>3</sub>S); 120.4 (CH(3)); 123.9 (CH(2,4)); 126.7, 128.6, 131.6 (C<sub>arom</sub>H); 153.8 (C<sub>arom</sub>-N); 165.5 (C(1,5)); 172.7 (C=N).

<sup>19</sup>F{<sup>1</sup>H}-NMR (THF-d<sub>8</sub>): δ = -79.6 (3 F, OTf); -128.0 (1 F, Ir-F).

Elemental analysis:

Calculated for  $C_{32}H_{45}F_4N_6O_3IrS_2 \cdot (3THF)$ : C 47.59, H 5.07, N 7.57;

Found: C 47.47, H 4.97, N 6.97.

### **[Ir(N<sub>3</sub>Me<sub>4</sub>)(Me)(OTf)(CH<sub>3</sub>CN)]OTf - 28**

[Ir(N<sub>3</sub>Me<sub>4</sub>)(Me)(OTf)<sub>2</sub>] **8** (20 mg, 23 μmol) was dissolved in acetonitrile. The color from green changed to red. The solvent was evaporated and the product was dissolved in THF/pentane and left to crystallize. The reaction was quantitative.

<sup>1</sup>H-NMR (CD<sub>2</sub>Cl<sub>2</sub>): δ = 0.84 (s, 3 H, Me); 2.18 (s, 6 H, 2 CH<sub>3</sub>); 2.21 (s, 3 H, CH<sub>3</sub>CN); 2.40 (s, 6 H, 2 CH<sub>3</sub>); 2.80 (s, 6 H, 2 CH<sub>3</sub>-CN); 7.23 (m, 6 H, CH<sub>arom</sub>); 8.24-8.35 (m, 3 H, CH(2, 3, 4)).

$^{13}\text{C}\{^1\text{H}\}$ -NMR ( $\text{CD}_2\text{Cl}_2$ ):  $\delta = 2.0$  (s,  $\text{CH}_3\text{CN}$ ); 16.9 (CN- $\text{CH}_3$ ); 17.4 ( $\text{CH}_3$ ); 17.6 ( $\text{CH}_3$ ); 23.3 (Ir- $\text{CH}_3$ ); 120.5 (CH(2,4)); 126.5-128.5 ( $\text{C}_{\text{arom}}\text{H}$ ); 139.3 (CH(3)); 141.6 ( $\text{C}_{\text{arom}}\text{-CH}_3$ ); 155.5 ( $\text{C}_{\text{arom}}\text{N}$ ); 181.0 (C=N).

$^{19}\text{F}\{^1\text{H}\}$ -NMR ( $\text{CD}_2\text{Cl}_2$ ):  $\delta = -79.50$  (s, 3F, OTf);  $-79.62$  (s, 3F, OTf).

### 6.2.3 Syntheses from Chapter 4

#### **[Ir(N<sub>3</sub>Me<sub>4</sub>)(H)Cl<sub>2</sub>] - 30**

Tris-(pentafluorophenyl)borane (44 mg, 86  $\mu\text{mol}$ ) was dissolved in 5 ml of dichloromethane and added to solid [Ir(N<sub>3</sub>Me<sub>4</sub>)OMe] **4** (50 mg, 84  $\mu\text{mol}$ ). The reaction mixture was stirred for 15 min. The color changed from green to brown. The solvent was evaporated and the crude product was washed with pentane (2  $\times$  2 ml) and dried in vacuo. The complex was recrystallized from  $\text{CH}_2\text{Cl}_2$ /pentane ( $-35^\circ\text{C}$ ).

Yield: 60 % (32 mg, 51  $\mu\text{mol}$ ).

$^1\text{H}$ -NMR ( $\text{CD}_2\text{Cl}_2$ )  $\delta = -18$  (s, 1 H, Ir-H); 2.02 (s, 6 H,  $\text{CH}_3$ ); 2.40 (s, 6 H,  $\text{CH}_3$ ); 2.60 (s, 6 H, CN- $\text{CH}_3$ ); 7.12 – 7.22 (m, 6 H,  $\text{CH}_{\text{arom}}$ ); 7.87 (t, 1 H,  $J = 8$  Hz, CH(3)); 8.27 (d, 2H,  $J = 8$  Hz, CH(2,4)).

$^{13}\text{C}\{^1\text{H}\}$ -NMR ( $\text{CD}_2\text{Cl}_2$ )  $\delta = 18.6$  (CN- $\text{CH}_3$ ); 22.1 ( $\text{CH}_3$ ); 22.3 ( $\text{CH}_3$ ); 129 (CH(3)); 129.8 (CH(2,4)); 132.4, 133.0, 133.8 ( $\text{C}_{\text{arom}}\text{H}$ ); 134.0 ( $\text{C}_{\text{arom}}\text{-CH}_3$ ); 142.7 ( $\text{C}_{\text{arom}}\text{N}$ ); 154.0 (C=N).

#### **[Ir(N<sub>3</sub>Me<sub>4</sub>)] [MeOB(C<sub>6</sub>F<sub>5</sub>)<sub>3</sub>] - 31**

Tris-(pentafluorophenyl)borane (17 mg, 33  $\mu\text{mol}$ ) was dissolved in 5 ml of diethyl ether and added to [Ir(N<sub>3</sub>Me<sub>4</sub>)OMe] **4** (20 mg, 33  $\mu\text{mol}$ ). The mixture was stirred for 30 min and the color changed from green to reddish-brown. The solvent was evaporated and the crude product was washed with pentane (3  $\times$  5 ml). After drying in vacuum no further purification was necessary.

Yield: 64 % (25 mg, 21  $\mu\text{mol}$ ).

$^1\text{H}$ -NMR (THF- $d_8$ ):  $\delta$  = 1.78 (s, 6 H, CN-CH<sub>3</sub>); 2.23 (s, 12 H, CH<sub>3</sub>); 2.99 (s, br, 3 H, BOMe(C<sub>6</sub>F<sub>5</sub>)<sub>3</sub>); 7.25 (m, 6 H, CH<sub>arom</sub>); 7.93 (d, 2 H,  $J$  = 8 Hz, CH(2,4)); 8.48 (t, 1 H,  $J$  = 8 Hz, CH(3)).

$^{13}\text{C}\{^1\text{H}\}$ -NMR (THF- $d_8$ ):  $\delta$  = 17.4 (CN-CH<sub>3</sub>); 18 (CH<sub>3</sub>); 25.3 (OMeB(C<sub>6</sub>F<sub>5</sub>)); 124.2 (CH(2,4)); 123.9 (C<sub>arom</sub>-CH<sub>3</sub>); 128.2, 129.7 (C<sub>arom</sub>H); 132 (CH(3)); 151.3 (C<sub>arom</sub>-N); 160.0 (C(1,5)); 178.0 (C=N).

$^{19}\text{F}\{^1\text{H}\}$ -NMR (THF- $d_8$ ):  $\delta$  = -133.9 (m, 6 F, *o*-F); -165.4 (t, 3 F, *p*-F); -168.4 (m, 6 F, *m*-F).

### **[Ir(N<sub>3</sub>Me<sub>4</sub>)(THF)]Al(pftb)<sub>4</sub> - 10-Al(pftb)<sub>4</sub>**

#### *Alternative syntheses*

1) from complex **4**

[H(Et<sub>2</sub>O)<sub>2</sub>][Al(pftb)<sub>4</sub>] (37 mg, 33  $\mu\text{mol}$ ) was dissolved in 5 ml of THF and added into a THF solution of [Ir(N<sub>3</sub>Me<sub>4</sub>)OMe] **4** (20 mg, 33  $\mu\text{mol}$ ). The color changed immediately from green to brownish-red. The mixture was stirred for 15 min and the solvent was evaporated. No further purification was necessary.

Yield: 94 % (50 mg, 31  $\mu\text{mol}$ ).

$^1\text{H}$ -NMR (THF- $d_8$ ):  $\delta$  = 1.78 (s, 6 H, CN-CH<sub>3</sub>); 2.24 (s, 12 H, CH<sub>3</sub>); 7.26 (m, 6 H, CH<sub>arom</sub>); 7.93 (d, 2 H,  $J$  = 8 Hz, CH(2,4)); 8.51 (t, 1 H,  $J$  = 8 Hz, CH(3)).

$^{13}\text{C}\{^1\text{H}\}$ -NMR (THF- $d_8$ ):  $\delta$  = 17.6 (CN-CH<sub>3</sub>); 18.2 (CH<sub>3</sub>); 120.9, 123.9 (C<sub>arom</sub>-CH<sub>3</sub>); 124.4 (CH(2,4)); 128.5, 129.9 (C<sub>arom</sub>H); 132.0 (CH(3)); 150.1 (C<sub>arom</sub>-N); 163.5 (C(1,5)); 178.0 (C=N).

$^{19}\text{F}\{^1\text{H}\}$ -NMR (THF- $d_8$ ):  $\delta$  = -75.6 (s, 36 F, Al(pftb)<sub>4</sub>).

Elemental analysis:

Calculated for C<sub>45</sub>H<sub>35</sub>AlF<sub>36</sub>IrN<sub>3</sub>O<sub>5</sub>: C 33.76, H 2.20, N 2.62;

Found: C 33.33, H 2.29, N 2.38.

2) from complex **10**

[Ir(N<sub>3</sub>Me<sub>4</sub>)THF]OTf **10** (30 mg, 38 μmol) was added to a solution of LiAl(pftb)<sub>4</sub> (37 mg, 38 μmol) in diethyl ether (10 ml). The mixture was stirred for 45 min. The color slightly changed from brown to reddish – brown. The mixture was filtered and the solvent was evaporated. The crude product was recrystallized from THF/pentane at –35 °C.

Yield: 95 % (55 mg, 36 μmol).

<sup>1</sup>H-NMR (THF-d<sub>8</sub>): δ = 1.78 (s, 6 H, CN-CH<sub>3</sub>); 2.23 (s, 12 H, CH<sub>3</sub>); 7.26 (m, 6 H, CH<sub>arom</sub>); 7.93 (d, 2 H, *J* = 8 Hz, CH(2,4)); 8.51 (t, 1 H, *J* = 8 Hz, CH(3)).

<sup>13</sup>C{<sup>1</sup>H}-NMR (THF-d<sub>8</sub>): δ = 17.6 (CN-CH<sub>3</sub>); 18.2 (CH<sub>3</sub>); 120.9, 123.9 (C<sub>arom</sub>-CH<sub>3</sub>); 124.4 (CH(2,4)); 128.5, 129.9 (C<sub>arom</sub>H); 132.0 (CH(3)); 150.1 (C<sub>arom</sub>-N) 163.5 (C(1,5)); 178.0 (C=N).

<sup>19</sup>F{<sup>1</sup>H}-NMR (THF-d<sub>8</sub>): δ = –75.6 (s, 36 F, Al(pftb)<sub>4</sub>).

3) from complex **19**

[H(Et<sub>2</sub>O)<sub>2</sub>][Al(pftb)<sub>4</sub>] (38 mg, 34 μmol) was dissolved in 5 ml of THF and added to a THF solution of [Ir(N<sub>3</sub>Me<sub>4</sub>)Ph] **19** (22 mg, 33 μmol). The color changed immediately from green to brownish-red. The mixture was stirred for 15 min and the solvent was evaporated.

Yield: 92 % (48 mg, 29 μmol).

**[Ir(N<sub>3</sub>Me<sub>4</sub>)H][Al(pftb)<sub>4</sub>]<sub>2</sub> - 33**

[H(Et<sub>2</sub>O)<sub>2</sub>][Al(pftb)<sub>4</sub>] (37 mg, 33 μmol) was dissolved in 5 ml of THF and added into a THF solution of [Ir(N<sub>3</sub>Me<sub>4</sub>)OMe] **4** (10 mg, 17 μmol). The color changed immediately from green to red. The mixture was stirred for 20 min and the solvent was evaporated. No further purification was necessary.

$^1\text{H}$ -NMR (THF- $d_8$ ):  $\delta = -33.1$  (s, 1 H, Ir-H); 2.17 (s, 6 H,  $\text{CH}_3$ ); 2.40 (s, 6 H,  $\text{CH}_3$ ); 2.83 (s, 6 H, CN- $\text{CH}_3$ ); 7.15-7.33 (m, 6 H,  $\text{CH}_{\text{arom}}$ ); 8.36 (t, 1 H,  $J = 8$  Hz, CH(3)); 8.22 (d, 2 H,  $J = 8$  Hz, CH(2,4)).

$^{13}\text{C}\{^1\text{H}\}$ -NMR (THF- $d_8$ ):  $\delta = 16.8$  ( $\text{CH}_3$ ); 17.0 (CN- $\text{CH}_3$ ); 18.1 ( $\text{CH}_3$ ); 119.1, 125.0 ( $\text{C}_{\text{arom}}\text{-CH}_3$ ); 128.8 (CH(2,4)); 123.5, 130.3 ( $\text{C}_{\text{arom}}\text{H}$ ); 142.0 (CH(3)); 145.3 ( $\text{C}_{\text{arom}}\text{-N}$ ); 162.9 (C(1,5)); 186.0 (C=N).

$^{19}\text{F}\{^1\text{H}\}$ -NMR (THF- $d_8$ ):  $\delta = -76.3$  (s, 72 F,  $\text{Al}(\text{pftb})_4$ ).

### **$[\text{Ir}(\text{N}_3\text{Me}_4)\text{C}_5\text{H}_{10}\text{O}][\text{Al}(\text{pftb})_4]$ - 34**

As already mentioned in Chapter 4, complex **10-Al(pftb) $_4$**  is soluble in diethyl ether, THF and DME and insoluble in non-polar solvents such as pentane, benzene and toluene. In order to obtain crystals from **10-Al(pftb) $_4$**  different solvent mixtures were tried either by layering non-polar solvent on top of the ether solution of **10-Al(pftb) $_4$** , or by vapor diffusion. Crystals were obtained from a diluted solution of  $\text{Et}_2\text{O}$ /pentane at  $-35$  °C by vapor diffusion. During crystallization of **10-Al(pftb) $_4$** , compound **34** was obtained.

$^1\text{H}$ -NMR ( $\text{Et}_2\text{O-}d_{10}$ ):  $\delta = 1.01$  (m,  $-\text{OCH}_2\text{CH}_3$ ); 1.42 (m,  $-\text{OCH}_2\text{CH}_3$ ); 2.03 (s, 6 H, CN- $\text{CH}_3$ ); 2.21 (s, 12 H,  $\text{CH}_3$ ); 4.21 (s, 2 H,  $\text{CH}=\text{CH}_2$ ); 5.57 (s, 1 H,  $\text{CH}=\text{CH}_2$ ); 7.43 (m, 6 H,  $\text{CH}_{\text{arom}}$ ); 8.28 (d, 2 H,  $J = 8$  Hz); 9.07 (t, 1 H,  $J = 8$  Hz).

$^{19}\text{F}\{^1\text{H}\}$ -NMR ( $\text{Et}_2\text{O-}d_{10}$ ):  $\delta = -79.0$  (s, 36 F,  $\text{Al}(\text{pftb})_4$ ).

### **$[\text{Ir}(\text{N}_3\text{Me}_4)(\eta^2\text{-CH}_2\text{O})][\text{Al}(\text{pftb})_4]$ - 35**

$[\text{Ir}(\text{N}_3\text{Me}_4)\text{OMe}]$  **4** (38 mg, 64  $\mu\text{mol}$ ) was dissolved in 5 ml of  $\text{C}_6\text{H}_6$  and then added to a yellow solution of  $\text{Ph}_3\text{CAI}(\text{pftb})_4$  (77 mg, 64  $\mu\text{mol}$ ) in  $\text{C}_6\text{H}_6$ . The mixture was stirred for 2 hours. The color changed from green to redish-brown. The solvent was evaporated and the crude product was washed with pentane to remove  $\text{Ph}_3\text{CH}$  (until colourless solution). The crude product was dissolved in diethyl ether. Crystals were obtained from a diluted solution of  $\text{Et}_2\text{O}$ /pentane at  $-35$  °C by vapor diffusion.

Yield: 64 % (64 mg, 41  $\mu$ mol).

$^1\text{H-NMR}$  (THF- $d_8$ ):  $\delta$  = 1.94 (s, 6 H, CN- $\text{CH}_3$ ); 2.10 (s, 12 H,  $\text{CH}_3$ ); 4.00 (s, 2 H,  $\text{CH}_2\text{O}$ ); 7.29 (m, 6 H,  $\text{CH}_{\text{arom}}$ ); 8.27 (d, 2 H,  $J$  = 8 Hz); 8.84 (t, 1 H,  $J$  = 8 Hz).

$^{13}\text{C}\{^1\text{H}\}$ -NMR (THF- $d_8$ ):  $\delta$  = 16.4 ( $\text{CH}_3$ ); 17.3 (CN- $\text{CH}_3$ ); 69.1 ( $\text{CH}_2\text{O}$ ); 125.6 ( $\text{CH}(2,4)$ ); 128.4, 128.5, 129.1 ( $\text{C}_{\text{aromH}}$ ); 136.0 ( $\text{CH}(3)$ ); (C(1,5)); 150.0 ( $\text{C}_{\text{arom-N}}$ ); 178.0 (C=N).

$^{19}\text{F}\{^1\text{H}\}$ -NMR (THF- $d_8$ ):  $\delta$  = -74.3 (s, 36 F,  $\text{Al}(\text{pftb})_4$ ).

IR (toluene):  $\nu_{\text{CO}}$  = 1031  $\text{cm}^{-1}$  (tentative).

Elemental analysis:

Calculated for  $\text{C}_{42}\text{H}_{37}\text{IrN}_3\text{O}_5\text{AlF}_{36}$ : C 32.33, H 2.37, N 2.69;

Found: C 33.35, H 2.25, N 2.55.

### **$[\text{Rh}(\text{N}_3\text{Me}_4)(\text{THF})][\text{Al}(\text{pftb})_4]$ – 36**

$[\text{H}(\text{Et}_2\text{O})_2][\text{Al}(\text{pftb})_4]$  (38 mg, 34  $\mu$ mol) was dissolved in 5 ml of THF and added to a THF (5 ml) solution of  $[\text{Rh}(\text{N}_3\text{Me}_4)\text{OMe}]$  **3** (17 mg, 34  $\mu$ mol). The mixture was stirred over the night and the color changed from green to reddish-brown. The solvent was evaporated. The crude product was left to crystallize from THF/pentane solution at  $-35$   $^\circ\text{C}$ .

Yield: 88 % (45 mg, 30  $\mu$ mol).

$^1\text{H-NMR}$  (THF- $d_8$ ):  $\delta$  = 1.98 (s, 6 H, CN- $\text{CH}_3$ ); 2.30 (s, 12 H,  $\text{CH}_3$ ); 7.19 (m, 6 H,  $\text{CH}_{\text{arom}}$ ); 7.92 (d, 2 H,  $J$  = 8 Hz,  $\text{CH}(2,4)$ ); 8.39 (t, 1 H,  $J$  = 8 Hz,  $\text{CH}(3)$ ).

$^{13}\text{C}\{^1\text{H}\}$ -NMR (THF- $d_8$ ):  $\delta$  = 16.5 (CN- $\text{CH}_3$ ); 18.4 ( $\text{CH}_3$ ); 119.5, 125.3 ( $\text{C}_{\text{arom-CH}_3}$ ); 126.9 ( $\text{CH}(2,4)$ ); 127.7, 129.7 ( $\text{C}_{\text{aromH}}$ ); 131 ( $\text{CH}(3)$ ); 148.1( $\text{C}_{\text{arom-N}}$ ) 158.8 (C(1,5)); 172.1 (C=N).

$^{19}\text{F}\{^1\text{H}\}$ -NMR (THF- $d_8$ ):  $\delta$  = -76.3 (s, 36 F,  $\text{Al}(\text{pftb})_4$ ).

Elemental analysis:

Calculated for  $C_{45}H_{35}AlF_{36}N_3O_5Rh$ : C 35.76, H 2.33, N 2.78;

Found: C 39.63, H 3.18, N 3.76.

### *Alternative synthesis*

$[Rh(N_3Me_4)OMe]$  (35 mg, 69.4  $\mu$ mol) dissolved in  $C_6H_6$  was added in to a yellow solution of  $Ph_3CAI(pftb)_4$  (84 mg, 69.4  $\mu$ mol) in  $C_6H_6$ . The mixture was stirred for 30 min. The color changed from green to reddish-brown. The solvent was evaporated and the crude product was washed with pentane to remove  $Ph_3CH$  and  $Ph_3COMe$  (until a colorless solution). The crude product was dried in high vacuum and was left to crystallize from THF/pentane solution at  $-35$  °C.

Yield: 38 % (40 mg, 26  $\mu$ mol).

### **$[Rh(N_3Me_4)C_6H_{10}O][Al(pftb)_4]$ - **37****

Complex **36** is soluble in diethyl ether, THF and DME and insoluble in non-polar solvents such as pentane, benzene and toluene. In order to obtain crystals from **36**, different solvent mixtures were attempted. Crystals were obtained by slow diffusion of pentane into a diethyl ether solution of **36** at  $-35$  °C. During crystallization compound **37** was obtained.

$^1H$ -NMR ( $Et_2O-d_{10}$ ):  $\delta$  = 0.87 (m,  $-OCH_2CH_3$ ); 2.07 (s, 6 H,  $CN-CH_3$ ); 2.30 (m,  $-OCH_2CH_3$ ); 2.43 (s, 12 H,  $CH_3$ ); 3.12 (br,  $CH=CH_2$ ), 5.45 (s,  $CH=CH_2$ ); 7.43 (m, 6 H,  $CH_{arom}$ ); 7.95 (d, 2 H,  $J$  = 8 Hz); 8.56 (t, 1 H,  $J$  = 8 Hz).

$^{19}F\{^1H\}$ -NMR ( $Et_2O-d_{10}$ ):  $\delta$  = -78.1 (s, 36 F,  $Al(pftb)_4$ ).

## 7 References

1. Lunsford, J. H., *Catal. Today* **2000**, 63, 165.
2. Periana, R. A., *C&E News* **2001**, 79, 287.
3. Periana, R. A.; Bhalla, G.; Tenn, W. J.; Young, K. J. H.; Liu, X. Y.; Mironov, O.; Jones, C. J.; Ziatdinov, V. R., *J. Mol. Catal. A: Chem.* **2004**, 220, 7.
4. Arndtsen, B. A.; Bergman, R. G.; Mobley, T. A.; Peterson, T. H., *Acc. Chem. Res.* **1995**, 28, 154.
5. Crabtree, R. H., *J. Chem. Soc., Dalton Trans.* **2001**, 2437.
6. Lipscomb, J. D., *Annu. Rev. Microbiol.* **1994**, 48, 371.
7. Feig, A. L.; Lippard, S. J., *Chem. Rev.* **1994**, 94, 759.
8. Baik, M. H.; Newcomb, M.; Friesner, R. A.; Lippard, S. J., *Chem. Rev.* **2003**, 103, 2385.
9. Meunier, B., *Chem. Rev.* **1992**, 92, 1411.
10. Austin, R. N.; Chang, H. K.; Zylstra, G. J.; Groves, J. T., *J. Am. Chem. Soc.* **2000**, 122, 11747.
11. Groothaert, M. H.; Smeets, P. J.; Sels, B. F.; Jacobs, P. A.; Schoonheydt, *J. Am. Chem. Soc.* **2005**, 127, 1394.
12. Elliott, S. J.; Zhu, M.; Tso, L.; Nguyen, H. H. T.; Yip, J. H. K.; Chan, S. I., *J. Am. Chem. Soc.* **1997**, 119, 9949.
13. Grapperhaus, C. A.; Mienert, B.; Bill, E.; Weyhermüller, T.; Wieghardt, K., *Inorg. Chem.* **2000**, 39, 5306.
14. Rohde, J. U.; In, J. H.; Lim, M. H.; Brennessel, W. W.; Bukowski, M. R.; Stubna, A.; Münck, E.; Nam, W.; Que Jr., L., *Science* **2003**, 299, 1037.
15. Kaizer, J.; Klinker, E. J.; Oh, N. Y.; Rohde, J. U.; Song, W. J.; Stubna, A.; Kim, J. H.; Münck, E.; Nam, W.; Que Jr., L., *J. Am. Chem. Soc.* **2004**, 126, 472.
16. Fenton, H. S. H., *J. Chem. Soc.* **1894**, 65, 899.
17. Walling, C., *Acc. Chem. Res.* **1975**, 8, 125.
18. Koppenol, W. H., *Redox Report* **2001**, 6, 229.
19. Haber, F.; Willstätter, R., *Chem. Ber.* **1931**, 64, 2844.
20. Haber, F.; Weiss, J., *Proc. R. Soc.* **1934**, 147, 332.
21. Weiss, J., *J. Phys. Chem.* **1937**, 41, 1107.
22. Gol'dshleger, N. F.; Tyabin, M. B.; Shilov, A. E.; Shteinman, A. A., *Zh. Fiz. Khim.* **1969**, 43, 2174.

23. Eskova, V. V.; Shilov, A. E.; Shteinman, A. A., *Kinet. Katal.* **1972**, 13, 534.
24. Shilov, A. E.; Shulpin, G. B., *Chem. Rev.* **1997**, 97, 2879.
25. Labinger, J. A.; Herring, A. M.; Bercaw, J. E., *J. Am. Chem. Soc.* **1990**, 112, 5628.
26. Periana, R. A.; Taube, D. J.; Evitt, E. R.; Loffler, D. G.; Wentrcek, P. R.; Voss, G.; Masuda, T., *Science* **1993**, 259, 340.
27. Periana, R.; Taube, D. J.; Gamble, S.; Taube, H.; Satoh, T.; Fujii, H., *Science* **1998**, 280, 560.
28. Burger, P., *Habilitationsschrift*, Universität Zürich: **2002**.
29. Holm, R. H., *Chem. Rev.* **1987**, 87, 1401.
30. Nugent, W. A.; Mayer, J. M., *Metal-Ligand Multiple Bonds* 6th ed.; J. Wiley & Sons: New York, Chichester, Brisbane, Toronto, Singapore, **1988**.
31. Hay-Motherwell, R. S.; Wilkinson, G.; Hussain-Bates, B.; Hursthouse, M. B., *Polyhedron* **1993**, 12, 2009.
32. Spaltenstein, E.; Corny, R. R.; C., C. S.; Mayer, J. M., *J. Am. Chem. Soc.* **1989**, 111, 8741.
33. Anderson, T. M.; Neiwert, W. A.; Kirk, M. L.; Piccoli, P. M. B.; Schultz, A. J.; Koetzle, T. F.; Musaev, D. G.; Morokuma, K.; Cao, R.; Hill, C., *Science* **2004**, 306, 2074.
34. Mayer, J. M., *Comm. Inorg. Chem.* **1988**, 8, 125.
35. Cinellu, M. A.; Minghetti, G.; Cocco, F.; Stoccoro, S.; Zucca, A.; Manassero, M., *Angew. Chem. Int. Ed.* **2005**, 117, 7052.
36. Nüchel, S.; Burger, P., *Angew. Chem. Int. Ed.* **2003**, 42, 1632.
37. Budzelaar, P. H. M.; De Bruin, B.; Gal, A. W.; Wieghardt, K.; van Lenthe, J. H., *Inorg. Chem.* **2001**, 40, 4649.
38. Susnjar, N., unpublished results, **2004**.
39. Luo, L.; Lanza, G.; Fragala, I. L.; Stern, C. L.; Marks, T. J., *J. Am. Chem. Soc.* **1998**, 120, 3111.
40. Alyea, E. C.; Merrel, P. H., *Inorg. Met.-Org. Chem* **1974**, 4, 535.
41. Small, L. B.; Brookhart, M.; Bennet, A. M. A., *J. Am. Chem. Soc.* **1998**, 120, 4049.
42. Fontana, F.; Minisci, F.; Barbosa, N. C. M.; Vismara, E., *Tetrahedron* **1990**, 46, 2525.
43. Haarman, F. H.; Bregman, R. F.; van Leeuwen, M. N. W. P.; Vrieze, K., *Organometallics* **1997**, 16, 979.
44. Nüchel, S.; Burger, P., *Organometallics* **2001**, 20, 4345.
45. Tanke, R. S.; Crabtree, R. H., *Inorg. Chem.* **1989**, 28, 3444.
46. Arthurs, M. A.; Bickerton, J.; Stobart, S. R.; Wang, J., *Organometallics* **1998**, 17, 2743.

47. Nüchel, S. PhD Thesis. Universität Zürich, **2002**.
48. Dias, L. E.; Brookhart, M.; White, S. P., *Organometallics* **2000**, 19, 4995.
49. Esteruelas, A. M.; Lopez, M. A.; Oro, A. L.; Perez, A.; Schulz, M.; Werner, H., *Organometallics* **1993**, 12, 1823.
50. Lunder, M. D.; Lobkovsky, E.; Streib, E. W.; Caulton, G. K., *J. Am. Chem. Soc.* **1991**, 113, 1837.
51. Luo, X. L.; Schulte, K. G.; Crabtree, H. R., *Inorg. Chem.* **1990**, 29, 682.
52. Connelly, G. N.; Geiger, E. W., *Chem. Rev.* **1996**, 96, 877.
53. Hermann, D.; Gandelman, M.; Rozenberg, H.; Shimon, W. J. L.; Milstein, D., *Organometallics* **2002**, 21, 812.
54. Kanzelberger, M.; Zhang, X.; Emge, J. T.; Goldman, S. A.; Zhao, J.; Incarvito, C.; Hartwig, F. J., hydride. *J. Am. Chem. Soc.* **2003**, 125, 13644.
55. Neve, F.; Ghedini, M.; Tiripicchio, A.; Ugozzoli, F., *Inorg. Chem.* **1989**, 28, 3084.
56. Gillard, R. D.; Mitchell, S. H.; Williams, P. A.; Vagg, R. S., *J. Coord. Chem.* **1984**, 13, 325.
57. Vogler, L. M.; Scott, B.; Brewer, K. J., *Inorg. Chem.* **1993**, 32, 898.
58. Hoogervorst, J. W.; Goubitz, K.; Fraanje, J.; Lutz, M.; Spek, L. A.; Ernsting, M. J.; Elsevier, J. C., *Organometallics* **2004**, 23, 4550.
59. Williams, W. E.; Lalor, F. J., *J. Chem. Soc., Dalton Trans.* **1973**, 1329.
60. Connelly, G. N.; Kitchen, M. D., *J. Chem. Soc., Dalton Trans.* **1977**, 931.
61. Beck, W.; Sünkel, K., *Chem. Rev.* **1988**, 88, 1405.
62. Barrera, J.; Sabat, M.; Harman, W. D., *J. Am. Chem. Soc.* **1991**, 113, 8178.
63. Krossing, I.; Brands, H.; Feuerhake, R.; Koenig, S., *J. Fluorine Chem.* **2001**, 112, 83.
64. Krossing, I.; Raabe, I., *Angew. Chem.* **2004**, 116, 2116.
65. Nubel, P. O.; Wilson, S. R.; Brown, T. L., *Organometallics* **1983**, 2, 515.
66. Jin, S.; Nieuwenhuyzen, M.; Wilkins, C. J., *J. Chem. Soc., Dalton Trans.* **1992**, 2071.
67. Buijs, W.; Comba, P.; Corneli, D.; Pritzkow, H., *J. Organomet. Chem.* **2002**, 641, 71.
68. Herrmann, W. A.; Bauer, C.; Plank, J.; Kalcher, W.; Speth, D.; Ziegler, M. L., *Angew. Chem. Int. Ed.* **1981**, 20, 193.
69. Yoo, B. W.; Choi, J. W.; Kim, D. Y.; Hwang, S. K.; Choi, K. I.; Kim, J. H., *Bull. Korean Chem. Soc.* **2002**, 23, 797.
70. Yoo, B. W.; Hwang, S. K.; Kim, D. Y.; Choi, J. W.; Kang, S. O.; Yoo, B. S.; Choi, K. I.; Kim, J. H., *Bull. Korean Chem. Soc.* **2004**, 25, 1633.
71. Holm, R. H.; Kennepohl, P.; Solomon, E. I., *Chem. Rev.* **1996**, 96, 2239.

72. Craig, C. J.; Purushothaman, K. K., *J. Org. Chem.* **1970**, 35, 1721.
73. Caron, A.; Palenik, G. J.; Goldish, E.; Donolme, J., *Acta Cryst.* **1964**, 17, 102.
74. Xu, X.; Goddard, W. A., *PNAS* **2004**, 101, 2673.
75. Desiraju, G. R., *Acc. Chem. Res.* **1996**, 29, 441.
76. Desiraju, G. R.; Kashino, S.; Coombs, M. M.; Glusker, J. P., *Acta Cryst.* **1993**, B49, 880.
77. Trost, M. B.; Braslau, R., *J. Org. Chem.* **1988**, 53, 532.
78. Campestrini, S.; Meunier, B., *Inorg. Chem.* **1992**, 31, 1999.
79. Wessel, J.; Crabtree, R. H., *J. Mol. Catal. A.* **1996**, 113, 13.
80. Pietikäinen, P., *Tetrahedron* **2000**, 56, 417.
81. Stahl, S. S., *Angew. Chem. Int. Ed.* **2004**, 43, 3400.
82. Sheldon, R. A.; Kochi, J. K., *Metal-Catalyzed Oxidation of Organic Compounds* **1981**, New York, (Academic Press).
83. Solomon, E. I.; Brunold, T. C.; Davis, M. I.; Kemsley, J. N.; Lee, S. K.; Lehnert, N.; Neese, F.; Skulan, A. J.; Yang, Y. S.; Zhou, J., *Chem. Rev.* **2000**, 100, 235.
84. Que, L.; Ho, R. Y. N., *Chem. Rev.* **1996**, 96, 2607.
85. Lewis, E. A.; Tolman, W. B., *Chem. Rev.* **2004**, 104, 1047.
86. Kim, E.; Chufan, E. E.; Kamaraj, K.; Karlin, K. D., *Chem. Rev.* **2004**, 104, 1077.
87. Egan, J. W.; Haggerty, B. S.; Rheingold, A. L.; Sendlinger, S. C.; Theopold, K. H., *J. Am. Chem. Soc.* **1990**, 112, 2445.
88. "Metal-dioxygen complexes", *Chem. Rev.* **1994**, 94, 567-856.
89. Berger, S.; S., B.; Kalinowski, H., *<sup>31</sup>P-NMR Spektroskopie* Georg Thieme Verlag, Stuttgart-New York: **1991**, 165.
90. Collman, J. P.; Boulatov, R.; Sunderland, C. J.; Fu, L., *Chem. Rev.* **2004**, 104, 561.
91. Poli, R., *Chem. Rev.* **1996**, 96, 2135.
92. Baird, M. C., *Chem. Rev.* **1988**, 88, 1217.
93. Hetterscheid, H. G. D.; Kaiser, J.; Reijerse, E.; Peters, J. P. T.; Thewissen, S.; Blok, J. N. A.; Smith, M. M. J.; de Gelder, R.; de Bruin, B., *J. Am. Chem. Soc.* **2005**, 127, 1895.
94. Limberg, C., *Angew. Chem. Int. Ed.* **2003**, 42, 5932.
95. Jewson, J. D.; Liable-Sands, L. M.; Yap, A. P. G.; Rheingold, A. L.; Theopold, K. H., *Organometallics* **1999**, 18, 300.
96. Hetterscheid, D. G. H.; De Bruin, B.; Smits, J. M. M.; Gal, A. W., *Organometallics* **2003**, 22, 3022.
97. Zhang, X. X.; Wayland, B. B., *J. Am. Chem. Soc.* **1994**, 116, 7897.
98. Zhang, X. X.; Parks, G. F.; Wayland, B. B., *J. Am. Chem. Soc.* **1997**, 119, 7938.

99. Miessler, G. L.; Tarr, D. A., *Inorganic Chemistry*. 3rd ed.; Pearson, Prentice Hall: **2004**.
100. van Koten, G.; Jastrzebski, J. T. B. H.; Vrieze, K., *J. Organomet. Chem.* **1983**, 250, 49.
101. Kaupp, M.; Stoll, H.; Preuss, H.; Kaim, W.; Stahl, T.; Van Koten, G.; Wissing, E.; Smeets, W. J. J.; Spek, L. A., *J. Am. Chem. Soc.* **1991**, 113, 5606.
102. Kooistra, M. T.; Hetterscheid, D. G. H.; Schwartz, E.; Knijnenburg, Q.; Budzelaar, P. H. M.; Gal, A. W., *Inorg. Chim. Acta.* **2004**, 357, 2945.
103. Blackmore, I. J.; Gibson, V. C.; Hitchcock, P. B.; Rees, C. W.; Williams, D. J.; White, A. J. P., *J. Am. Chem. Soc.* **2005**, 127, 6012.
104. Braese, S.; Gil, C.; Knepper, K.; Zimmerman, V., *Angew. Chem. Int. Ed.* **2005**, 44, 5188.
105. Laubender, M.; Werner, H., *Angew. Chem. Int. Ed.* **1998**, 37, 150.
106. Hu, X.; Meyer, K., *J. Am. Chem. Soc.* **2004**, 126, 16323.
107. Shay, T. D.; Yap, A. P. G.; Zakharov, N. L.; Rheingold, L. A.; Theopold, H. K., *Angew. Chem. Int. Ed.* **2005**, 117, 1532.
108. Dai, X.; Kapoor, P.; Warren, H. T., *J. Am. Chem. Soc.* **2004**, 126, 4799.
109. MacKay, A. B.; Fryzuk, D. M., *Chem. Rev.* **2004**, 104, 385.
110. Squillacote, M.; De Felippis, J., *J. Org. Chem.* **1994**, 59, 3564.
111. Simeonov, A. M., *J. Org. Chem.* **1995**, 60, 1897.
112. Yamada, H.; O'Leary, M. H., *J. Am. Chem. Soc.* **1977**, 99, 1661.
113. Gibson, V. C.; Humphries, J. M.; Tellman, P. K.; Wass, F. D.; White, P. J. A.; Williams, J. D., *Chem. Comm.* **2001**, 2252.
114. Crabtree, R. H., *The organometallic chemistry of the transition metals*. 2nd ed.; John Wiley & Sons: **1994**.
115. Brookhart, M., unpublished results, **1999**.
116. Kulzick, M. A.; Price, R. T.; Andersen, R. A.; Muetterties, E. L., *J. Organomet. Chem.* **1987**, 333, 105.
117. Faller, J. W.; Crabtree, R. H.; Habib, A., *Organometallics* **1985**, 4, 929.
118. Kubas, G. J., *Metal Dihydrogen and  $\sigma$ -Bond Complexes* Kluwer Academic, New York: **2001**, 200.
119. Limbach, H. H.; Ulrich, S.; Gruendemann, S.; Buntkowsky, G.; Sabo-Etienne, S.; Chaudret, B.; Kubas, G. J.; Eckert, J., *J. Am. Chem. Soc.* **1998**, 120, 7929.
120. Matthes, J.; Gründemann, S.; Toner, A.; Guari, Y.; Donnadiou, B.; Spandl, J.; Sabo-Etienne, S.; Clot, E.; Limbach, H. H.; Chaudret, B., *Organometallics* **2004**, 23, 1424.
121. Crabtree, R. H.; Lavin, M.; Bonnevot, L., *J. Am. Chem. Soc.* **1986**, 108, 4032.
122. Heinekey, D. M.; Oldham Jr., W. J., *Chem. Rev.* **1993**, 93, 913.

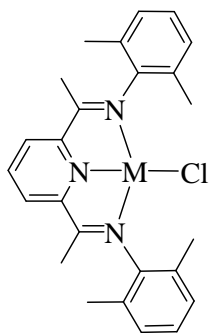
123. Sabo-Etienne, S.; Chaudret, B., *Chem. Rev.* **1998**, 98, 2077.
124. Ingleson, M. J.; Brayshaw, S. K.; Mahon, M. F.; Ruggiero, G. D.; Weller, A. S., *Inorg. Chem.* **2005**.
125. Bernskoetter, W. H.; Lobkovsky, E.; Chirik, P. J., *J. Am. Chem. Soc.* **2005**, 127, 7901.
126. Gusev, D. G., *J. Am. Chem. Soc.* **2004**, 126, 14249.
127. Burger, P., unpublished results. **2004**.
128. Lin, Z., *Chem. Soc. Rev.* **2002**, 31, 239.
129. Corey, J. Y.; Braddock-Wilking, J., *Chem. Rev.* **1999**, 99, 175.
130. Doherty, M. N.; Hoffman, W. N., *Chem. Rev.* **1991**, 91, 553.
131. Grushin, V. V.; Marshall, W. J., *J. Am. Chem. Soc.* **2004**, 126, 3068.
132. Marshall, W. J.; Grushin, V. V., *Organometallics* **2004**, 23, 3343.
133. Yahav, A.; Goldberg, I.; Vigalok, A., *J. Am. Chem. Soc.* **2003**, 125, 13634.
134. Yahav, A.; Goldberg, I.; Vigalok, A., *Inorg. Chem.* **2005**, 44, 1547.
135. Murphy, F. E.; Murugavel, R.; Roesky, W. H., *Chem. Rev.* **1997**, 97, 3425.
136. Vicente, J.; Rubio, G. J.; Bautista, D., *Inorg. Chem.* **2001**, 40, 2636.
137. Farnham, W. B.; Dixon, D. A.; Middleton, W. J.; Calabrese, J. C.; Harlow, R. L.; Whitney, J. F.; Jones, G. A.; Guggenberger, L. J., *J. Am. Chem. Soc.* **1987**, 109, 476.
138. Borrmann, T.; Lork, E.; Mews, R.; Stohrer, W.-D., *J. Fluorine Chem.* **2004**, 125, 903.
139. Thalladi, V. R.; Weiss, H. C.; Bläser, D.; Boese, R.; Nangia, A.; Desiraju, G. R., *J. Am. Chem. Soc.* **1998**, 120, 8702.
140. Kryachko, E.; Scheiner, S., *J. Phys. Chem. A* **2004**, 108, 2527.
141. Brook, M. A., *Silicon in Organic, Organometallic and Polymer Chemistry*. Wiley, New York: **2000**; 28-38.
142. Sun, H.; DiMagno, G. S., *J. Am. Chem. Soc.* **2005**, 127, 2050.
143. West, R., *J. Am. Chem. Soc.* **1954**, 76, 6012.
144. Steward, W. O.; Pierce, R. O., *J. Am. Chem. Soc.* **1961**, 83, 1916.
145. Frankiss, G. S., *J. Phys. Chem.* **1967**, 71, 3418.
146. Williams, S. B.; Goldberg, K. I., *J. Am. Chem. Soc.* **2001**, 123, 2576.
147. Mann, G.; Incarvito, C.; Rheingold, A. L.; Hartwig, F. J., *J. Am. Chem. Soc.* **1999**, 121, 3224.
148. Widenhoefer, R. A.; Buchwald, S. L., *J. Am. Chem. Soc.* **1998**, 120, 6504.
149. Canty, A. J.; Jin, H.; Skelton, B. W.; White, A. H., *Inorg. Chem.* **1998**, 37, 3975.
150. Hartwig, J. F., *Acc. Chem. Res.* **1998**, 31, 852.
151. Crumpton, D. M.; Goldberg, K. I., *J. Am. Chem. Soc.* **2000**, 122, 962.

152. Williams, S. B.; Goldberg, K. I., *J. Am. Chem. Soc* **2001**, 123.
153. Fekl, U.; Kaminsky, W.; Goldberg, K. I., *J. Am. Chem. Soc.* **2003**, 125, 15286.
154. Fekl, U.; Kaminsky, W.; Goldberg, K. I., *J. Am. Chem. Soc* **2001**, 123, 6423.
155. Bartlett, K. L.; Goldberg, K. I.; Borden, W. T., *J. Am. Chem. Soc* **2000**, 122, 1456.
156. Kalinowski, H.; Berger, S.; S., B. In *<sup>13</sup>C-NMR-Spektroskopie*, Georg Thieme Verlag, Stuttgart-New York: **1984**; 448.
157. Hahn, C.; Sieler, J.; Taube, R., *Polyhedron* **1998**, 17, 1183.
158. Hahn, C.; Spiegler, M.; Herdweck, E.; Taube, R., *Eur. J. Inorg. Chem.* **1999**, 435.
159. Dias, L. E.; Brookhart, M.; White, P. S., *Chem. Comm.* **2001**, 423.
160. Ortmann, D. A.; Gevert, O.; Laubender, M.; Werner, H., *Organometallics* **2001**, 20, 1776.
161. Carmona, D.; Ferrer, J.; Lorenzo, M.; Santander, M.; Ponz, S.; Lahoz, F. J.; Lopez, J. A.; Oro, A. L., *Chem. Comm.* **2002**, 870.
162. Melenkivitz, R.; Hillhouse, G. L., *Chem. Comm.* **2002**, 660.
163. Cabrera, L.; Hollink, E.; Stewart, J. C.; Wei, P.; Stephan, D. W., *Organometallics* **2005**, 24, 1091.
164. Yue, N. L. S.; Stephan, D. W., *Organometallics* **2001**, 20, 2303.
165. Krossing, I.; Reisinger, A., *Eur. J. Inorg. Chem.* **2005**, 1979.
166. Deem, M. L.; Iobst, E. J.; Zink, M. D., *Inorg. Chim. Acta.* **1989**, 157, 153.
167. Harman, W. D.; Chen, H., *J. Am. Chem. Soc* **1996**, 118, 5672.
168. Raubenheimer, H. G.; Esterhuysen, M. W.; Timoshkin, A.; Chen, Y.; Frenking, G., *Organometallics* **2002**, 21, 3173.
169. Budzelaar, P. H. M.; Moonen, N. N. P.; de Gelder, R.; Smits, J. M. M.; Gal, A. W., *Eur. J. Inorg. Chem.* **2000**, 753.
170. Fujita, K.; Nakaguma, H.; Hanasaka, F.; Yamaguchi, R., *Organometallics* **2002**, 21, 3749.
171. Baird, G. J.; Davies, S. G.; Jones, R. H.; Prout, K.; Warner, P., *Chem. Comm.* **1984**, 12, 745.
172. Veya, P.; Floriani, C.; Chiesi-Villa, A.; Rizzoli, C., *Organometallics* **1994**, 13, 214.
173. Schröder, W.; Pörschke, K.; Tsay, Y. H.; Krüger, C., *Angew. Chem. Int. Ed.* **1987**, 26, 919.
174. Thiyagarajan, B.; Michalzyk, L.; Bollinger, J. C.; Huffman, J. C.; Bruno, J. W., *Organometallics* **1996**, 15, 1989.

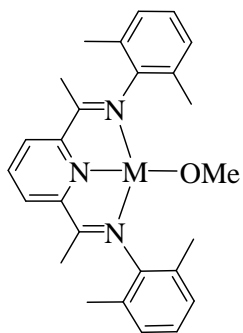
175. Hesse, M.; Meier, H.; Zeeh, B., *Spektroskopische Methoden in der organischen Chemie*. 3rd ed.; Thieme, Stuttgart: **1987**; 140.
176. Huang, Y. H.; Gladysz, J. A., *J. Chem. Educ.* **1988**, 65, 298.
177. Gibson, D. H.; Owens, K.; Mandal, S. K.; Sattich, W. E.; Franco, J. O., *Organometallics* **1989**, 8, 498.
178. Reinartz, S.; Brookhart, M.; Templeton, J. L., *Organometallics* **2002**, 21, 247.
179. Gambarotta, S.; Floriani, C.; Chiesi-Villa, A.; Guastini, C., *Organometallics* **1986**, 5, 2425.
180. Wells, A. F., *Structural Inorganic Chemistry*. 3rd ed.; Oxford Press: **1962**; 717.
181. Clark, G. R.; Headford, C. E. L.; Mardsen, K.; Roper, W. R., *J. Organomet.Chem.* **1982**, 231, 335.
182. Buhro, W. E.; Patton, A. T.; Strouse, C. E.; Gladysz, J. A.; McCormick, F. B.; Etter, M. C., *J. Am. Chem. Soc.* **1983**, 105, 1056.
183. Klein, D. P.; Gladysz, J. A., *J. Am. Chem. Soc.* **1991**, 114, 8710.
184. Mendez, N. Q.; Seyler, J. W.; Arif, A. M.; Gladysz, J. A., *J. Am. Chem. Soc.* **1993**, 115, 2323.
185. Gambarotta, S.; Floriani, C.; Chiesi-Villa, A.; Guastini, C., *J. Am. Chem. Soc.* **1983**, 105, 1690.
186. Erker, G.; Kropp, K.; Krüger, C.; Chiang, A. P., *Chem. Ber.* **1982**, 115, 2447.
187. Bryndza, H. E.; Calabrese, J. C.; Marsi, M.; Roe, D.; Tam, W.; Bercaw, J. E., *J. Am. Chem. Soc.* **1986**, 108, 4805.
188. Blum, O.; Milstein, D., *J. Am. Chem. Soc.* **1995**, 117, 4582.
189. Blum, O.; Milstein, D., *Angew. Chem. Int. Ed.* **1995**, 34, 229.
190. Hammond, G. S., *J. Am. Chem. Soc.* **1955**, 77, 334.
191. Armarego, W. L. F.; Chai, C. L. L., *Purification of Laboratory Chemicals* **2003**, 322.
192. Sheldrick, G. *SHELXTL*, Universität Göttingen: Göttingen, **1988**.
193. Sheldrick, G. *SHELXL 97*, Universität Göttingen: Göttingen, **1997**.
194. Cramer, R.; McCleverty, J. A.; Bray, J., *Inorg. Synth.* **1990**, 28, 86.
195. Huisgen, R.; Bayerlein, F.; Heydkamp, W., *Chem. Ber.* **1959**, 92, 3223.
196. Krossing, I., *Chem. Eur. J.* **2001**, 7, 490.
197. Britovsek, G. J. P.; Bruce, M.; Gibson, C. V.; Kimberley, B. S.; Maddox, P. J.; Mastroianni, S.; McTavish, S. J.; Redshaw, C.; Solan, G. A.; Strömberg, S.; White, A. J. P.; Williams, D. J., *J. Am. Chem. Soc.* **1999**, 121, 8728.

## 8 Appendix

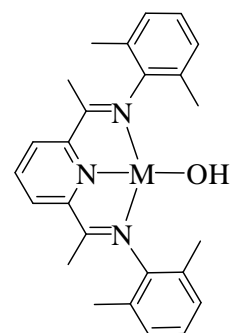
### 8.1 Starting materials (1 – 7, 9)<sup>44, 49</sup>



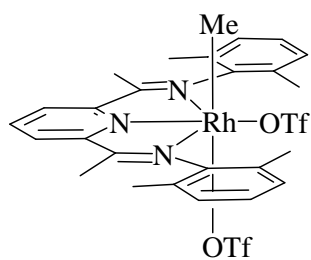
Rh **1**  
Ir **2**



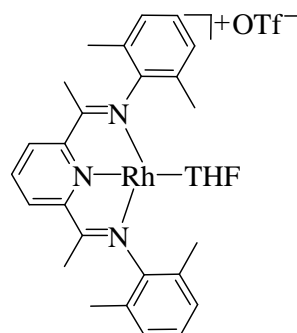
Rh **3**  
Ir **4**



Rh **5**  
Ir **6**

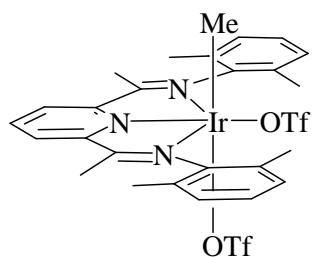


**7**

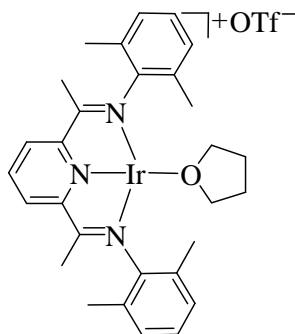


**9**

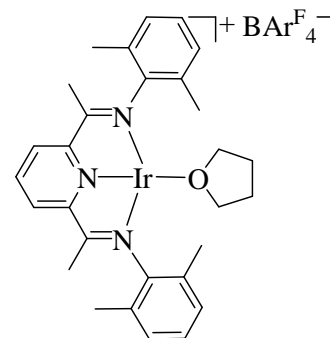
### 8.2 Isolated complexes (8-36)



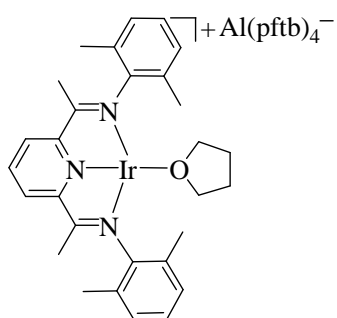
**8**



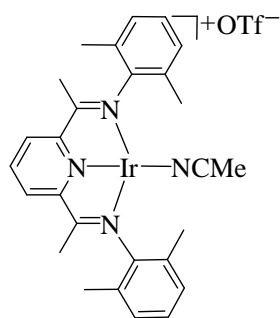
**10**



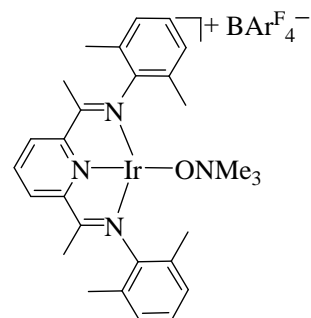
**10-BArF<sub>4</sub>**



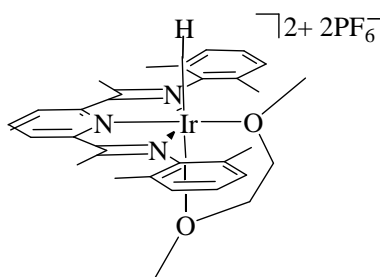
**10-Al(pftb)<sub>4</sub>**



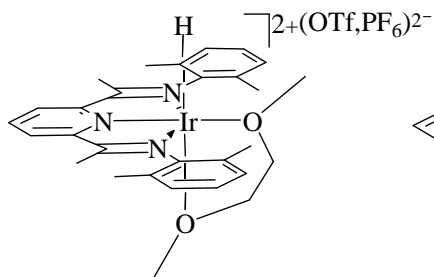
**10-MeCN**



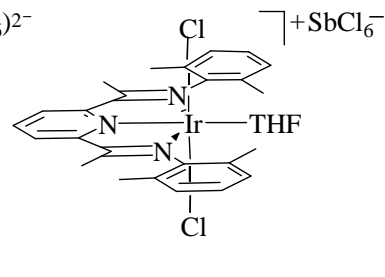
**10b**



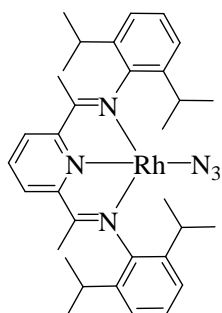
**11**



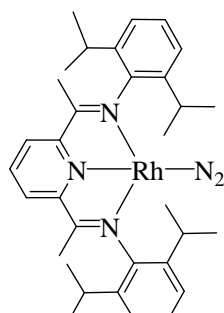
**12**



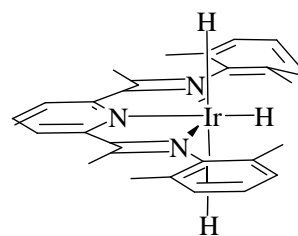
**13**



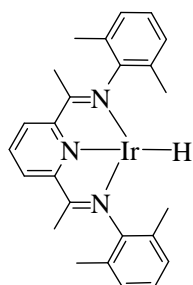
**15**



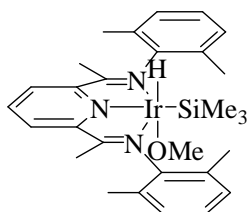
**17**



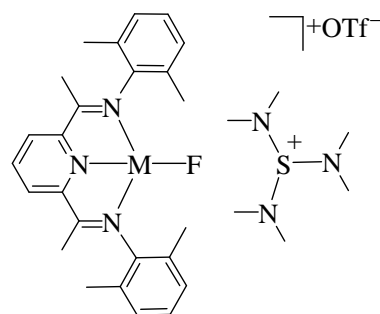
**20**



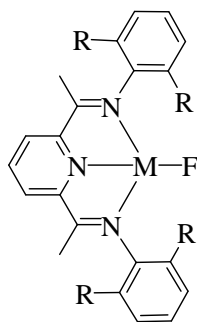
**20c**



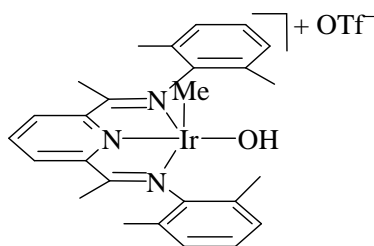
**21**



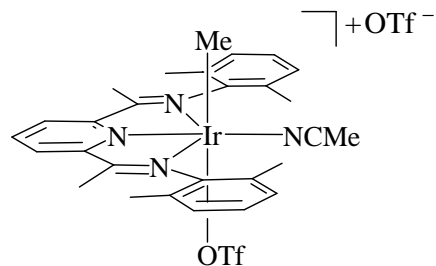
**Rh 22**  
**Ir 23**



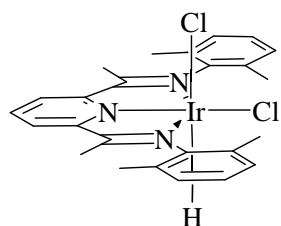
M = Rh; R = Me **24**  
 M = Ir; R = Me **25**  
 M = Rh; R = <sup>i</sup>Pr **26**



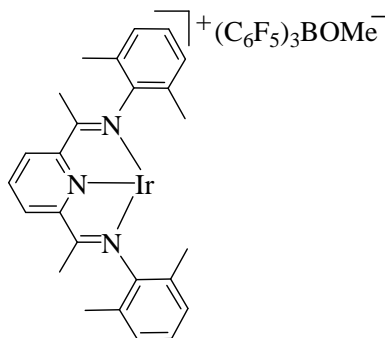
**27**



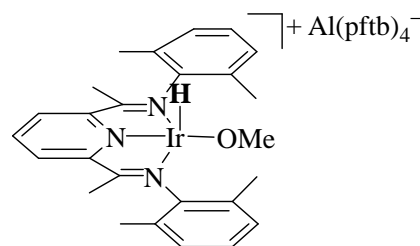
**28**



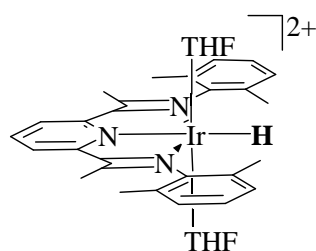
**30**



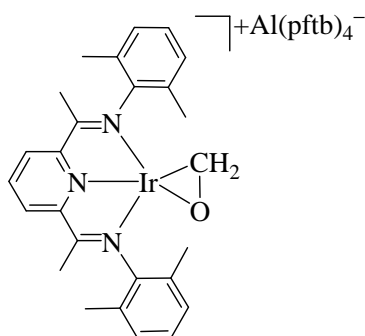
**31**



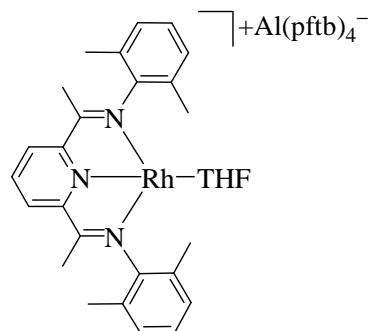
**32**



**33**

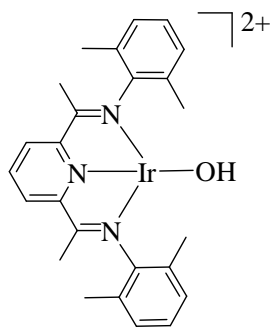


**35**

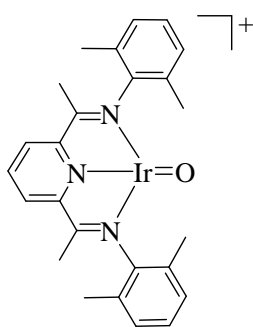


**36**

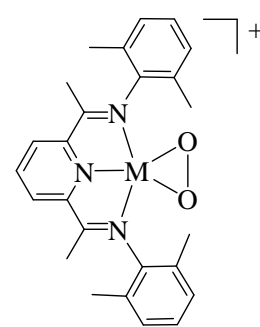
### 8.3 Summary of postulated complexes



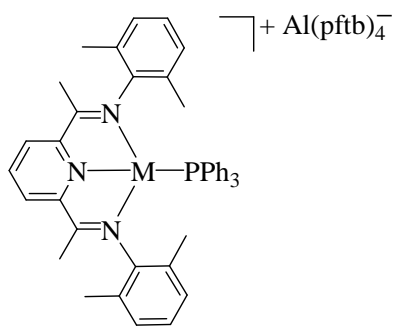
**I**



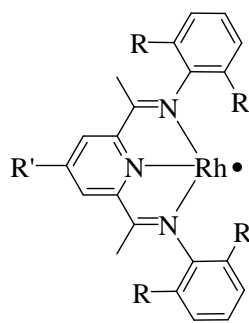
**II**



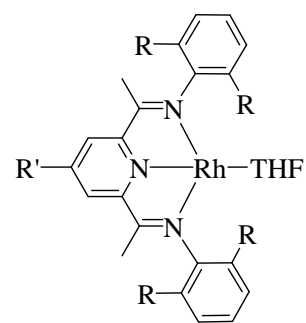
**III** M = Ir, Rh



Rh, **IVa**; Ir, **IVb**

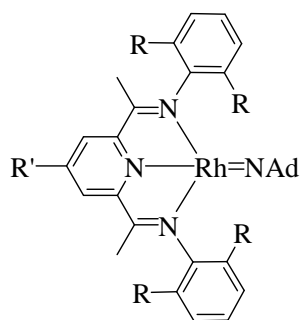


**V**



**Va**

R = Me, iPr  
R' = H, t-Bu



**VI**

## 8.2 X-ray crystallographic data and parameters

Complex	[Ir(N <sub>3</sub> Me <sub>4</sub> )THF]OTf <b>10</b>	[Ir(N <sub>3</sub> Me <sub>4</sub> )(DME)(H)](PF <sub>6</sub> ) <sub>2</sub> <b>11</b>
Empirical formula	C <sub>30</sub> H <sub>35</sub> F <sub>3</sub> IrN <sub>3</sub> O <sub>4</sub> S	C <sub>37</sub> H <sub>58</sub> F <sub>12</sub> IrN <sub>3</sub> O <sub>6</sub> P <sub>2</sub>
Formula weight [g/mol]	782.87	1123.00
Crystal size [mm]		0.14 x 0.11 x 0.10
Crystal system	monoclinic	monoclinic
Space group	P2 <sub>1</sub> /c, No. 14	P2 <sub>1</sub> /c, No. 14
a [Å]	13.7740(11)	16.3156(12)
b [Å]	15.9555(16)	12.3642(7)
c [Å]	14.8682(11)	22.3933(18)
α [°]		
β [°]	106.767(9)	99.166(9)
γ [°]		
V [Å <sup>3</sup> ]	3128.7(5)	4459.7(5)
Z	4	4
D <sub>calc.</sub> [g/cm <sup>3</sup> ]	1.662	1.673
Temperature [K]	193	183
λ [Å], Mo-Kα	0.71073	0.71073
2 Θ [°]	2.55, 25.82	1.89, 23.92
Refln. collected, unique	5785, 5785	26773, 6881
No. of parameters	359	566
GooF, S	0.923	0.940
R <sub>1</sub> (I>2σ(I))	0.0477	0.0323
wR <sub>2</sub> (I>2σ(I))	0.1176	0.0485
ρ <sub>min,max</sub> [e/ Å <sup>3</sup> ]	2.716, -1.757	0.720, -0.505

<b>Complex</b>	<b>[Ir(N<sub>3</sub>Me<sub>4</sub>)(THF)Cl<sub>2</sub>]SbCl<sub>6</sub>·2THF <b>13</b></b>	<b>[Rh(N<sub>3</sub><sup>i</sup>Pr<sub>4</sub>)N<sub>2</sub>] <b>17</b></b>
Empirical formula	C <sub>37</sub> H <sub>51</sub> Cl <sub>8</sub> IrN <sub>3</sub> O <sub>3</sub> Sb	C <sub>33</sub> H <sub>43</sub> N <sub>5</sub> Rh
Formula weight [g/mol]	1183.40	612.63
Crystal size [mm]		0.72 x 0.26 x 0.07
Crystal system	monoclinic	orthorhombic
Space group	C2/c, No. 15	P2 <sub>1</sub> 2 <sub>1</sub> 2 <sub>1</sub> , No. 19
a [Å]	27.406(3)	8.4292(4)
b [Å]	9.1101(6)	18.0316(9)
c [Å]	37.6923(6)	20.3519(10)
α [°]		
β [°]	107.235(16)	
γ [°]		
V [Å <sup>3</sup> ]	8988.2(10)	3093.3(3)
Z	8	4
D <sub>calc.</sub> [g/cm <sup>3</sup> ]	1.611	1.315
Temperature [K]	193	153
λ [Å], Mo-Kα	0.71073	0.71073
2 θ [°]	2.37, 22.15	1.51, 32.58
Refln. collected, unique	2355, 2172	83054, 11219
No. of parameters	465	353
Goof, S	1.003	1.047
R <sub>1</sub> (I>2σ(I))	0.0266	0.0364
wR <sub>2</sub> (I>2σ(I))	0.0602	0.0760
ρ <sub>min,max</sub> [e/ Å <sup>3</sup> ]	0.437, -0.664	0.885, -0.788

<b>Complex</b>	<b>[Rh(N<sub>3</sub><sup>1</sup>Pr<sub>4</sub>)N<sub>3</sub>].2THF <b>15</b></b>	<b>[Rh(N<sub>3</sub>Me<sub>4</sub>)F]((Me<sub>2</sub>N)<sub>3</sub>SOTf) <b>22</b></b>
Empirical formula	C <sub>41</sub> H <sub>59</sub> N <sub>6</sub> O <sub>2</sub> Rh	C <sub>32</sub> H <sub>45</sub> F <sub>4</sub> N <sub>6</sub> O <sub>4</sub> RhS <sub>2</sub>
Formula weight [g/mol]	770.85	820.77
Crystal size [mm]	0.6 x 0.14 x 0.05	0.58 x 0.48 x 0.05
Crystal system	triclinic	orthorhombic
Space group	P-1, No. 2	Pbca, No. 61
a [Å]	9.967(3)	13.3966(14)
b [Å]	14.173(4)	20.791(2)
c [Å]	15.899(4)	26.391(3)
α [°]	111.602(4)	
β [°]	94.160(4)	
γ [°]	103.753(4)	
V [Å <sup>3</sup> ]	1996.1(9)	7350.8(13)
Z	2	8
D <sub>calc.</sub> [g/cm <sup>3</sup> ]	1.283	1.483
Temperature [K]	153	153
λ [Å], Mo-Kα	0.71073	0.71073
2 θ [°]	1.40, 27.53	1.54, 28.11
Refln. collected, unique	23205, 8802	81686, 8739
No. of parameters	427	443
GooF, S	1.215	0.911
R <sub>1</sub> (I>2σ(I))	0.1075	0.0773
wR <sub>2</sub> (I>2σ(I))	0.1794	0.1634
ρ <sub>min,max</sub> [e/ Å <sup>3</sup> ]	1.896, -0.752	1.011, -0.987

<b>Complex</b>	<b>[Ir(N<sub>3</sub>Me<sub>4</sub>)F]((Me<sub>2</sub>N)<sub>3</sub>SOTf) <b>23</b></b>	<b>[Ir(N<sub>3</sub>Me<sub>4</sub>)(H)Cl<sub>2</sub>]·CH<sub>2</sub>Cl<sub>2</sub> <b>30</b></b>
Empirical formula	C <sub>32</sub> H <sub>45</sub> F <sub>4</sub> IrN <sub>6</sub> O <sub>3</sub> S <sub>2</sub>	C <sub>26</sub> H <sub>30</sub> Cl <sub>4</sub> IrN <sub>3</sub>
Formula weight [g/mol]	894.06	718.57
Crystal size [mm]	0.31 x 0.24 x 0.05	
Crystal system	orthorhombic	monoclinic
Space group	Pbca, No. 61	C2/c, No.15
a [Å]	13.3815(13)	34.592(7)
b [Å]	20.840(2)	8.2610(17)
c [Å]	26.333(3)	18.520(4)
α [°]		
β [°]		108.37(3)
γ [°]		
V [Å <sup>3</sup> ]	7343.6(12)	5022.7(18)
Z	8	8
D <sub>calc.</sub> [g/cm <sup>3</sup> ]	1.617	1.879
Temperature [K]	153	153
λ [Å], Mo-Kα	0.71073	0.71073
2 θ [°]	2.10, 25.16	2.32, 22.15
Refln. collected, unique	69716, 6478	2791, 2791
No. of parameters	429	294
GooF, S	0.747	1.049
R <sub>1</sub> (I>2σ(I))	0.0444	0.0520
wR <sub>2</sub> (I>2σ(I))	0.0741	0.1521
ρ <sub>min,max</sub> [e/ Å <sup>3</sup> ]	1.265, -1.034	1.420, -1.509

<b>Complex</b>	<b>[Ir(N<sub>3</sub>Me<sub>4</sub>)(CH<sub>2</sub>O)]Al(pftb)<sub>4</sub> <b>35</b></b>	<b>[Ir(N<sub>3</sub>Me<sub>4</sub>)(Me)(MeCN)OTf]<sup>+</sup> <b>28</b></b>
Empirical formula	C <sub>42</sub> H <sub>29</sub> AlF <sub>36</sub> IrN <sub>3</sub> O <sub>5</sub>	C <sub>30</sub> H <sub>33</sub> F <sub>6</sub> IrN <sub>4</sub> O <sub>6</sub> S <sub>2</sub>
Formula weight [g/mol]	1558.83	915
Crystal size [mm]	0.47 x 0.07 x 0.07	0.05 x 0.2 x 0.3
Crystal system	orthorhombic	monoclinic
Space group	Pna2 <sub>1</sub> , No. 33	P2 <sub>1</sub> /c, No. 14
a [Å]	20.6915(7)	16.031(7)
b [Å]	19.9295(7)	12.433(6)
c [Å]	13.0509(5)	20.423(10)
α [°]		
β [°]		102.141(8)
γ [°]		
V [Å <sup>3</sup> ]	5381.8(3)	3980(3)
Z	4	4
D <sub>calc.</sub> [g/cm <sup>3</sup> ]	1.917	1.392
Temperature [K]	153	153
λ [Å], Mo-Kα	0.71073	0.71073
2 θ [°]	1.42, 28.03	1.30, 27.82
Refln. collected, unique	63451, 12616	21038, 7969
No. of parameters	755	449
Goof, S	0.955	1.146
R <sub>1</sub> (I>2σ(I))	0.0486	0.1651
wR <sub>2</sub> (I>2σ(I))	0.0845	0.3817
ρ <sub>min,max</sub> [e/ Å <sup>3</sup> ]	1.431, -0.764	3.997, -3.561

<b>Complex</b>	<b>Me<sub>2</sub>PhNO</b>	<b>MePh<sub>2</sub>NO</b>
Empirical formula	C <sub>8</sub> H <sub>11</sub> NO	C <sub>13</sub> H <sub>13</sub> NO
Formula weight [g/mol]	137.18	199.24
Crystal size [mm]	0.55 x 0.19 x 0.12	0.1 x 0.1 x 0.3
Crystal system	orthorhombic	orthorhombic
Space group	Pbca, No. 61	Pna2 <sub>1</sub> , No. 33
a [Å]	6.8945(6)	23.660(3)
b [Å]	10.7108(9)	15.685(2)
c [Å]	20.2513(17)	5.5041(8)
α [°]		
β [°]		
γ [°]		
V [Å <sup>3</sup> ]	1495.5(2)	2042.6(5)
Z	8	8
D <sub>calc.</sub> [g/cm <sup>3</sup> ]	1.219	1.296
Temperature [K]	153	153
λ [Å], Mo-Kα	0.71073	0.71073
2 θ [°]	2.01, 28.02	1.56, 28.01
Reflex. collected, unique	16617, 1776	23605, 4771
No. of parameters	92	272
GooF, S	0.975	1.062
R <sub>1</sub> (I>2σ(I))	0.0385	0.0692
wR <sub>2</sub> (I>2σ(I))	0.0948	0.1258
ρ <sub>min,max</sub> [e/ Å <sup>3</sup> ]	0.219, -0.213	0.276, -0.254

<b>Complex</b>	<b>[Ir(N<sub>3</sub>Me<sub>4</sub>)(C<sub>6</sub>H<sub>13</sub>O)]<sup>+</sup> <b>34</b></b>	<b>[Rh(N<sub>3</sub>Me<sub>4</sub>)(C<sub>6</sub>H<sub>13</sub>O)]<sup>+</sup> <b>37</b></b>
Empirical formula	C <sub>47</sub> H <sub>41</sub> AlF <sub>36</sub> IrN <sub>3</sub> O <sub>5</sub>	C <sub>47</sub> H <sub>41</sub> AlF <sub>36</sub> RhN <sub>3</sub> O <sub>5</sub>
Formula weight [g/mol]	1631.02	1542.00
Crystal size [mm]	0.6 x 0.12 x 0.05	0.1 x 0.14 x 0.7
Crystal system	monoclinic	monoclinic
Space group	P2 <sub>1</sub> /n, No. 14	P2 <sub>1</sub> /n, No. 14
a [Å]	14.3008(18)	14.152(2)
b [Å]	12.4646(15)	12.5538(19)
c [Å]	31.920(4)	31.806(5)
α [°]		
β [°]	96.387(2)	95.020(2)
γ [°]		
V [Å <sup>3</sup> ]	5654(12)	5629.1(14)
Z	4	4
D <sub>calc.</sub> [g/cm <sup>3</sup> ]	1.911	1.779
Temperature [K]	153	153
λ [Å], Mo-Kα	0.71073	0.71073
2 θ [°]	1.28, 28.04	1.29, 25.06
Refln. collected, unique	65759, 13179	54757, 9920
No. of parameters	839	829
GooF, S	1.087	1.029
R <sub>1</sub> (I>2σ(I))	0.0661	0.0772
wR <sub>2</sub> (I>2σ(I))	0.1543	0.1920
ρ <sub>min,max</sub> [e/ Å <sup>3</sup> ]	1.724, -1.554	0.743, -0.722

## 8.3 Lebenslauf

---

### Persönliche Daten

**Name:** Nevena Šušnjar

**Geboren am:** 23.09.1976

**Geburtsort:** Belgrad

**Nationalität:** Serbisch

---

### Ausbildung

1983 - 1991	Grundschule "Karadjordje"
1991 - 1995	XII bgd Gymnasium "Dimitrije Tucovic"
1995 - 2001	Universität Belgrad, Fakultät der Chemie
06/2001 - 11/2001	Diplomarbeit im Institut für Anorganische Chemie, Universität Belgrad bei Prof. Dr. S. Sovilj Thema: <i>Co(II)</i> , <i>(III)</i> , <i>Ni(II)</i> and <i>Cu(II)</i> dithiocarbamato Complexes
19/11/2001	Dipl. Chemiker
2002 - 2006	Doktorandin bei Prof. Dr. P. Burger zum Thema: <i>Towards Rhodium and Iridium oxo complexes</i>
2002 - 2003	Anorganisch-chemischen Institut der Universität Zürich
2003 - 2006	Institut für Anorganische und Angewandte Chemie der Universität Hamburg

---

### Anstellungsverhältnis

10/2003 - 02/2006    Wissenschaftliche Mitarbeiterin an der Universität Hamburg

---

### Konferenzen und Fortbildungen

08/2003	XV Fechem - Zürich, Switzerland - Posterbeitrag
09/2003	Summer school on computational chemistry - Heidelberg, Germany
09/2004	Molecular modeling and DFT calculations - Heidelberg, Germany
09/2005	XVI Fechem - Budapest, Hungary – Posterbeitrag

The research presented within, was carried out by the author at the University of Zürich and University of Hamburg. It is the author's original work and contains nothing that is a result of the work carried out in collaboration and has not been submitted in whole or in part for a degree at any other university.

Hamburg, February 2006

Filename: Towards Ir and Rh oxo complexes-small versons1  
Directory: D:\Documents and Settings\Andy and  
Nele\Desktop\Nele Work\Thesis-fin  
Template: D:\Documents and Settings\Andy and Nele\Application  
Data\Microsoft\Templates\Normal.dot  
Title: 1 Introduction  
Subject:  
Author: nevena  
Keywords:  
Comments:  
Creation Date: 23.02.2006 13:50  
Change Number: 16  
Last Saved On: 13.04.2006 16:48  
Last Saved By: Nevena Susnjar  
Total Editing Time: 181 Minutes  
Last Printed On: 25.04.2006 21:32  
As of Last Complete Printing  
Number of Pages: 147  
Number of Words: 51.933 (approx.)  
Number of Characters: 296.020 (approx.)